Development of an NMR method for the *In vitro* characterisation of enzyme activity present in honey bee venom against mammalian bioactive molecules

A thesis submitted to the Department of Pure and Applied Chemistry, in fulfilment of the regulations for the Degree of Doctor of Philosophy in Chemistry.

Jennifer Wallace

2017

This thesis is the result of the author's original research. It has been composed by the author and has not been previously submitted for examination which has led to the award of a degree.

Signed:

Date:

Acknowledgements

I would like to start by thanking the Korean Government KIAT Scheme, and Beesen Co. for all of the funding support throughout the duration of my work.

Secondly I would like to thank both my supervisors; Dr Mark Dufton and Dr John Parkinson. Dr Mark Dufton, my main supervisor and first point of contact for any assistance and guidance, has been incredibly supportive and encouraging. Dr Dufton's support has been vital throughout and his encouragement has allowed me to continually challenge myself.

Dr John Parkinson has also been incredibly supportive and encouraging. Dr Parkinson's support, in particular the assistance given to me in regards to the NMR technique, has been invaluable throughout all of my work.

Special thanks also goes to Strathclyde University NMR Technician Craig Irving, who has also been available for technical support for the NMR instrument.

I would like to thank members of the Cormack group (Tim, Amaia, Omer, Ali, Danny, Ain, and many more). All of these people, who I was fortunate to share an office with, were of immense help throughout the project. Not only were they there for academic support, but they also made the experience more enjoyable than I could have ever hoped, and I hope to stay in touch with in the future.

I would also like to extend my thanks to the other members of the bee venom team (Jonans Tusiimire, Dr Dave Watson, Carol Clements and Louise Young) for their valuable input during the monthly meetings for the project as a whole.

Lastly my final thanks go to my friends and family for their support and encouragement throughout my entire time at University. Special thanks go to Craig who has supported and believed in me and had encouraged me to take this particular academic path.

Abstract

The venoms of snakes and insects are complex mixtures of toxins and enzymes that produce profound physiological and behavioural consequences when injected into prey creatures. Understanding how these consequences are achieved from very small amounts of venom in short time intervals sheds light on the principles of venom action and the defence mechanisms that may have to be overcome. In addition to the possibility of better treatments for envenomed humans, wider insights into drug discovery are also promised.

This thesis describes an investigation into the chemical effects of Honey Bee (*Apis mellifera*) venom. The toxic effects of some bee venom components (such as melittin and phospholipase A2) are well known, but the venom's capacity to respond to potential defensive reactions (as represented by the biomolecules commonly released by mammals in response to wounding and the injection of toxins) has not been so well studied.

Using the technique of Real-time NMR, specially adapted to this research, purified whole bee venom was challenged with a range of bioactive molecules that a mammalian victim could potentially release in response to the presence of the venom (i.e. adrenalin, cortisol, angiotensin, bradykinin, substance P and opioid peptides). Reactions were carried out in the NMR spectrometer under physiological conditions (pH 7.4, 37°C) and full spectrum "snapshots" were taken at frequent intervals. Subsequent analysis revealed whether or not any transformation had taken place, and, if so, what intermediates and products were generated.

It was found that only substance P and the opioid peptides were acted upon by the bee venom, implying the venom contained one or more appropriate peptidase activities.

Further experimentation with the opioids Met- and Leu-enkephalin, and their N-terminal fragment Tyr-Gly-Gly, established that the peptidase activity was primarily that of a dipeptidyl dipeptidase, supported by a dipeptidase. Subsequent kinetic studies implied that these substrates were not ideal and so other opioid peptides (Endomorphin I, Endomorphin II and Casomorphin 1-7) were also tested. It was found that Endomorphin I was the "best" substrate.

The substrate specificity of the venom dipeptidyl peptidase shows consistencies with the known mammalian dipeptidyl peptidases III and IV. The presence of a DPP IV – like enzyme (i.e. an evolutionary homologue of the human version) in bee venom has been predicted from gene sequence analysis and the generation of melittin from its precursor. This bee protein is also known as Api m 5 and is a notable allergen. Consequently, the bee venom was challenged with a model substrate and a model inhibitor for human DPP IV. The model substrate was readily converted and the model inhibitor reduced the rate of conversion of the opioid peptides. Two synthetic variants of the inhibitor were tested, but they were not as effective. Although bee venom Api m 5 shares structural and preferred substrate/inhibitor similarities with human DPP IV, some contrasts remain (for example the former's ability to act on enkephalin peptides).

It is proposed that the role of the bee venom DPP-IV like enzyme (i.e. Api m 5) is primarily to destroy opioid peptides released by mammalian sting victims in response to the physical and toxicological impact of the venom. Opioid peptides bind to skin nociceptors to limit pain perception following injury, so fragmentation of these peptides could lead to prolonged pain from the sting site(s) and therefore behaviour that serves the interests of the bees (i.e. avoidance, retreat or stopping in the case of a mammal foraging a hive).

Preliminary experiments were conducted to follow the action of the hyaluronidase in bee venom which breaks up the extra cellular matrix carbohydrate to speed up the tissue spread of the venom components. The NMR method again proved to be useful.

Table of Contents

Acknowledgements.....I

Abstract..... II

Abbreviations IX

Chapter 1 1

1.0 Bee Venom 1

1.0.1 Introduction 1

1.0.2 Composition of Bee Venom 5

1.0.2.1 Melittin..... 7

1.0.2.2 Phospholipase A2 11

1.0.2.3 Hyaluronidase 15

1.0.2.4 Mast Cell Degranulation Peptide 18

1.0.2.5 Apamin..... 19

1.0.2.6 Api m 5..... 20

1.0.3 Bee venom versus snake venom 25

1.1 Skin Physiology 27

1.1.1 Introduction 27

1.1.2 Keratinocytes 28

1.1.3 Corneocytes..... 28

1.1.4 The Stratum Corneum..... 29

1.1.5 Extracellular Matrix 30

1.2 Defence Bio-actives to be Investigated Experimentally..... 32

1.2.1 Adrenalin..... 33

1.2.2 Cortisol 37

1.2.3 Enkephalin 38

1.2.4 Bradykinin 40

1.2.5 Angiotensin II 41

1.2.6 Substance P 42

1.3 Therapeutic Applications of Bee Venom 44

1.3.1 Arthritis 44

1.3.2 Cancer 45

1.3.3 Parkinson's Disease 46

1.3.4 Cosmetics 48

1.4 Nuclear Magnetic Resonance 49

1.4.1 Introduction 49

1.4.2 Principles of NMR 50

1.4.2.1 Chemical Shift 51

1.4.2.2 Spin-spin Coupling 52

1.4.2.3 Spin Relaxation 53

1.4.2.4 NMR Instrumentation 53

1.4.3 Reaction Monitoring by NMR 53

1.4.3.1 In tube mixing 55

1.4.3.2 Sampling from external reaction 55

1.4.3.3 Flow NMR 56

1.4.3.4 In situ mixing 56

1.5 Aims 57

Chapter 2 58

2.0 Determination of Limit of Detection (LoD) and Limit of Quantification (LoQ) for BV by NMR spectroscopy 58

2.1 Introduction 58

2.2 Experimental 59

2.2.1 Instrumentation 59

2.2.2 Method 59

2.2.3 Materials 61

2.2.4 Solution Preparation 62

2.3 Results and Discussion 63

2.4 Summary 72

Chapter 3 73

3.0 Bioactive Screening 73

3.1 Introduction 73

3.2 Experimental 73

3.2.1 Materials 73

3.2.2 Substrate Solutions 73

3.2.3 NMR Experimental 74

3.3 Results of all Control Experiments for Bioactive Molecules/BV 76

3.4 Results of all Bioactive Molecules Experiments 78

3.4.1 YGGFL Results 80

3.4.2 YGGFM Results 85

3.4.3 Substance P Results 89

3.5 Determination of Substrate Cleavage Sites 91

3.6 Summary 101

4.0 Characterisation of Peptidase Activity 102

4.1 Introduction 102

4.2 Experimental 111

4.2.1 Materials 111

4.3 Results 113

4.3.1 Results of Other Opioid Substrate Experiments 113

4.3.2 Results of Human DPP IV Substrate – GP-X 124

4.3.3 Results of Michaelis-Menten Kinetics Experiments 128

4.4 Summary 136

Chapter 5 139

5.0 Investigation of Enzyme Inhibition 139

5.1 Introduction 139

5.2 Experimental 140

5.2.1 Materials 140

5.2.2 Methods 140

5.3 Results 144

5.3.1 IPI Controls 144

5.3.2 IPG Controls 147

5.3.3 FPI Controls 150

5.3.4 Substrate Controls 153

5.3.5 Inhibitor + Substrate Controls 159

5.3.6 Results of BV + IPI + Substrate Experiments 162

5.3.7 Results of BV + FPI + Substrate Experiments 168

5.4 Summary 174

Chapter 6 175

6.0 Discussion of results 175

6.1 Quality Control 175

6.2 Enzyme Activity 176

6.2.1 Enkephalin and Nociceptin Fragments 176

6.2.2 The Enkephalin Peptides – YGGFM and YGGFL 178

6.2.3 Human DPP IV Substrate – GP-7-amido-4-methylcoumarin hydrobromide 179

6.3 Enzyme Inhibition 180

6.4 Substrate Specificity 186

6.5 Identification of Enzyme 187

General Conclusions 194

Collaborative Work 196

Future Work 198

References 200

Appendix 1 215

Appendix 2 218

Appendix 3 219

Appendix 4 220

Appendix 5 225

Appendix 6 228

Appendix 7 231

Abbreviations

AA	Arachidonic Acid
ACE	Angiotensin converting enzyme
ACTH	Adrenocorticotrophin
ADA	Adenosine deaminase
APN	Aminopeptidase N
BV	Bee venom
BVT	Bee venom therapy
cAMP	Cyclic adenosine monophosphate
CE	Cornified envelope
CNS	Central nervous system
COMT	Catechol-O-methyl transferase
COSY	Correlation spectroscopy
COX	Cyclooxygenase
CW	Continuous wave
DMSO-d_6	Dimethyl sulfoxide-d_6
DNA	Deoxyribonucleic acid
DOR	δ-opioid receptor
DPP	Dipeptidyl peptidase
DRs	Death receptors
ECM	Extracellular matrix
ES-complex	Enzyme/substrate-complex
EXSY	Exchange spectroscopy
FBS	Foetal bovine serum
FT	Fourier transformation
GAG	Glycosaminoglycan
GC-MS	Gas chromatography – mass spectrometry
GR	Glucocorticoid receptor

HA	Hyaluronic acid
HIV	Human immunodeficiency virus
HPA	Hypothalamic pituitary adrenocortical
HPLC	High pressure liquid chromatography
HSQC	Heteronuclear single quantum coherence spectroscopy
ICH	International Council on Harmonisation
iNOS	Inducible nitric oxide synthase
IUPAC	International Union of Pure and Applied Chemistry
JAK	Janus kinase
Km	Michaelis constant
KOR	κ-opioid receptor
LAAO	L-amino acid oxidase
LoD	Limit of Detection
LoQ	Limit of Quantification
MCD	Mast cell degranulation peptide
MMPs	Matrix metalloproteinases
MOA	Monoamine oxidase
MOR	μ-opioid receptors
MSH	Melanocyte stimulating hormone
NEP	Neutral endopeptidase
NF-κB	Nuclear factor kappa-light-chain-enhancer of activated B cells
NMR	Nuclear magnetic resonance
NO	Nitric oxide
NOESY	Nuclear Overhauser Effect spectroscopy
NSAIDS	Non-steroidal anti-inflammatory drugs
OFQ/N	Orphanin FQ/nociceptin
PAF	Platelet activating factor
PD	Parkinson’s disease
PENK	Pro-enkephalin gene

PGE_2	Prostaglandin A_2
PLA_2	Phospholipase A_2
PPM	Parts per million
RA	Rheumatoid arthritis
RF	Radiofrequency
ROS	Reactive oxidative species
SC	Stratum corneum
S/N	Signal-to-noise ratio
STAT3	Signal transducer and activator of transcription 3
TEWL	Transepidermal water loss
TOCSY	Total correlation spectroscopy
UV	Ultraviolet
Vmax	Maximum velocity
WBV	Whole bee venom
WHO	World Health Organisation
YGG	Tyr-Gly-Gly
YGGFL	Leu-enkephalin
YGGFM	Met-enkephalin
YPFF	Endomorphin II
YPWF	Endomorphin I
YPFPGPI	Casomorphin 1-7

Chapter 1

1.0 Bee Venom

1.0.1 Introduction

Bees are thought to have arisen around the time that flowering plants first appeared.[1] In terms of evolution bees arose from the spheciform wasps, sometimes referred to as *sphecidae* or sphecoid wasps.[1] *Apis mellifera* (honey bees) are part of the Hymenoptera order in the Insecta class.[2–4] The Hymenoptera order of insects includes thousands of species of wasps, ants, sawflies and bees.[5] The Hymenoptera classification is shown in figure 1.0.1.1. The *Apis* insect classification, an ancient line of bees, is thought to have originated in tropical Eurasia which migrated and ended up in Europe around ten thousand years ago.[5] Honey bees are *ca.* 15-20 mm in size, they live in natural hives, tree cavities and artificial hives and are generally nonaggressive.[6]

In a honey bee colony the hierarchy begins with a queen bee followed by workers and then drones.[7] There is usually only one queen bee in a hive that lays eggs, producing offspring, along with tens of thousands of worker bees that are involved in foraging, protecting the hive, and caring for the offspring.[5,7] Worker bees are sterile meaning they cannot reproduce. The queen bee lifespan is much longer than that of the worker bees (*ca.* 10 times longer).[5]

Honey bees, like other insects, have an open circulatory system which is known as a hemolymph. This means that the body fluid within an insect flows freely and there is no distinction between the blood and interstitial fluid.[8] This can be compared to the mammalian circulatory system which is a closed system with the blood contained within capillaries. These different circulatory systems mean that the bee defence mechanisms have to overcome the different physical barriers within mammals for effective action. However, when bees use their defence mechanisms against other insects, the open circulatory system makes it easier to have an effective action.

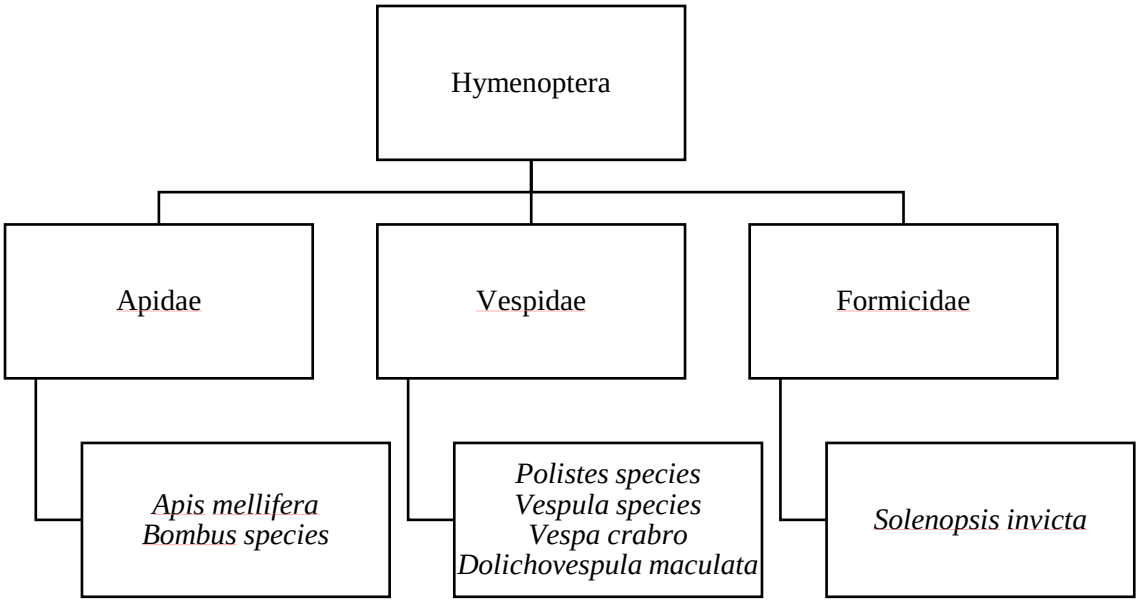

Figure 1.0.1.1: Hymenoptera taxonomy. Adapted from Casale and Burks, 2014.[6]

Insects do not have an adaptive immune system but have evolved an innate immune system meaning that they can distinguish between foreign and non-foreign molecules.[8] The innate immune system of insects works *via* both cellular and humoral mechanisms.[8,9] The cellular mechanisms involve phagocytosis, capture by hemocytes and confining of pathogens by nodule formation.[9] The humoral mechanisms involve the release of antimicrobial peptides into the hemolymph from fat bodies, clotting within the hemolymph and melanisation, which is the formation of melanin.[9] Insects are vulnerable to many microorganisms as well as other insects and vertebrates, meaning they not only require an established immune response but also a defence mechanism. It is well known from literature that bees are stinging insects which inject venom as a defence mechanism. However honey bees generally will not sting unless provoked.[3]

The venom reservoir is where the bee venom is stored, which is secreted from the poison and accessory glands.[10] Envenomation is the process by which bees insert their sting into their victim. The sting of Hymenoptera insects has evolved from ovipositors, which were used to lay eggs and therefore only female Hymenoptera insects are capable of stinging.[4,6] Honey bees have a barbed stinger meaning that they leave

behind the sting and venom sac when they pull away and this continues to inject venom into the victim.[2,11] A diagram showing the barbed stinger is shown in figure 1.0.1.2. The sting only detaches from the bee when it injects into a vertebrate whereas it stays attached to the bee when it stings other insects. This is an adaptation specifically against vertebrates.[4] There is a nerve ganglion attached to the sting which helps embed the sting into the flesh and is responsible for the continuous injection of venom into the wound after it is detached from the bee.[12] The venom then causes a series of different reactions by the various components of the venom.

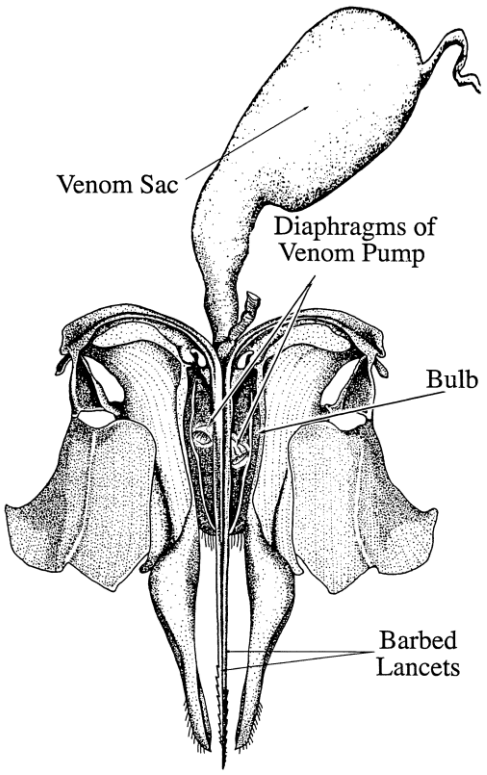

Figure 1.0.1.2: Diagram of the honey bee sting. [4] (reproduced with permission)

Bee venom (BV) is a mixture of various molecules ranging from small molecules (< 10 kDa) to larger molecules (100 kDa).[4,11,13,14] It is known that there are at least 18 different components to the BV.[13] The composition of BV is described in detail in section 1.0.2. Venom is produced by honey bees as a defence mechanism against predators. Hymenoptera social insects will use their sting to defend against anything

that is a threat to their hive.[4] The venom has evolved over time to defend against different threats with the majority of threats to a honey bee being other insects. When honey bees sting other insects the venom causes paralysis and death. However, when they sting humans the main effect is to cause pain and distraction.[4] The sting and the mandibular gland produce what are known as pheromones, the main component being isopentyl acetate, which evaporates and gives a smell (like bananas) to warn other bees about potential danger.[4,15]

Generally a bee sting in humans will cause a local reaction such as pain, swelling, redness and itching.[16] The areas of the body which have the highest level of pain after a bee sting are the mouth/nose.[17] The treatment of local reactions would be with H_1-antihistamines (which target H_1 histamine receptors) glucocorticoid creams/ointments, analgesics or ice/cold compresses.[6] The honey bee can inject up to 147 µg of its venom into its victim in one sting.[2] In some people a single sting from a honey bee can cause a hypersensitivity reaction instantly, resulting in anaphylaxis.[2,16] Death from a bee sting is rare; however it can occur after just one sting.[4,16,18] The cause of death from a bee sting commonly involves respiratory dysfunction via anaphylaxis or cardiovascular failure.[6]

There are four types of hypersensitivity reactions (type I, II, III and IV), which have been classified by Gell and Coombs according to the immune response.[19] Type I hypersensitivity reactions, which lead to anaphylaxis, are a result of IgE antibodies[20] being released in response to BV allergens known as phospholipase A_2 and hyaluronidase.[4] These allergens are discussed in greater detail in section 1.0.2. This type of reaction occurs only in sensitized individuals. The venom-specific IgE are found on mast cells, which cause numerous mast-cell mediators to be released. These mediators include histamine, leukotrienes, prostaglandins and platelet activating factor.[6] The clinical symptoms of an anaphylactic reaction to honey bee venom include urticaria, angioedema, tachycardia, asphyxia, nausea and myocardial infarction.[6,18] The treatment of an anaphylactic shock reaction would be by injectable epinephrine, H_1-antihistamines, oxygen and β2 agonists.[6]

1.0.2 Composition of Bee Venom

BV is a complex mixture of various components. Table 1.0.2.1 below shows some of the main components with their molecular weight, biological action and their dry weight present in BV.

Table 1.0.2.1: Components of BV

Component	Molecular Weight (kDa)	% present in BV	Action of Component
PLA_2 (Api m 1)	16	10 – 12 %	Disruption of cell membranes
Hyaluronidase (Api m 2)	39	< 3 %	Hydrolyses hyaluronic acid
Acid phosphatase (Api m 3)	43	1 %	Releases histamine and induces wheal and flare in the skin
Melittin (Api m 4)	2.840	40 – 60 %	Synergism with PLA_2 and has lytic activity
Venom dipeptidyl peptidase IV (Api m 5)	100	-	Cleaves pro-melittin Sequence similarity to human DPP IV
Api m 6	7.190, 7.400, 7.598 and 7.808	-	4 isoforms exist: Api m 6.01, 6.02, 6.03 and 6.04. Recent allergen found in 40 % of BV hypersensitive patients.
CUB Serine protease (Api m 7)	39	-	Cleaves peptide bonds using serine at the catalytic site
References [10,11,14,21–24]			

Table 1.0.2.1 continued

Component	Molecular Weight (kDa)	% present in BV	Biological Action
Carboxylesterase -6 (Api m 8)	70	-	Hydrolysis of carboxylic esters
Serine carboxypeptidase (Api m 9)	60	-	Cleaves peptide bonds using serine at the catalytic site
Icarapin-like precursor (Api m 10)	50 – 55	-	-
Major royal jelly protein (Api m 11)	50	-	-
Vitellogenin (Api m 12)	200	-	Provides nutrients
Apamin	2.036	2 – 3 %	Inhibits Ca^{2+} dependent K^+ channels and acts as a neurotoxin
Mast Cell Degranulation Peptide (MCD)	2.588	1 – 3 %	Releases histamine, anti-inflammatory and analgesic. Inhibitor of K^+ channels.
Adolapin	11.5	1 %	Anti-inflammatory and inhibits PLA_2 and COX activity.
Histamine	0.307	1.5 %	Agonist at histamine receptors
References [10,11,14,21–24]			

Other components and their dry weight in BV include amines (dopamine (0.13 – 1 %) and noradrenaline (0.1 – 0.7 %)), enzymes (Lysophospholipase (1 %), and α-

Glucosidase (0.6 %)) and carbohydrates (2 % - fructose and glucose).[13,21,25] Citrate is also found in BV, and a study has shown evidence that this may inhibit the BV phospholipase A2.[26]

1.0.2.1 Melittin

Melittin is the major toxic component of the dry weight of bee venom. It has 26 amino acid residues and it exists as an amphiphilic structure.[10,14] The amino acid sequence of melittin is:

GIGAVLKVLTTGLPALISWIKRKRQQ.[13]

Melittin is fundamentally a hydrophobic molecule but has 6 positive charges at physiological pH.[27] Located towards the carboxy-terminal end of the melittin molecule there are four amino acids (Lys21-Arg22-Lys23-Arg24)[27] with positive charges along with 6 other amino acid residues at this end giving hydrophilicity to this part of the molecule.[10] Located towards the amino-terminal end of the melittin molecule there are two amino acids[27] with positive charges along with 20 other amino acid residues giving hydrophobicity to this part of the molecule.[10] The crystal structure of melittin is shown in figure 1.0.2.1.1.

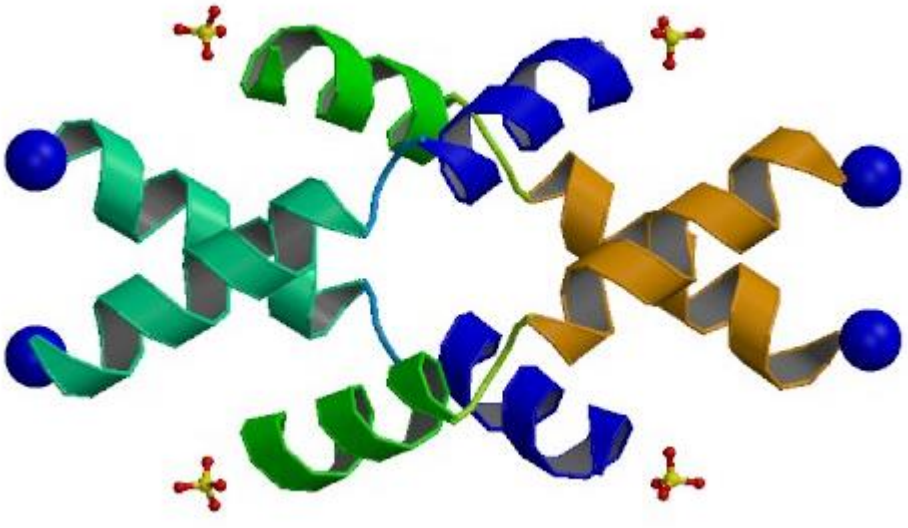

Figure 1.0.2.1.1: Ribbon structure of melittin. This structure was obtained at a resolution of 2.0 Å using four sulfate ions as ligands. The structure was taken from the RCSB protein data bank.[28] The blue balls are modified N-terminals (NH_3). The bend in each chain is shown in light blue and light green. Dark green/dark blue and orange/aqua segments represent chains either side of the bend.

Melittin is synthesized *via* cleavage of two precursor molecules. The first of these precursor molecules is called prepromelittin, which is a 70 amino acid peptide with a methionine at the amino end of the peptide.[29] This is not detected in the venom gland. It is thought that there is rapid cleavage of prepromelittin to the second precursor molecule promelittin,[29] which would make it difficult to detect prepromelittin. Promelittin, which is found in the venom gland and is composed of 49 amino acids,[30] is hydrolysed releasing melittin into the venom gland.[27,29,31] The enzyme responsible for the hydrolysis of promelittin to release melittin was found to be a dipeptidyl peptidase IV-like enzyme.[30] This enzyme is mentioned in table 1.0.2.1 and is discussed in more detail in section 1.0.2.6.

The conformation and self-association of melittin has been widely studied due to its complexity. When melittin is in its α-helical conformation, it is asymmetric meaning there are polar and non-polar amino acids on either side of the peptide. This asymmetry formed by the arrangement of amino acids gives melittin its amphiphilic structure.[27,32] Melittin is monomeric when the concentration is low and forms tetramers when the

concentration is high.[13,27] These structural conformations are important for the various actions of melittin.

The tetramer conformation is dependent on various factors which includes melittin monomer concentration (as previously mentioned), salt concentration, and pH.[27] These factors result in a reduction of the overall charge of melittin and stimulates the aggregation of melittin monomers into tetramers. This reduction in charge is necessary as the high charge density of melittin means that there would be electrostatic repulsion occurring between the monomers which would therefore prevent aggregation into tetramers.[27] A study by Talbot *et al.* looked at the conformation of melittin using fluorescence measurements, gel filtration and optical rotatory dispersion. These results found that melittin is a monomer when there is low concentration of melittin and low ionic strength at physiological pH.[33] This study also showed that high monomer concentration and high ionic strength causes aggregation at physiological pH.

When melittin is in its tetrameric form the hydrophobic side chains of each melittin chain are all positioned towards the inner part of the tetramer making the tetramer core apolar. The hydrophilic and charged amino acids are mostly positioned towards the outer part of the tetramer giving the tetramer a hydrophilic surface which protects the hydrophobic residues from the solvent. Electrostatic repulsion is thought to be the reason that melittin tetramers are soluble in solution and prevents the higher order aggregation of tetramers since the four melittin chains in a tetramer contain only positive charges.[32]

There is a bend in the melittin chain between amino acid residues 11 and 12 (Thr-Gly respectively). On either side of this bend there are two α-helical regions. There is no hydrogen bonding between the amino acid Thr10 carbonyl oxygen and amino acid Pro14. This may give Pro14 involvement in the formation of the bend as this would destabilise the α-helix between amino acid residues 10 – 14.[32]

The main biological action of melittin is that it is cytolytic.[31] Melittin can incorporate into both synthetic and natural phospholipid bilayers of membranes forming pores, therefore causing interference with the bilayer structure.[27] The mechanism by which antimicrobial peptides, including melittin, form pores has been widely studied. Two main mechanisms for pore formation have been suggested, a diagram showing these

two mechanisms is shown in figure 1.0.2.1.2. One of these mechanisms is known as the barrel-stave model where the peptides incorporate into the hydrophobic region of the bilayer with the hydrophilic regions of the peptide forming the centre region of the pore.[34,35] The other mechanism is known as the toroidal model where the peptides interact with the polar head groups, pulling these head groups from the top and bottom of the bilayer together causing them to bend. This lines the pore with both the polar head groups of the bilayer and the peptide.[35]

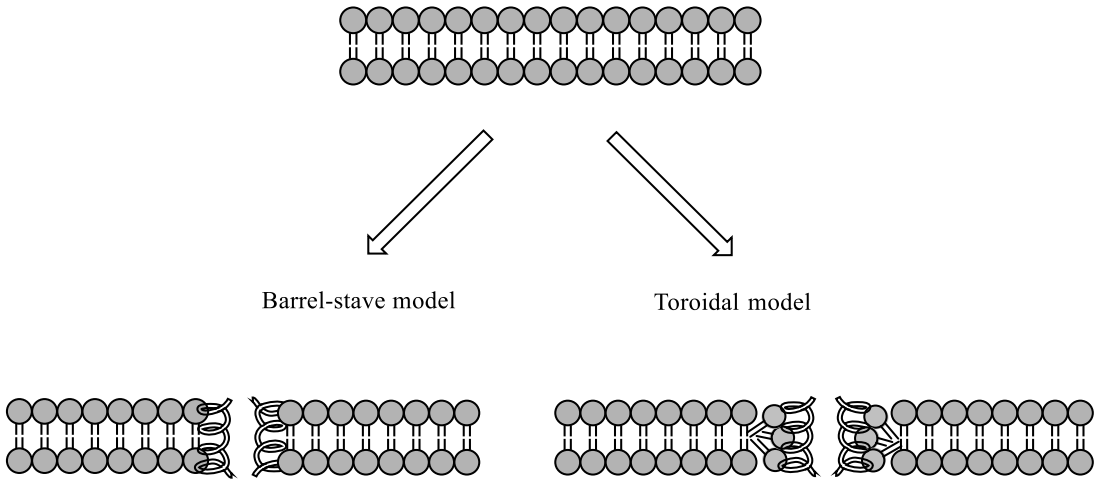

Figure 1.0.2.1.2 Schematic of pore formation by antimicrobial peptides (adapted from Sengupta *et al.*, 2008)[36]

The mechanism melittin uses to form pores remains controversial in the literature. Some papers suggest that melittin follows the barrel-stave model;[37] however others suggest the toroidal model.[35] The process of forming pores appears to be complex with several factors affecting the way melittin incorporates into membranes. Another action of melittin is that it acts in synergy with phospholipase A_2, which is discussed in the next section.

1.0.2.2 Phospholipase A2

Phospholipase A_2 (PLA_2) is one of the enzymes found in BV. In general PLA_2 enzymes act at the *sn*-2 position of membrane phospholipids to release a fatty acid, for example arachidonic acid (AA), and a lysophospholipid. [38,39] AA is a precursor molecule for signalling molecules such as eicosanoids, which include prostaglandins and leukotrienes.[39] Prostaglandins and leukotrienes are formed when AA is metabolized by the enzymes lipoxygenase and cyclooxygenase.[40,41] Lysophosphatidylcholine is an example of a lysophospholipid which can be released by PLA_2. These molecules are also the precursor molecules for other signalling molecules such as platelet-activating factor (PAF). [23,24] Eicosanoids and PAF play a key role in the inflammatory response.[41] A diagram showing a membrane phospholipid bilayer is shown in figure 1.0.2.2.1 and the general structure of a phospholipid is shown in figure 1.0.2.2.2.

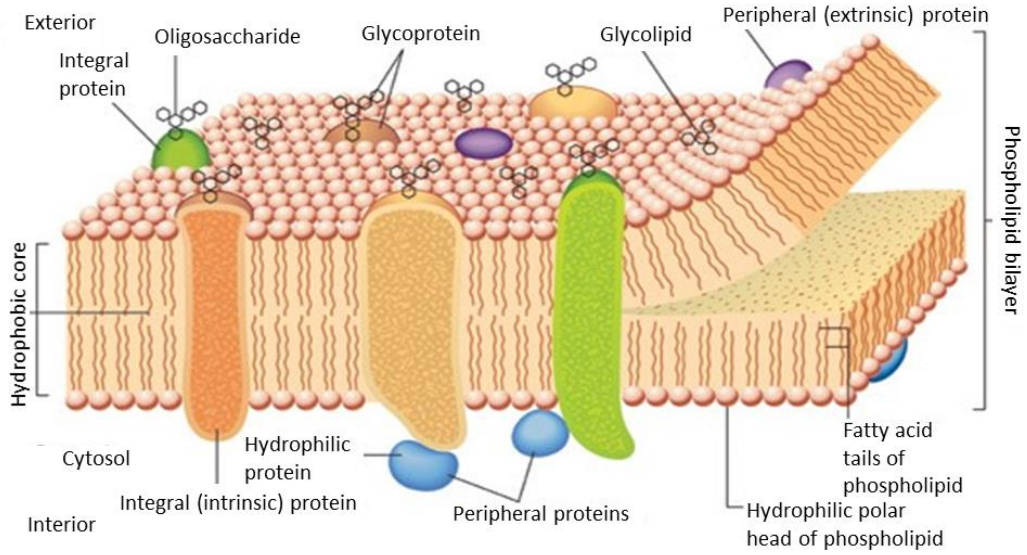

Figure 1.0.2.2.1: Image of a phospholipid bilayer, this image was taken from rsc.org.[42]

The general group of PLA_2 enzymes has been classified into numerous different groups according to nucleotide and amino acid sequence.[39,41,43] Table 1.0.2.2.1 gives details of the PLA_2 enzyme classification which was adapted from Schaloske and Dennis.[43] There is also a broader classification which groups the PLA_2 enzymes into three groups; secretory PLA_2, cytosolic PLA_2 and cytosolic Ca^{2+}-independent PLA_2.[39,41] The majority of PLA_2 enzymes require mM concentrations of Ca^{2+} for optimal catalytic activity.[39]

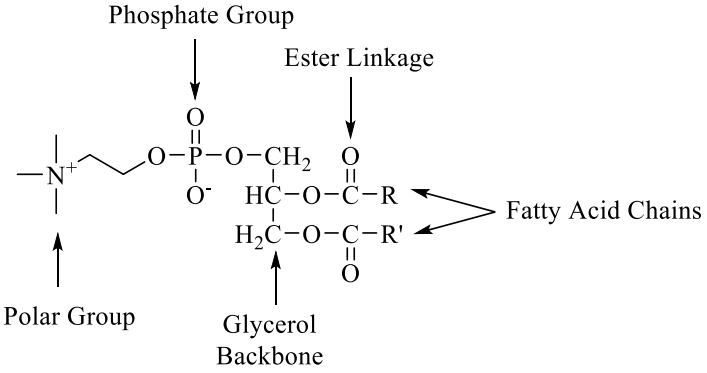

Figure 1.0.2.2.2: General structure of a phospholipid

PLA_2 is one of the components in BV which results in an allergic response and is therefore considered one of the major allergens in BV. On its own BV PLA_2 is non-toxic; however together with melittin it is hemolytic.[2,4] The amino acid sequence of the BV PLA_2 was determined and compared to vertebrate PLA_2 amino acid sequences. The result showed that the BV PLA_2 has a distinct structure compared to the class I/II superfamily of PLA_2 enzymes.[44,45] BV PLA_2 is part of group III PLA_2 enzymes, which have a molecular weight of *ca.* 15-18 kDa and have 5 disulfide bridges.[41] BV PLA_2 is comprised of 134 amino acids and is glycosylated at the Asn13 residue.[45]

The BV PLA_2 enzyme is only structurally similar to vertebrate PLA_2 enzymes at the active site which contains histidine and aspartic acid residues, the Ca^{2+} binding loop and certain cysteine residues.[46] The triad of a hydroxyl-imidazole-carboxylate (Tyr87-His34-Asp35 in the case of BV PLA_2) is a common feature in the active site of enzymes which catalyse the hydrolysis of esters.[46] In the catalytic site of BV PLA_2 the

His34 residue is followed by the Ca^{2+} binding Asp35 residue. The Asp64 residue interacts with the His34 residue. However, mutant BV PLA_2 enzymes lacking this Asp64 residue still show catalysis of phospholipids showing this residue is not essential for enzyme activity.[46] It is thought that the Asp64 residue is there to stabilize the imidazole of His34 into the optimum position for catalysis. BV PLA_2 contains only one conserved tyrosine residue (Tyr87) in comparison to the class I and II families which have two conserved tyrosine residues.[44]

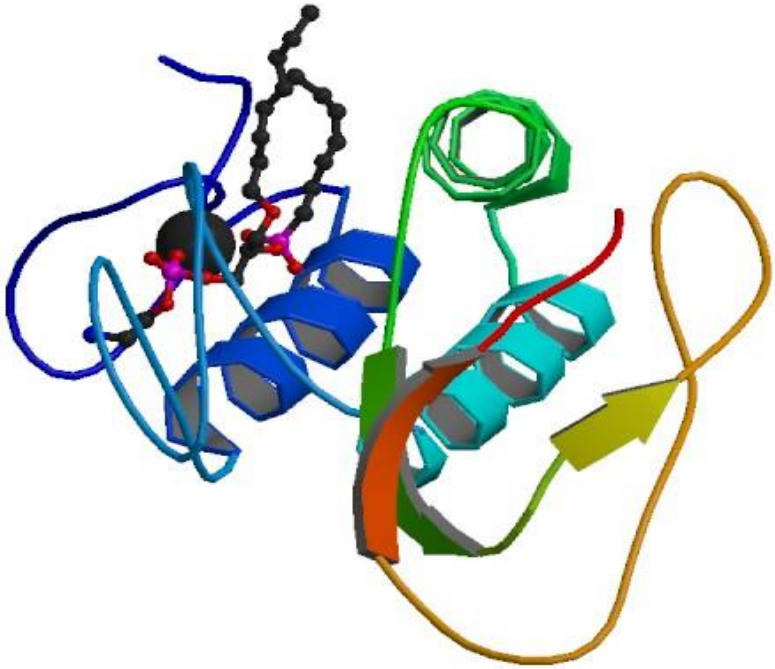

Figure 1.0.2.2.3: Ribbon Structure of BV PLA_2. This structure was obtained at a resolution of 2.0 Å while in a complex with a transition state analogue. The structure was taken from the RCSB protein data bank.[47] The black beaded molecule is a transition state molecule (diC8(2Ph)PE). The different colours relate to the individual secondary structures (α helices and β sheets) of the protein. There are also two calcium ions present.

Table 1.0.2.2.1: Classification of PLA_2 Enzymes

Group	Sub-group	Source	Molecular Weight (kDa)
I	A, B	Cobras, Krait, Human/porcine pancreas	13 - 15
II	A, B, C, D, E, F	Rattlesnakes, human synovial, Gaboon viper, Rat/murine testis, Human/murine pancreas, spleen, brain, heart, uterus, testis, embryo	13 - 17
III	-	Bee/human/murine/lizard	15 - 55
IV	A, B, C, D, E, F	Human/murine	61 - 114
V	-	Human/murine heart, lung, macrophage	14
VI	A_1, A_2, B, C, D, E, F	Human/murine	28 - 146
VII	A, B	Human, murine, porcine, bovine	40 - 45
VIII	A, B	Human	26
IX	-	Snail venom (conodipine-M)	14
X	-	Human spleen, thymus, leukocyte	14
XI	A, B	Green rice shoots	12 - 13
XII	-	Human/murine	19
XIII	-	Parvovirus	< 10
XIV	-	Symbiotic fungus, bacteria	13 - 19
XV	-	Human, murine, bovine	45

Reference [43]

1.0.2.3 Hyaluronidase

Hyaluronidases are glycosidase enzymes which hydrolyse hyaluronic acid (HA).[48] These enzymes are classified into three different groups and the details of these groups are shown in table 1.0.2.3.1. These enzymes are found in mammals, insects, leeches and bacteria.[49] The substrate for these enzymes, hyaluronic acid (HA), is found in the majority of tissues but is most abundantly found in the extracellular matrix (ECM).[50] HA is also found in connective tissue near the collagen and elastin fibres and is able to bind a vast quantity of water (which may contribute to the hydration of the skin).[51] HA, also known as hyaluronan, is a glycosaminoglycan (GAG) which is produced by fibroblasts and keratinocytes and is known to decrease with age.[51] HA has a linear structure and is made up of repeating units known as disaccharide units (figure 1.0.2.3.1). The two repeating disaccharide units present in HA are β-D-(1-3) glucuronic acid and β-D-(1-4)-N-acetylglucosamine.[52]

Table 1.0.2.3.1: Hyaluronidase Enzymes

	(1) Mammalian hyaluronidase	**(2) Hyaluronate-3-glycanohydrolases**	**(3) Microbial hyaluronidases**
Numerical Classification	E.C. 3.2.1.35	E.C. 3.2.1.36	E.C. 4.2.99.1
Cleavage	β-1-4 glycosidic linkages in HA, chondroitin and chondroitin sulfate	Glucoronate linkages of HA	β-1-4 glycosidic linkages in HA, using β-elimination process
Product	Even numbered oligosaccharides	Tetra- and hexa-saccharides	Δ4-5 unsaturated oligosaccharides
Reference [50]			

The ribbon structure of BV hyaluronidase has been solved at a resolution of 1.6 Å.[49] The BV hyaluronidase ribbon structure is shown in figure 1.0.2.3.2. The structure of the BV hyaluronidase in a complex with a HA tetramer suggests that the catalytic mechanism is an acid-base mechanism. This occurs by Glu113 acting as a proton donor and the N-acetyl group on the substrate acting as a nucleophile. Asp111 and Glu113 amino acids are the only conserved carboxylic residues found in the catalytic binding groove. Glu113 showed a distance of 2.6 Å between the carboxyl side chain and the glycosidic oxygen, placing it in a good position to act as a proton donor. However the Asp111 carboxyl oxygens were 5 Å away from the glycosidic oxygen suggesting the Glu113 may be more important for catalysis.[49]

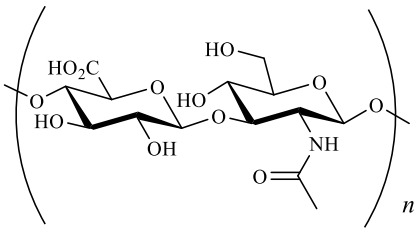

Figure 1.0.2.3.1 Structure of Hyaluronic Acid

Hyal-1, the predominant mammalian hyaluronidase, has a similarly folded structure ((β/α)8-barrel) to the BV hyaluronidase.[48] It is known that initial cleavage of this occurs by transfer of a proton from the glutamic acid residue (Glu131 in Hyal-1) to the C4 oxygen. A water molecule then replaces the HA leaving group where it is thought that the Glu131 and Tyr202 residues polarize this water molecule. This results in a nucleophilic attack on the C1 carbon therefore completing the hydrolysis of the glycosidic bond.[48] Given the similar folding of mammalian hyaluronidase and BV hyaluronidase, it is possible that this is the mechanism used by BV hyaluronidase to degrade HA.

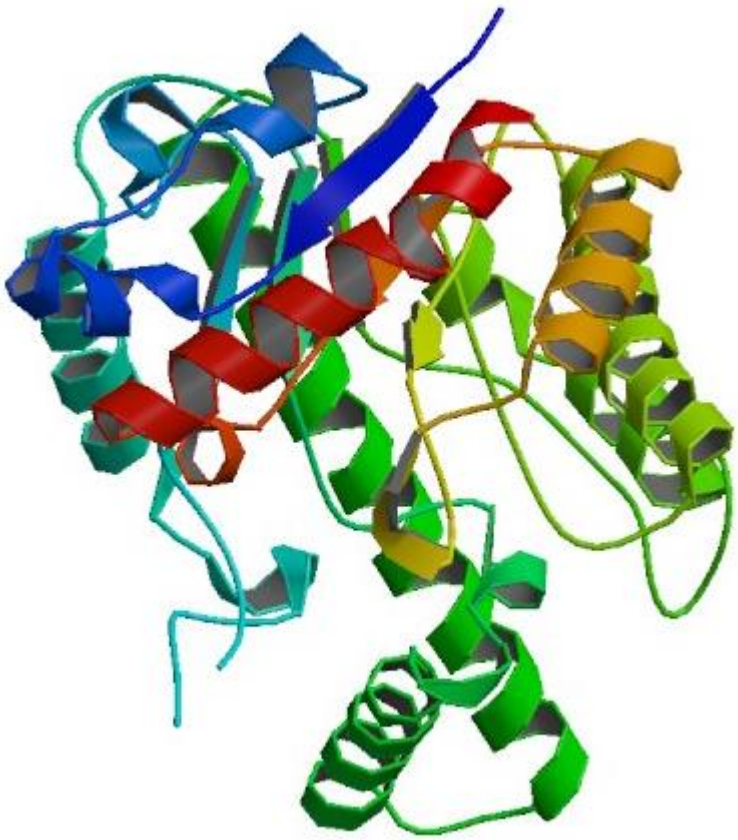

Figure 1.0.2.3.2 Ribbon Structure of BV Hyaluronidase. This structure was obtained at a resolution of 1.6 Å. The structure was taken from the RCSB protein data bank.[53] The tetramer structure is not shown here. The different colours relate to the individual secondary structures (α helices and β sheets) of the protein.

It is well known that hyaluronidase is a major allergen found in BV.[4,49] Studies carried out have shown that over 70 % of people had IgE present in their serum specifically against recombinant hyaluronidase.[54] BV hyaluronidase is made up of 350 amino acids. It has four possible glycosylation sites (N-X-T where X is any amino acid), and has two disulfide bridges.[49,54] It has been found that two of the four possible glycosylation sites are glycosylated (Asn115 and Asn263).[54] The BV hyaluronidase also shares *ca.* 30 % sequence similarity to that of mammalian hyaluronidase.[48,49] BV hyaluronidase degrades HA found in the ECM of the skin which helps aid the spread of venom throughout the body and is therefore considered the major 'spreading factor'.[4,48,49]

1.0.2.4 Mast Cell Degranulation Peptide

Mast cell degranulation (MCD) peptide is 22 amino acids long with the following amino acid sequence:

IKCNCKRHVIKPHICRKICGKN.[11,13]

MCD peptide has actions which are strongly linked with allergies.[13] MCD peptide releases histamine from mast cells at a low concentration. However, at higher concentrations it prevents the degranulation of mast cells.[11,13] MCD therefore acts as both an anti-inflammatory and inflammatory agent. MCD contains two disulfide bridges between the Cys3 and Cys15 and the Cys5 and Cys19 residues. These disulfide bridges result in a compact cyclic structure of two asymmetric loops.[55] The primary structure is shown in figure 1.0.2.4.1.

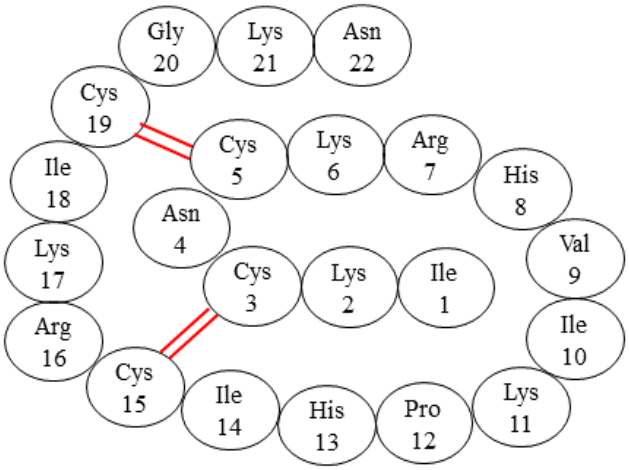

Figure 1.0.2.4.1 Primary structure of MCD adapted from Gauldie *et al,* 1978.[56]

The process of mast cell degranulation involves several steps and is initiated by the binding of antigens to IgE molecules. This is then followed by the cross linking of two IgE molecules resulting in dimerization of IgE receptors. This initiates several cellular processes beginning with phospholipase C activation (via Ca^{2+} ion mobilization) followed by protein phosphorylation, PLA_2 activation, finally resulting in lysolecithin

formation. Lysolecithin mediates the fusion of mast cell granules with the plasma membrane resulting in the release of various mediators such as histamine.[55]

1.0.2.5 Apamin

Apamin is 18 amino acids long with the following amino acid sequence:

CNCKAPETALCARRCQQH.[11]

The primary structure of apamin is shown in figure 1.0.2.5.1. Apamin has a similar structure to the MCD peptide previously described. However, it acts at different receptors and has a different physiological action.[56] Apamin is a small neurotoxin which blocks the Ca^{2+}-activated potassium channels.[11,13]

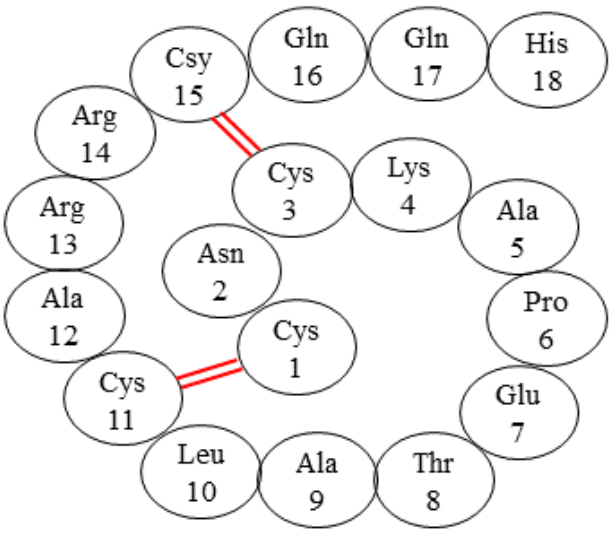

Figure 1.0.2.5.1 Primary structure of apamin adapted from Gauldie *et al.*, 1978.[56]

1.0.2.6 Api m 5

Genome studies identified a protein (Api m 5) present in BV with 32 % sequence homology to the human DPP IV enzyme.[57] A study has identified an enzymatic activity for this BV component, which is the sequential cleavage of dipeptides from pro-melittin to release melittin.[30] This is the only known action of BV DPP IV in the literature. However, the human DPP IV has been studied extensively.

Human DPP-IV (EC 3.4.14.5) is a type II cell surface integral glycoprotein which has a vast array of functions.[58–60] It was originally known as CD26 (cluster of differentiation 26), a lymphocyte T cell surface marker, which is composed of 766 amino acids in total.[58–62] The DPP IV molecule has a short intracellular cytoplasmic domain composed of 6 amino acids (MKTPWK), a transmembrane domain composed of 22 amino acids (VLLGLLGAAALVTIITVPVVLL) which is hydrophobic in nature and an extracellular domain which contains the catalytic region and various N-terminal glycosylation sites; this domain is composed of the remaining 738 amino acids.[58–60]

The catalytic region is a triad of the amino acids Ser630, Asp708, and His740 with Ser630 (a crucial catalytic residue) found in a pocket, which is created by an α/β hydrolase region and a β propeller domain, which has the active sequence GWSYG.[58–60] DPP IV is an uncharacteristic serine protease as the residues within the catalytic triad (Ser630-Asp708-His740) are inverted when compared with a typical serine protease, which has the catalytic triad sequence of His-Asp-Ser.[59,60] A schematic showing a simplistic image of DPP IV is shown in figure 1.0.2.6.1. The ribbon structure of human DPP IV has been determined and is shown in figure 1.0.2.6.2.

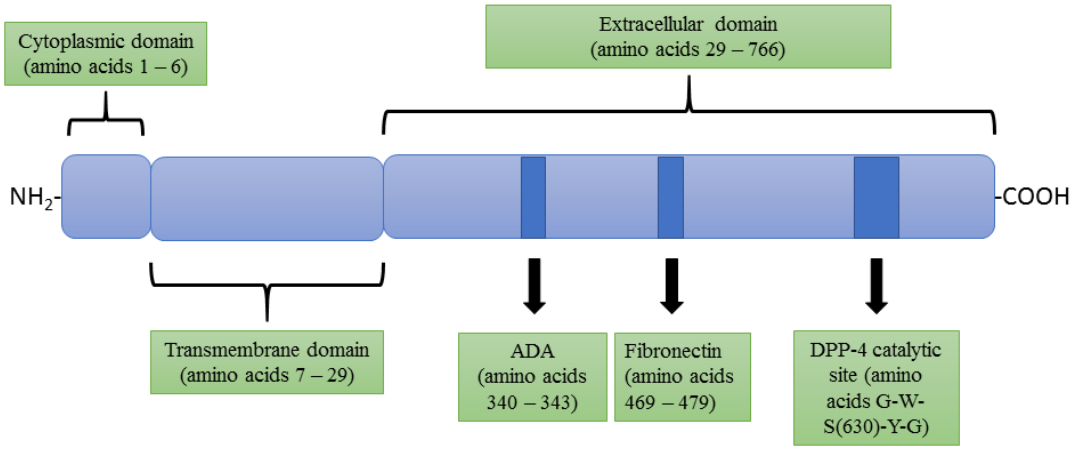

Figure 1.0.2.6.1: Diagram of DPP IV molecule found in humans, this image was adapted and reproduced from Ohnuma, K. et al.

The gene for human DPP IV/CD26 is found on the long arm of chromosome 2 (2q24.3)[60,61,63] and is expressed in various different cell types such as epithelial cells of the liver, intestine, kidney, prostate tissue and corpus luteum, T-helper cells and there is a soluble form found in plasma and urine.[59,63] One of the main functions of DPP IV is that it cleaves dipeptides (N-terminal) from peptides which preferentially have proline or alanine at the penultimate position.[58,59,61,63] It has also been found that peptides with other amino acids at the penultimate position, such as glycine and leucine, can also be hydrolysed. However, this occurs at slower rates when compared with proline/alanine in this position.[60] Natural substrates for human DPP IV are cytokines, neuropeptides, bioactive peptides and hormones.[58,59] Other functions include acting as an anchor for the enzyme adenosine deaminase (ADA), binding to collagen and fibronectin. It can act as a co-receptor for gp120, which is a protein found in the HIV envelope, and is also involved in glucose homeostasis.[58,59,63]

Figure 1.0.2.6.2: Ribbon Structure of human DPP IV, this structure was obtained at a resolution of 2.6 Å. The structure was taken from the RCSB protein data bank.[64]

Substrates can access the human DPP IV catalytic site via two ways.[65,66] One of these routes is by a side opening which is found at the point where the hydrolase and β–propeller domains meet. The other route is entry through a channel formed by the β-propeller domain.[65,66] These openings are shown in figure 1.0.2.6.3.

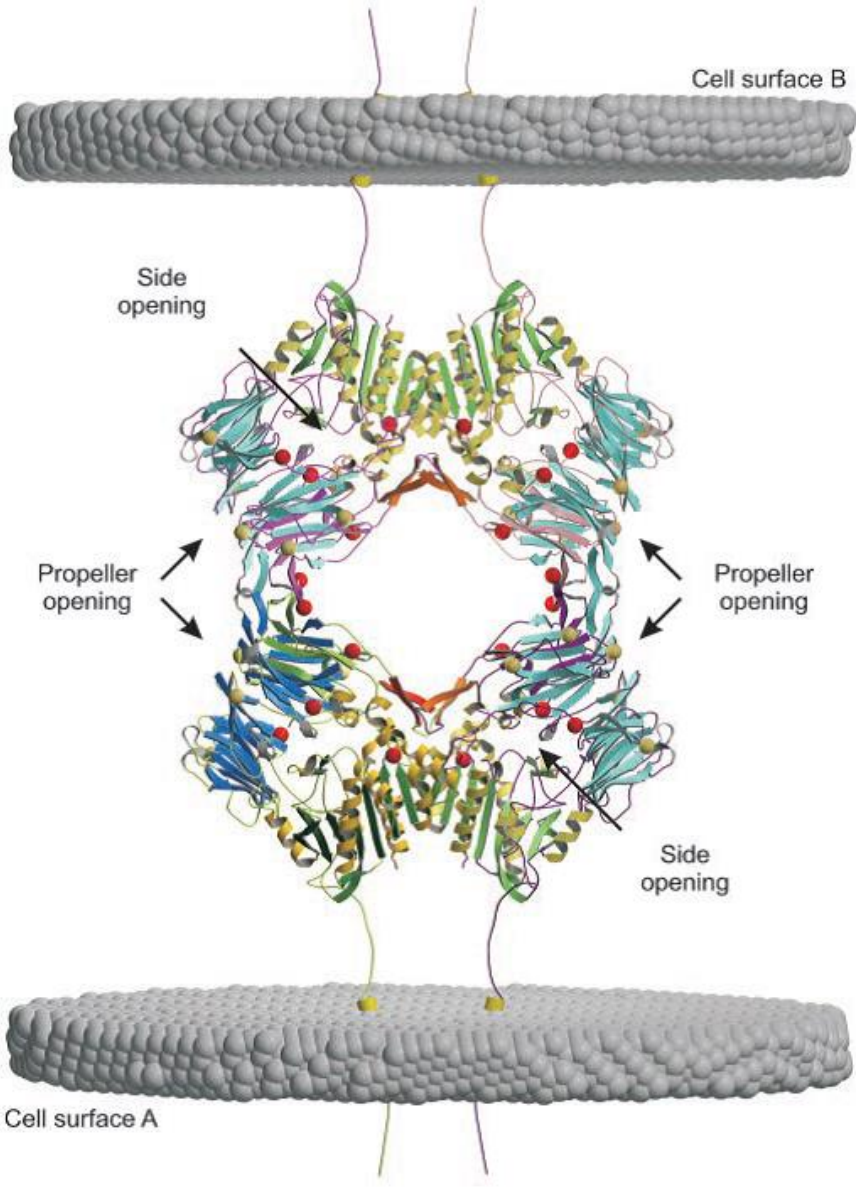

Figure 1.0.2.6.3: Crystal structure of porcine DPP IV forming a dimer of dimers with 222 symmetry. Red spheres are crystal modifications, grey spheres are possible glycosylation sites. This tetramer was modified to show how DPP IV can facilitate cell-to-cell contact. Porcine and human DPP IV have 88 % sequence identity. The image was obtained from Engel *et al.*, 2003[65] with permission from PNAS. "Copyright 2003 National Academy of Sciences" The side opening is a distance of 20 Å from the surface of the protein to the active site compared to the longer distance of 37 Å for the β-propeller opening.[65] Larger substrates have to unfold to gain access to the β-propeller opening. The shorter distance of the side opening appeared to be the preferred route for products to leave the catalytic site.

The human DPP IV catalytic mechanism involves a catalytic triad of residues Ser630, Asp708, and His740.[59] Ser630 is the essential catalytic residue which is found in the "nucleophilic elbow" of human DPP IV and is formed of the sequence Gly628-Trp629-Ser630-Tyr631-Gly632.[59,67] The Ser630 residue is H-bonded to the His740 residue and an oxygen atom on Asp708 is H-bonded to His740.[59] Ser630 attacks the scissile bond as the nitrogen on the His740 residue accepts the hydrogen from the Ser630 –OH group. Asp708 H-bonding with the His740 makes the nitrogen on this residue more electronegative therefore completing the catalytic triad.

During catalysis by human DPP IV an oxyanion tetrahedral intermediate is formed. This is stabilised by the Tyr547 –OH group along with H-bonding to the –NH group of Tyr631.[59,67] A study using mutagenesis by replacing the Tyr547 with a phenylalanine and therefore removing the –OH group showed that the –OH group on Tyr547 was crucial for catalysis.[67] Another study using mutagenesis identified residues Glu205 and Glu206 as having an important role in the substrate binding.[68] Mutation at these amino acid sites stopped the human DPP IV activity.

1.0.3 Bee venom versus snake venom

Insects are not the only species known to produce venom. Therefore a comparison between the honey bee and snake venoms will be useful to show the similarities and differences between two different venom-producing species. There are differences in the components of the different snake venoms. However, for the purpose of this research only a general review of the major snake venom components will be considered. Table 1.0.3.1 shows the comparison between the major components found in bee and snake venom. It is possible that some of the components found in snake venom are present in BV.

Table 1.0.3.1: Comparison of the major components in bee/snake venom

Component	Bee Venom	Snake Venom
Phospholipase A_2	✓	✓
Hyaluronidase	✓	✓
Melittin	✓	×
MCD-Peptide	✓	×
Apamin	✓	×
Other neurotoxins	×	✓
Histamine	✓	×
Cardiotoxins	×	✓
Myotoxins	×	✓
L-amino acid oxidase	×	✓
Metalloproteinases	×	✓
Serine proteases	✓	✓
Bradykinin potentiating peptide	×	✓
References [22,69–72]		

The cardiotoxins, myotoxins and neurotoxins found in snake venoms are collectively involved in the killing of snake prey during hunting and defence. Cardiotoxins are described as lytic factors where they increase muscle contraction, cause lysis of red blood cells and result in cardiac arrest.[73] Cardiotoxins show some similarities to the lytic peptide, melittin, found in BV.[74] The myotoxins are involved in causing muscle necrosis resulting in paralysis and also inducing an inflammatory response.[75] The neurotoxins in snake venom damage the nerve tissue by interrupting the transmission of neurons at the intramuscular junction which results in paralysis.[76] Bees do not sting unless provoked; their venom has not evolved to kill mammals but rather to cause a distraction to the mammal. However snakes use their venom for both hunting and defending. Hence, snake venom has evolved to contain more toxin components used for killing mammals.

The L-amino acid oxidase (LAAO) activity found in snake venoms is also found in other organisms such as bacteria, fungi and fish,[77,78] giving a possibility that BV also has this activity. The LAAO enzymes transform L-amino acids into their α-keto acid form via oxidative deamination. This results in oxidative stress via the production of H_2O_2.[78] The snake venom LAAOs have molecular masses between 120 and 150 kDa where they are homodimers.[78] Several of the snake venom LAAOs are involved in either inducing or inhibiting platelet aggregation.[77] These enzymes are also involved in apoptosis, hemolysis, cytotoxicity and edema, amongst other biological actions.[78]

Snake venom metalloproteinases are enzymes which rely on zinc for their activity. These enzymes play an important role in tissue damage by snake venom. They are responsible for the hemorrhagic effect of snake venom along with causing damage to muscles and play a role in inflammatory responses.[79]

The bradykinin potentiating peptides increase bradykinin (described in section 1.2.4) activity and inhibit the angiotensin converting enzyme which is responsible for degrading angiotensin.[80] This increases the permeability of blood vessels along with vasodilation which lowers the blood pressure in mammals.

1.1 Skin Physiology

1.1.1 Introduction

The skin protects internal organs from invasion of foreign substances and hazardous environmental factors such as bacteria/viruses and harmful chemicals. An understanding of the skin physiology is important as this is where a bee inserts the stinger. The skin is made up of various layers of different cells, namely the epidermis and dermis.[81] The epidermis can subsequently be subdivided into four sub-layers known as the stratum corneum, stratum granulosum, stratum spinosum and the stratum basale.[81,82] The main constituent of the epidermis is keratinocytes and others include melanocytes, Langerhans cells, and Merkel cells.[82] The dermis can also be subdivided into two layers known as the papillary and reticular dermis. The reticular dermis is mainly composed of loose connective tissue and elastic fibres which run parallel to the papillary dermis.[81] The papillary dermis is composed of a mesh network of fibrous proteins such as collagen and elastic fibres.[81,83] Figure 1.1.1.1 shows a diagram of the different skin layers with a bee stinging, releasing bee venom which includes but is not exclusive to hyaluronidase, PLA_2 and melittin. Also shown in this diagram is the defence bio-actives which could be released in response to a bee sting.

The thickness of the skin varies in different parts of the body. For example the skin on the eye lids is much thinner than the skin of the forearm. With that in mind the thickness of the epidermis is in the range of 20 - 150 μm and the dermis is in the range of 2000 – 3000 μm.[84] The lancet of a honey bee sting is around 1.4 mm long[85] meaning that it would reach the dermis layer of the skin.

There are numerous receptors found within the skin. These include the nociceptors which are involved in pain perception, mechanoreceptors which are involved in touch and pressure stimuli, thermoreceptors which are involved in temperature control, and also the pruriceptors which are involved in pain and itching.[86]

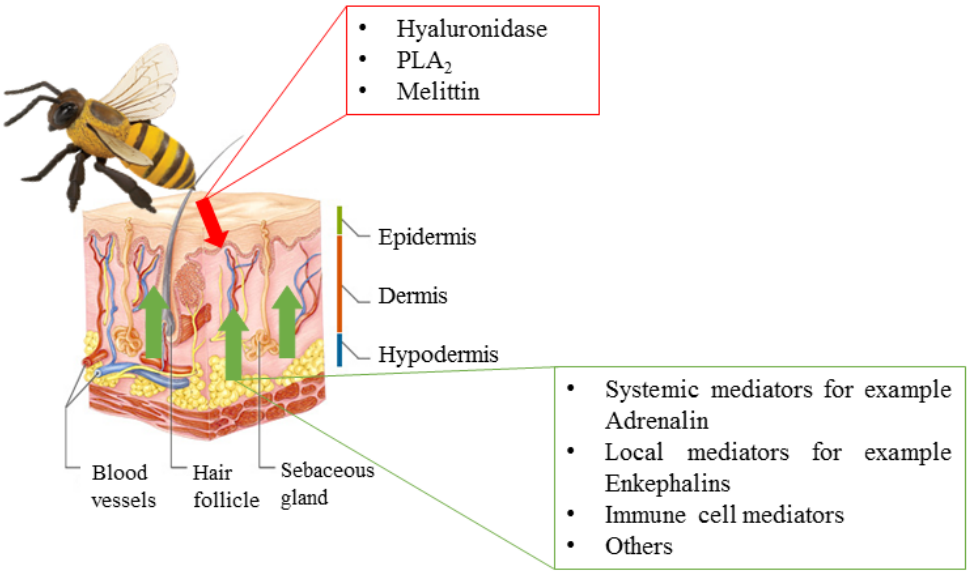

Figure 1.1.1.1: Diagram showing a bee stinging and the response to the bee venom.

1.1.2 Keratinocytes

Keratinocytes, found in the epidermis, are highly proliferative and have the ability to self-renew.[87] Keratin is a protein with a protective role which is synthesised by keratinocytes[87] and results in a network of filaments giving the epidermis its strength.[83,87] Keratinocytes differentiate into corneocytes and during this process their structure changes where they become flattened and laden with keratin filaments. These keratin filaments within the newly formed corneocytes form a dense array and interact with filaggrin (a matrix protein) causing the keratin filaments to form tight bundles.[88]

1.1.3 Corneocytes

The average thickness of corneocytes is about 1 µm and there are about 15 layers of these cells in the stratum corneum.[89] Corneocytes are formed from the differentiation of keratinocytes and are flat and anucleated cells.[88] Corneocytes are laden with keratin

filaments which are encapsulated in proteins which are known as the cornified envelope (CE).[88,89] Keratin filaments have the ability to bind to water and are connected through intra- and interkeratin filament disulfide bonds giving a stable structure.[89] The CE has a lipid monolayer which is composed of covalently bound, long-chain ceramides on the outer layer giving a hydrophobic surface.[89] The structure of an example ceramide is shown in figure 1.1.3.1. The chain length of ceramides varies and the predominant ceramides in the stratum corneum (SC) are longer chains ($> C_{20}$).[89]

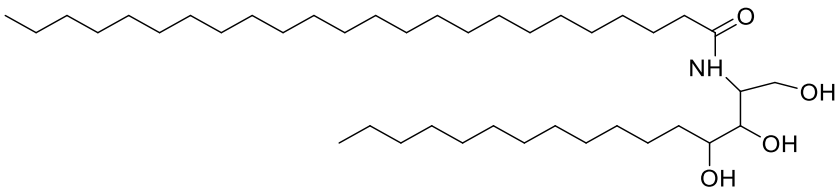

Figure 1.1.3.1: Structure of Ceramide NP[90]

1.1.4 The Stratum Corneum

The SC is the outer most layer of the epidermis, which provides a permeability barrier to the most vital organs and is composed mainly of corneocytes. The impermeable barrier to water can be attributed to the complex array of lipids in the SC.[89–91] This barrier to water is essential for life as it ensures the skin is hydrated and therefore gives the skin its elasticity.[91] However, there is a small amount (10 ml/kg hour) of water loss through the SC to the atmosphere and this is known as transepidermal water loss (TEWL).[90]

Desmosomes and hemidesmosomes, attached to corneocytes of the SC,[89] are linked by keratin filaments, giving a strong surface to the epidermis.[87] This linkage along with the contents which are secreted from lamellar bodies gives a brick and mortar structure.[82,89] This structure contributes to the impermeable barrier provided by the SC. Lipids within the intercellular spaces of the SC that are important for the barrier function include cholesterol, ceramides and fatty acids which are found at varying

amounts; 25, 50 and 10 % respectively. The structure of cholesterol is shown in figure 1.1.4.1. It has also been noted that there is the presence of some cholesterol sulfate and cholesterol esters.[88,89,91] These lipids have a range of functions such as providing flexibility to the skin and giving structure to the lipid bilayer of the SC.[89,90]

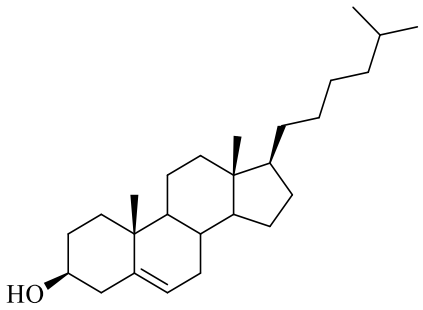

Figure 1.1.4.1: Structure of Cholesterol

1.1.5 Extracellular Matrix

The strength and elasticity of the skin can also be attributed to the connective tissue in the dermis known as the extracellular matrix (ECM). This dermal ECM is a complex arrangement made up of various fibrous proteins such as collagen and elastic fibres and also glycosaminoglycans (GAG).[51,81] Large complexes can be formed by these fibrous proteins to give skin its structure. They also help with adhesion of cells and the control of cell signalling.[81] GAGs give skin its outward appearance; they also have the ability to bind to water molecules. An example of a GAG found in the skin is HA, which has been discussed in section 1.0.2.3.

The strength of the skin can be attributed largely to the main component of the dermal ECM, collagen, or more specifically collagens I and III.[81,92] There are many different types of collagens. The differences in the types of collagen relate to the structure of the collagen. Almost a third of the known types of collagen are fibrillar collagens (types I-III, V and XI). Fibrillar collagens have a banding pattern where three α chains form a helix structure. The remaining types of collagens are known as non-fibrillar. These are further divided into various groups which are shown in table 1.1.5.1.

Table 1.1.5.1: Non-fibrillar collagens

Group	Type of Collagen
Fibril associated with interrupted triple helices (FACIT)	IX, XII, XIV, XVI and XIX
Network forming collagens	IV, VIII and X
Beaded filament collagens	VI
Transmembrane collagens	XIII and XVII
Basement membrane collagens	VII
References [93,94]	

Collagen VII is also found in the extracellular matrix and anchors fibrils to the basement of the dermis. This is important for the structure and function of the skin.[83] Collagen IV is known to help provide stability to the skin, and reduced levels of this in wrinkles suggests that it plays an important role in the formation of wrinkles.[51]

Elastic fibres which are found in the dermal ECM consist of an elastin core, surrounded by microfibrils which are predominantly composed of the glycoprotein, fibrillin-1.[95] It is these fibres which give skin its elastic nature but there are enzymes such matrix metalloproteinases (MMPs) which can cleave these microfibrillar structures, resulting in a loss of elasticity which is evident in ageing skin.[96]

1.2 Defence Bio-actives to be Investigated Experimentally

Homeostasis is the maintenance of an equilibrium which constantly has to overcome intrinsic or extrinsic factors.[97] Stress is a term which refers to a threat or challenge to the body. These threats can be physiological or psychological causing a cascade of responses,[98] which would therefore disrupt homeostasis. In mammals a sting from an insect such as a bee would consequently cause stress and the initiation of the 'fight or flight' response.

The 'fight or flight' response is a cascade of cellular actions resulting in the release of adrenalin and noradrenaline. This is part of the systemic response. These neurotransmitters result in increased smooth muscle contraction and increased heart rate.[99] This is accompanied by the release of various other biologically active mediators such bradykinin, cortisol, substance P, angiotensin II and the enkephalins which are produced locally. These mediators together result in inflammation to help to close down the pathogen, pain and changes to heart rate.[100] This cascade of responses will help to regain homeostasis as quickly as possible by inactivating the pathogen (bee venom) and stopping its spread throughout the body.

A delayed response will also involve the adaptive immune response (for example antibodies) being stimulated.[101] However, for the purpose of this investigation the immediate response is the most important. Therefore, aspects of the adaptive immune response will not be discussed. A description of those substances to be used primarily in determining if there is any action of the enzymes in BV against these substances are described below. These substances were all chosen as they are part of a mammal's immediate response to a threat, and therefore BV may come into contact with them.

1.2.1 Adrenalin

Adrenalin, also referred to as epinephrine,[102] is a catecholamine which is synthesised from the amino acid L-tyrosine.[103] The biosynthesis of adrenalin is shown in figure 1.2.1.1. Adrenalin is a neurotransmitter which is released from the adrenal medulla during the 'fight or flight' response.[99] The release of adrenalin occurs when the preganglionic neurons in the sympathetic nervous system are stimulated by the neurotransmitter acetylcholine.[100] It acts on the adrenergic receptors, also called adrenoceptors, giving various responses.[104]

There are two subtypes of adrenoceptors known as α and β, these are further subdivided into α_{1A}, α_{1B}, α_{1D}, α_{2A}, α_{2B}, α_{2C}, and β_1, β_2 and β_3.[104] Adrenoceptors are G-protein coupled receptors which are found in almost all peripheral tissues and groups of neurones.[105] Adrenalin acts on both the α and β adrenoceptors causing two distinct effects; vasodilation and vasoconstriction.[100] Some examples are used to explain these contradictory effects of adrenalin and are listed in table 1.2.1.1.

The relaxation of the gastrointestinal tract is to get rid of unwanted waste to make it easier to escape from the threat a mammal is facing. The contraction and relaxation of the blood vessels will increase the rate and force of contraction of the heart, which will help to get oxygen around the body quicker. This effect occurs simultaneously and allows the body to control blood to specific areas of the body.[100,105]

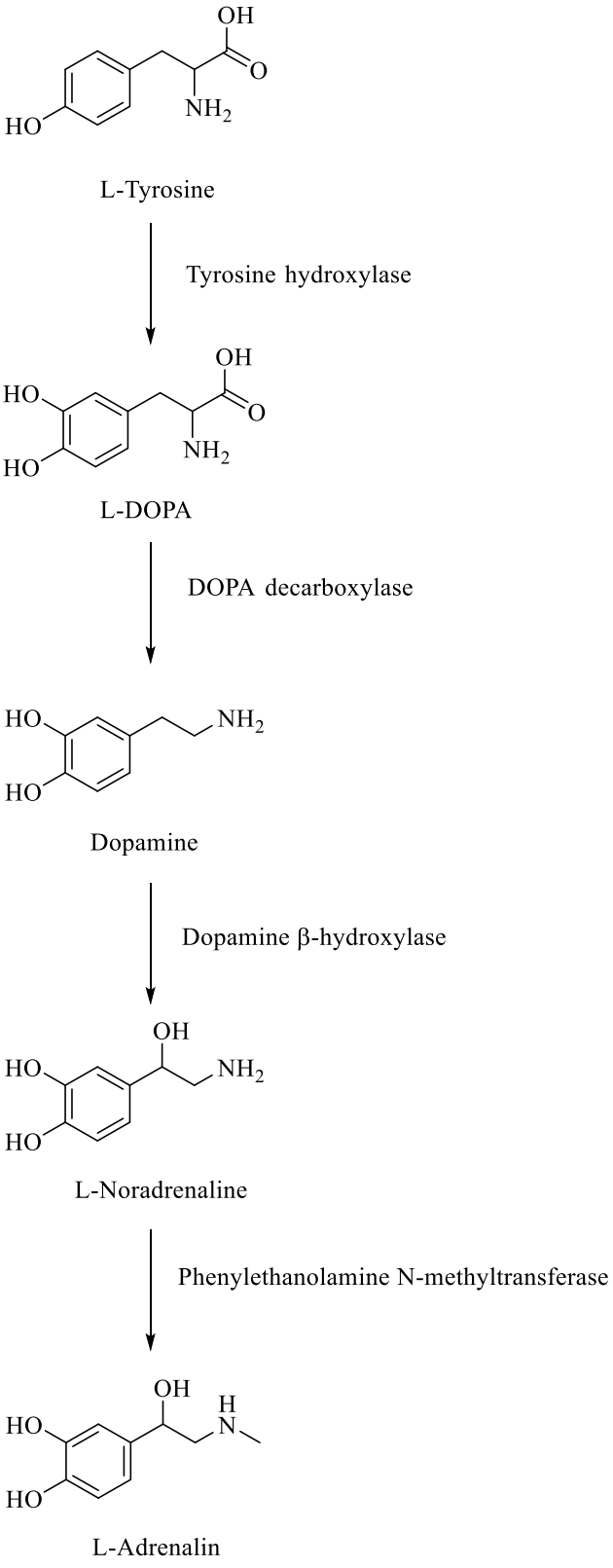

Figure 1.2.1.1: Adrenalin biosynthesis. Adopted and reproduced with permission from Kvetnansky *et al.*, 2009.[106] DOPA, dihydroxyphenylalanine.

Adrenalin is metabolised by two enzymes known as monoamine oxidase (MAO) and catechol-O-methyl transferase (COMT). MAO is located intracellularly and converts adrenalin to its corresponding aldehyde, which can then be metabolised by aldehyde dehydrogenase to a carboxylic acid. COMT is also located intracellularly and metabolises adrenalin by one of the hydroxyl groups becoming methylated.[100] The metabolism of adrenalin is shown in figure 1.2.1.2. As adrenalin plays an important role in the 'fight or flight' response it would be released in response to a bee sting.

Table 1.2.1.1: Different actions of adrenalin

Adrenoceptor	Action
α_1	Relaxation of the gastrointestinal tract smooth muscle
	Vasoconstriction of blood vessels
α_2	Contraction of the smooth muscle of blood vessels
β_1	Increase heart rate
β_2	Relaxation of the bronchi
	Vasodilation of blood vessels
	Relaxation of gastrointestinal tract
Reference [100]	

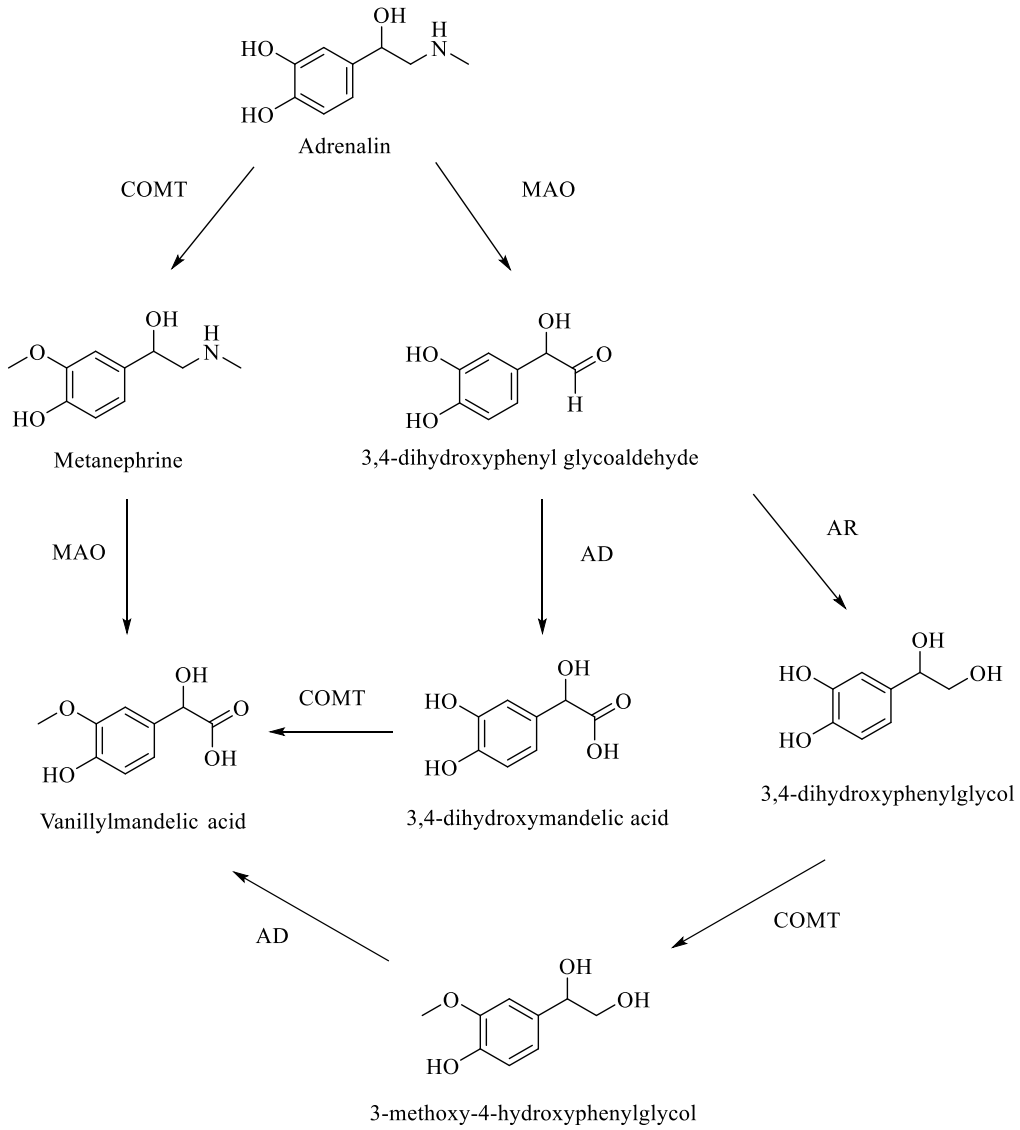

Figure 1.2.1.2: Metabolism of adrenalin. Adopted and reproduced with permission from Kvetnansky *et al.*, 2009.[106] MAO, monoamine oxidase; COMT, catechol-O-methyl transferase; AD, aldehyde dehydrogenase; AR, aldehyde reductase.

1.2.2 Cortisol

Cortisol is a glucocorticoid hormone synthesized and released from the adrenal cortex;[107] the structure is shown in figure 1.2.2.1. The release of cortisol is controlled by the hypothalamic-pituitary-adrenocortical (HPA) axis which is activated in response to a stress-induced stimulus.[108–110] A stimulus such as a bee sting would therefore cause this hormone to be released and therefore may be a target for BV. The glucocorticoid receptor (GR) is where cortisol binds with high affinity to exert its effect. The cortisol-glucocorticoid receptor complex interacts with DNA by promoting transcription factors for some mediators as well as reducing transcription of others and in doing so inhibits inflammation.[100,107] Glucocorticoids like cortisol are also involved in immunosuppression, glucose metabolism and general homeostasis.[110] Cortisol is inactivated via the 11β-hydroxysteroid dehydrogenase process. The two enzymes involved are known as 11β-HSD1 and 11β-HSD2; these enzymes convert cortisol to the inactive hormone cortisone.[111]

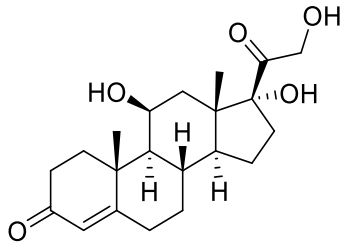

Figure 1.2.2.1: Structure of Cortisol

1.2.3 Enkephalin

The first opioid peptides to be discovered were the pentapeptides named met- and leu-enkephalin.[112] The amino acid sequences of met- and leu-enkephalin are YGGFM and YGGFL respectively.[113,114] For reference, a table detailing the coding used for all amino acids is found in appendix 7. The structures of these molecules are shown in figure 1.2.3.1. The enkephalins produce an analgesic effect similar to morphine by acting on the δ-opioid receptors.[114,115] This analgesic effect is reversed in the presence of the opioid antagonist naloxone.[115] The enkephalins have very short half-lives with a range of 20 seconds to 13 minutes, depending on species, due to their rapid metabolism.[116,117] Given the rapid hydrolysis of these peptides it has been difficult to obtain an accurate half-life. Three enzymes are known to be responsible for the hydrolysis of the enkephalin peptides. These enzymes work by hydrolysing different bonds within the peptide. A schematic showing the cleavage points of enkephalins is shown in figure 1.2.3.2.

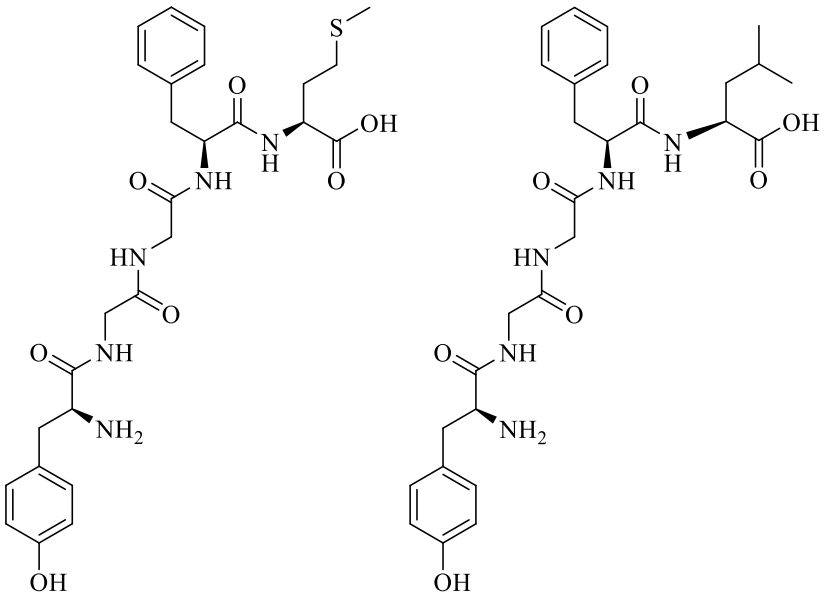

Figure 1.2.3.1: Structure of Met-enkephalin (left) and Leu-enkephalin (right)

Hydrolysis of the enkephalin peptides in humans seems to be dominated by the cleavage of the Tyr1-Gly2 bond by the aminopeptidase, aminopeptidase N (APN/CD13), releasing free tyrosine.[117–119]

Neutral endopeptidase 24.11 (NEP), a transmembrane enzyme, cleaves the Gly3-Phe4 bond of enkephalins releasing the tripeptide Tyr1-Gly2-Gly3 and the dipeptide Phe4-Leu/Met5.[120]

A dipeptidyl aminopeptidase that has been identified as being involved in enkephalin hydrolysis is known as dipeptidyl peptidase III (DPP III).[121] This enzyme is found intracellularly and is sometimes referred to as enkephalinase B.[122,123] DPP III works by cleaving dipeptides from the N terminus, which would result in Tyr1-Gly2 being released during enkephalin hydrolysis.

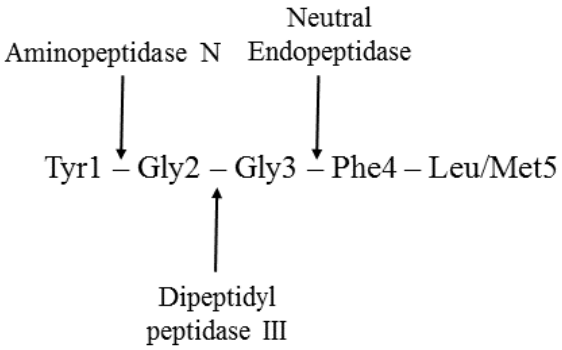

Figure 1.2.3.2: Hydrolysis sites in enkephalin peptides

1.2.4 Bradykinin

Bradykinin is released from precursor substrates known as kininogens by enzymes known as kallikreins at the site of inflammation.[124] The amino acid sequence of bradykinin is RPPGFSPFR;[124] the structure is shown in figure 1.2.4.1. Bradykinin exerts its affect via the bradykinin receptors, B_1 and B_2, which are seven transmembrane G-protein coupled receptors.[125] Bradykinin is metabolised by enzymes known as kinase I and kinase II. The kinase II enzyme is a peptidyl dipeptidase (identical to angiotensin converting enzyme) which cleaves the Pro7-Phe8 bond releasing the dipeptide Phe8-Arg9.[100] The biological effects of bradykinin are vasodilation resulting in increased blood flow and decreased blood pressure, inflammation, and pain.[126,127] This therefore may be a target for BV as inflammation would reduce the spread of BV.

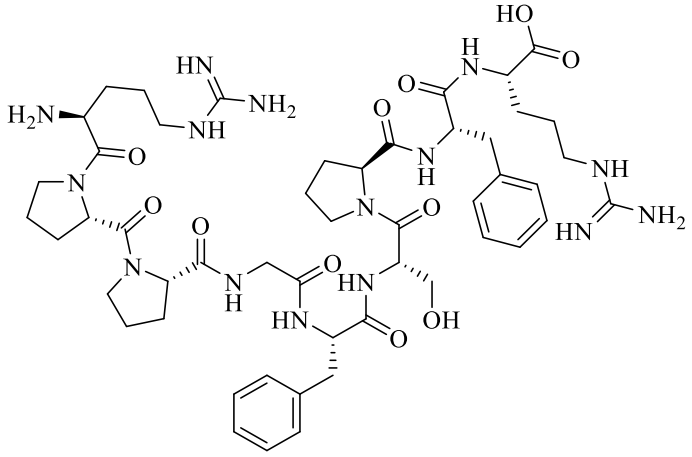

Figure 1.2.4.1: Structure of Bradykinin

1.2.5 Angiotensin II

Angiotensin II is a hormone comprised of 8 amino acid residues with the following sequence; DRVYIHPF.[128,129] Angiotensin II is formed from the cleavage of angiotensin I by the angiotensin converting enzyme (ACE), which is identical to kinase II described above for bradykinin metabolism.[100,129,130] ACE therefore inactivates bradykinin and converts angiotensin I to angiotensin II.[100] The structure of this octapeptide hormone is shown in figure 1.2.5.1. Angiotensin II has a role in the homeostasis of the cardiovascular system and is the active product in the endocrine renin-angiotensin system.[129–131] It is a strong vasoconstrictor by acting on the angiotensin type I and II receptors (AT_1 and AT_2), which are G-protein coupled receptors.[130] As angiotensin II is involved in vasoconstriction it may be a target for the BV as vasoconstriction would reduce the spread of the venom.

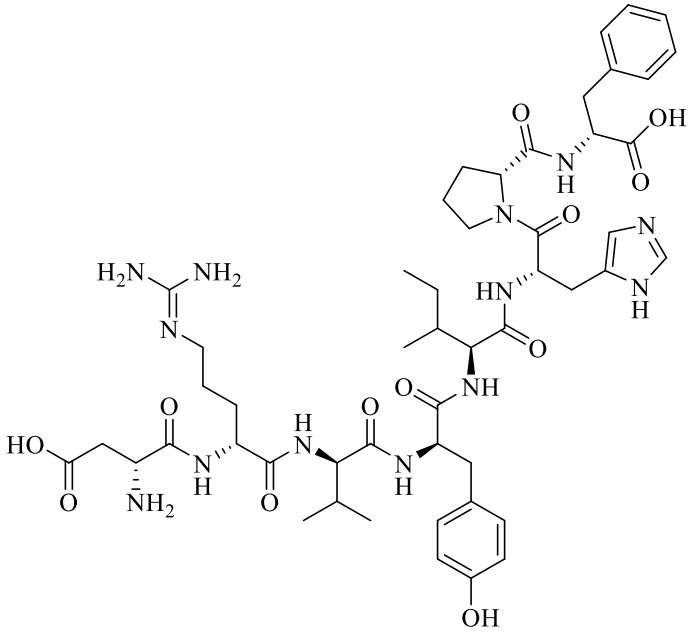

Figure 1.2.5.1: Structure of Angiotensin II

1.2.6 Substance P

Substance P is found within the central and peripheral nervous systems.[132] The amino acid sequence of substance P is RPKPQQFFGLM.[133] The structure of substance P is shown in figure 1.2.6.1. It belongs to a family of peptides which have a similar structure called the tachykinins.[133] The tachykinin family also includes neurokinin A and B which, along with substance P, have a similar C-terminal amino acid sequence (FXGLM, where X is either F or V).[132] Substance P acts on the neurokinin-1 (NK1) receptor where it is thought to act as a neurotransmitter, neuromodulator or co-transmitter.[133,134] Substance P is involved in many biological processes which includes the regulation of the transmission of pain, nociception, respiration, contraction of gastrointestinal tissue, inflammation, and immune responses.[132–134] A review of substance P in the literature found that there were a number of enzymes involved in the degradation of this peptide. These enzymes are listed in table 1.2.6.1. All of these enzymes hydrolyse substance P in various ways releasing different products. This therefore may be a target of the BV as this would restrict the spread of the venom and would be released during a stressful situation such as a bee sting.

Table 1.2.6. 1: Enzymes involved in substance P metabolism

Enzyme	Reference
Neutral endopeptidase (NEP)	135
Substance P-degrading enzyme	136
Angiotensin-converting enzyme	137
Dipeptidyl aminopeptidase IV	138
Post-proline endopeptidase	139
Cathepsin-D	140
Cathepsin-E	140

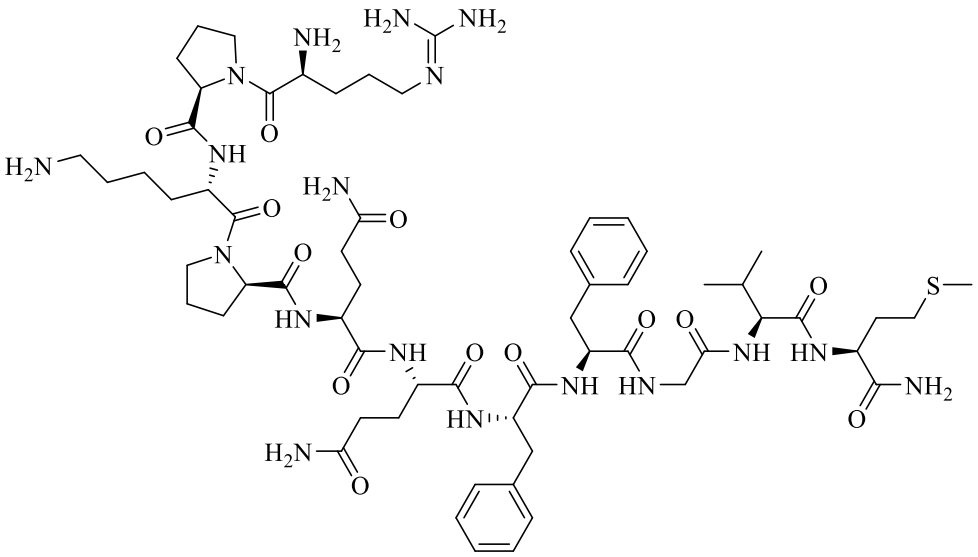

Figure 1.2.6.1: Structure of Substance P

1.3 Therapeutic Applications of Bee Venom

Bee venom has been used in various ways to help treat a variety of health problems for thousands of years. The use of BV for a therapeutic purpose is known as bee venom therapy (BVT). BVT dates back to ancient Egypt, Greece and China that has been used in the treatment of cancer, arthritis, wounds, burns and pain relief.[11] Bee venom acupuncture (BVA) is a form of BVT which involves the injection of dilute BV into acupuncture points.[141] There is a lot of controversy in the literature over the value of BVT as a means of therapeutic treatment; some of these will now be discussed.

1.3.1 Arthritis

Some studies have suggested that BV has anti-inflammatory properties and would therefore be useful in osteoarthritis and autoimmune diseases such as rheumatoid arthritis.[142,143] Autoimmune diseases occur when the body's immune response attacks healthy cells within the body.[101] Rheumatoid arthritis (RA) is caused by inflammation primarily in the joints causing pain and stiffness.[13] However, the inflammation also occurs systemically sometimes resulting in death.[144] Osteoarthritis (OA) is caused by damage to different parts of the joint such as the articular cartilage being worn out.[145] The treatment of arthritis involves the management of pain using analgesic drugs such as opioids and reducing inflammation using NSAIDS (non-steroidal anti-inflammatory drugs).[146]

Studies claim that the BV is involved in the inhibition of inflammatory mediators. Park *et al.* carried out an investigation into the anti-arthritic effect of BV and melittin where the results showed that BV had an inhibitory effect on the expression of the following inflammatory mediators: cyclooxygenase 2 (COX 2), cytosolic phospholipase A_2 ($cPLA_2$), inducible nitric oxide synthase (iNOS), prostaglandin E_2 (PGE_2), and nitric oxide (NO).[142] This study also claims that BV causes inhibition of these mediators by inhibiting the activation of NF-κB (transcription factor involved in iNOS, COX 2 and $cPLA_2$ expression) by binding to the p50 subunit (has a role in activation of NF-κB). These results are supported by with the study carried out by Moon *et al.*[147] which also

showed that BV inhibited the expression of these inflammatory mediators. However this latter study claims that BV inhibits expression of inflammatory mediators by preventing the degradation of IκBα (inhibitor of κBs) pathway and also inhibiting the Akt (signalling molecule which regulates NF-κB) and JNK (c-Jun N-terminal kinase, a mitogen-activated protein kinase) pathways. This is a different claim to the previous study showing the need for more experiments to establish the mechanism of BV anti-inflammatory activity. A third study by Stuhlmeier has claimed that bee venom and melittin do not inhibit the activation of NF-κB and also do not inhibit the degradation of IκB previously mentioned for other studies.[21] This study showed that bee venom increased the ability of leukocyte cells to release oxygen radicals. This paper also claimed that the concentration of BV or melittin used to supress the NF-κB-p50-DNA interaction actually causes the collapse of the cells. These studies are small and carried out on cell lines *in vitro* and are therefore only indicative. *In vivo* experiments are required to establish the clinical significance of the anti-inflammatory effects of BV.

1.3.2 Cancer

Cancer is disease where there is uncontrolled proliferation and spread of abnormal cells. Within the developed world cancer is one of the biggest causes of death. There are many different types of cancer. These include but are not limited to bowel, lung, breast and prostate cancer. Cancer is normally treated by chemotherapy, surgery or radiation therapy and usually a combination of two if not all of these interventions.[100] As cancer is so prevalent in the developed world there is a huge interest in finding better treatments. Some studies have looked into the effect BV has on cancer cells.

Orsolic *et al.* looked into the ability of BV to inhibit tumour growth along with inhibition of metastasis both *in vitro* and *in vivo*. The results showed that BV was able to inhibit the proliferation of carcinogenic cells *in vitro* and also reduce tumour progression *in vivo*.[148] The results also showed that the point of BV injection played a role in the ability of BV to inhibit tumour growth. The inhibition of tumour progression was shown to also increase responses from localised lymph nodes therefore increasing the release of lytic cells from the lymph nodes. Although this study showed promising

results with animal experiments there is still a need to show the effectiveness of this in clinical studies. There is also a question about the selectivity of melittin as it may also damage healthy cells.

Another study carried out by Jo *et al*. investigated the effect of melittin, and whole BV on ovarian cancer cells.[149] This study used the two cells lines, SKOV3 and PA-1 ovarian cancer cells. The results showed that both melittin and BV increased the expression of some death receptors (DRs). The expression of DRs is connected with the induction of apoptosis. Apoptosis, also known as programmed cell death, plays a vital role in treating cancer. This study also showed that melittin and BV inhibited STAT3 (signal transducer and activator of transcription 3), which is involved in a variety of roles such as cell growth, metastasis, apoptosis and proliferation. This pathway, known as the JAK/STAT3 signal pathway, is involved in many different types of cancer so is an important target for cancer treatment. The inhibition of this pathway in ovarian cancer cells was shown to reduce cell growth of these cells. It was therefore concluded in this study that melittin and BV inhibited ovarian cancer cell growth by amplifying the expression of DR3, DR4 and DR6 and also inhibition of STAT3. However this study is only carried out on cell lines *in vitro* meaning there is a need for clinical studies to show the effectiveness of BV/melittin in treating this type of cancer.

1.3.3 Parkinson's Disease

Parkinson's disease (PD) is a neurodegenerative disease of the central nervous system (CNS) where there is degeneration of dopaminergic neurons within the substantia nigra pars compacta part of the brain. This degeneration causes motor insufficiencies such as tremor and stiffness.[141,150,151] The pathogenesis of PD is still unclear; however, exposure to 1-methyl-4-phenyl-1,2,3,6-tetrahydropyridine (MPTP) in humans causes neurodegeneration of dopamine neurons and results in a syndrome which resembles PD.[151,152] Treatment of this disease is the use of the drug Levodopa (also known as L-DOPA or L-3,4-dihydroxyphenylalanine) which increases the concentration of dopamine in the brain.[141,150] However there are side effects such as dyskinesia

(involuntary movements) and problems with motor function due to the use of this drug in the longer term.[141] Therefore there is a need to find alternative treatments for PD. Studies have shown that BV may be useful in the treatment of neurodegenerative diseases such as Parkinson's disease.[151,153] A brief discussion of how BV may have potential benefits in the treatment of PD will now be discussed.

A study carried out by Chung *et al.* looked at the effect of BV in the MPTP mouse model of PD.[151] The results showed that BV inhibited microglial activation (which have a role in degeneration of dopamine neurons) and reduced the infiltration of CD4+ T cells to the substantia nigra of mice which had been injected with MPTP. The results also showed that BV increased the peripheral regulatory T cell concentration which play a role in immune homeostasis and help to control destruction at the site of inflammation. Although the results presented here show promise for the use of BV as a treatment for PD in animal studies there is still a need for clinical studies to show the true effectiveness of BV to help treat PD.

Another study carried out by Alvarez-Fischer *et al.* looked at the neuroprotective effect of whole BV along with the single BV component apamin.[153] This study used the MPTP mouse model to examine the effect of BV/apamin on dopaminergic neurons. The results from this study showed that BV had a protective effect on the dopaminergic neurons which is consistent with the previous study already discussed. The results also found that apamin on its own had a reduced effect in comparison to whole BV suggesting that there may be synergy within the whole BV to increase the effect of apamin. In control experiments the results showed that apamin actually significantly ($p<0.05$) decreased the concentration of dopamine in the brain suggesting a harmful effect on healthy mice compared to the MPTP-induced mouse model of PD. This study is relatively small and uses only a maximum of 8 animals per experiment. The results shown here are therefore only indicative and further clinical studies would be required to show how effective BV/apamin would be *in vivo* for humans with PD.

1.3.4 Cosmetics

Bee venom has also become a growing interest within the cosmetic industry where it is thought to have anti-ageing effects. There are various products already on the market which include Rodial, Forapin, Apiven and Manuka Doctor. These products are generally skin ointments/creams which are formulated using whole bee venom. However it is very difficult to find literature with scientific data showing evidence for the anti-aging effects of BV. Hence there is a lot of controversy about how these bee venom cosmetic products produce an effect (if any). On the Rodial website for their bee venom moisturiser they claim that bee venom 'plumps and smoothes fine lines and wrinkles'.[154] However, there is no link to a scientific study which shows that BV has these effects. Likewise on the Manuka Doctor website for their Apinourish collection the claim is that 'Purified Bee Venom and Manuka Honey have powerful age-defying benefits; these active ingredients from the hive help with rejuvenating the skin's appearance'.[155] Again there is no link to scientific data for this claim to show that BV has anti-aging effects.

A small study found in the literature by Han *et al.* looked at the effects of a serum containing purified BV on the appearance of wrinkles on the face.[156] The results from this study showed that after 12 weeks the number of wrinkles, depth of wrinkles and area of wrinkles appeared to be reduced. However this study was based on visual appearance of wrinkles and only used 22 subjects to look at the effect of this BV containing serum. There is no suggestion for the scientific mechanism for how BV reduces wrinkles. There is therefore a need to have scientific studies to prove if BV has any anti-aging properties.

1.4 Nuclear Magnetic Resonance

1.4.1 Introduction

Nuclear magnetic resonance (NMR) is a powerful technique which has the ability to give structural data on unknown substances, conduct quantitative experiments and also show changes to a molecule as it undergoes a chemical reaction. NMR was discovered in 1945 by Bloch and Purcell, who performed the first NMR experiments independently of one another.[157] The original NMR instruments were based on the continuous wave (CW) method, which involved a fixed radiofrequency (RF),[158] but now the modern instruments use the Fourier transformation (FT) method.[159] NMR has developed over many years and the imaging application is now used for non-invasive medicinal purposes, known as magnetic resonance imaging (MRI). [160]

NMR the spectroscopic application, has developed over the last 50 years so that experiments can be carried out not only in one dimension (1D) but in two dimensions (2D) and more. There are numerous different two dimensional techniques which can be used and these include exchange spectroscopy (EXSY), cross-relaxation (NOESY), correlation spectroscopy (COSY), and total correlation spectroscopy (TOCSY). The use of 2D NMR is of a major advantage as it provides a clearer picture of interactions occurring within a molecule.[161]

Solids, liquids and sometimes gases can be analysed by NMR. NMR is frequently used by chemists to analyse proteins and peptides to get a better understanding of their nature. This is therefore a useful technique in the analysis of WBV enzyme activity against various substrates. Advances in the NMR technique allows for reactions to be monitored *in situ*. This is therefore a useful technique for the work to be carried out in this project. An NMR method will be developed to monitor the action of the enzyme activity in BV against various substrates.

1.4.2 Principles of NMR

In NMR, electromagnetic radiation, in the radio wave region, is applied to atoms causing the atoms to align with or against the magnetic field (B_o) direction. The majority of atomic nuclei possess spin, known as the spin quantum number (*I*). A selection of atomic nuclei *I* are shown in table 2. To determine the nuclear spin states of an atom the following equation can be used:

$$\text{No. of energy levels} = 2I + 1$$

This means that ^{1}H, which has a *I* of 1/2, has two spin states, with or against the magnetic field (B_o). This splitting between the energy levels is known as the Zeeman splitting.[162]

The magnetic moment (μ) of a substance is where it has the ability to interact with a magnetic field. When a nuclei is spinning it has angular momentum (P) and charge which produces a specific magnetic moment (μ):

$$\mu = \gamma P$$

where γ is the gyromagnetic ratio which can show how strong the magnetic properties are of the nuclei.[163] A positive value of γ indicates that the magnetic moment is parallel to the angular momentum and vice versa for a negative value of γ.[162]

The Larmor frequency is the rate of precession of a nucleus. The rate of precession (Larmor precession) is where the static field causes the magnetic moment to rotate about an axis in a circular motion which then rotates about the axis of the applied field. The Larmor frequency equation is:

$$\nu = \frac{-\gamma B_o}{2\pi}$$

Where ν is the Larmor frequency in Hertz. Nuclei change their spin state when they absorb energy from electromagnetic radiation which is applied to the nuclei and must be the same as the Larmor frequency to allow resonance to occur.[163]

Free-induction decay (FID) is induced by applying a magnetic field and then letting the nuclei to come to equilibrium. A radio frequency (RF) pulse is then applied which

rotates the spin polarisations. The RF signal produced while the precessional motion of the spin is resumed in the magnetic field is detected,[162] and this is what produces the NMR signal.

1.4.2.1 Chemical Shift

A magnetic field applied to a nucleus causes the atoms to produce their own magnetic field; this therefore affects the Larmor frequency. This magnetic field created by electrons in an atom can either add to or take away from the external magnetic field.[162] This causes the NMR signal to shift. Protons which have a high electron density have a lower δ (chemical shift) value, known as shielding, and resonate at a higher field. Electronegative groups can withdraw electrons and therefore reduce the electron density causing the δ value to increase, known as de-shielding, and resulting in a resonance at a lower field.[159,161] The magnetic field at the nucleus (B) can be expressed as follows:

$$B = B_0(1- \sigma)$$

where σ is the shielding constant and B_0 is the applied magnetic field. σ is expressed in ppm, a dimensionless unit, reliant on the chemical surroundings of the nucleus.[161,164]

A reference signal is often used to determine an NMR signal relative to a compound added to the sample. Tetramethylsilane (TMS) is a common reference standard which is used in NMR. The chemical shift (δ) value of TMS is 0, it is relatively unreactive and gives a sharp peak which is well separated from sample peaks making it a good reference standard. The position of an NMR signal is often expressed in terms of part per million (ppm). The following equation can be used to determine the position of an NMR signal when using a reference standard:

$$\delta = \frac{\nu - \nu_{TMS}}{\nu_{TMS}}$$

where ν is the Larmor frequency of a certain nuclei and ν_x is the Larmor frequency of the same nuclei in the reference compound.[162]

1.4.2.2 Spin-spin Coupling

Resonance signals in NMR can be split into various lines and is often referred to as J-coupling, scalar coupling or spin-spin coupling.[164] Coupling occurs from the valence electrons and so is a property of the molecule which cannot be changed by means of the external conditions. The coupling constant (J) is measured in Hz and is independent of the external magnetic field. Signals can be split into various numbers of lines such as a doublet (two lines), a triplet (three lines), a quartet (four lines) and so on. The number of lines a resonance will be split into can be calculated as M = n + 1, where m is the multiplicity and n is the number of protons three bonds away from the resonating group. The expected intensities of the line in a multiplet can be predicted using Pascal's triangle. The protons in a multiplet are aligned in various ways for example in a triplet there are three lines where the proton spins are aligned in three different ways as shown below.[161]

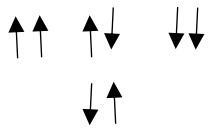

Figure 1.4.2.2.1 is a diagram of Pascal's triangle which shows the expected intensities of the lines in a multiplet.

1	Singlet
1 1	Doublet
1 2 1	Triplet
1 3 3 1	Quintet
1 4 6 4 1	
1 5 10 10 5 1	

Figure 1.4.2.2.1: Pascal's triangle showing the splitting pattern and line intensity in NMR spectroscopy.[163]

1.4.2.3 Spin Relaxation

After a nucleus has been placed in a magnetic field the nuclear spins are required to come back to their original equilibrium; if this did not happen then NMR would not be possible.[158] There are two different relaxation processes, these are spin-lattice relaxation and spin-spin relaxation.[158,162] Spin-lattice relaxation or longitudinal relaxation as it is sometimes known as, is where the spins establish their Boltzmann population values. Spin-spin relaxation, also known as transverse relaxation, is where nuclear spins lose their coherence and the signal dissipates over time. These relaxation processes are defined by a time, T_1 is the spin-lattice relaxation time and T_2 is the spin-spin relaxation time.[158,161,162]

1.4.2.4 NMR Instrumentation

The main components of an NMR spectrometer are the probe, pulse programmer, superconducting magnet, RF transmitter, receiver and data acquisition/processing computer.[165] The superconducting solenoid transmits a constant current through coils of resistant-free alloys. This is capable of producing a magnetic field which is strong, homogenous (within one part in 10^9) and stable which gives high resolution NMR spectroscopy.[158] The probe has an RF coil around it and the sample sits on top of the probe where the sample is spun and becomes locked in a homogenous magnetic field.[162] The RF transmitter is responsible for producing the RF signals which are at the Larmor frequency of the isotope being studied.[162]

1.4.3 Reaction Monitoring by NMR

NMR has the major advantage of being non-invasive and non-destructive. There has been a lot of work in developing software to assist with the reaction monitoring method. Recent advances in this technology now mean that reactions can be monitored through flow methods as well as static methods.[166] The method used for this work is a static method where a reaction takes place in a standard NMR tube within the probe.

An advantage of using the static method is that small volumes (*ca.* 600 µL) can be used. There is a large disadvantage associated with the static method: there is a delay in collecting the initial spectrum due to the requirement to lock and shim the sample to obtain an optimised field homogeneity prior to collection of the first data set.[167]

Original flow methods for reaction monitoring in NMR involved altered static NMR tubes where the reactants were injected into the tube which was in the probe. This involved the development of flow probes where there is a flow cell within the coil area of the NMR probe. This had the advantage of allowing the dynamics of the reaction to be detected quickly. However this approach meant there was less control over reaction conditions.[168] There are numerous disadvantages of using flow probes as they are expensive, have a narrow temperature range, can normally only detect one nucleus and can become blocked if there are particulates present.[166,168] Another disadvantage of the flow method is that larger sample volumes are required for cleaning the flow lines before a reaction takes place.

Advances in technology then led to the development of a flow cell which allowed the analysis of continuous flow or stopped flow reactions.[166] This method involves a reaction vessel outside of the NMR instrument, where the reaction takes place, and is fed into the NMR tube via the flow cell for analysis. The advantage of this approach over the flow probe approach is that no modifications to the NMR instrument are required and it was compatible with typical 5 mm probes meaning there was a wider range of nuclei available for analysis.[166] There are, however, various disadvantages to this method: the NMR analysis has a lag period associated with it meaning fast reactions can be difficult to detect; the temperature of connecting lines may have varying temperatures which could have a large effect on the reaction kinetics.[168]

The most recent developments came from a group who looked at maintaining the advantages of a flow probe and flow cell while reducing the disadvantages of these approaches.[168] This group designed an NMR flow tube with several considerations beforehand. These considerations included the need to design a device with versatility, the ability to control reaction conditions throughout the experiment, and to shorten the delay of a sample leaving a reaction vessel to being detected in the flow cell. The

success of this device was demonstrated through monitoring the reaction of *p*-phenylenediamine and isobutyraldehyde to form a diimine.

Software such as MestreNova's reaction monitoring module has been developed to extract the relevant information from reactions monitored by NMR. This software can extract kinetic values from the data and can help to visualise the changes in signal intensity as a product is formed. This software can also be used for data processing in a manner similar to TopSpin.[169] Bruker have also recently developed software, called InsightMR, which is integrated to a Bruker NMR instrument. This software allows for the integration of acquisition and processing features giving rapid handling of many spectra and gives the ability to change acquisition parameters based on the real-time data. Advances in software such as those mentioned above and others make reaction monitoring via NMR a much simpler process.[170] However there are some limitations to these software packages as sometimes more than one package has to be used to extract the relevant data.

There are various methods by which reaction monitoring can be carried out. These methods will now be briefly described.

1.4.3.1 In tube mixing

The reactants are mixed in the tube, which is then transferred to the NMR instrument. This is the method of choice for this study of work.

1.4.3.2 Sampling from external reaction

Aliquots are taken from a reaction vessel and transferred into a tube which can then be transferred to the NMR instrument for analysis.

1.4.3.3 Flow NMR

This method involves flowing a reaction mixture from a reaction vessel into an NMR tube, which is in the NMR probe.

1.4.3.4 In situ mixing

Reactants can be mixed in a tube which is already in the coil detection area of the probe.

1.5 Aims

Venoms are produced by many different species and are essentially natural products. Natural products are a rich source of bioactivity and many are used as drugs. There is a large amount of research on bee venom (BV) found in the literature. However an area of research which has been neglected is the action of BV on the mammalian defence system. This is therefore an area of research which requires attention.

The aims of this work are:

1. To development an enzyme assay under physiological conditions, using real time NMR as the analytical technique (chapter 2).
2. To establish the transformative (i.e. enzyme) activity of WBV *in vitro* against mammalian defence response bioactive molecules (chapter 3).
3. Having established such activity in WBV, the next aim is to search for related substrates that WBV modifies (chapter 4).
4. Characterise the kinetic properties of any enzyme identified (chapter 4).
5. To search for potential inhibitors of any enzyme activity (chapter 5).
6. Identify the component in WBV responsible for the activity (chapter 6).
7. To propose the role of any activities found (chapter 6).

Chapter 2

2.0 Determination of Limit of Detection (LoD) and Limit of Quantification (LoQ) for BV by NMR spectroscopy

2.1 Introduction

Reaction monitoring by NMR is a viable technique for carrying out and observing enzyme action in venoms. This method had to ensure that there was efficient water suppression and had to ensure that all the signals from WBV could be observed. It is also important to determine the analytical performance of the 600 MHz NMR instrument on which this work was carried out to get a clearer understanding of its capabilities and limitations. An attractive advantage of NMR as the analytical technique is that only small amounts of solution are required (550 µL). It is also possible to maintain a consistent temperature while carrying out analyses providing confidence that the experiments are always carried out at a constant temperature.

A method was therefore developed with the concept of producing qualitative and quantitative data that is reliable. It is thus important to find out the lowest concentration of BV solution that gives a signal which is distinct from the background. This is known as the Limit of Detection (LoD) and is defined by various regulatory organisations, such as WHO, IUPAC and ICH, as a signal-to-noise ratio greater than 3. This is the standard ratio used for various instruments and is therefore an accepted signal-to-noise ratio. The Limit of Quantification (LoQ) is the lowest concentration of sample that gives a signal which is obtained with good precision and accuracy. The LoQ is therefore higher than the LoD and the signal-to-noise ratio needs to be greater than ten.

Obtaining the LoD/LoQ of whole BV is a valuable quality control step when analysing the presence of BV in a formulation. The development of a suitable NMR method will then be applied to monitoring enzymatic reactions of BV with a range of substrates at known WBV and substrate concentrations.

2.2 Experimental

2.2.1 Instrumentation

NMR data were acquired under Topspin (version 2.1, Bruker Biospin, Karlsruhe) using a Bruker AVANCE III 600 NMR spectrometer operating at a proton resonance frequency of 600.13 MHz and equipped with a TBI [^{1}H, ^{13}C, ^{31}P–^{15}N]-z triple resonance probe-head fitted with an actively shielded gradient coil for delivery of pulsed-field gradients.

2.2.2 Method

One-dimensional ^{1}H NMR data were typically acquired using an excitation sculpting approach (Bruker pulse program zgpr) on samples equilibrated at a calibrated temperature of 310 K. Data were accumulated and centred at the solvent resonance with 64 transients over a frequency width of 7.22 kHz into 32,000 data points for an acquisition time aq = 2.27 s with a recycle delay d1 = 2 s between transients using a 90° radiofrequency (r.f.) pulse (p1 = 10.48 µs at a power level of 0.9 dB attenuation).

The acquisition parameters are noted below in table 2.2.2.1. The AV600 TBI probe was tuned manually using a solution of 100 mM potassium phosphate buffer at 310 K. The probe was then allowed to cool down to 298 K to allow a cold sample to be inserted and equilibrated to the correct temperature. 550 µL of each concentration was transferred into clean NMR tubes for analysis.

A cleaning process was developed to ensure that all glassware (NMR tubes, volumetric flasks etc.) were cleaned to a good standard. This process involved using a 1 % HCl solution to remove any contaminants present on the glassware. This was then followed by copious amounts of double distilled water to neutralise the glassware.

Details of the pulse programme mentioned in table 2.2.2.1 are shown in appendix 1. A diagram showing the pulse programme described in appendix 1 is shown in appendix

2. This reaction was carried out under automation. Therefore, details of the automation programme are shown in appendix 3.

This pulse sequence has been applied as it effectively attenuates the large, broad water peak which can affect the quality of spectra. This pulse sequence uses an echo effect which involves a pulse field gradient being applied before and after a refocusing element. This results in transverse magnetisation being returned to its original position.[171] The double gradient in this pulse sequence is shown in appendix 2. It should be noted that the second pair of gradients are less intense and hence why these are shown in the figure as slightly smaller. This pulse sequence effectively works by using a soft and hard $180_x°$ pulse sequence with the soft pulse being applied directly to the water resonance resulting in everything but the water being inverted.[171] Issues were still seen with the water peak not being suppressed properly. Our studies showed that this was due to dissolved gas being released from the solution causing tiny bubbles which severely degrades magnetic homogeneity. Hence the buffer is de-gassed by sonication prior to use to reduce this effect. De-gassing appears to have effectively resolved this issue and the pulse sequence works successfully to remove this large peak. The effect of a bubble present in an NMR tube during acquisition is shown in figure 2.2.2.1.

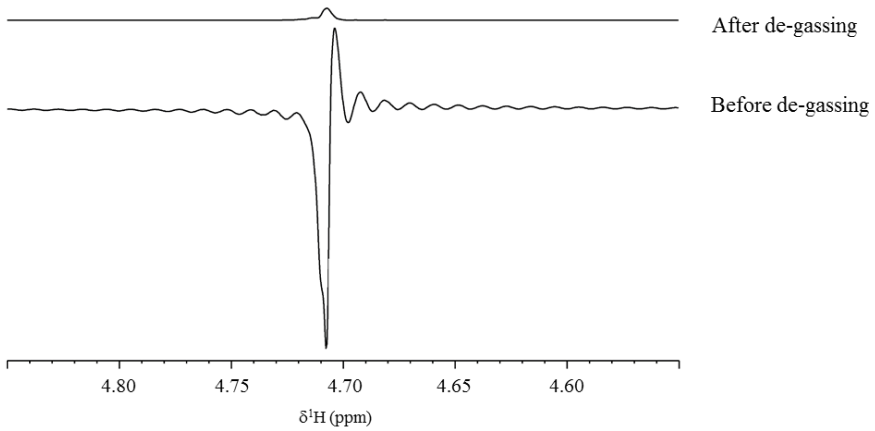

Figure 2.2.2.1: Effect of small bubble present in NMR tube

Table 2.2.2.1: Acquisition Parameters

Parameter	Setting
Probe	TBI
Solvent	H_2O:D_2O (90:10)
Temperature	310 K
Receiver Gain	128
SW (ppm) [Hz]	11.9878 [7194.245]
O1P (ppm) [Hz]	4.710 [2826.61]
TD	32768
AQ (s)	2.2774260
DW (µs)	69.500
Number of Scans	16, 64, 256 and 1024
Nucleus	^1H
Pre-acquisition Delay (D20)	0.5 s
Experimental Time	*ca.* 2 hours
Experiment	N@es1d_k

2.2.3 Materials

BV was provided by Beesen Co. (a South Korean company), lot number WCB010113. BV was collected via a commercial product developed by Beesen Co. which leaves the bees unharmed. The bees are given a small electric shock from a landing pad in front of the bee hive. This causes them to sting into a mesh gauze where the BV can be collected. Water used for this experiment was double distilled and D_2O was obtained from Sigma-Aldrich. NMR tubes were Wilmad (535-PP-7) 5 mm thin 7" long, 600 MHz rated tubes. Sodium azide, dipotassium deuterium phosphate and potassium dideuterium phosphate were bought from Sigma-Aldrich.

2.2.4 Solution Preparation

A description how of all the solutions used throughout this work were prepared is detailed below.

2.2.4.1 Sodium Azide

Sodium azide (6.5 mg) was dissolved in H_2O (10 mL) in a volumetric flask (10 mL) to yield a 0.01 M (10 mM) solution of sodium azide in water. This solution was stored in the fridge until required.

2.2.4.2 Potassium Phosphate Buffer

K_2DPO_4 (1.355 g) and KD_2PO_4 (312 mg) were transferred into a 100 mL volumetric flask. 1 mL of the 0.01 M sodium azide solution was added to the flask, 10 mL of D_2O was then added and the flask was made up to the mark with double distilled H_2O. This gave a 100 mM potassium phosphate buffer solution with 0.1 mM sodium azide at pH 7.4. This buffer solution was then degassed by sonication at 37 °C for 15 minutes. This solution was stored at 3 – 5 °C until required.

2.2.4.3 Bee Venom Solutions

An amount of BV (50.4 mg) was weighed out into 10 mL volumetric flask. This was dissolved in 100 mM potassium phosphate buffer. This solution was then filtered using 0.22 µm pore filters to remove any insoluble particulates and microbial enzymes present. BV solutions were then stored at 0 °C until they were required.

2.2.4.4 Dilutions

Serial dilutions were carried out using a stock solution of BV. These dilutions were carried out using 100 mM potassium phosphate buffer. The concentrations used were as follows: 1.008, 0.504, 0.252, 0.126, 0.063, 0.032, 0.016, 0.008, 0.004, 0.002 and 0.001 mg/mL. These solutions were stored in the fridge until required. The accuracy of these dilutions relates to the automatic pipette (± 3.6 – 9.5 µL) and the volumetric flasks (± 0.025 mL).

2.3 Results and Discussion

Solutions of BV at varying concentrations were analysed using the method described in section 2.2.2. For each tube four experiments were carried out sequentially with the same conditions each time but with an increase in the number of scans. The number of scans used is shown in table 2.2.2.1. Each tube was therefore in the NMR probe for *ca.* 2 hours. Increasing the number of scans improves the signal-to-noise ratio so it is expected that the lowest concentration with a signal-to-noise of greater than 3 will be at the highest number of scans. A control was also run at the same time as these solutions. The potassium phosphate buffer on its own was used as the control; this was used to show there were no obvious contaminants present in the buffer. To ensure consistency with results each solution of BV used for analysis had its own assigned NMR tube. Therefore, for repeat experiments, an aliquot of the same concentration of solution went into the same NMR tube as used in the previous experiment. This ensured that there were no contaminants left behind from a solution of different concentration, which would obviously affect results.

Initially the potassium phosphate buffer was being made up using the protonated salts (K_2HPO_4 and KH_2PO_4). However when running controls using this buffer, it was found that there were many unidentifiable peaks present. Various actions were taken such as making up fresh buffer and cleaning all glassware (mentioned in section 2.2.2). When initial spectra were taken of the buffer shortly after the buffer was made the spectrum showed no signals. However if the buffer control was run 24 hours later there

were many peaks present. It was therefore decided to use the deuterated salts instead. The deuterated salts were cleaner compared to the protonated salts.

The results from the control showed that, at 1024 scans, there were still some unidentifiable peaks present using the deuterated salts. The glassware the buffer was made up in was cleaned thoroughly again and the buffer was made up again as described above in section 2.2.4.2. The NMR tubes were also cleaned thoroughly again. A buffer control was then run for each of the NMR tubes being used. However these peaks still remained so it was decided that as these peaks are present in the buffer they could be excluded from the BV spectra. There were fewer signals present in the buffer using the deuterated salts when compared with the protonated salts. The deuterated salts therefore gave a cleaner spectrum so these salts were used for all experiments. The signal region in the BV spectra that was chosen for the signal-to-noise calculation was not at same ppm as the unidentifiable peaks in the buffer.

Figure 2.3.2 is a diagram which highlights the signal region and the noise region which were used to calculate the signal-to-noise ratio in Topspin. The noise region was a region at the end of the spectrum where there were no signals from the BV present. The signal region was of the largest signal in the BV spectrum. All data were processed in the same way so that direct comparisons could be made between the data points.

The SINO calculation carried out in topspin calculates the signal-to-noise ratio using the following formula:

$$\text{SINO} = \frac{maxval}{2 \,.\text{noise}}$$

where *maxval* is the highest intensity signal in the defined signal region (shown in figure 2.3.3), the noise is calculated using the following formula from the Bruker command documentation:

$$noise = \sqrt{\frac{\sum_{i=-n}^{n} y(i)^2 - \frac{1}{N}\left(\left(\sum_{i=-n}^{n} y(i)\right)^2 + \frac{3.\left(\sum_{i=1}^{n} i(y(i) - y(-i))\right)^2}{N^2 - 1}\right)}{N - 1}}$$

where N is the total number of points in the noise region (shown in Figure 2.3.2), n = (N-1)/2, and y(i) is the nth point in the noise region.

The signal chosen to calculate the signal-to-noise is that of citrate.[164] The structure of citrate is shown in figure 2.3.1. A study carried out by Fenton *et al.* showed that citrate is a component present in BV by GC-MS. Therefore using this signal region ensures that this method for determining LoD/LoQ is robust. This signal is shown in figure 2.3.2.

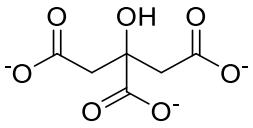

Figure 2.3.1: Structure of Citrate

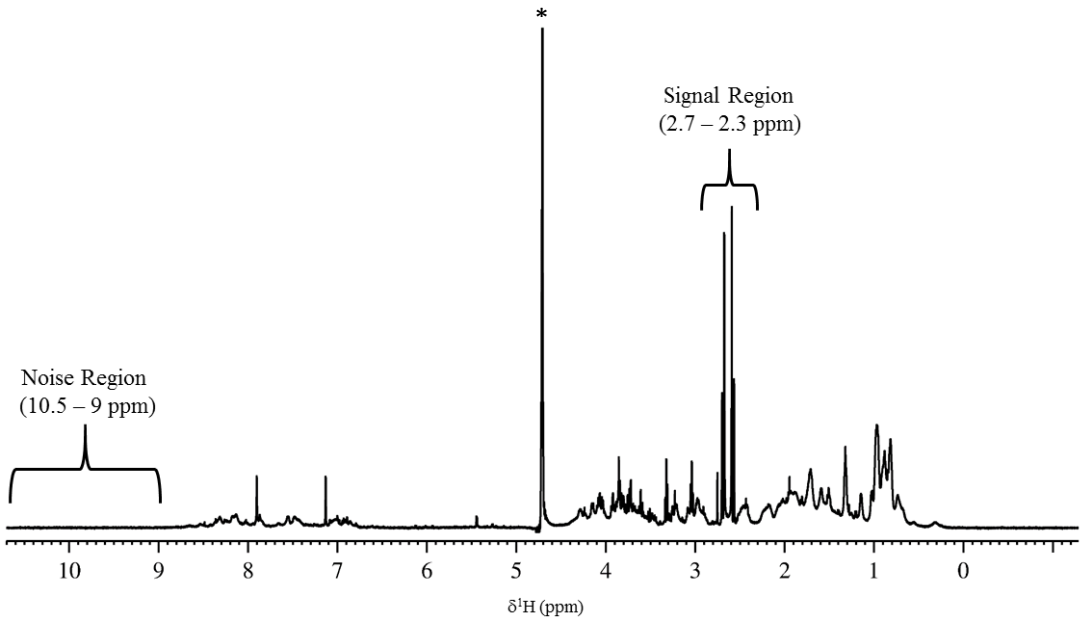

Figure 2.3.2: ^{1}H NMR spectra of BV showing signal and noise regions used to calculate the signal-to-noise ratio. The signal denoted with * is the signal which arises from the solvent.

Figure 2.3.3 and table 2.3.1 show the results from the data obtained at 16 scans. Table 2.3.1 shows three results for each concentration, this arises from taking three different aliquots of a stock solution. From figure 2.3.3 it is clear, as expected, that there is a linear response; as the concentration increases the signal-to-noise ratio increases. The R^2 value (shown in figure 2.3.3) shows that there is good correlation between the data points. R^2 is a measure of how close the data points are to the line of best fit. Therefore the lower the R^2 value the closer the data are to the line of best fit, and the data therefore has good linear regression. At 16 scans the LoD was found to be at a concentration of 0.032 mg/mL and the LoQ was found to be 0.063 mg/mL.

In table 2.3.1 the standard deviation has been calculated and shows that as the concentration increases the standard deviation increases. A possible explanation for the increased variation as the concentration increases is that there are a lot of small proteins and peptides present in BV, so at higher concentrations these could be affecting other signals. At lower concentrations all molecules are reduced in concentration. This means that components of the WBV which are present in small quantities become so diluted they are not detected by NMR.

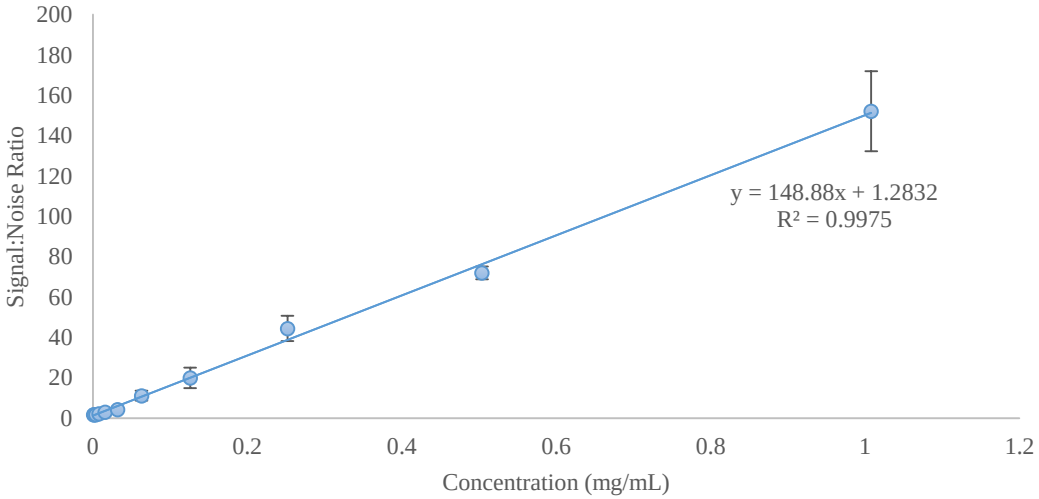

Figure 2.3.3: LoD/LoQ at 16 scans. Concentrations = 0.001, 0.002, 0.004, 0.008, 0.016, 0.032, 0.063, 0.126, 0.252, 0.504 and 1.008 mg/mL BV, n = 3.

Table 2.3.1: Tabulated data from NMR spectra at 16 scans

Concentration (mg/mL)	S/N 1	S/N 2	S/N 3	Mean	STD
0.001	1.55	1.79	1.8	1.713	0.142
0.002	1.63	1.71	1.89	1.743	0.133
0.004	1.57	1.86	1.64	1.690	0.151
0.008	2.3	2.19	2.23	2.240	0.056
0.016	2.98	2.09	3.85	2.973	0.880
0.032	4.9	4.12	3.6	4.207	0.654
0.063	12.43	12.61	8.28	11.107	2.450
0.126	23.39	22.28	14.18	19.950	5.028
0.252	41.63	40.11	51.59	44.443	6.236
0.504	72.53	74.98	68.67	72.060	3.181
1.008	169.12	156.81	130.44	152.123	19.761

S/N = signal to noise ratio and STD = standard deviation.

Figure 2.3.4 shows the results of data analysed at 64 scans. Similar to the results seen for 16 scans, there is good correlation as the R^2 value is low, showing good linearity. The LoD was found to be at a concentration of 0.008 mg/mL BV and the LoQ was found to be at a concentration of 0.063 mg/mL BV.

The standard deviation was calculated and is shown in table 2.3.2. Table 2.3.2 shows three results for each concentration, this arises from taking three different aliquots of a stock solution. A similar pattern is seen in these data to the data at 16 scans. However higher standard deviations are seen for lower concentrations when compared with the data at 16 scans. It can be assumed that as increasing the number of scans gives a better signal there are more small proteins and peptides being detected which are possibly causing the variation.

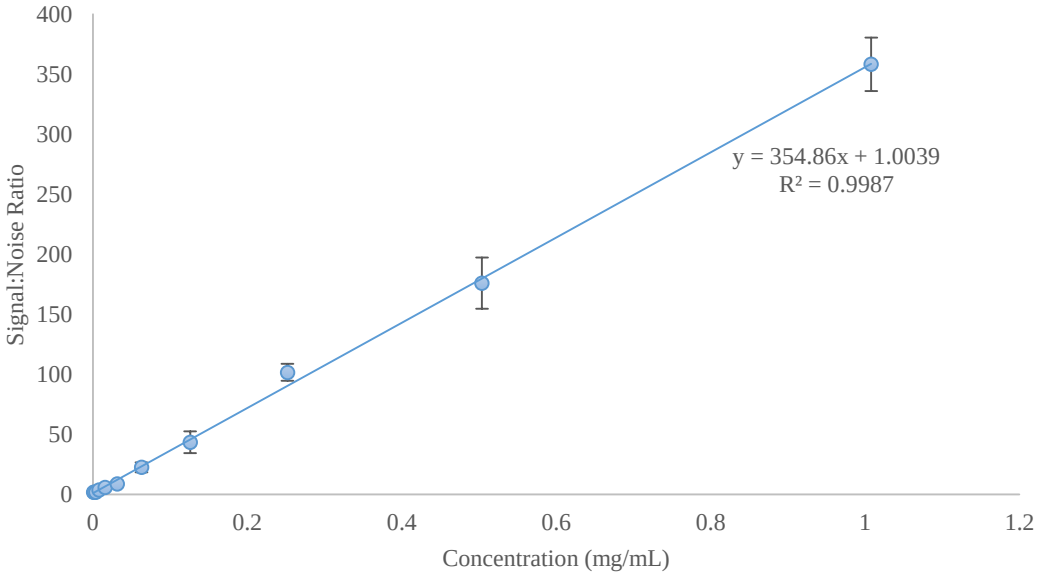

Figure 2.3.4: LoD/LoQ at 64 scans. Concentrations = 0.001, 0.002, 0.004, 0.008, 0.016, 0.032, 0.063, 0.126, 0.252, 0.504 and 1.008 mg/mL BV, n = 3.

Table 2.3.2: Tabulated data from NMR spectra at 64 scans

Concentration (mg/mL)	S/N 1	S/N 2	S/N 3	Mean	STD
0.001	1.82	2.11	1.88	1.937	0.153
0.002	1.96	1.79	1.95	1.900	0.095
0.004	1.89	1.49	2.49	1.957	0.503
0.008	2.94	3.1	5.36	3.800	1.353
0.016	6.67	3.84	7.01	5.840	1.740
0.032	10.27	9.72	6.25	8.747	2.180
0.063	24.86	25.02	17.83	22.570	4.106
0.126	49.8	47.68	33.04	43.507	9.126
0.252	94.18	102.4	108.4	101.660	7.139
0.504	151.6	191.54	184.53	175.890	21.326
1.008	370.47	371.83	332.67	358.323	22.227

S/N = signal to noise ratio and STD = standard deviation.

The results for data at 256 scans are shown in figure 2.3.5. These results are similar to both 16 and 64 scans, with good correlation (low R^2 value) meaning there is good linearity. The LoD was found to be at a concentration of 0.004 mg/mL BV and the LoQ was found to be at a concentration of 0.008 mg/mL BV. Table 2.3.3 shows three results for each concentration, this arises from taking three different aliquots of a stock solution.

The standard deviation was calculated and is shown in table 2.3.3. A similar pattern is seen in these data to the data at 16 and 64 scans. Again higher standard deviations are seen for lower concentrations when compared with the data at 16 and 64 scans.

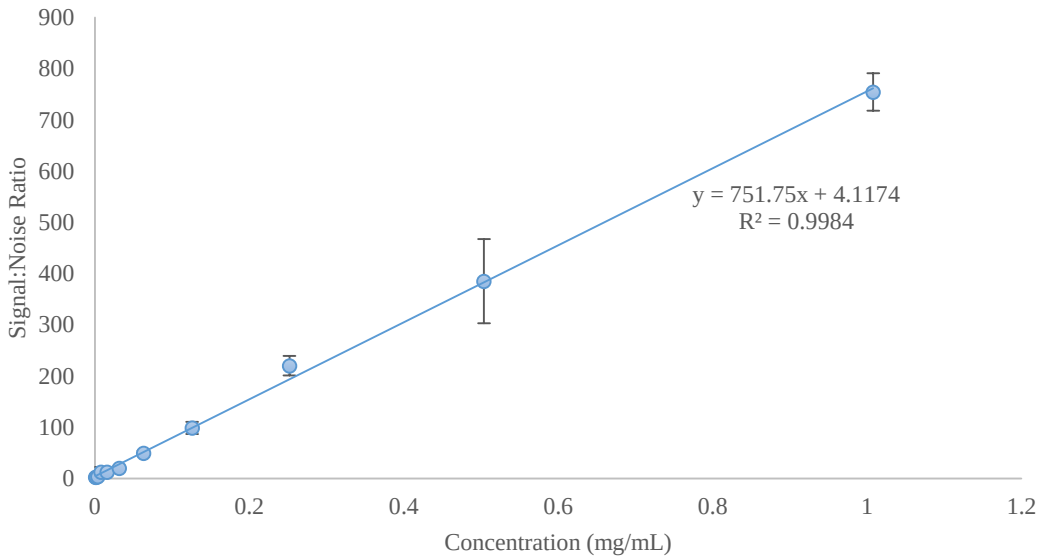

Figure 2.3.5: LoD/LoQ at 256 scans. Concentrations = 0.001, 0.002, 0.004, 0.008, 0.016, 0.032, 0.063, 0.126, 0.252, 0.504 and 1.008 mg/mL BV, n = 3.

Table 2.3.3: Tabulated data from NMR spectra at 256 scans

Concentration (mg/mL)	S/N 1	S/N 2	S/N 3	Mean	STD
0.001	2.03	2.16	2.48	2.223	0.232
0.002	2.25	1.77	3.24	2.420	0.750
0.004	3.15	2.16	4.81	3.373	1.339
0.008	5.97	6.89	23.7	12.187	9.981
0.016	13.41	7.87	15.62	12.300	3.992
0.032	23.19	21.21	14.98	19.793	4.284
0.063	51.6	52.67	44.01	49.427	4.721
0.126	104.5	106.29	85.11	98.633	11.746
0.252	198.33	228.18	233.63	220.047	19.004
0.504	301.67	466.16	387.35	385.060	82.269
1.008	712.27	773.55	778.29	754.703	36.825

S/N = signal to noise ratio and STD = standard deviation

Finally, results for data at 1024 scans are shown in figure 2.3.6. These results are similar to 16, 64 and 256 scans, with good correlation (low R^2 value) meaning there is good linearity. The LoD was found to be at a concentration of 0.001 mg/mL BV and the LoQ was found to be at a concentration of 0.008 mg/mL BV. Table 2.3.4 shows three results for each concentration, this arises from taking three different aliquots of a stock solution.

The standard deviation was calculated and is shown in table 2.3.4. A similar pattern is seen in these data to the data at 16, 64 and 256 scans. Again higher standard deviations are seen for lower concentrations when compared with the data at 16, 64 and 256 scans.

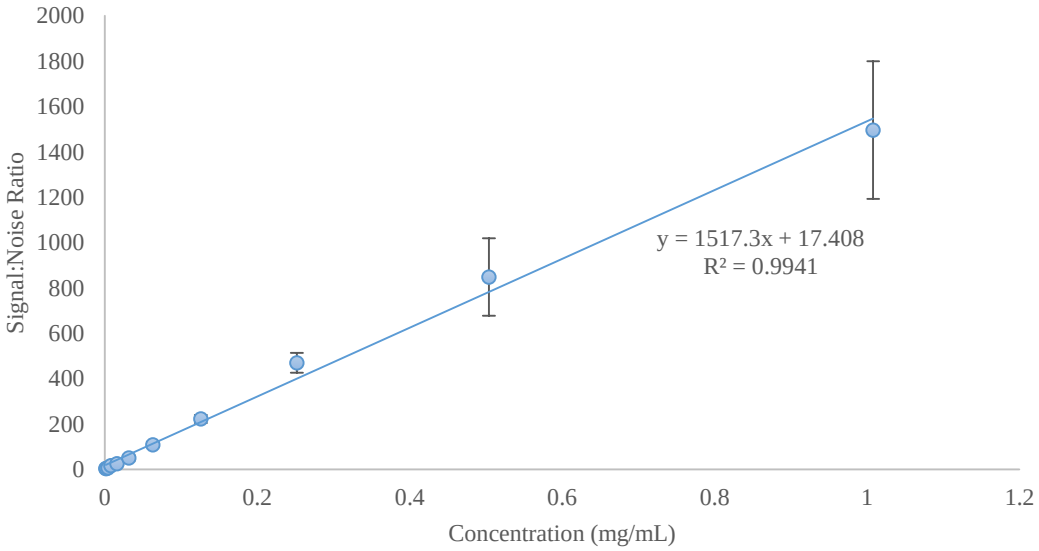

Figure 2.3.6: LoD/LoQ at 1024 scans. Concentrations = 0.001, 0.002, 0.004, 0.008, 0.016, 0.032, 0.063, 0.126, 0.252, 0.504 and 1.008 mg/mL BV, n = 3.

Table 2.3.4: Tabulated data from NMR spectra at 1024 scans

Concentration (mg/mL)	S/N 1	S/N 2	S/N 3	Mean	STD
0.001	3	3.74	3.53	3.423	0.381
0.002	4.42	2.26	6.04	4.240	1.896
0.004	8.2	3.66	7.74	6.533	2.499
0.008	15.33	16.05	18.58	16.653	1.707
0.016	26.9	18.07	29.36	24.777	5.937
0.032	52.81	60.38	35.71	49.633	12.638
0.063	110.42	119.13	95.38	108.310	12.015
0.126	202.41	228.31	234.97	221.897	17.201
0.252	424.64	473.24	511.47	469.783	43.518
0.504	651.38	964.87	926.58	847.610	171.015
1.008	1329.7	1312.52	1846.48	1496.233	303.444

S/N = signal to noise ratio and STD = standard deviation

2.4 Summary

In summary, the overall LoD is 1 µg/mL BV at 1024 scans and the overall LoQ is 8 µg/mL BV which can be obtained at both 256 and 1024 scans. These data will be important for obtaining reliable results when testing the presence of BV in formulations, which is part of a larger project.

The NMR method used here gave sufficient water suppression and good signal detection. This method was therefore applied to the monitoring of the enzyme reactions. The results here also showed that this method was robust and reliable giving confidence in its application to reaction monitoring. The results of the enzyme reactions via reaction monitoring NMR are described in chapter 3.

Chapter 3

3.0 Bioactive Screening

3.1 Introduction

All the substrates which will be used for this study and are potentially released in response to a bee sting in mammalian systems have been described in section 1.2, along with the molecular structure and amino acid sequence (if applicable) of each one. The single amino acid tyrosine (Y) was also tested to assess if there was L-amino acid oxidase (LAAO) activity present in BV.

3.2 Experimental

3.2.1 Materials

Hydrocortisone (cortisol), epinephrine, angiotensin II, GG, and bradykinin, were all bought from Sigma Aldrich. YGG was bought from Bachem. Substance P was bought from Merck Chemicals Ltd. YG was bought from Apollo Scientific Ltd. Met-enkephalin was bought from Synpeptide Co., Ltd. Leu-enkephalin was brought from both Tocris bioscience and Bachem. The supplier of BV was already mentioned in chapter 2.

3.2.2 Substrate Solutions

An amount of substrate was weighed out into a 5 mL volumetric flask. All substrates were dissolved in 100 mM^{-1} potassium phosphate buffer, with the exception of cortisol which was dissolved in DMSO-d_6 due to solubility in aqueous solutions. These solutions were then degassed by sonication at 37 °C for 15 minutes.

Details of the instrumentation and BV solution preparation has already been described in section 2.2 so will therefore not be mentioned here.

3.2.3 NMR Experimental

To carry out this work 400 µL of WBV (*ca.* 5 mg/mL) was mixed, by pipetting, with 400 µL of a substrate solution in an Eppendorf tube on ice. These reactions are detailed in table 3.2.3.1. However, there is an exception to this protocol, which is the cortisol experiment. This experiment used 600 µL of 5.04 mg/mL WBV and 50 µL of 100 mM^{-1} cortisol. This was done on ice to reduce any enzyme activity occurring before analysis. The substrate solution was sonicated at 37 °C beforehand to ensure the substrate was fully dissolved and degassed. The reaction mixture was then transferred to an NMR tube, which was subsequently placed in the NMR probe at 298 K. The sample was then locked and shimmed, and when the instrument was ready to start analysis the temperature was increased to 310 K.

Table 3.2.3.1: Solution details for substrate reactions

Substrate	Stock Substrate Concentration (mM^{-1})	Working Substrate Concentration (mM^{-1})	Stock BV Concentration (mg/mL)	Working BV Concentration (mg/mL)
Angiotensin II	4	2	4.85	1.21
Bradykinin	0.94	0.47	5.02	1.26
Substance P	0.342	0.171	5.04	1.008
Leu-enkephalin	2.25	1.13	5.02	1.26
Met-enkephalin	5	2.5	4.85	1.21
Epinephrine	5	2.5	4.85	1.21
Cortisol	100	7.69	5.04	4.65
Tyr (Y)	5	2.5	4.85	1.21

To monitor these reactions via NMR over time, the same NMR method used for the LoD/LoQ experiments was used for these experiments. However, the D20 delay parameter was altered. This delay pauses the pulse sequence before the acquisition begins. As a reaction takes place it will start to slow down the longer it goes on. This therefore means there is no need to acquire a spectrum every minute. This delay is therefore used to reduce the amount of spectra collected. The details of the delays used are shown in table 3.2.3.2. Therefore, each experiment was *ca.* 12.5 hours long.

Table 3.2.3.2: Pre-acquisition Delays

D20
0.5 s for 75 spectra
10 s for 40 spectra
20 s for 40 spectra
40 s for 40 spectra
80 s for 10 spectra

3.3 Results of all Control Experiments for Bioactive Molecules/BV

To be sure that any observed action against a substrate is the result of the BV, the necessary controls were run. The substrates and BV were run individually to ensure they were stable over the length of the experiment. The data were collected in the same way as the BV/substrate reactions, therefore mimicking the reaction procedure. For these experiments an aliquot from the stock solution was used and dissolved in an equal amount of buffer to keep concentrations consistent. The concentrations are shown in table 3.2.3.1.

The results of the controls found that all of the substrates and BV were stable at 37 °C over the 12 hour period. Figure 3.3.1 is an example of a substrate control. This displays the results of the control of met-enkephalin. It is shown that there are no changes to any of the signals meaning the peptide is stable. The results from the rest of the substrate controls can be found in appendix 4.

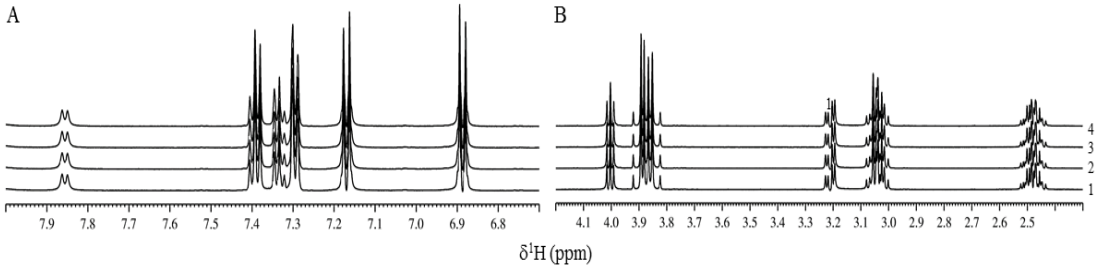

Figure 3.3.1: ^{1}H Met-enkephalin control aromatic (A) and aliphatic (B) region showing spectrum 1 (0 hours), 2 (after 1 hour), 3 (after 6 hours) and 4 (after 12.5 hours).

Figure 3.3.2 displays the results of the BV control. There is some autodigestion of the BV which occurs and is shown by very small changes in the signals in both the aromatic and aliphatic regions (figure 3.3.2). However the BV is stable for the first hour which would be the most critical stage of any enzyme activity by the BV.

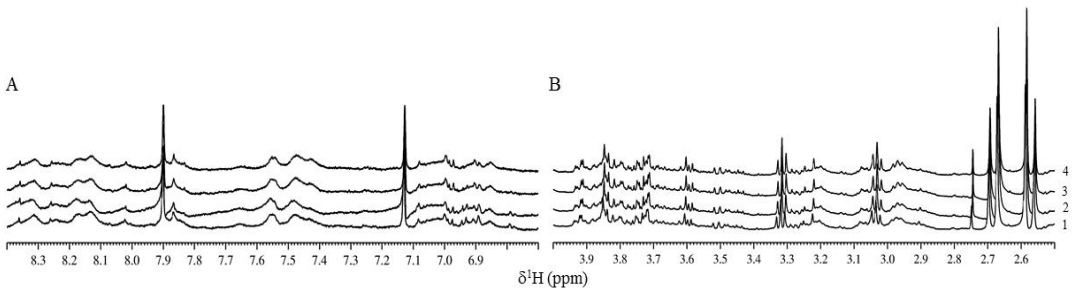

Figure 3.3.2: ^{1}H BV control aromatic (A) and aliphatic (B) region showing spectrum 1 (0 hours), 2 (after 1 hour), 3 (after 6 hours) and 4 (after 12.5 hours).

3.4 Results of all Bioactive Molecules Experiments

Reactions of BV with the substrates were then carried out. There was a delay of 10-15 minutes from the point of mixing until the first ^{1}H NMR spectrum was collected this is due to the time taken for sample equilibration and to carry out a topshim to get the best possible line shape. Topshim is a tool for an easy way to carry out automatic shimming. Results have shown that BV mixed independently with angiotensin II, bradykinin, epinephrine, cortisol and tyrosine resulted in the substrate remaining unchanged throughout the experiment. The spectra of these reactions are shown in figure 3.4.1, 3.4.2, 3.4.3, 3.4.4, and 3.4.5 respectively. In these figures the first and last spectrum is shown, which shows that there is no change in the substrate signals. These results mean that these substrates are not a target for any of the enzymes present in BV. The result from the tyrosine reaction means that BV does not have the L-amino acid oxidase activity that is present in some snake venoms.[77]

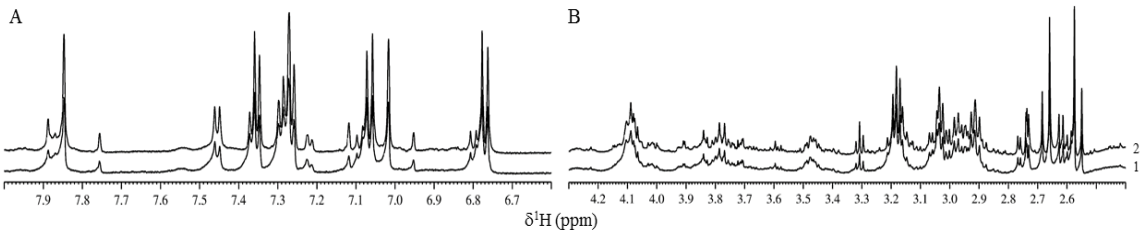

Figure 3.4.1: ^{1}H BV + Angiotensin II aromatic (A) and aliphatic (B) region showing spectrum 1 (0 hours) and 2 (after 12.5 hours).

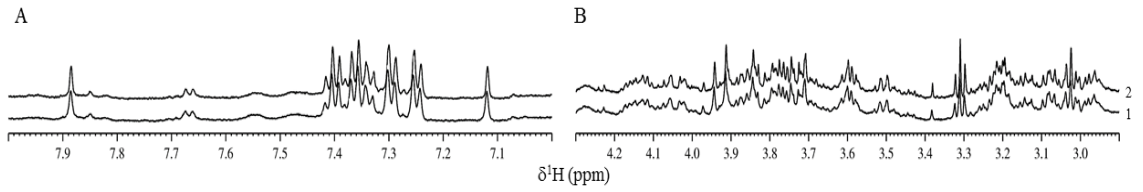

Figure 3.4.2: ^{1}H BV + Bradykinin aromatic (A) and aliphatic (B) region showing spectrum 1 (0 hours) and 2 (after 12.5 hours).

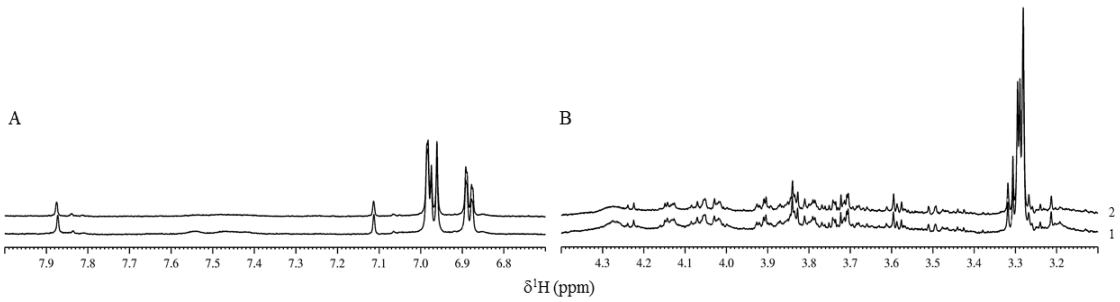

Figure 3.4.3: ^{1}H BV + Epinephrine aromatic (A) and aliphatic (B) region showing spectrum 1 (0 hours) and 2 (after 12.5 hours).

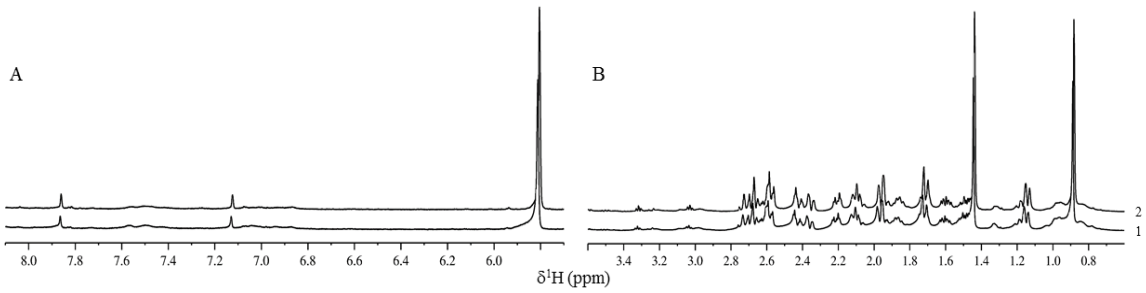

Figure 3.4.4: ^{1}H BV + Cortisol aromatic (A) and aliphatic (B) region showing spectrum 1 (0 hours) and 2 (after 12.5 hours).

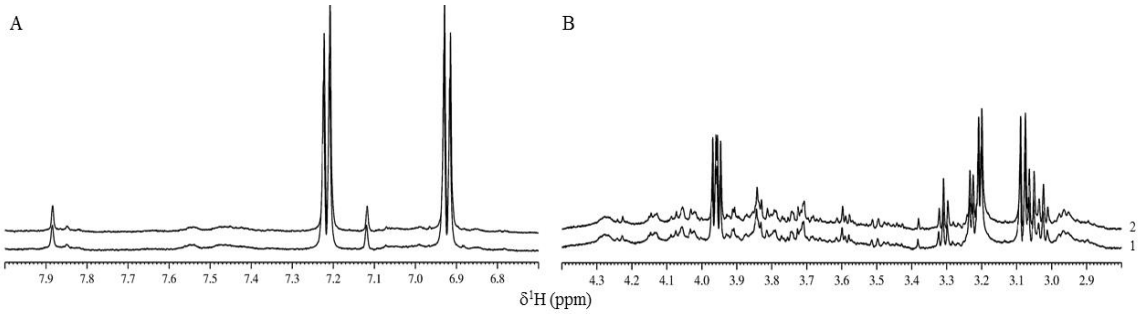

Figure 3.4.5: ^{1}H BV + Tyrosine aromatic (A) and aliphatic (B) region showing spectrum 1 (0 hours) and 2 (after 12.5 hours).

The results from the reactions of BV and the substrates YGGFL, YGGFM and substance P showed that these substrates were modified. These results are described

in sections 3.4.1, 3.4.2 and 3.4.3 for YGGFL, YGGFM and substance P respectively. There are significant changes in the substrate signals, which decrease in intensity as degradation occurs along with the appearance of new signals relating to a product.

3.4.1 YGGFL Results

In figure 3.4.1.1 there are clear changes in the aromatic region (δ 7.5 – 6.8 ppm) where the signals in this region relate to those from the Y and F amino acid residues. There are also new signals which are seen developing clearly in the aliphatic region (δ 3.8 – 3.6 ppm). This region shows ^{1}H signals arising from the alpha carbons within the molecule.

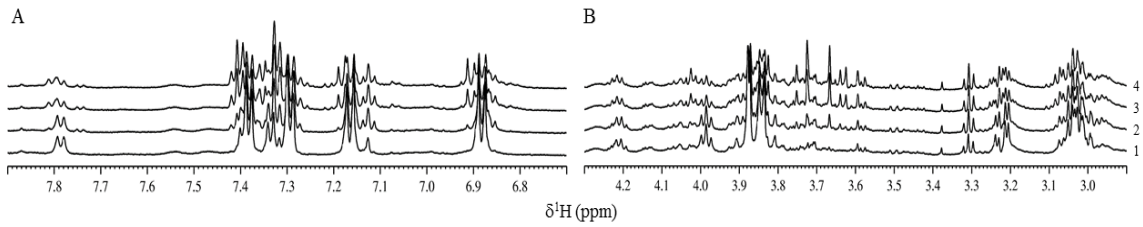

Figure 3.4.1.1: ^{1}H BV + YGGFL aromatic (A) and aliphatic (B) region showing spectrum 1 (0 hours), 2 (after 1 hour), 3 (after 6 hours) and 4 (after 12.5 hours).

The modification of YGGFL in the presence of BV is shown graphically in figure 3.4.1.2. The signal represented by δ 7.19 – 7.14 ppm relates to two of the protons on the tyrosine residue and the signal represented by δ 3.67 – 3.63 ppm relates to protons on the product molecule, which most likely relates to a glycine residue in the product.

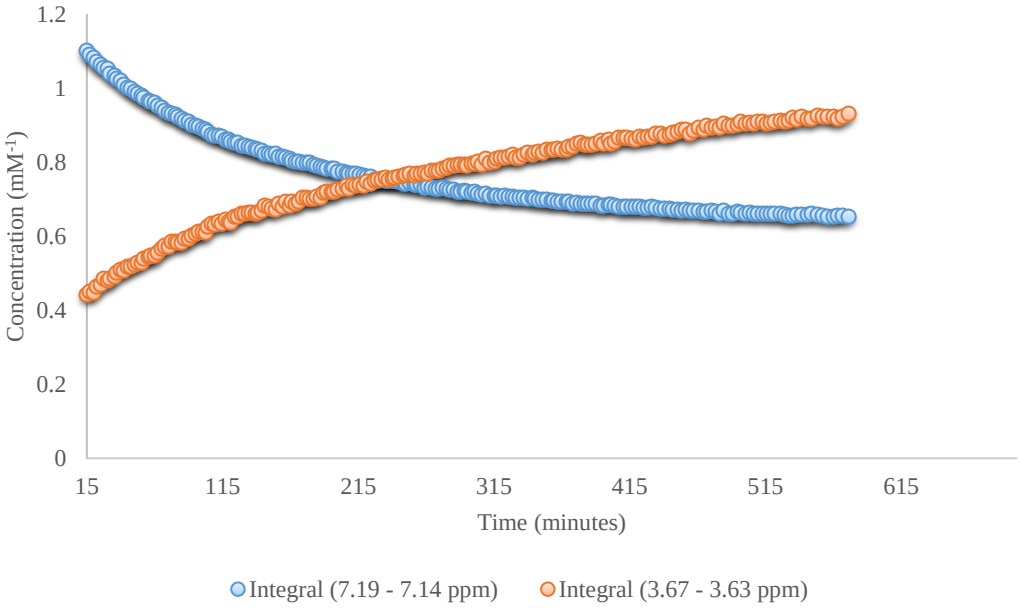

Figure 3.4.1.2: Graphical representation of YGGFL modification by BV.
Integral 7.19 – 7.14 ppm represents equivalent protons on Y in YGGFL peptide.
Integral 3.67 – 3.63 ppm represents protons on product molecule.

It should be noted that due to software and experimental issues these results are not absolute and therefore only indicative. The software used to extract this information from the data does not allow a time 0 point to be added where the concentration of product would be 0. This has therefore caused the results to show some molar differences between starting material and product. A way of overcoming this issue would be to use an internal standard of known concentration, this can then be used to obtain the concentration of starting material and product more accurately. The 15 minutes delay, previously mentioned, associated with the instrument equilibrium stage is an issue that is being addressed with the development of new hardware. This is the same issue for all experiments in the remained of this chapter and throughout the rest of this work. The levelling out of the results shown in figure 3.4.1.2 at the end of the experiment could be due to the enzyme becoming denatured. There are also no error bars shown on the graphs in this chapter and the remained of the thesis due to the experiments only being completed once. This was due to time and the cost of the substrates being used.

Figure 3.4.1.3 shows the assignment of YGGFL. There are 29 protons (excluding OH and NH protons) in this peptide. However in this ^{1}H spectrum there are only 28 protons shown (excluding signal A). The proton marked with an X, which has not been assigned is close to the solvent signal and is suppressed as a result. This would corroborate with the fact there is a proton missing from the spectrum. Signal A relates to an amide and has not been assigned. Signal G also integrates to half a proton, the rest of this signal is lost as suppression of the H_2O signal takes place. The partial assignment details of YGGFL are shown in table 3.4.1.1.

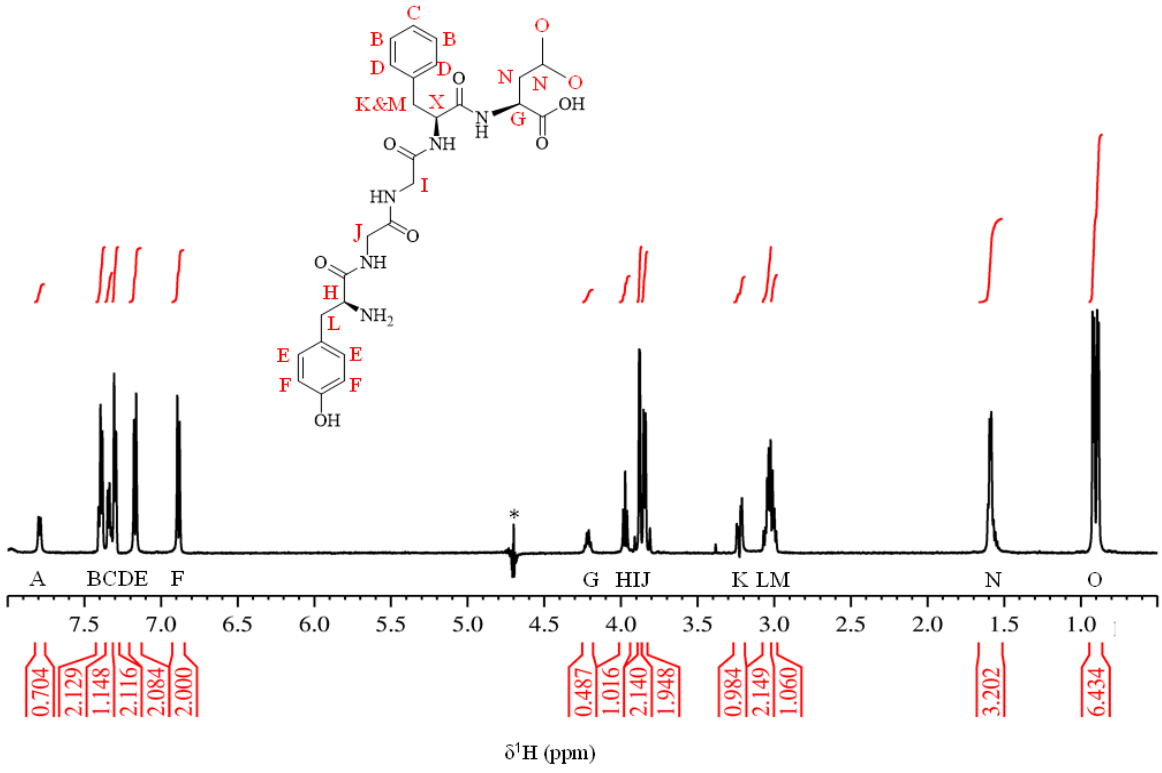

Figure 3.4.1.3: ^{1}H YGGFL Partial Assignment. The signal denoted with * is the signal which arises from the solvent.

Table 3.4.1.1: YGGFL Assignment Details

^{1}H Label	^{1}H Integral	δ (ppm)	J_{HH}-coupling (Hz)	Multiplicity
A	1	7.789	8.30	d
B	2	7.392	7.26	t
C	1	7.333	7.08	t
D	2	7.296	7.63	d
E	2	7.166	8.69	d
F	2	6.883	8.69	d
G	1	4.215	-	m
H	1	3.971	7.76	t
I	2	3.878	2.76	d
J	2	3.843	7.98	d
K	1	3.238	5.06, 14.88	dd
		3.214	5.22, 14.88	
L	2	3.050	-	m
M	1	3.003	-	dd
N	3	1.581	-	m
O	6	0.916	6.29, 17.93	dd
		0.886	6.18, 17.83	

This data was obtained by comparing YGGFL with fragments of this peptide. This is shown in figure 3.4.1.4. By comparing these fragments with the YGGFL peptide the signal assignment of YGGFL could be made without the need for 2D experiments.

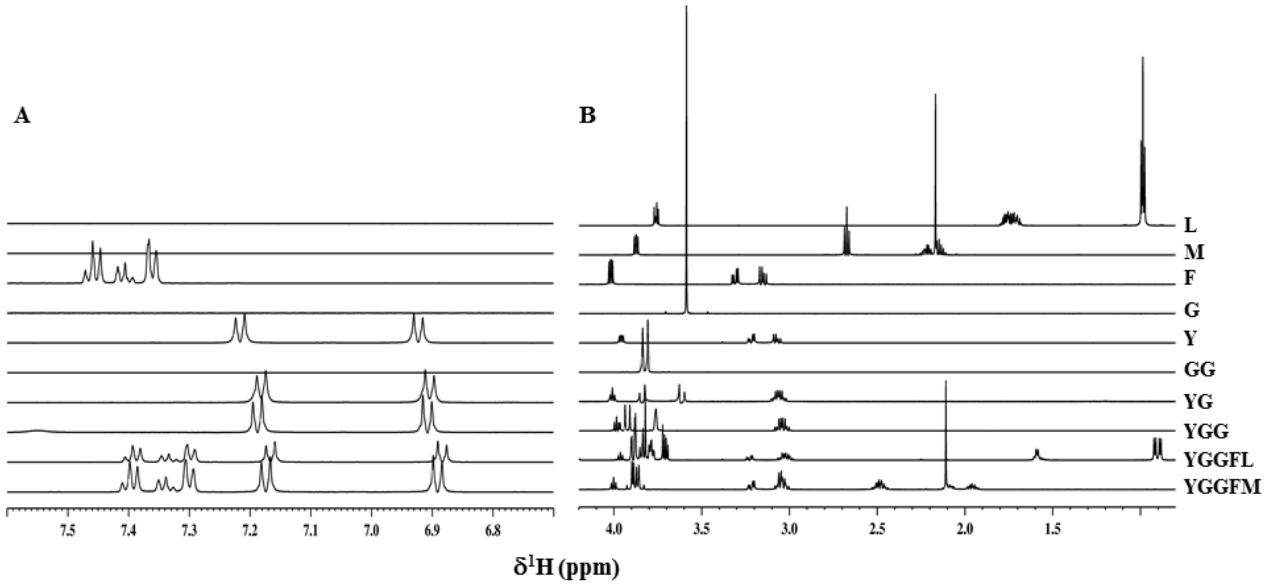

Figure 3.4.1.4: Comparison of YGGFM/YGGFL with fragments

3.4.2 YGGFM Results

In figure 3.4.2.1 there are similar signal changes seen in both the aromatic and aliphatic regions as previously mentioned for the YGGFL results. There is also a change in the signal at *ca.* δ 2.1 ppm, which relates to the methyl group of the methionine residue. As the reaction progresses there is the appearance of several new signals at a slightly higher chemical shift value which will relate to the methionine being part of a product peptide.

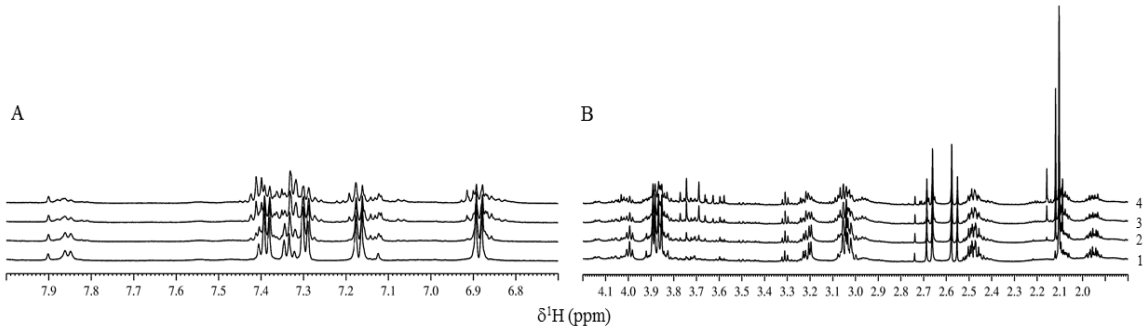

Figure 3.4.2.1: ^{1}H BV + YGGFM aromatic (A) and aliphatic (B) region showing spectrum 1 (0 hours), 2 (after 1 hour), 3 (after 6 hours) and 4 (after 12.5 hours).

The modification of YGGFM in the presence of BV is shown graphically in figure 3.4.2.2. The signal represented by δ 7.19 – 7.14 ppm relates to two of the protons on the tyrosine residue and the signal represented by δ 3.78 – 3.72 ppm relates to protons on the product molecule. The points on the graph at the beginning of the reaction for integral δ 3.78 – 3.72 ppm which show a large increase compared to the rest of the points on the line are due to an issue with the water suppression as these signals lie close to the water signal at δ 4.70 ppm. See previous note regarding the levelling out of the graphs towards the end of this experiment and also the difference in molar balance (section 3.4.1).

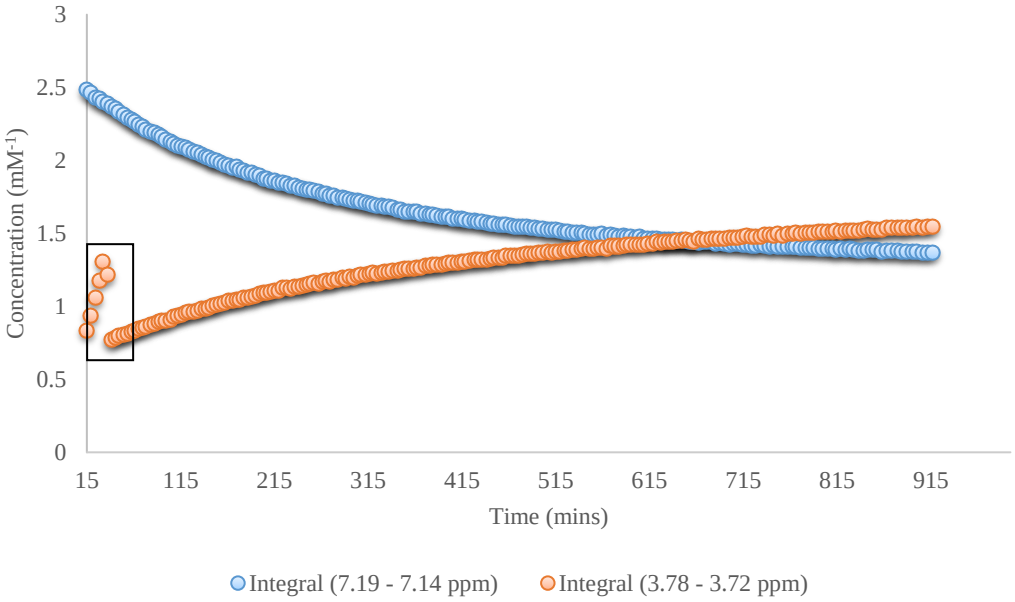

Figure 3.4.2.2: Graphical representation of YGGFM modification by BV. Integral 7.19 – 7.14 ppm represents equivalent protons on Y in YGGFM peptide. Integral 3.78 – 3.72 ppm represents protons on product molecule. Highlighted data points in the box are due instrumentation error which settles out as the experiment continues.

Figure 3.4.2.3 shows the partial assignment of YGGFM. There are 27 protons (excluding OH and NH protons) in this peptide, however in this ^{1}H spectra there are only 26 protons shown (excluding signal A). Similar to the YGGFL peptide there is a proton marked with an X which has not been assigned; this signal is close to the solvent signal. This would corroborate with the fact that there is a proton missing from the spectrum. Signal A relates to an amide and has not been assigned. Signal G also integrates to half a proton, the rest of this signal is also lost as the solvent suppression takes place. The partial assignment details of YGGFM are shown in table 3.4.2.1. This assignment was carried out by comparing YGGFM with various fragments of this peptide (figure 3.4.1.4). This meant that 2D data did not need to be acquired.

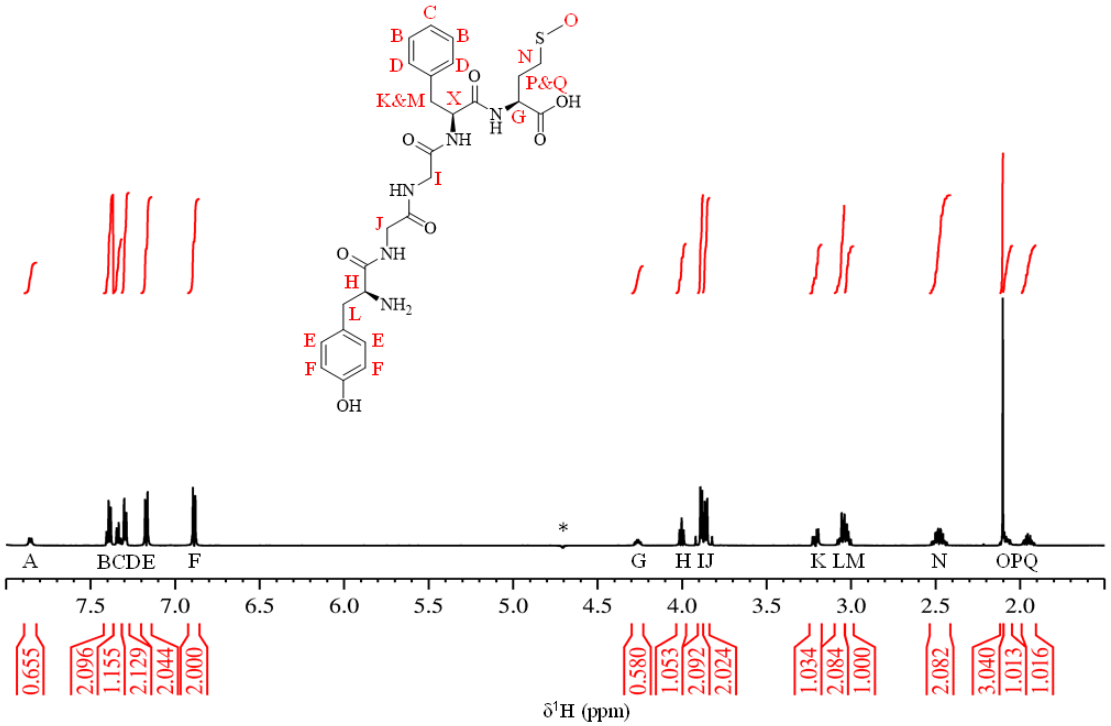

Figure 3.4.2.3: ^{1}H YGGFM Partial Assignment. The signal denoted with * is the signal which arises from the solvent.

Table 3.4.2.1: YGGFM Partial Assignment Details

^{1}H Label	^{1}H Integral	δ (ppm)	J_{HH}-coupling (Hz)	Multiplicity
A	1	7.856	7.84	d
B	2	7.393	7.50	t
C	1	7.334	7.28	t
D	2	7.294	7.27	d
E	2	7.170	8.78	d
F	2	6.886	8.78	d
G	1	4.263	-	m
H	1	4.003	7.45	t
I	2	3.887	6.61	d
J	2	3.859	8.66	d
K	1	3.224	5.68, 14.55	dd
		3.199	5.65, 14.31	
L	2	3.055	-	m
M	1	3.022	-	dd
N	2	2.480	-	m
O	3	2.103	-	s
P	1	2.076	-	m
Q	1	1.950	-	m

3.4.3 Substance P Results

The results for the BV and substance P reaction are shown figure 3.4.3.1. There were solubility issues with this peptide which therefore meant a very low concentration had to be used. In the aromatic region, where the signals relate to the two phenylalanine amino acids in the peptide, there are clear changes in the initial signals. However the formation and disappearance of signals in the aliphatic region becomes more difficult to see due to the low concentration of peptide used. To show more clearly the modification of this peptide a graphical representation is shown in figure 3.4.3.2. This graph shows that as one of the doublets in the aromatic region decreases in intensity, another doublet increases in intensity at a slightly higher chemical shift. From this graph is it clear that modification of substance P has occurred after *ca.* 100 minutes. See previous note regarding the levelling out of the graphs towards the end of this experiment and also the difference in molar balance (section 3.4.1).

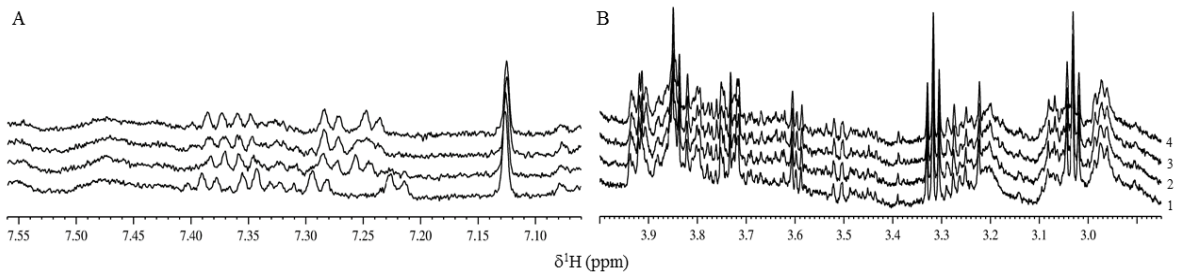

Figure 3.4.3.1: ^{1}H BV + Substance P aromatic (A) and aliphatic (B) region showing spectrum 1 (0 hours), 2 (after 1 hour), 3 (after 6 hours) and 4 (after 15 hours).

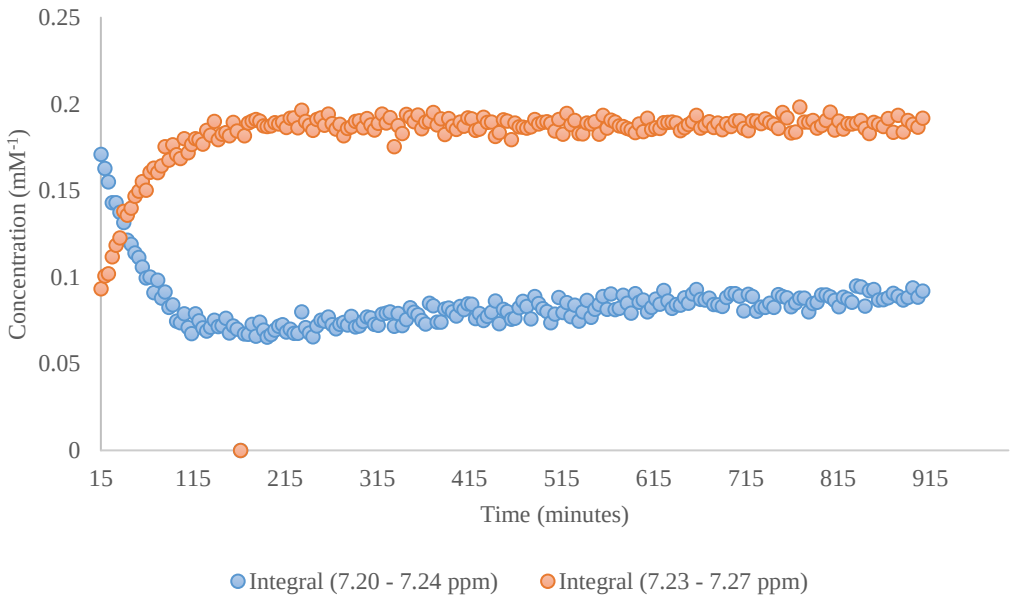

Figure 3.4.3.2: Graphical representation of substance P modification. Integral 7.20 – 7.24 ppm represents proton(s) on amino acid residue in substance P peptide. Integral 7.23 – 7.27 ppm represents protons on product molecule.

One conclusion which can be made is that BV does not have L-amino acid oxidase activity. This is due to the results of WBV mixed with Y showing no activity. Another conclusion from these results is that both met- and leu-enkephalin and substance P are being modified by BV. There are four peptide bonds within the enkephalin peptides and several peptide bonds within the substance P peptide which could be broken by an enzyme. There are also a number of side chains on the amino acid residues which could be modified. From the results shown here it is not clear how these peptides are being modified. Further analysis is required to deduce the modification pathway which will be discussed in section 3.5.

3.5 Determination of Substrate Cleavage Sites

Due to the issues with substance P it was decided to look further into the modification of the enkephalin peptides. A model peptide, YGG, was used as it is the first three amino acids of the enkephalin peptide sequences. This model peptide was used as a cheaper alternative for the leu- and met-enkephalin (YGGFL and YGGFM respectively). The possible fragments of this peptide were also analysed; this includes glycine, YG and GG. Details for the experiments are shown in table 3.5.1. A full signal assignment of YGG is shown in figure 3.5.1 and table 3.5.2. This assignment was carried out by comparing YGG with various fragments of this peptide (figure 3.4.1.4). This meant that 2D data did not need to be acquired.

Table 3.5.1: Solution details for substrate reactions

Substrate	Stock Substrate Concentration (mM^{-1})	Working Substrate Concentration (mM^{-1})	Stock BV Concentration (mg/ml)	Working BV Concentration (mg/ml)
YGG	5	2.5	5.02	1.26
YG	5	2.5	4.85	1.21
GG	5	2.5	4.85	1.21
G	5	5	n/a	n/a

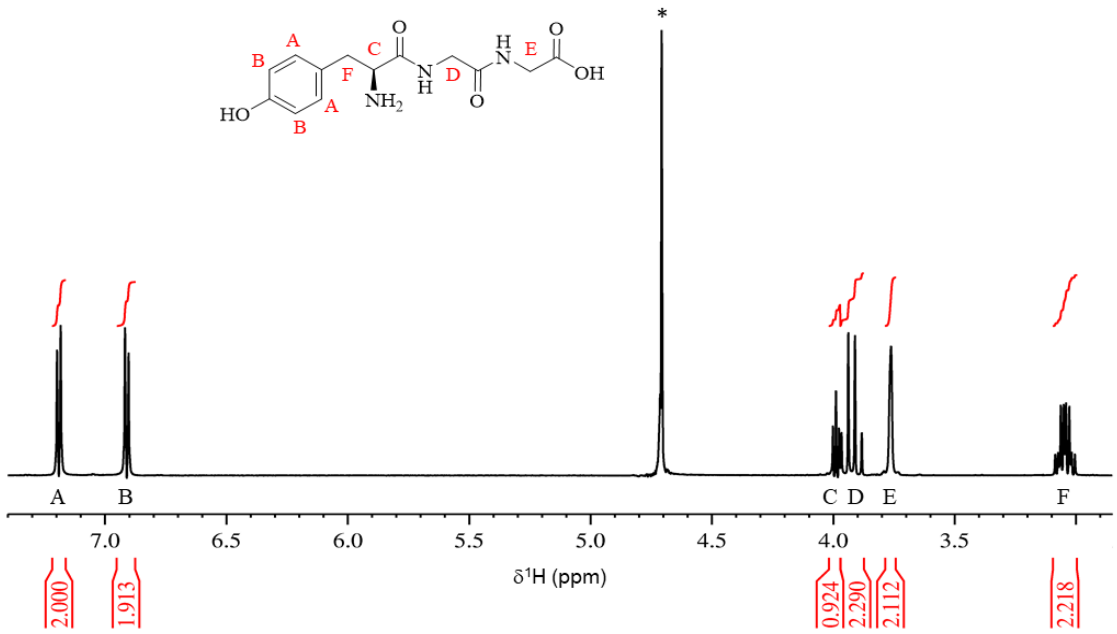

Figure 3.5.1: ^{1}H signal assignment of YGG peptide. The signal denoted with * is the signal which arises from the solvent.

Table 3.5.2: YGG ^{1}H signal assignment details

^{1}H Label	^{1}H Integral	δ (ppm)	J_{HH}-coupling (Hz)	Multiplicity
A	2	7.19	8.76	d
B	2	6.91	8.82	d
C	1	3.99	7.44	t
D	2	3.95, 3.89	16.82, 16.82	dd
E	2	3.76	-	s
F	2	3.06	7.00, 13.92	dd
		3.02	8.03, 13.92	dd

A control experiment was carried out for this peptide in the same way as the others previously described. The results found that the YGG peptide was stable over a period of 12.5 hours, the results are shown in appendix 4 (4H). YGG was then mixed with

BV in the same way as all other reactions and the results of this reaction are shown in figure 3.5.2.

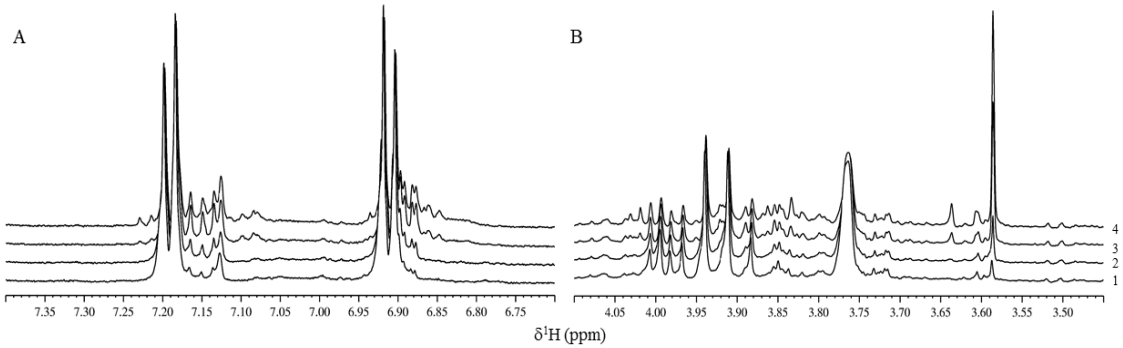

Figure 3.5.2: ^{1}H BV + YGG aromatic (A) and aliphatic (B) regions showing spectrum 1 (0 hours), 2 (after 1 hour), 3 (after 6 hours) and 4 (after 12.5 hours).

In figure 3.5.2 there is a clear transformation of YGG in the presence of BV. The two doublets at *ca.* δ 7.2 and 6.9 ppm in figure 3.5.2 represent the protons A and B respectively (figure 3.5.1), found on the aromatic ring of the tyrosine amino acid in this peptide. The results show that over time there is a decrease in the size of these signals and sequentially the formation of new signals at the lower chemical shift value of *ca.* δ 7.16 and 6.88 ppm.

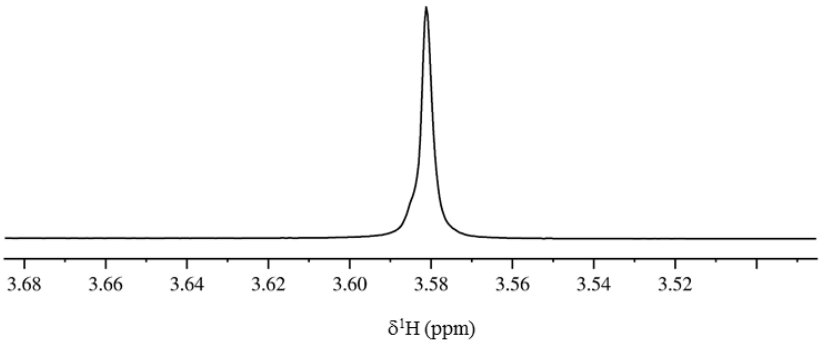

Figure 3.5.3: ^{1}H Glycine

A large distinctive signal at δ 3.58 ppm is formed at the same time as the doublets at δ 7.2 and 6.9 ppm decrease. This signal is that of the alpha carbon of free glycine. The ^{1}H NMR spectrum of free glycine is shown in figure 3.5.3, which shows that there is a single signal at *ca.* δ 3.6 ppm. This therefore confirms that the formation of the signal at *ca.* δ 3.6 ppm during the transformation of YGG by BV is that of free glycine. This result means that BV is cleaving the YGG peptide between the two glycine residues to form YG and G which is shown in figure 3.5.4.

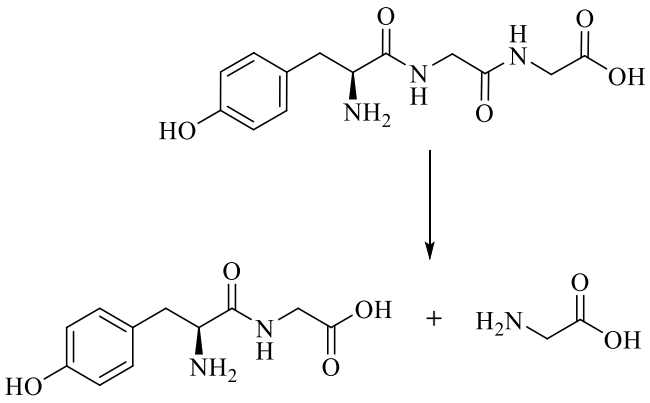

Figure 3.5.4: Cleavage Pathway of YGG

The modification of YGG in the presence of BV is shown graphically in figure 3.5.5. The signal represented by δ 7.22 – 7.16 ppm relates to two of the protons on the tyrosine residue and the signal represented by δ 3.59 – 3.58 ppm relates to two protons on the product molecule which is free glycine. Some of the points towards the end of the reaction stand out compared with the general trend of the line, this is due to the water suppression failing possibly because of the formation of a gas bubble, resulting in loss of magnetic field homogeneity across the sample.

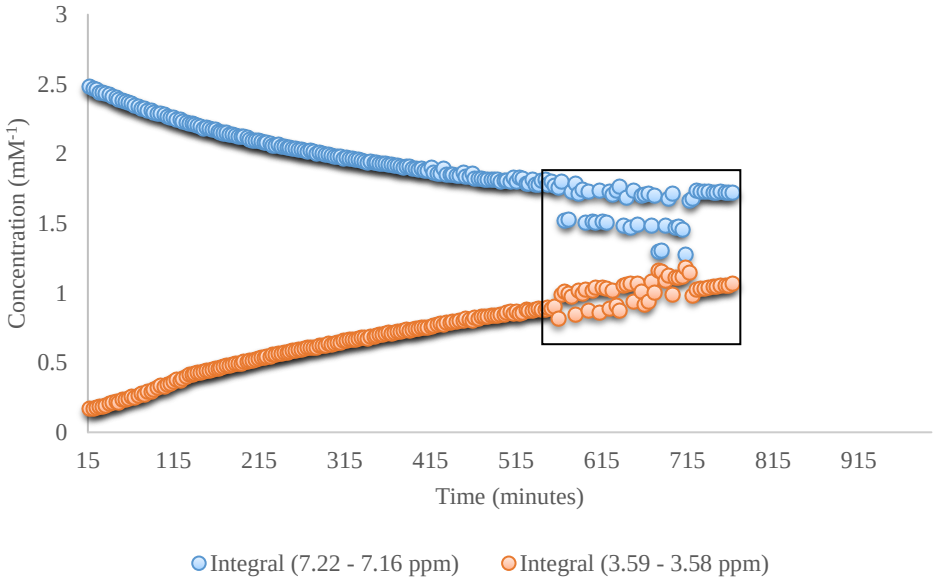

Figure 3.5.5: Graphical representation of YGG modification by BV. Integral 7.22 – 7.16 ppm represents equivalent protons on Y in YGG peptide. Integral 3.59 – 3.58 ppm represents protons on product molecule. Highlighted data points in the box are due instrumentation error which settles out as the experiment continues.

Further experiments were then carried out to look closely at the degradation pathway of YGG. The dipeptides YG and GG were analysed confirming that the YGG peptide is hydrolysed at the GG bond. The molecular structure of YG and GG are shown in figure 3.5.6 and 3.5.9 respectively. A signal assignment of the YG peptide is shown in figure 3.5.7 along with the details of this assignment in table 3.5.3. This assignment was carried out by comparing YG with various fragments of this peptide (figure 3.4.1.4). This meant that 2D data did not need to be acquired. A signal assignment for the GG peptide is not shown as there are only two singlets in the ^{1}H spectrum for this peptide; these represents the four protons attached to the two alpha carbons (two protons on each carbon).

The controls of YG and GG are both shown in appendix 4 (4I and 4J respectively), which show that these dipeptides are stable for the length of the experiment (*ca.* 5 hours). The D20 delay parameter for these experiments was not altered and was kept at 0.5 s for 70 spectra. This was due to the data being collected for a much shorter period of time in comparison to the other substrate/BV reactions. These experiments

were carried out for a much shorter period of time as they were being conducted to confirm previous results. To show the delayed hydrolysis of the YGG hydrolysis product YG so therefore only a short analysis was required.

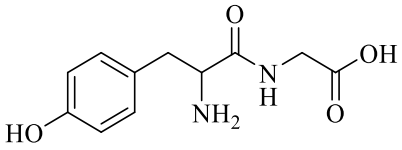

Figure 3.5.6: Structure of YG

The results of these experiments are shown in figure 3.5.8 and 3.5.10 for YG and GG respectively. The results for the reaction of BV with GG show that the substrate remains intact throughout the experiment. The GG spectrum shows two singlets at *ca.* δ 3.82 ppm which are not present in the spectra during the YGG hydrolysis, this therefore rules out GG being a product in the YGG degradation. These results also mean that the enzymes present in BV responsible for the hydrolysis are unable to break the GG bond without the Y residue being present. This shows the significance of this amino acid for the binding of the substrate YGG to the enzyme. Y has a hydrophobic side chain which may be a required chemical property that is important for the binding of the YGG substrate and subsequently the enkephalin peptides

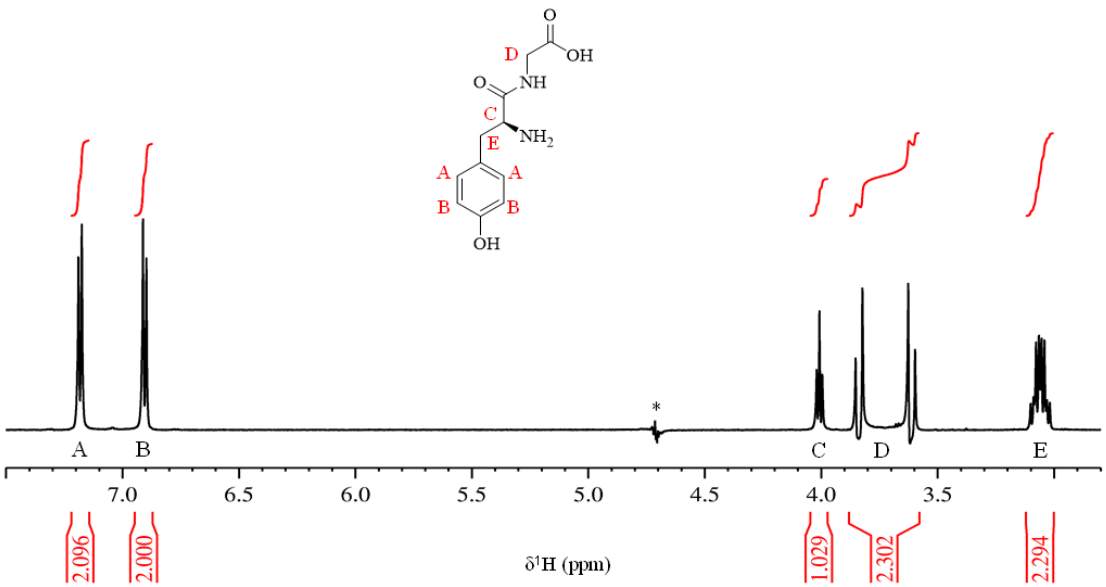

Figure 3.5.7: ^{1}H signal assignment of YG peptide. The signal denoted with * is the signal which arises from the solvent.

Table 3.5.3: YG ^{1}H signal assignment details

^{1}H Label	^{1}H Integral	δ (ppm)	J_{HH}-coupling (Hz)	Multiplicity
A	2	7.182	8.80	d
B	2	6.904	8.74	d
C	1	4.008	7.32	t
D	2	3.838	17.68, 135.65	dd
		3.614	17.68, 135.81	
E	2	3.060	-	m

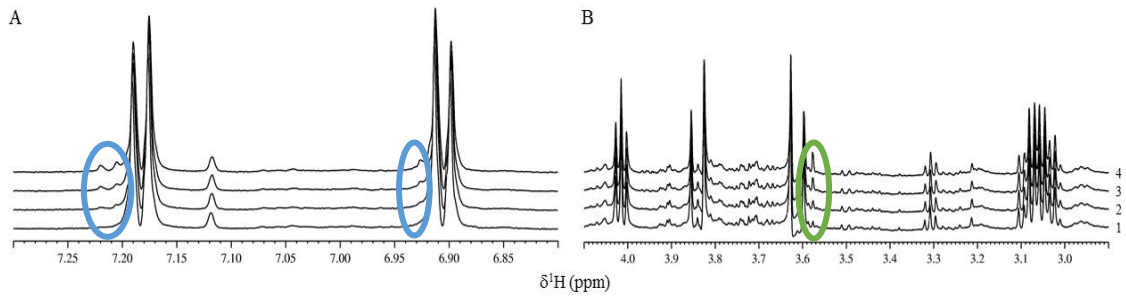

Figure 3.5.8: ^{1}H BV + YG aromatic (A) and aliphatic (B) regions showing spectrum 1 (0 hours), 2 (after 1 hour), 3 (after 2.5 hours) and 4 (after 5 hours). The signal highlighted in green represents the formation of free glycine. The signals highlighted in blue represent the formation of free tyrosine.

The results for BV with YG on the other hand showed that YG was broken down. There is the development of a singlet at *ca.* δ 3.58 ppm which is similar to the YGG hydrolysis. This has already been confirmed as the development of free G, and this is being produced as YG is broken down forming Y and G.

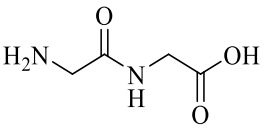

Figure 3.5.9: Structure of GG

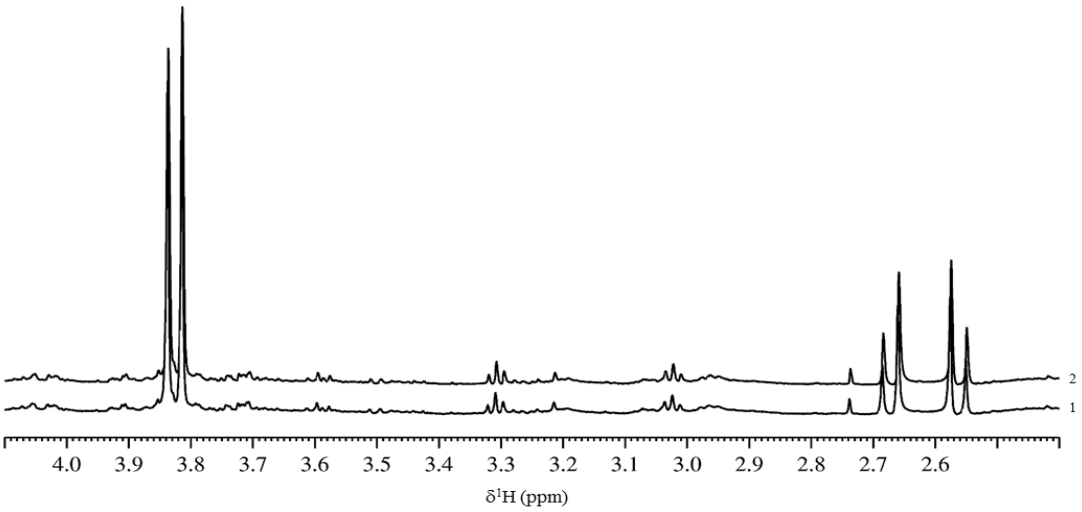

Figure 3.5.10: ^{1}H BV + GG showing spectrum 1 (0 hours) and 2 (after 5 hours).

The cleavage pathway for this experiment is shown in figure 3.5.11. As YG is only a dipeptide, the enzyme responsible for this hydrolysis cannot be a dipeptidyl peptidase.

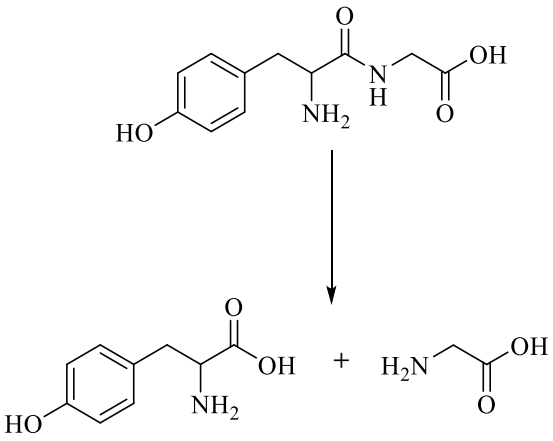

Figure 3.5.11: Cleavage Pathway of YG

A graph showing the relative rates of reaction of these substrates (YGGFM, YGGFL, YGG and YG), except substance P, is shown in figure 3.5.12. Substance P was excluded from this graph as the concentration used for this substrate was not comparable to the other substrates used. This graph shows the relative rates at which

these peptides are modified. The doublet at δ 7.19 ppm representing the Y amino acid in all four of these substrates was used to obtain these relative rates. The graph only shows the first 60 minutes of each reaction as this is the most important part of the process.

Table 3.5.4 Tabulated data showing the relative rates for four peptides

Substrate	% Conversion at 20 mins	Relative Rate (μM/min^{-1}) after 20 mins
YG	0 %	0
YGGFL	3.2 %	4
YGG	3.6 %	4.5
YGGFM	4 %	5

There are no statistics shown for these experiments as they were only conducted once. Repeat experiments could not be carried out due to the time and cost of carrying out these experiments.

The graph in figure 3.5.12 shows that YGGFM is modified the quickest followed by the model peptide YGG and then YGGFL (table 3.5.4). Also shown is that the YG dipeptide remains the same over the 60 minute period. This is expected as this dipeptide was a degradation product of the YGG peptide meaning that YG degradation will be a slower process.

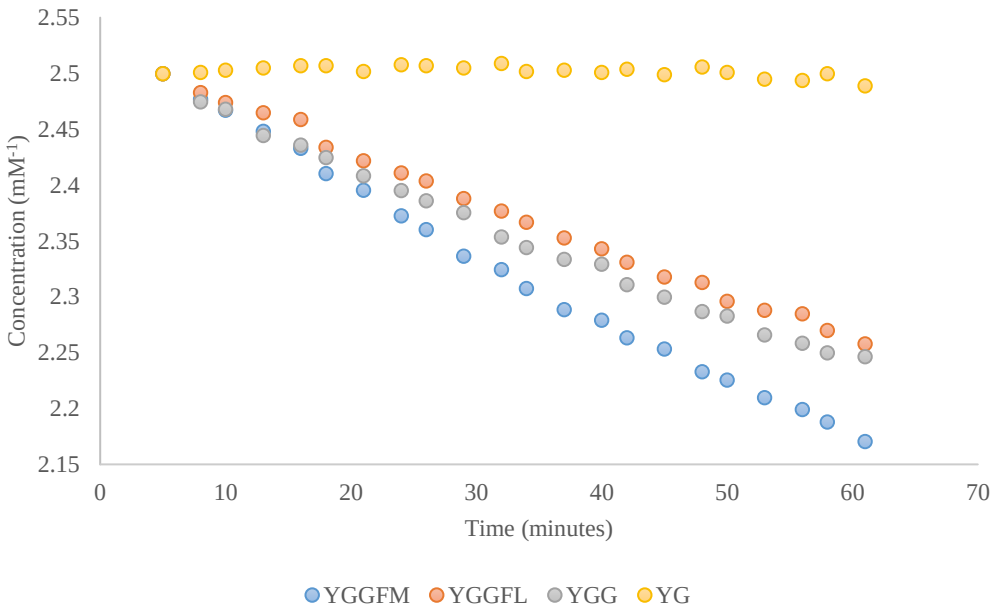

Figure 3.5.12: Graphical representation of the relative rates

3.6 Summary

To summarise, the results presented here show that of all the substrates which were tested only the met- and leu-enkephalin (YGGFM and YGGFL respectively) and substance P peptides were modified by the BV. Further analysis into a model peptide (YGG) for the enkephalin peptides showed that this peptide was hydrolysed between the GG bond forming YG and free G. The results also showed that the product, YG, was hydrolysed to form free tyrosine and free glycine, but comparatively slower.

The results here have indicated that the enzyme which may be responsible for this activity is a dipeptidyl peptidase (DPP) enzyme. From the literature it is known that a component in BV (known as Api m 5) shows sequence homology to the human dipeptidyl peptidase IV (DPP IV). Therefore the next step was to look for substrates which are related to the enkephalin peptides and may be substrates of a DPP IV enzyme.

Chapter 4

4.0 Characterisation of Peptidase Activity

4.1 Introduction

Following on from the substrate screening study for the peptidase activity, the next logical step was to look in more detail at other peptides which may be modified by the BV. From the previous results it was concluded that the BV appears to be targeting peptides like the enkephalin peptides. Therefore, this led to testing other opioid peptides (table 4.1.1). There are other opioid peptides (endorphins and dynorphins) which were not tested, as the first amino acids in the sequences of these peptides are that of met- and leu-enkephalin respectively. This is due to the expense of these other peptides.

Table 4.1.1: Experimental Peptides

Peptide	Amino Acid Sequence
Met-enkephalin	YGGFM
Leu-enkephalin	YGGFL
Substance P	RPKPQQFFGLM
Endomorphin I	YPWF
Endomorphin II	YPFF
Casomorphin 1-7	YPFPGPI
Nociceptin fragment	FGG

Opium is a substance which is found in poppy seeds of the *Papaver somniferum* poppy. This led to the discovery of the opioid system due to the analgesic and euphoric properties associated with opium.[112,172] The active ingredient present in opium is the strong analgesic morphine which has been used for many years as a pain killer.[112] The

opioid system plays a role in an array of different physiological responses such as nociception, emotional behaviour, stress, learning and memory and the reward system.[112,173]

Various endogenous opioid peptides have been discovered which include the endorphins, enkephalins, dynorphins and endomorphins.[114,172] Gene studies have been carried out and the precursor molecules for the enkephalins, endorphins and dynorphins have been deduced.[172] The gene for the precursor molecule of the endomorphins has not yet been deduced. Prepro-enkephalin (PENK), prepro-opiomelanocortin (POMC) and prepro-dynorphin (PDYN) are the respective genes which code for the precursor molecules for the enkephalin peptides, β-endorphin and the dynorphin peptides.[112,114,172]

The opioid peptides share a common amino acid sequence at the N-terminus which is known as the "opioid motif". This sequence is YGGF which is then extended towards the C-terminal in a range of 5 to 31 amino acid residues.[113,114,172] There is however an exception to this common N-terminal sequence as the endomorphin peptides do not contain this "opioid motif".[113] The endomorphin peptides are discussed further in section 4.1.2.

4.1.1 Opioid Receptors

The opioid receptors have been divided into three groups and these groups are known as the μ-opioid receptor (MOR), the δ-opioid receptor (DOR) and the κ-opioid receptor (KOR).[113,114,172] These receptors are encoded by the Oprm1, Oprd1 and Oprk1 genes respectively.[174] These receptor groups have been subdivided further giving the MOR subtypes as μ_1, μ_2, and μ_3, the DOR subtypes as δ_1 and δ_2 and the KOR subtypes as κ_1, κ_2 and κ_3.[172] Opioid receptors in humans are most commonly found in the cortex, limbic system and the brain stem.[112]

The endogenous opioid peptide ligands for these receptors have different affinities for different receptor subtypes. The enkephalin peptides have a ×20 higher affinity for the δ receptors than the μ receptors.[173] The endomorphin peptides have a high affinity for

the μ receptors and the β-endorphins have a higher affinity for the μ receptors. The dynorphin peptides preferentially bind to the κ receptors.[114,173] There has also been the discovery of another receptor which is known as the orphanin/nociception receptor (also known as OLR-1) with which an endogenous ligand has been termed oprhanin/nociceptin FQ.[175]

These receptors are membrane bound receptors with high sequence homology to the seven-helix bundle transmembrane G protein-coupled receptor family.[113,114,172,176] The G proteins these receptors couple to are the Go/Gi subtypes which produce the cellular effects.[172,173] These effects include inhibition in both the production of cyclic adenosine monophosphate (cAMP) and the N-type Ca^{2+} voltage gated channels. Hyperpolarization also occurs by exciting inward moving K^{+} channels.[114,172,173] This hyperpolarization results in reduced neuronal activity and the decrease in the intracellular Ca^{2+} concentration caused by inhibiting the Ca^{2+} channels resulting in decreased neurotransmitter release.[114,173] The different groups of substrates for these receptors will be discussed with the exception of the enkephalin peptides as these have already been discussed.

4.1.2 Endomorphins

There are two known endomorphin peptides which are termed endomorphin I and endomorphin II.[177] These peptides differ from each other by one amino acid with the endomorphin I amino acid sequence being YPWF and the endomorphin II amino acid sequence being YPFF.[177,178] Endomorphin I is found predominately in the brain and endomorphin II is found predominately in the spinal cord.[179] The endomorphin peptides acting on the μ-opioid receptors have an anti-nociception effect in the supraspinal, spinal and peripheral areas.[177,178,180]

The endomorphin peptides are metabolised by several enzymes such as the human dipeptidyl peptidase IV enzyme, which cleaves the Pro2-Trp3 bond in endomorphin I and the Pro2-Phe3 bond in endomorphin II.[181] This releases the dipeptides YP for both endomorphin I and II and WF for endomorphin I and FF for endomorphin II. This cleavage can also occur by the aminopeptidase M enzyme.[182] These dipeptides are then

further metabolised to free amino acids. Aminopeptidase P can cleave the Tyr1-Pro2 bond which releases free Y and leaves the tripeptides PWF for endomorphin I and PFF for endomorphin II.[183] Human carboxypeptidase Y and proteinase A enzymes convert the amide at the C-terminus of the endomorphin peptides into a carboxyl group. Hydrolysis then followed cleaving the Trp2-Phe3 bond in endomorphin I and FF bond in endomorphin II.[182] From BV genome studies a protein equivalent to the human DPP IV enzyme has been found.

4.1.3 Endorphins

The endorphins are perceived as the explanation for a "runner's high/runner's addiction" due to their hypoalgesic effects.[184] Post translational processing of the prepro-opiomelanocortin (POMC) precursor releases several active peptides which includes β-lipotropin, β-endorphin, adrenocorticotropic hormone (ACTH), melanocyte stimulating hormone (MSH) and γ-lipotropin.[185,186] β-endorphin is released from the pituitary gland during exercise, pain and excitement.[187] β-endorphin produces euphoric and analgesic effects when released.[172] The amino acid sequence of β-endorphin is:

YGGFMTSEKSQTPLVTLFKNAIIKNAYKKGE.[114]

The β-endorphin amino acid sequence is part of the β-lipotropin amino acid sequence, specifically amino acids 61-91. [185] The release of β-endorphin normally results in increased ACTH levels, which is an indication of a stress response to exercise.[184] Studies have shown that β-endorphin is metabolised by the insulin-degrading enzyme which cleaves the F18-K19 bond followed by the L17-F18 bond. This produces the α–endorphin (β-endorphin amino acids 1-16) and γ–endorphin (β-endorphin amino acids 1-17) fragments.[188] These peptides were not studied in this project due to their cost. However, as the first five amino acids (YGGFM) of the β-endorphin peptide is met-enkephalin it is likely that these peptides would be modified by BV.

4.1.4 Dynorphins

There are multiple peptides known so far which make up the dynorphin family of peptides. The peptides released after cleavage of the precursor prodynorphin by the enzyme proprotein convertase 2 (PC) are dynorphin A, dynorphin B and α/β neo-endorphin.[114,189] There are also varying lengths of the amino acid sequence of dynorphin A (DYN A) and dynorphin B (DYN B) peptide which are shown in table 4.1.4.1.

The first five amino acids from the N-terminus is the amino acid sequence of leu-enkephalin, which is found in all of these peptides. These peptides act via the κ-opioid receptor in both the central and peripheral nervous systems.[172,189,190] The dynorphins are involved in the physiological actions pain, learning and memory, stress and emotion.[189] It is thought that the action of dynorphins in certain areas of the brain result in an involvement in drug addiction.[191] This has therefore been an area of study to understand drug addiction.

The metabolism of the dynorphin peptides is complex and involves several enzymes. Studies have suggested that there are aminopeptidases involved in the degradation of the dynorphin peptides. One study showed that puromycin-sensitive aminopeptidase and aminopeptidase M showed specificity for the dynorphin peptides.[192] One study also showed that the human angiotensin-converting enzyme-related carboxypeptidase (ACE_2) was involved in the hydrolysis of dynorphin 1-13.[193] A dynorphin-converting endopeptidase has been found in the human spinal cord and shows specificity for the dynorphin B peptide. It cleaves the Arg6-Arg7 bond to release YGGFLR.[194,195] Similarly to the endorphin peptides these peptides were not studied in this project due to their cost. However, as the first five amino acids (YGGFL) of the dynorphin peptides is leu-enkephalin there is a strong possibility that these peptides would be modified by BV.

Table 4.1.4.1: Name and amino acid sequence of peptides derived from the precursor prodynorphin[196]

Peptide Name	Amino Acid Sequence
DYN A 1-8	YGGFLRRI
DYN A 1-13	YGGFLRRIRPKLK
DYN A 1-17	YGGFLRRIRPKLKWDNQ
DYN B 1-13	YGGFLRRQFKVVT
Big-DYN	YGGFLRRIRPKLKWDNQKRYGGFLRRQFKVVT
α-neo-endorphin	YGGFLRKYPK
β-neo-endorphin	YGGFLRKYP
Leumorphin	YGGFLRRQFKVVTRSQEDPNAYYEEDPNAYYEELFDV

4.1.5 Orphanin FQ/Nociceptin

Orphanin FQ (OFQ/N), which is sometimes referred to as nociceptin, has an amino acid sequence of FGGFTYARKSARKLANQ.[197] This peptide has a significant sequence homology to the dynorphin A peptide.[175,198] OFQ/N however has little affinity for the μ-, δ- and κ-opioid receptors.[199] The receptor that OFQ/N acts on is called opioid receptor-like 1 (ORL_1) which has a significant sequence homology to the opioid receptors.[200] The cellular action of OFQ/N is similar to that of the opioid peptides, which is inhibition of cAMP production and activation of K^+ channels.[201]

The OFQ/N peptide can be hydrolysed by the aminopeptidase N (APN) enzyme, which cleaves the FG bond to release free F. This activity is blocked in the presence of APN inhibitors. Endopeptidase 24.15 is also involved in the hydrolysis of OFQ/N by cleaving the Ala7-Arg8, Ala11-Arg12 and Arg12-Lys13 bonds.[202] For this project the full peptide was not studied due to expense. However, a small fragment (FGG) of this peptide was used instead. This fragment was not a good model for the nociception peptide as there are four positive charges in this peptide (attributed to the Lys and Arg amino acids) which could affect entry to the catalytic site.

4.1.6 Exogenous Opioid Peptides

There are a number of bioactive peptides which can be found in dairy products such as milk. These bioactive peptides include casomorphins, lactorphins, lactoferroxins, casoxins, casokinins and others.[203] In the literature there are review articles which discuss all of these bioactive peptides. However, for the purpose of this work only the casomorphins will be discussed.[203,204] One group of these peptides is known as the β casomorphins and consist of fragments of a precursor protein, β-casein.[205] The β casomorphin fragments are found in the 60-70 amino acid region (YPFPGPIPNSL) of the β-casein sequence.[203,205] Many fragments can be released from this short sequence, these are listed in table 4.1.6.1. These fragments predominately act on the μ opioid receptors upon release.[203,205,206] The casomorphins are hydrolysed by the human dipeptidyl peptidase IV enzyme. This enzyme cleaves the Pro2-Phe3 bond releasing the dipeptide Tyr1-Pro2.[207,208] It would continue to sequentially cleave after each proline residue in the sequence.

Table 4.1.6.1: Fragments from the β Casein Protein

Peptide Name	Amino Acid Sequence	Precursor Fragment	Reference
β casomorphin-5	YPFPG	β casein amino acids 60-64	205
β casomorphin-7	YPFPGPI	β casein amino acids 60-66	205
β casomorphin-11	YPFPGPIPNSL	β casein amino acids 60-70	209

4.1.7 Gly-Pro-7-amido-methylcoumarin

Another substrate which was of interest to test was that of GP-7-amido-4-methylcoumarin hydrobromide. This substrate will be referred to as GP-X where X is 7-amido-4-methylcoumarin hydrobromide. The human dipeptidyl peptidase (DPP) IV enzyme shows specificity for this substrate. This substrate has a proline residue which is a desirable diagnostic indicator for the human DPP IV enzyme. The human DPP IV enzyme has optimal activity against substrates with proline at the penultimate position.[59] The structure of this molecule is shown in figure 4.1.7.1. Genetic studies have indicated that an enzyme similar to human DPP IV is present in BV. A study, previously mentioned, has also shown that an enzyme similar to the human DPP IV enzyme was responsible for the conversion of pro-melittin to melittin.[30] Testing this substrate with BV will therefore help to confirm if the DPP IV-like enzyme (Api m 5) in BV is the enzyme responsible for the modifications of the substrates tested so far.

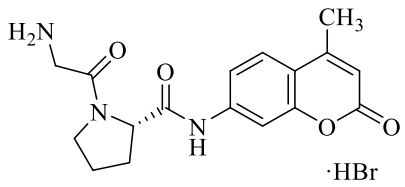

Figure 4.1.7.1: Structure of GP-7-amido-4-methylcoumarin hydrobromide

4.1.8 Kinetics Experiments

Enzyme kinetics experiments will then be carried out. These experiments are a useful way to look at how an enzyme works in action as they provide information such as the mechanism of action. The Michaelis-Menten equation is way of describing the rate of enzyme action by relating the initial reaction velocity (V_0) to the substrate concentration [S].[210] The following equation is the Michaelis-Menten equation:

$$V = \frac{Vmax[S]}{Km + [S]}$$

Where Km is the substrate concentration at which the reaction rate is half of Vmax, and Vmax is the maximal rate of the reaction. There are certain assumptions made when applying the Michaelis-Menten equation to an enzyme reaction, namely:

- The concentration of substrate [S] is much larger than the concentration of enzyme [E].
- A steady state is formed i.e. the rate of formation of enzyme-substrate [ES] is equal to the rate of dissociation of [ES].

4.2 Experimental

4.2.1 Materials

Endomorphin I & II, and casomorphin 1-7 were all purchased from Sigma Aldrich. FGG was purchased from Bachem. GP-7-X was purchased from Apollo Scientific Ltd.

Details of the sample preparation and instrumentation have already been described in sections 2.2 and 3.2 so will therefore not be discussed here. Table 4.2.1.1 shows the details of the solutions used in BV/substrate experiments (opioid peptides and human DPP IV substrate). The mole ratios for all the BV/substrate experiments are shown in table 4.2.1.2.

Table 4.2.1.1: Solution mixing details for substrate reactions

Substrate	Stock Substrate Concentration (mM^{-1})	Working Substrate Concentration (mM^{-1})	Stock BV Concentration (mg/ml)	Working BV Concentration (mg/ml)
YPWF	4.1	2.05	5.11	1.28
YPFF	1	0.5	1.02	0.255
YPFPGPI	3.2	1.6	5.11	1.25
FGG	5	2.5	5.11	1.28
GP-X	5	2.5	5.28	1.32

Table 4.2.1.2: Ratios of BV to substrate for each experiment

Experiment	Ratio (BV:Substrate)
BV + YPWF	1.3:2.1
BV + YPFF	1.2:2
BV + YPFPGPI	1.3:1.6
BV + FGG	1.3:2.5
BV + GP-X	1.3:2.5

The NMR method used for the BV + GP-X experiment was slightly different from the @es1d_k experiment used for all other acquisitions. For this experiment a pure echo with water suppression experiment (@PEW5_k) was used which improved the quality of the data for this sample. This NMR method is described by Adams, R. W. et al., 2013.[211] There were different D20 delays used for this experiment, these are shown in table 4.2.1.3.

Table 4.2.1.3: Pre-acquisition delays

D20
0.5 s for 75 spectra
10 s for 40 spectra
600 s for 20 spectra
900 s for 20 spectra
1200 s for 20 spectra

4.3 Results

The results of the additional opioid peptides (endomorphin I and II and casomorphin 1-7) will be reported first, followed by the results from the human DPP IV substrate experiment and finally the kinetic experiments will be reported. The opioid substrate experiments were carried out in the same way as the reactions in the substrate screening study. The details of the substrate/BV solutions are shown in table 4.2.1.1. The FGG tripeptide (figure 4.3.1) was used as a model peptide for the nociception peptide as a cheaper alternative.

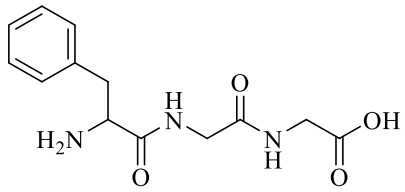

Figure 4.3.1: Structure of FGG

4.3.1 Results of Other Opioid Substrate Experiments

4.3.1.1 Stability

Controls of all the opioid substrates showed that they were all stable in the phosphate buffer solution used (pH 7.4). The NMR spectra of all the stable opioid substrates are found in appendix 4.

4.3.1.2 Results for YPWF

The ^{1}H NMR results for the reaction of BV with YPWF are shown in figure 4.3.1.2.1. At the end of the analysis period it is clear that the initial structure has been completely modified. This is due to the complete disappearance of signals which relate to the intact YPWF peptide. This substrate, along with two others tested (YPFF and YPFPGPI) have a common N-terminal sequence of Y-P-X where X is either W or F (see table 4.1.1). The FGG peptide is an exception to this as the N-terminal sequence is different. Proline residues can adopt two different conformations (cis and trans). The YPFPGPI peptide has three proline residues meaning it has 2^3 possible conformations. This is important to consider as certain conformations may react more than others. However, it appears from the results of all three substrates that conformation is not an issue. These conformations make it difficult to establish the specific pathway by which BV modifies these peptides due to the presence of signals for each conformation.

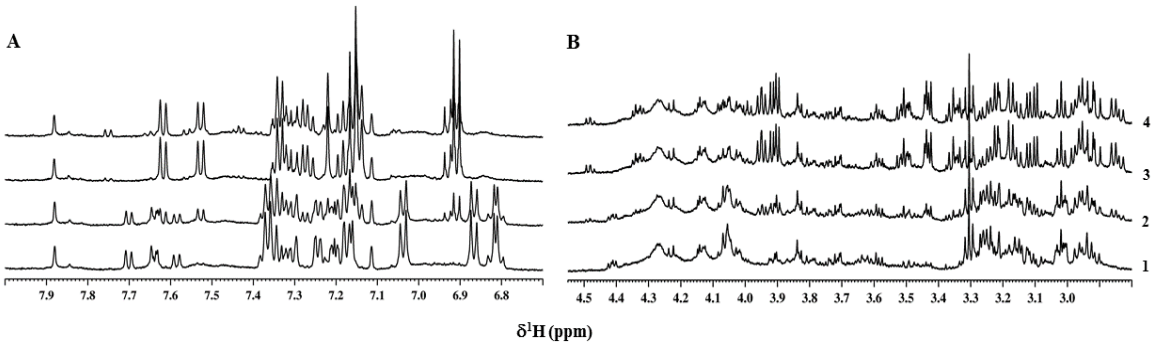

Figure 4.3.1.2.1: ^{1}H BV + YPWF aromatic (A) and aliphatic (B) region showing spectrum 1 (0 hours), 2 (after 1 hour), 3 (after 6 hours) and 4 (after 15 hours).

Shown in figure 4.3.1.2.2 is a graphical representation of the BV + YPWF reaction. The integral represented by δ 7.73 – 7.67 ppm is a signal from the intact substrate and relates to the W amino acid, which decreases as the peptide is modified. This leads to the development of a product which is represented by the integral at δ 7.55 – 7.50 ppm; this signal also relates to the W amino acid. Comparison of the YPWF ^{1}H spectrum to the ^{1}H spectrum of the YPFF spectrum, confirms that these signals must relate to W as they are not present in the YPFF spectrum which does not contain a W amino acid.

From the graph it is clear to see that the intact endomorphin I peptide is completely modified after 5 hours. Modification of the product formed can also be seen as the product line in the graph increases, plateaus off and then starts to slowly decrease.

As previously mentioned there is a lag phase of *ca.* 15 minutes associated with this experiment due to the time it takes from mixing BV with the substrate to starting analysis. See previous note regarding the levelling out of the graphs towards the end of this experiment and also the difference in molar balance (section 3.4.1).

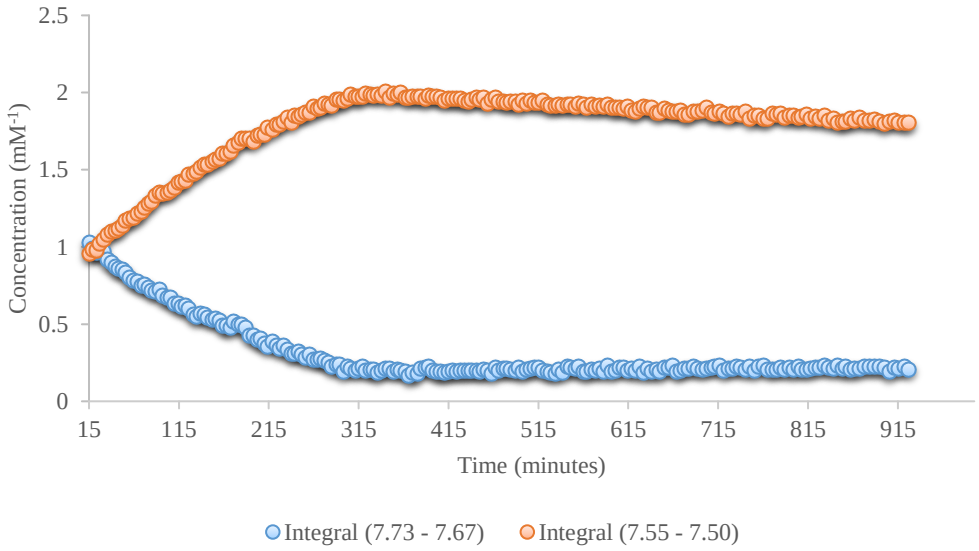

Figure 4.3.1.2.2: Degradation of YPWF by BV. Integral 7.73 – 7.67 ppm represents protons on an amino acid residue in YPWF peptide. Integral 7.55 – 7.50 ppm represents protons on product molecule.

4.3.1.3 Results for YPFF

The ^{1}H data for YPFF in the presence of BV is shown in figure 4.3.1.3.1. The data shows that the YPFF peptide is modified by BV, as signals relating to the unaltered peptide completely disappear along with the appearance of new signals relating to the modified peptide.

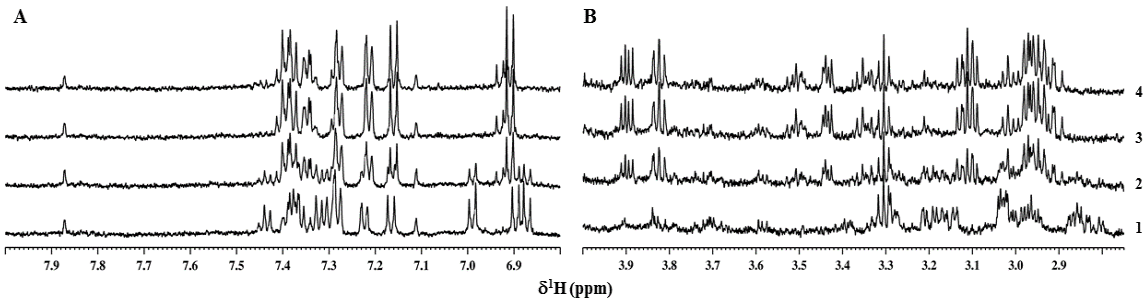

Figure 4.3.1.3.1: ^{1}H BV + YPFF aromatic (A) and aliphatic (B) region showing spectrum 1 (0 hours), 2 (after 1 hour), 3 (after 6 hours) and 4 (after 15 hours).

Shown in figure 4.3.1.3.2 is a graphical representation of the BV + YPFF reaction. The integral represented by δ 7.02 – 6.96 ppm is a signal from the Y amino acid in the intact substrate, which decreases as modification occurs. This leads to the development of a product which is represented by the integral at δ 3.93 – 3.87 ppm which relates to the alpha carbon in the Y amino acid in the modified peptide. From the graph it is clear to see that the intact YPFF peptide is completely modified after 3.5 hours. See previous note regarding the levelling out of the graphs towards the end of this experiment and also the difference in molar balance (section 3.4.1).

Comparing this to the BV + YPWF reaction it appears that this peptide is modified at a slower rate. This is a good comparison as the mole ratios of both of these reactions are almost identical (see table 4.2.1.2). However for a better understanding of which peptide is modified quicker, the enzyme kinetics will have to be determined.

The graph for the BV + YPFF reaction (figure 4.3.1.3.2) shows that the data points are not as close together when compared with the BV + YPWF reaction graph (figure

4.3.1.2.2). This is due to the smaller concentration of endomorphin II being used meaning there is more noise in the NMR spectra.

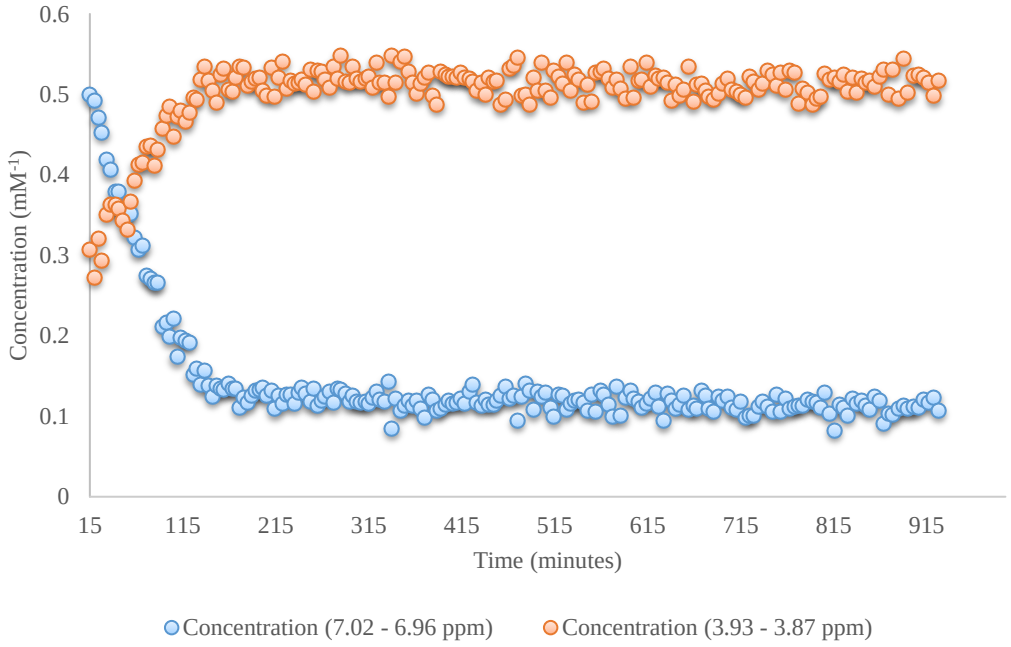

Figure 4.3.1.3.2: Degradation of YPFF by BV. Integral 7.02 – 6.96 ppm represents equivalent protons on Y in YPFF peptide. Integral 3.93 – 3.87 ppm represents protons on product molecule.

4.3.1.4 Results for YPFPGPI

The ^{1}H data for YPFPGPI in the presence of BV is shown in figure 4.3.1.4.1. The data shows that the YPFPGPI peptide is modified by BV, as signals relating to the unaltered peptide completely disappear along with the appearance of new signals relating to the modified peptide.

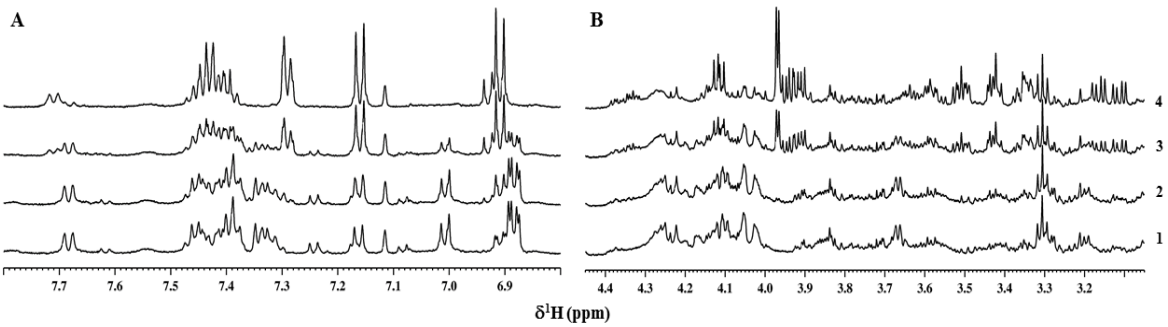

Figure 4.3.1.4.1: ^{1}H BV + YPFPGPI aromatic (A) and aliphatic (B) region showing spectrum 1 (0 hours), 2 (after 1 hour), 3 (after 6 hours) and 4 (after 15 hours).

Shown in figure 4.3.1.4.2 is a graphical representation of the BV + YPFPGPI reaction. The integral represented by δ 6.90 – 6.86 ppm is a signal from the Y amino acid in the intact substrate which decreases as modification occurs. This leads to the development of a product which is represented by the integral δ 3.98 – 3.96 ppm which relates to the P amino acid in the modified peptide. From the graph it is clear to see that the intact YPFPGPI peptide is completely modified after 15 hours. There is a point on the graph which is an outlier; this could have been caused by an instrumentation error. See previous note regarding the levelling out of the graphs towards the end of this experiment and also the difference in molar balance (section 3.4.1). A comparison of these results to the YPWF and YPFF experiments show that YPFPGPI is modified at a slower rate. The change in chemical shift of the aromatic signals associated with the tyrosine residue when compared with YPFF could be due to the differences in concentration of the substrate used.

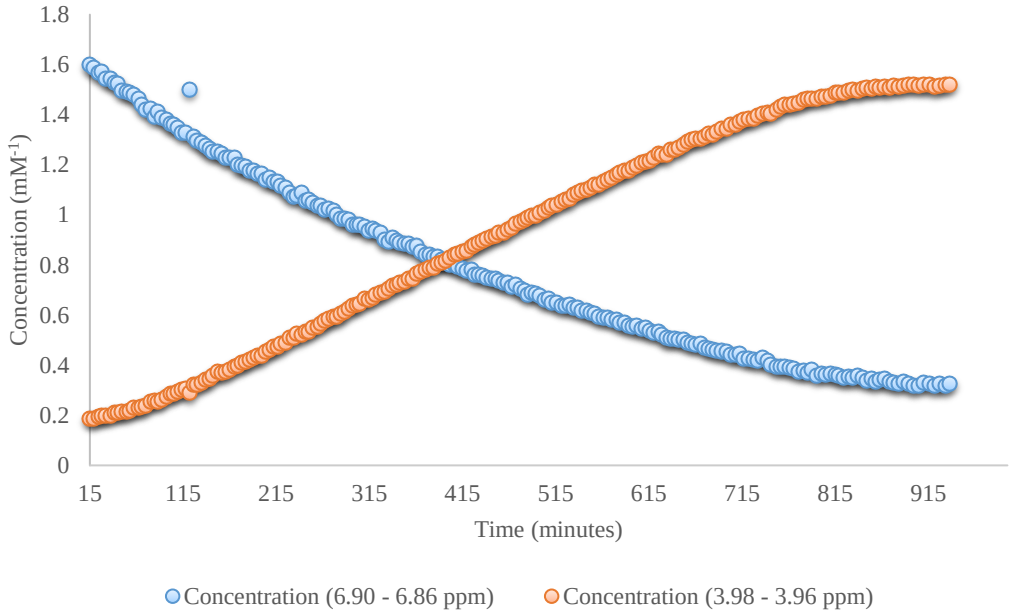

Figure 4.3.1.4.2: Degradation of YPFPGPI by BV. Integral 6.90 – 6.86 ppm represents equivalent protons on Y in YPFPGPI peptide. Integral 3.98 – 3.96 ppm represents protons on product molecule.

4.3.1.5 Results for FGG

The results of the reaction of BV with the nociceptin fragment, FGG, are shown in figure 4.3.1.5.1. The FGG peptide showed similar results to the YGG peptide (previously discussed, section 3.5) which showed the development of a free glycine signal (at δ 3.58 ppm) meaning the GG bond was hydrolysed. This result therefore suggests the same enzyme responsible for the YGG hydrolysis is the same for FGG hydrolysis.

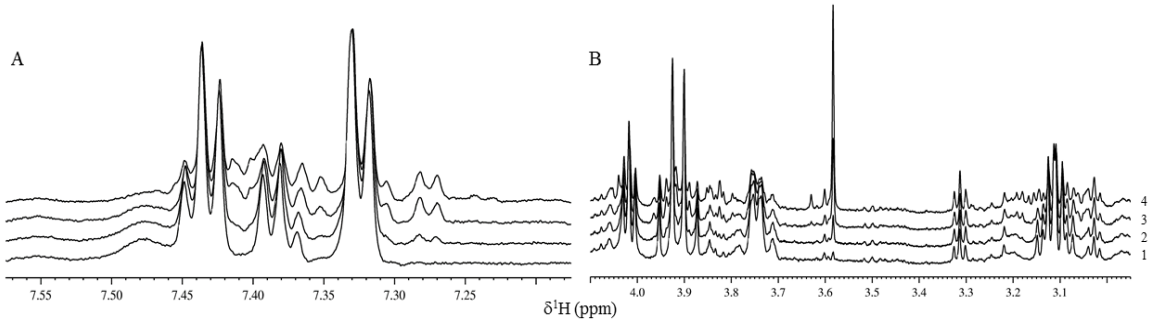

Figure 4.3.1.5.1: ^{1}H BV + FGG aromatic (A) and aliphatic (B) region showing spectrum 1 (0 hours), 2 (after 1 hour), 3 (after 6 hours) and 4 (after 19 hours).

Figure 4.3.1.5.2 shows a full signal assignment of the FGG peptide with the details of the assignment shown in table 4.3.1.5.1. As mentioned for previous signal assignments a comparison was made of small fragments (figure 3.4.1.4) to deduce the signal assignment of FGG without carrying out 2D experiments.

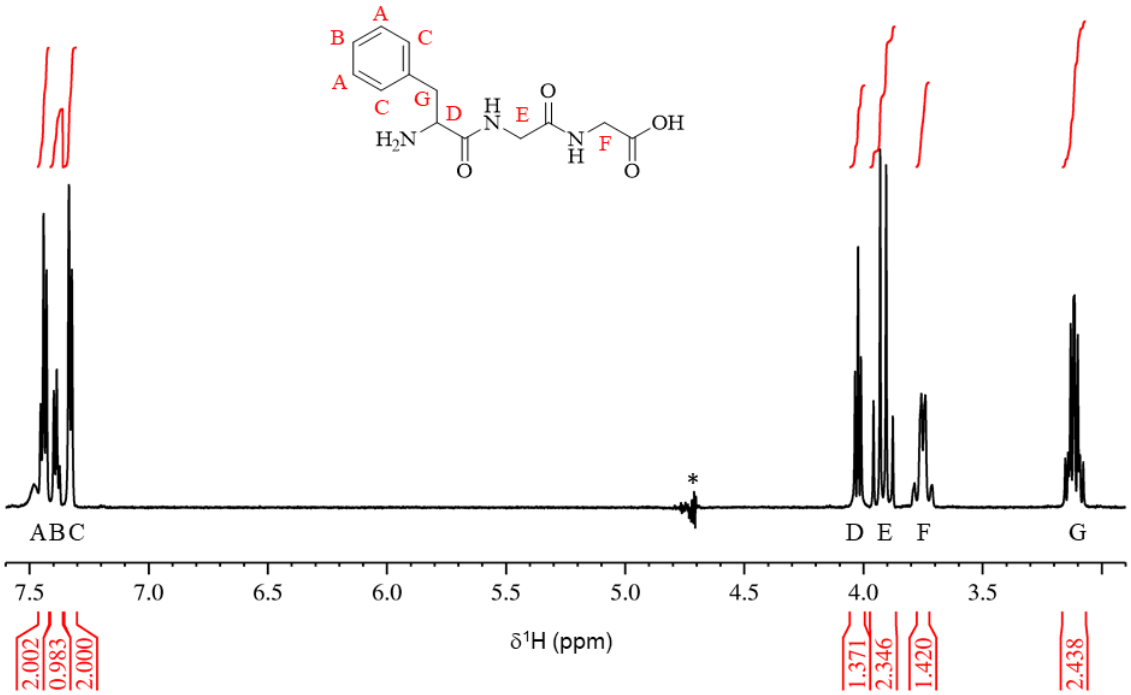

Figure 4.3.1.5.2: ^{1}H signal assignment of FGG Peptide, the signal denoted with * is the signal which arises from the solvent.

Table 4.3.1.5.1: FGG ^{1}H signal assignment details

^{1}H Label	^{1}H Integral	δ (ppm)	J_{HH}-coupling (Hz)	Multiplicity
A	2	7.44	7.56	t
B	1	7.38	7.32	t
C	2	7.32	7.35	d
D	1	4.02	7.41	t
E	2	3.94	16.95	dd
		3.88	16.72	
F	2	3.77	17.39	dd
		3.72	16.59	
G	2	3.13	7.14, 13.83	dd
		3.09	7.95, 13.71	dd

The results of the hydrolysis of FGG by BV is shown graphically in figure 4.3.1.5.3. This figure shows the development of the free G which is represented by δ 3.60 – 3.57 ppm. Also shown is the decrease of one of the F signals which is represented by δ 7.35 – 7.30 ppm. See previous note regarding the levelling out of the graphs towards the end of this experiment and also the difference in molar balance (section 3.4.1). Figure 4.3.1.5.4 shows the cleavage pathway for this enzyme.

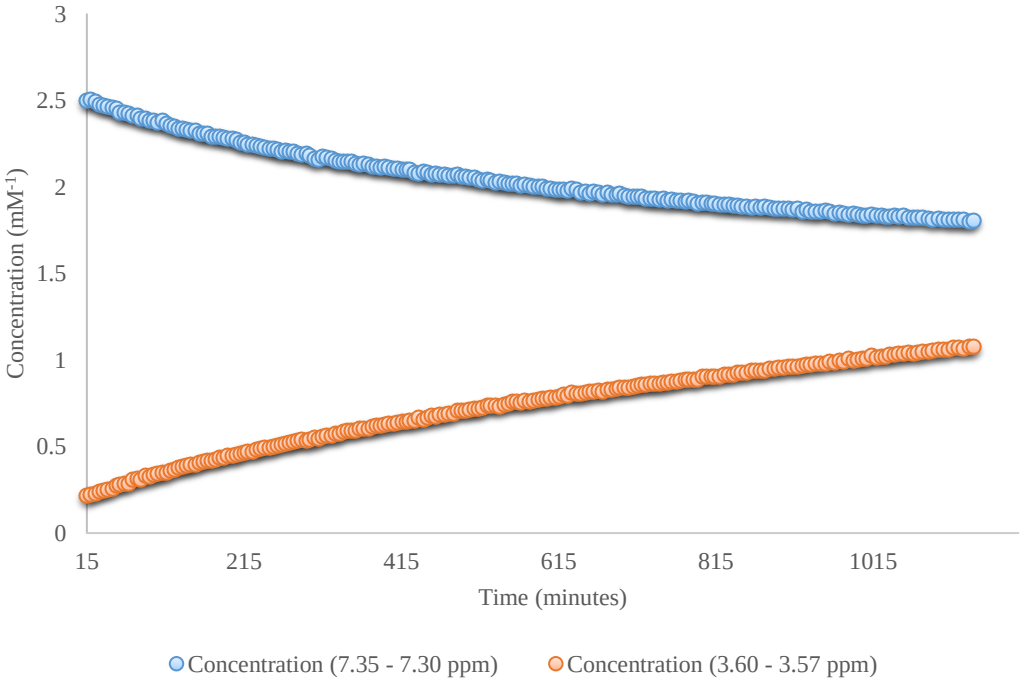

Figure 4.3.1.5.3: Degradation of FGG by BV. Integral 7.35 – 7.30 ppm represents equivalent protons on F in FGG peptide. Integral 3.60 – 3.57 ppm represents protons on product molecule.

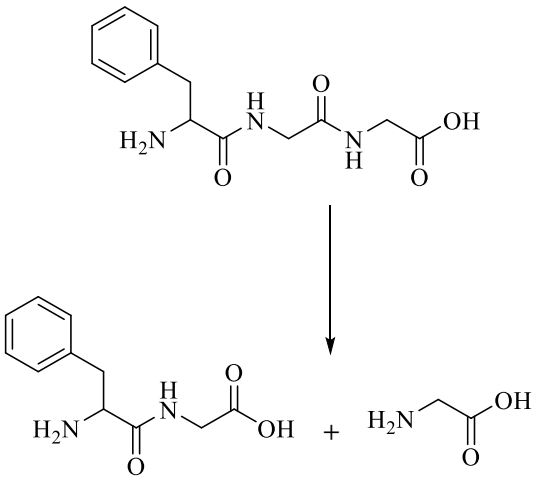

Figure 4.3.1.5.4: Cleavage pathway of FGG

A comparison of the crossover times for all the peptides analysed in this study are shown in table 4.3.1.5.2. The crossover time is that point at which 50 % of the intact peptide has been modified by BV. The results show that YPWF is modified the quickest with FGG being modified the slowest. As the YPWF peptide is modified quicker than the YPFF this suggests that the BV enzyme works optimally with the W amino acid residue at the penultimate position over F.

Table 4.3.1.5.2: 50 % Peptide Modification Times

Peptide	Crossover Time (mins)
YPWF	15
YPFF	50
YPFPGPI	393
FGG	> 1145

4.3.2 Results of Human DPP IV Substrate – GP-X

The details of the solutions used for this experiment are shown in table 4.2.1.1. Figure 4.3.2.1 shows the results from the control experiment of this substrate. The control shows that this molecule is slowly modified over time. Within the aromatic region two new doublets appear at *ca.* δ 7.53 and 6.79 ppm along with two new singlets at *ca.* δ 6.62 and 6.08 ppm. From these data it appears that the modification of GP-X is occurring at the Pro-7-amido-4-methylcoumarin bond of the molecule as the signals in the aromatic region reflect this part of the molecule. This would result in the formation of an NH_2 on the free methylcoumarin part of the cleaved molecule (figure 4.3.2.2). This therefore affects the chemical shift values of the protons on the benzene ring which result in the formation of new signals in the aromatic region. There are also some notable changes within the aliphatic region where there is also the development of new signals.

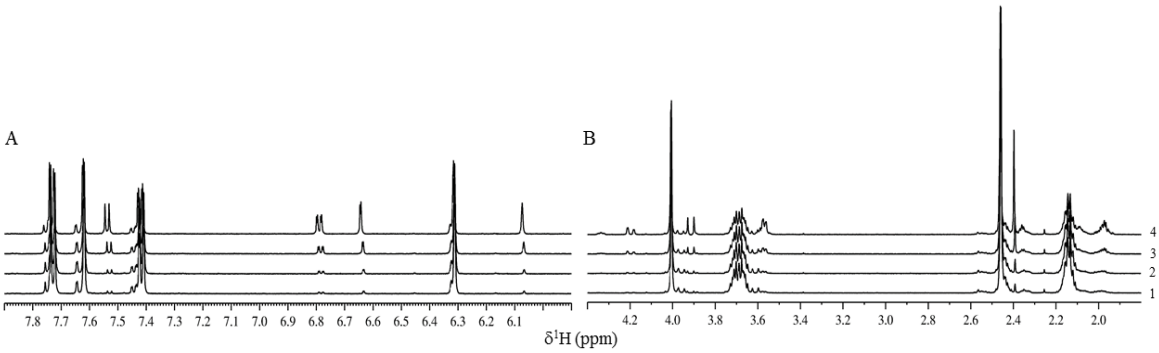

Figure 4.3.2.1: ^{1}H GP-X in buffer aromatic (A) and aliphatic (B) region showing spectrum 1 (0 hours), 2 (after 1 hour), 3 (after 6 hours) and 4 (after 19 hours).

In the presence of BV GP-X is also modified. The results of the BV + GP-X experiment showed that GP-X was completely modified within 3.5 hours. The ^{1}H NMR results of this are shown in figure 4.3.2.3 which shows the complete disappearance of several signals in both the aromatic and aliphatic region which represent GP-X before modification.

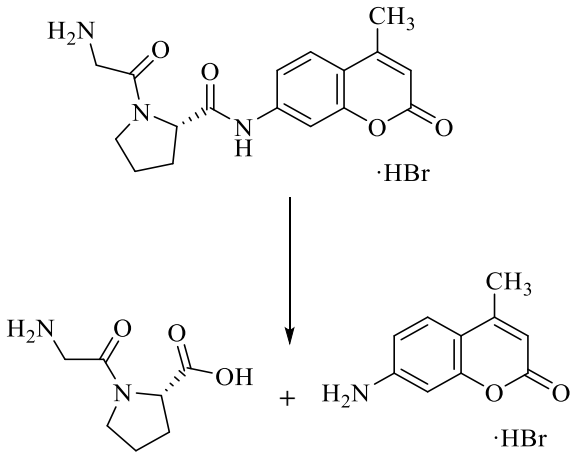

Figure 4.3.2.2: Cleavage pathway of GP-7-amido-4-methylcoumarin hydrobromide

The signals appearing at *ca.* δ 6.7 – 6.8 ppm appear at a slightly different chemical shift when compared with the control in figure 4.3.2.1. This could be caused by the presence of BV.

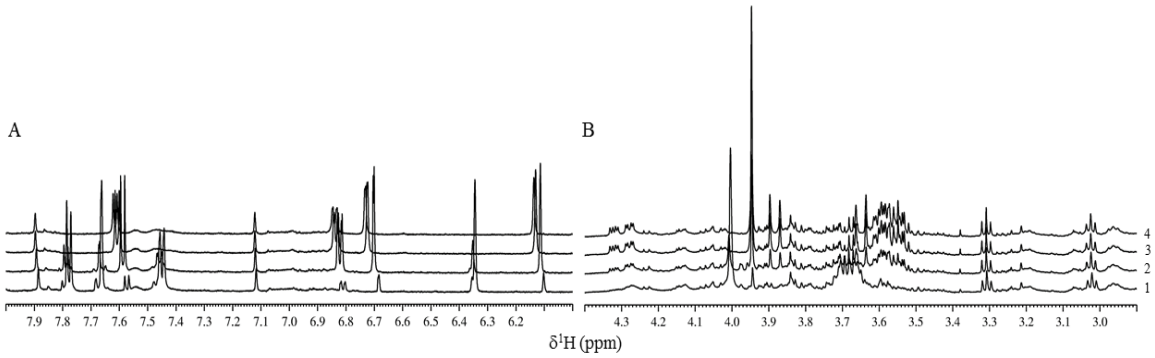

Figure 4.3.2.3: ^{1}H BV + GP-X aromatic (A) and aliphatic (B) region showing spectrum 1 (0 hours), 2 (after 1 hour), 3 (after 6 hours) and 4 (after 19 hours).

Figure 4.3.2.4 shows a graphical representation of the modification of GP-X by BV. The signal δ 7.50 – 7.40 ppm represents one of the protons found on the methylcoumarin part of the intact molecule and the δ 7.61 – 7.56 ppm signal represents one of the protons from the methylcoumarin part of the modified molecule. The

product signal (δ 7.61 – 7.56 ppm) shows an increase and then begins to decrease meaning there is further modification of the product molecule. This is possibly due to another enzyme found in the BV.

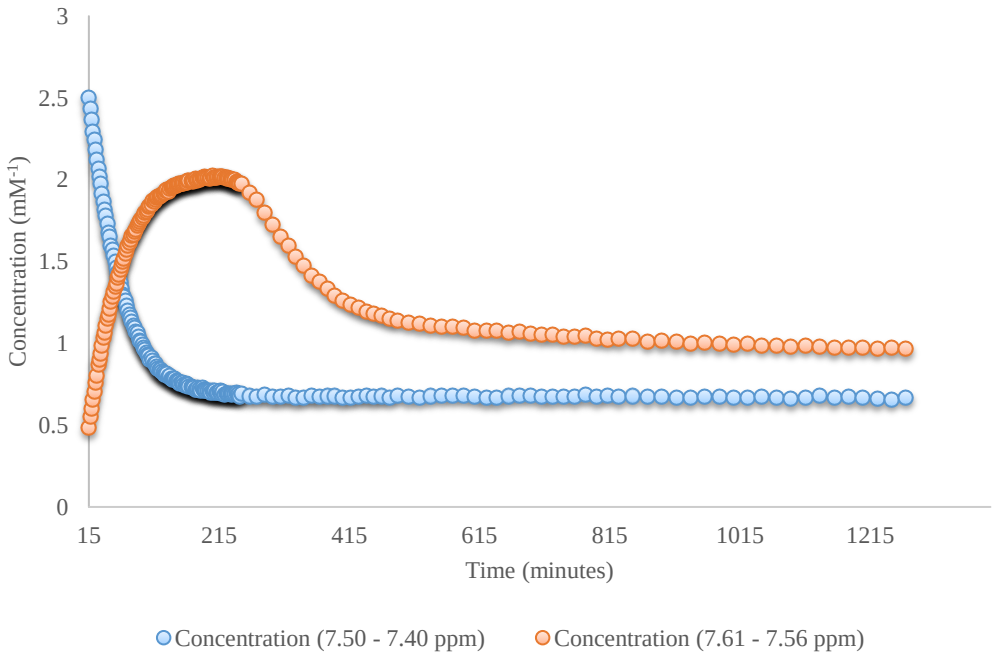

Figure 4.3.2.4: Graphical representation of GP-X in the presence of BV. Integral 7.50 – 7.40 ppm represents protons on an amino acid residue in GP-X. Integral 7.61 – 7.56 ppm represents protons on product molecule.

A graphical representation showing a comparison between GP-X control and the GP-X + BV is shown in figure 4.3.2.5. It is clear that in the presence of BV GP-X is modified much quicker than the slow modification of GP-X in buffer. There is a steep decline of the signal relating to intact substrate in the presence of BV compared with the control which is much slower.

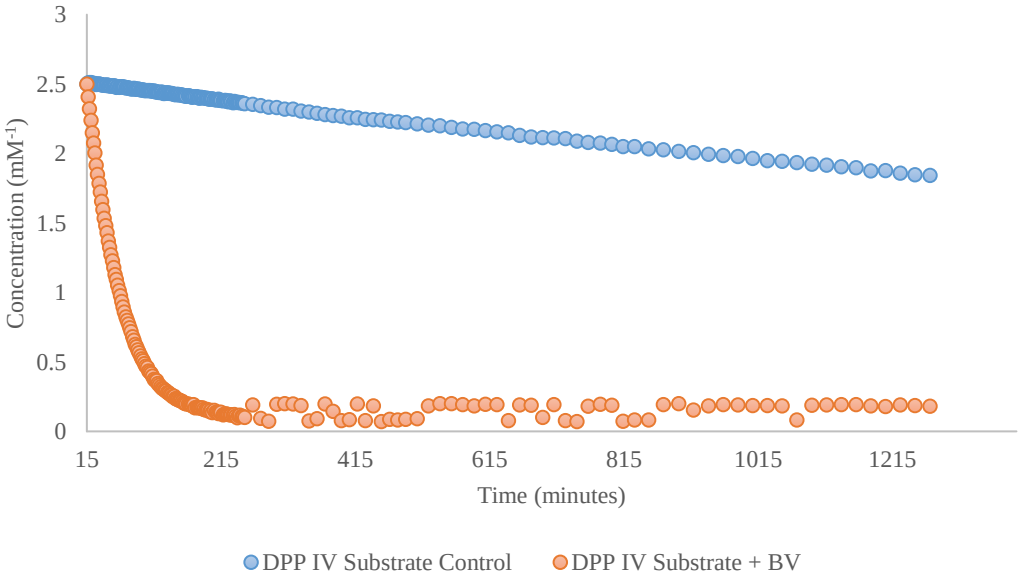

Figure 4.3.2.5: Comparison of GP-X in buffer with GP-X in the presence of BV.

4.3.3 Results of Michaelis-Menten Kinetics Experiments

For the enzyme kinetics experiments the concentration of BV was kept constant and the substrate concentration was varied. The details of the solutions used for the enzyme kinetic experiments are shown in table 4.3.3.1. The substrates used were YGG, FGG, YGGFM and YGGFL. These were used as they were the cheapest peptides which were shown to be modified by BV.

The kinetics experiment reactions were only run for *ca.* 2 hours to obtain the initial reaction velocity. Substrate solutions were always sonicated at 37 °C for 15 minutes beforehand to ensure they were fully dissolved and degassed. The kinetics values to be obtained are the Vmax and Km. From the point of mixing the substrate with the BV and transferring the mixture into the NMR probe there is a delay of approximately 10 to 15 minutes. This means that capturing the very beginning of the reaction was lost due to this delay. The results shown here are therefore less accurate than if a stop flow method for the NMR was used. The results will however still give a good indication of the enzyme behaviour.

Table 4.3.3.1: Solution mixing details for YGG, YGGFM, YGGFL and FGG kinetics experiments

Stock Substrate Concentration (mM^{-1})	Working Substrate Concentration (mM^{-1})	Stock BV Concentration (mg/ml)	Working BV Concentration (mg/ml)
5	2.5	5.11	1.28
2.5	1.25	5.11	1.28
1	0.5	5.11	1.28
0.5	0.25	5.11	1.28
0.4	0.2	5.11	1.28
0.25	0.125	5.11	1.28

4.3.3.1 Kinetics results for YGG

This method was initially optimized using the YGG peptide as it was a cheaper model peptide for the enkephalin peptides (met- and leu-enkephalin). The results of this experiment initially produce a graph (figure 4.3.3.1.1) which shows that as substrate concentration increases the initial velocity increases until there is saturation of the enzyme. To obtain the kinetics values the reciprocal of this graph is taken which produces a straight line (figure 4.3.3.1.2), known as a Lineweaver-Burk plot. The graph is fitted with a line of best fit and then extrapolated back until it crosses the X-axis, this gives -1/Km and where the line crosses the Y-axis gives 1/Vmax. There are no error bars shown in figure 4.3.3.1.1 as this experiment was only repeated once due to the cost and time of carrying out these experiments. This is same for all of the kinetics experiments discussed in the remained of this chapter.

To obtain the results for the BV + YGG reaction, the development of the free glycine signal at *ca.* δ 3.58 ppm was used. In table 4.3.3.1.1 the results from the MNOVA output are detailed. The initial velocity for YGG hydrolysis was calculated as follows:

$$\frac{C2 - C1}{T2 - T1}$$

where C2 is the concentration of free glycine after 15 minutes and C1 is the free glycine concentration at initial mixing (0 mM). T2 is 15 minutes after mixing and T1 is time 0. The Lineweaver-Burk plot for YGG shows that the Km is 0.111 mM^{-1} and the Vmax is 0.0172 mM/min^{-1}.

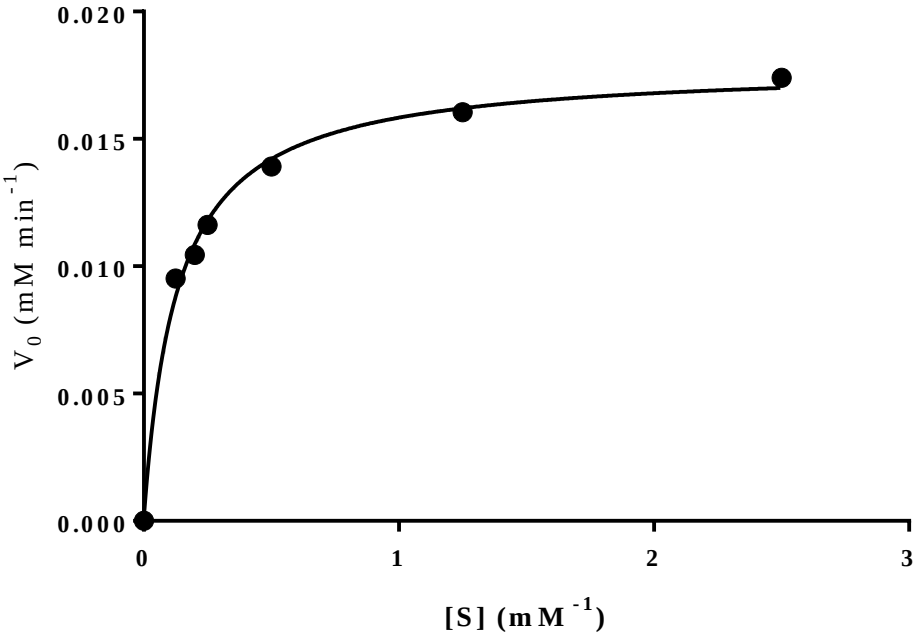

Figure 4.3.3.1.1: BV + YGG kinetics experiment results.

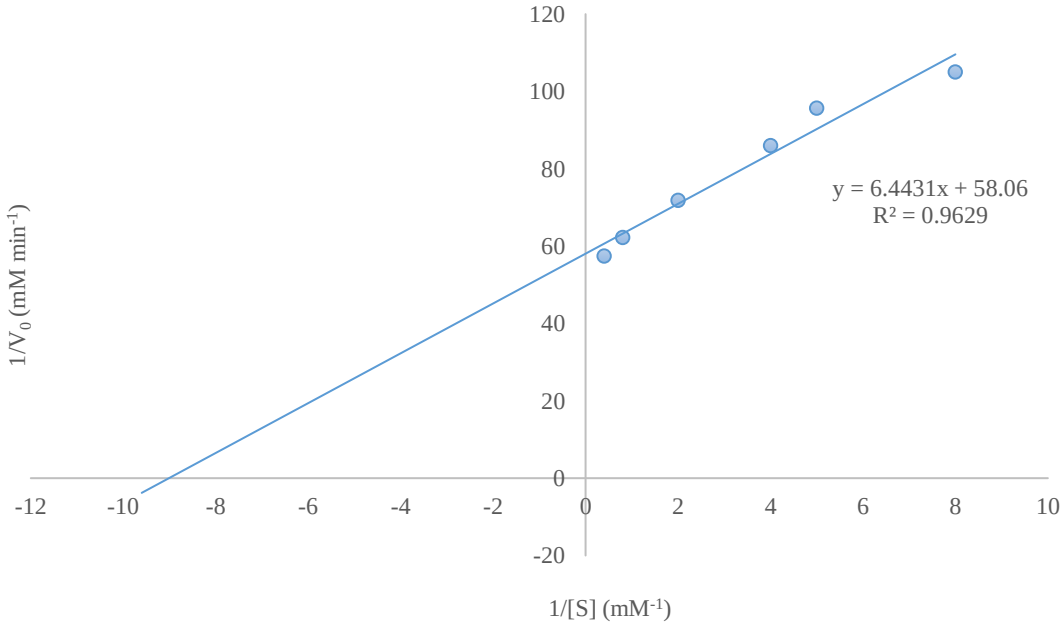

Figure 4.3.3.1.2: Lineweaver-Burk Plot of the BV + YGG reaction

Table 4.3.3.1.1: MestReNova Output of BV + YGG

Initial Concentration of YGG (mM^{-1})	Concentration of Free Glycine after 15 mins (mM^{-1})	Initial Velocity (V_0) (mM/min^{-1})
2.5	0.261	0.0174
1.25	0.241	0.0161
0.5	0.209	0.0139
0.25	0.174	0.0116
0.2	0.157	0.0105
0.125	0.143	0.00953

4.3.3.2 Kinetics results for YGGFM

To calculate the initial velocity of YGGFM (figure 4.3.3.2.1) and YGGFL (figure 4.3.3.3.1) peptides the same calculation was carried out. However C2 is the concentration of a Y containing product after 8 minutes and C1 is the Y containing product concentration at initial mixing (0 mM^{-1}). T2 is 8 minutes after mixing and T1 is time 0. The Lineweaver-Burk plot for YGGFM show that the Km is 0.922 mM^{-1} and the Vmax is 0.0356 mM/min^{-1}. The associated data used to produce this graph is shown in table 4.3.3.2.1.

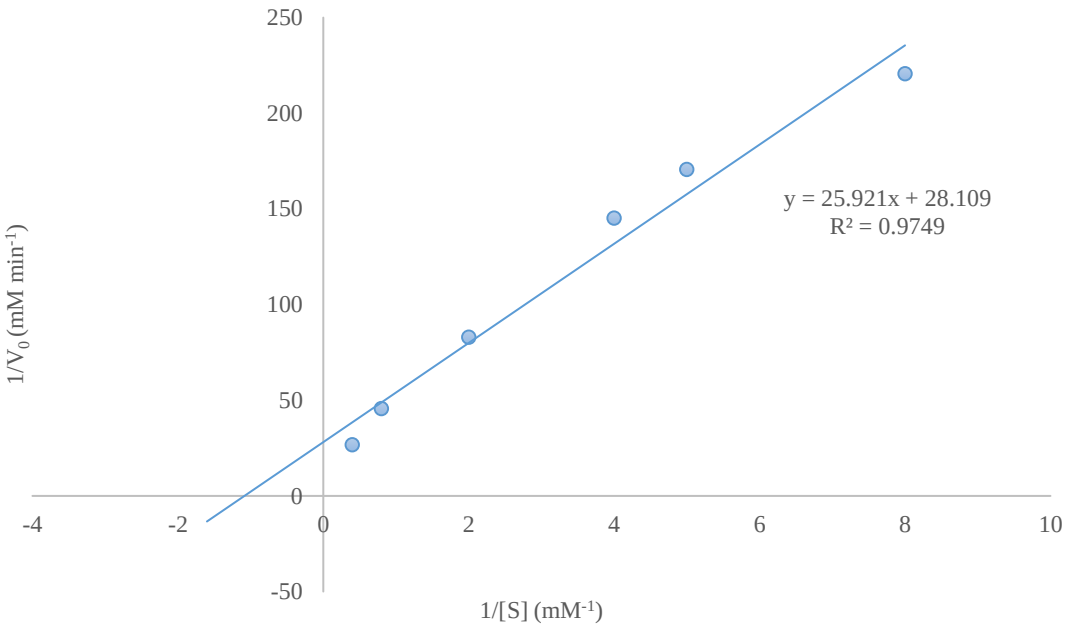

Figure 4.3.3.2.1: Lineweaver-Burk Plot for the BV + YGGFM reaction

Table 4.3.3.2.1: MestReNova Output of BV + YGGFM

Initial Concentration of YGGFM (mM^{-1})	Concentration of Y product after 8 mins (mM^{-1})	Initial Velocity (V_0) (mM/min^{-1})
2.5	0.299	0.0373
1.25	0.175	0.0219
0.5	0.0844	0.0106
0.25	0.0550	0.00688
0.2	0.0469	0.00586
0.125	0.0363	0.00454

4.3.3.3 Kinetics results for YGGFL

The Lineweaver-Burk plot (figure 4.3.3.3.1) for YGGFL show that the Km is 0.889 mM^{-1} and the Vmax is 0.0362 mM/min^{-1}. The associated data used to produce this graph is shown in table 4.3.3.3.1. This Lineweaver-Burk plot also shows a point that does not fall on the line of best fit. This point is for the final substrate concentration of 0.5 mM^{-1} YGGFL. This could be due to experimental error during sample preparation or be caused by line shape which affects the intensity of the peaks in the NMR spectrum. This variance could also be due to the presence of another enzyme acting simultaneously.

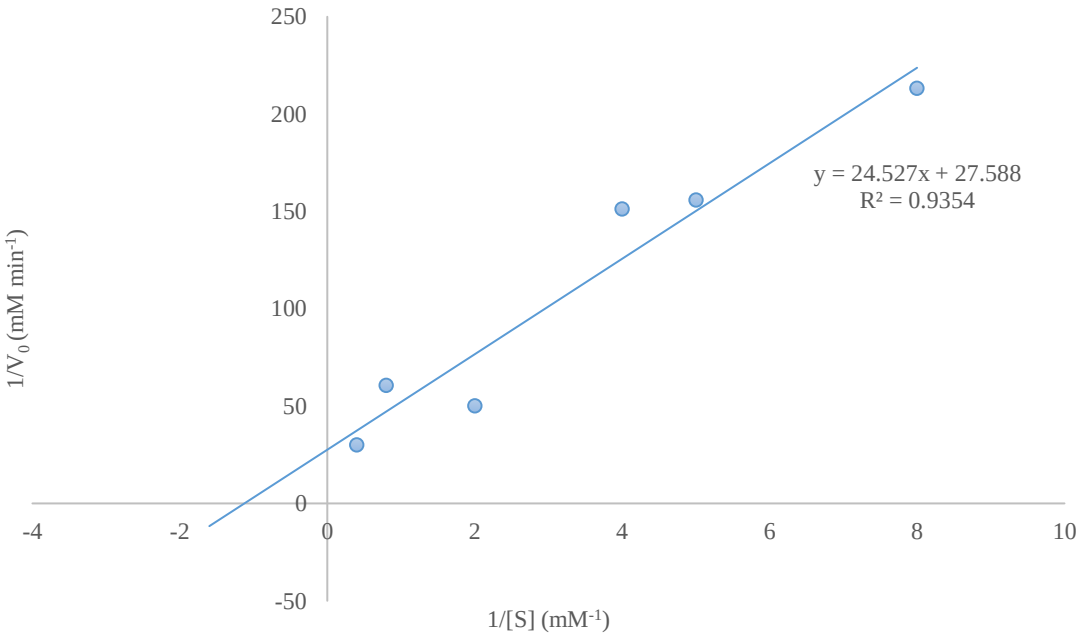

Figure 4.3.3.3.1: Lineweaver-Burk Plot for the BV + YGGFL reaction

Table 4.3.3.3.1: MestReNova Output of BV + YGGFL

Initial Concentration of YGGFL (mM^{-1})	Concentration of Y product after 8 mins (mM^{-1})	Initial Velocity (V_0) (mM/min^{-1})
2.5	0.266	0.0333
1.25	0.132	0.0165
0.5	0.160	0.0200
0.25	0.0529	0.00661
0.2	0.0513	0.00641
0.125	0.0375	0.00469

4.3.3.4 Kinetics results for FGG

The Lineweaver-Burk plot (figure 4.3.3.4.1) for FGG show that the Km is 0.0347 mM^{-1} and the Vmax is 0.0115 mM/min^{-1}. The associated data used to produce this graph is shown in table 4.3.3.4.1. This Lineweaver-Burk plot also shows that there is a point which does not sit on the line of best fit. This point is for the final concentration of 0.2 mM^{-1} FGG. As the rest of the points all follow a linear line it can be assumed that this point is lower due to experimental error. Due to this point being lower than expected this has caused the R^2 value to be lower.

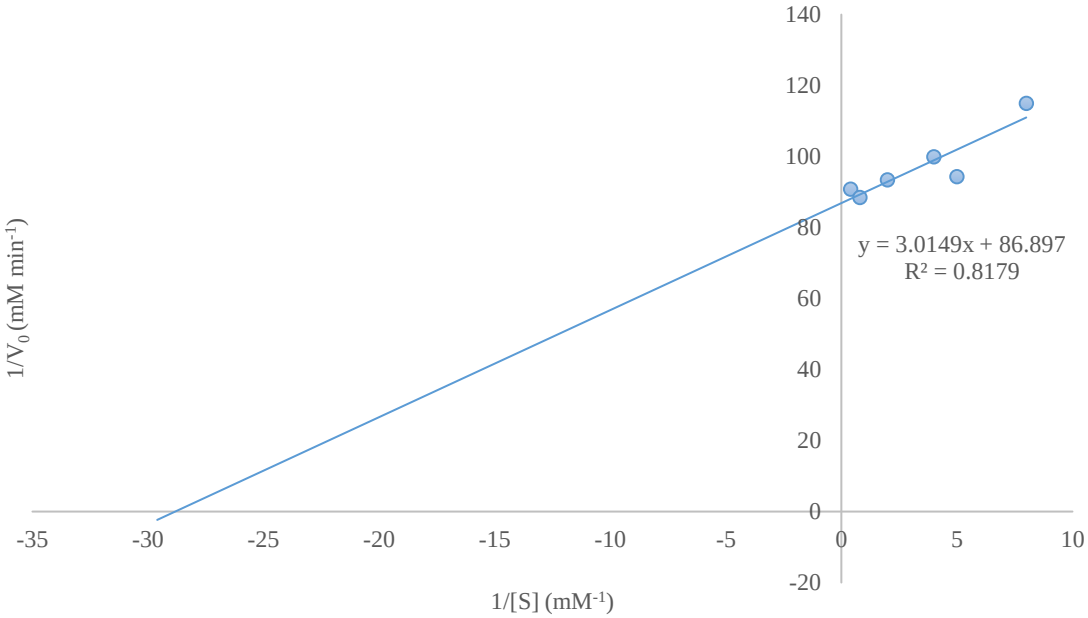

Figure 4.3.3.4.1: Lineweaver-Burk Plot for the BV + FGG reaction

Table 4.3.3.4.1: MestReNova Output of BV + FGG

Initial Concentration of FGG (mM^{-1})	Concentration of Free Glycine after 16 mins (mM^{-1})	Initial Velocity (V_0) (mM/min^{-1})
2.5	0.176	0.0110
1.25	0.181	0.0113
0.5	0.171	0.0107
0.25	0.160	0.0100
0.2	0.169	0.0106
0.125	0.139	0.00869

4.4 Summary

These results will be discussed further in chapter 6. However, BV modified all of the additional opioid substrates tested (YPWF, YPFF, YPFPGPI and the nociception model peptide FGG). This showed further evidence for BV specifically targeting the opioid peptides. Due to the complexity of the data for YPWF, YPFF and YPFPGPI, the specific details of how these peptides are degraded have not been deduced.

BV also modified the human DPP IV substrate (GP-X). This result shows evidence that the DPP IV-like enzyme known to be present in BV may be responsible for the modification of the other substrates.

The Km and Vmax values were deduced for each of the substrates using the equation from the line of best fit in the Lineweaver-Burk plot. These values are shown in table 4.4.1. From the results it can be concluded that YGGFM and YGGFL are both modified by a similar method. The Km/Vmax for both of these substrates are directly comparable to each other as the same signal region (δ 7.16 – 7.12 ppm) was used for each substrate. This signal region relates to the shift of one of the Y signals as modification takes place.

Table 4.4.1: Enzyme Kinetics Values

Substrate	Km (mM^{-1})	Vmax (mM/min^{-1})	Kcat (mM/s^{-1})
YGG	0.111	0.0172	0.804
YGGFM	0.922	0.0356	1.668
YGGFL	0.889	0.0362	1.698
FGG	0.0347	0.0115	0.539

The results for the YGG and FGG peptides are also directly comparable to one another as the same signal region (δ 3.59 – 3.55 ppm) was used. This is the signal for free glycine which appears clearly in both of these reactions. These results show remarkable differences to one another. The Km for the FGG peptide is *ca.* 3 times

smaller than the Km value for YGG. This means that the BV has a higher affinity for the FGG peptide compared to the YGG peptide. The FGG peptide is therefore acting like an inhibitor rather than a substrate as it has a low Kcat and Km.

Looking at the Km values overall it appears the BV enzyme binds to the substrates with the following affinity; FGG > YGG > YGGFL > YGGFM. The rate of modification which is represented by the Vmax value shows the following efficiency of degrading substrate; FGG > YGG > YGGFM > YGGFL.

As the Km and Vmax values for all substrates were not obtained due to time and cost, a comparison between crossover times was used instead. The crossover time is the point at which 50 % of the peptide substrate has been modified by BV. This comparison is detailed in table 4.4.1 The BV concentration (mg/mL) to substrate concentration (mM^{-1}) ratio has also been shown to highlight the differences in concentration.

The difference in concentration ratios between YGGFM and YGGFL mean that a direct comparison cannot be made using the crossover times. Therefore the data obtained during the kinetic experiments can be used as the same concentrations were used for each peptide. The Vmax values, 0.0356 mM/min^{-1} and 0.0362 mM/min^{-1} for YGGFM and YGGFL respectively, show that there is a marginal difference in the rate of hydrolysis of these peptides by BV.

A comparison between the relative rates of the enkephalin peptides and the endomorphin peptides shows that the BV enzyme, like the human DPP IV enzyme, binds more strongly to proline at the penultimate position. There is a substantial difference in the peptide crossover times with the endomorphin peptides which have proline in the P1’ position.

Table 4.4.1: 50 % Peptide Modification Times

Peptide	Crossover Time (mins)	Ratio (BV:Substrate)
YGGFM	627	1:2.1
YGGFL	240	1:0.9
YPWF	15	1:1.6
YPFF	50	1:1.7
RPKPQQFFGLM	36	1:0.2
YPFPGPI	393	1:1.2
GP-X	57	1:1.9
YGG	> 768	1:1.9
FGG	> 1145	1:1.9

There are no statistics shown for these experiments as they were only conducted once. Repeat experiments could not be carried out due to the time and cost of carrying out these experiments.

Chapter 5

5.0 Investigation of Enzyme Inhibition

5.1 Introduction

Further investigations of the possibility of the DPP IV-like enzyme in BV being responsible for the enzyme action in BV was carried out. There are four different types of enzyme inhibition; competitive, noncompetitive, uncompetitive and partial.[212] Competitive inhibition is when the inhibitor binds to the free enzyme and blocks substrate access to the catalytic site. Noncompetitive inhibition is when the inhibitor is able to bind to both the enzyme/substrate (ES)-complex and the free enzyme. Uncompetitive inhibition is when the inhibitor binds to the ES-complex. Partial inhibition is when the inhibitor binds to the ES-complex but the enzyme still has the ability to form a product but at a much reduced rate.

There are a vast range of enzymes known which all have different inhibitors. There are a number of factors to consider when selecting an inhibitor, these include the structure of the catalytic site and the catalytic mechanism. For example inhibition of aminopeptidases, which mostly use a metal ion for catalytic activity, involves the development of a molecule with a functional group which can complex with the metal ion and also contain a group capable of recognising the catalytic site.[213] For the purpose of this work selection of an inhibitor had to be carefully made. The results so far have indicated that a component in BV showed similarity to human dipeptidyl peptidase IV. Therefore, the first step at looking to inhibit the BV enzyme was to use a specific inhibitor which is used for the human DPP IV enzyme known as diprotin A. This is a tripeptide with the amino acid sequence Ile-Pro-Ile (IPI).[214]

This study will therefore look at the effect of this inhibitor on the BV enzyme action. From here on in diprotin A will be referred to as IPI. Any observed inhibition of action by BV in the presence of the inhibitor will provide further evidence that the enzyme present in BV is similar to the human DPP IV enzyme. Subsequently modifications will be made to the IPI peptide to see if inhibition can be improved. The two modified peptides tested were FPI and IPG. Glycine was used as previous results indicated slow

hydrolysis with this amino acid in this position (YGG) and phenylalanine was used as previous results showed that this amino acid in this position results in a higher Km (FGG).

5.2 Experimental

5.2.1 Materials

IPI was all bought from Sigma Aldrich. FPI and IPG were bought from Synpeptide Co., Ltd.

5.2.2 Methods

For this work 250 µL of BV (*ca.* 5 mg/mL) was mixed with 250 µL of 0.5 mM^{-1} inhibitor on ice and then pre-incubated at 37 °C for 30 minutes. This was done to allow the inhibitor to bind to the enzyme. 250 µL of a 5 mM^{-1} substrate was then added to this mixture on ice, which was then placed in the NMR instrument for analysis. Table 5.2.2.2 displays the details of the solutions used in this study. All substrates and inhibitor were sonicated at 37 °C for 15 minutes prior to any experiment to ensure they were fully dissolved. Details of the NMR experiment used are shown in table 5.2.2.1.

Table 5.2.2.1: NMR method used in experiments

Experiment	NMR Method
BV + IPI + GP-X	@PEW5_k
BV + IPI + YGG	@es1d_k
BV + IPI + FGG	@es1d_k
BV + IPI + YGGFM	@es1d_k
BV + IPI + YGGFL	@PEW5_k

Table 5.2.2.2: Solution details for BV + inhibitor + substrate reactions

Substrate (S) or Inhibitor (I)	Stock S or I Concentration (mM^{-1})	Working S or I Concentration (mM^{-1})	Stock BV Concentration (mg/ml)	Working BV Concentration (mg/ml)
IPI (I)	0.5	0.167	5.28	0.59
FPI (I)	0.5	0.167	5.04	0.56
YGG (S)	5	1.67	5.28	0.59
FGG (S)	5	1.67	5.04	0.56
YGGFM (S)	5	1.67	5.28	0.59
YGGFL (S)	5	1.67	5.28	0.59
GP-X* (S)	5	1.67	5.28	0.59

*X = 7-amido-4-methylcoumarin hydrobromide

5.2.2.1 Inhibitor Control Experiments

Control experiments were run for the inhibitor in the presence of BV and in the absence of BV. This was done to test the stability of the inhibitor in the phosphate buffer along with testing to see if BV had an effect on the inhibitor peptide.

- BV + IPI + buffer
- Buffer + IPI + buffer
- BV + IPG + buffer
- Buffer + IPG + buffer
- BV + FPI + buffer
- Buffer + FPI + buffer

These experiments were carried out the same way as the BV + inhibitor + substrate experiments, using the same concentrations. However, 100 mM^{-1} potassium phosphate buffer was used to replace the substrate and/or BV. This ensured the concentrations were kept constant between control experiments and BV + inhibitor + substrate experiments.

5.2.2.2 Substrate Control Experiments

To be able to make direct comparisons and ensure that any inhibition of the modification of substrates by BV is due to the inhibitor, it was necessary to run controls. It is important to point out that these controls are different from experiments mentioned previously. For this study the controls which were carried were as follows:

- BV + buffer + GP-X
- BV + buffer + YGG
- BV + buffer + FGG
- BV + buffer + YGGFL
- BV + buffer + YGGFM

These experiments were carried out the same way as the BV + inhibitor + substrate experiments, using the same concentrations. However, 100 mM^{-1} potassium phosphate buffer was used to replace the inhibitor. This ensured the concentrations were kept constant between control experiments and BV + inhibitor + substrate experiments.

5.2.2.3 Inhibitor + Substrate Control Experiments

Another set of controls were run to ensure there was no interaction between the substrate and the inhibitor. This was not carried out for the IPG peptide as results showed BV to modify this peptide very quickly (i.e. is a good substrate) and would therefore be an unsuitable inhibitor. Therefore, the following controls were also carried out:

- IPI + GP-X
- IPI + YGG
- IPI + FGG
- IPI + YGGFM
- IPI + YGGFL
- FPI + GP-X

- FPI + YGG
- FPI + FGG
- FPI + YGGFM
- FPI + YGGFL

These controls were carried out by mixing 400 µL of the substrate with 400 µL of the inhibitor. An ^{1}H NMR was taken and then these samples were left at room temperature for 7 days. After this period another ^{1}H NMR was taken and compared to the initial spectrum.

5.3 Results

5.3.1 IPI Controls

The buffer + IPI + buffer control experiment was run to ensure that IPI was stable in the potassium phosphate buffer. The results from this control experiment showed that IPI is stable on its own in the potassium phosphate buffer (figure 5.3.1.1). This is also shown clearly in figure 5.3.1.2 where there is a graphical representation of the IPI control. From this graph it is clear that there are no changes in signal intensity over the 20 hour period meaning the IPI remained intact throughout the analysis. The signal represented by δ 1.05 – 1.10 ppm relates to one of the methyl groups on the unmodified peptide. The signal represented by δ 1.10 – 1.14 ppm relates to a region of the spectra where there are no signals present. This was done so that a comparison between this control and IPI in the presence of BV could be made.

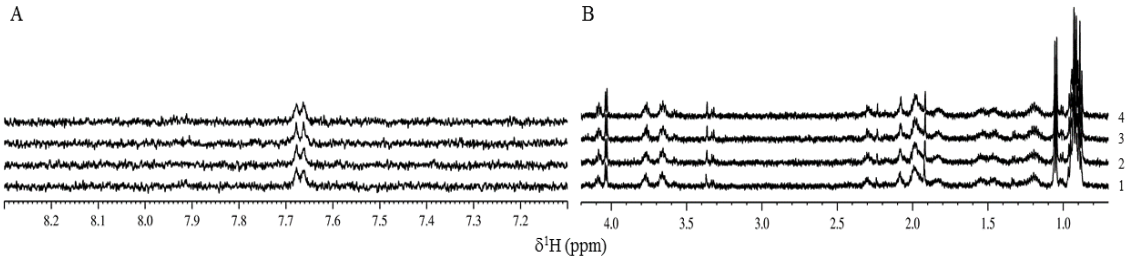

Figure 5.3.1.1: ^{1}H Buffer + IPI + buffer control aromatic (A) and aliphatic (B) region showing spectrum 1 (0 hours), 2 (after 1 hour), 3 (after 6 hours) and 4 (after 20.5 hours).

Comparing the results shown in figure 5.3.1.2 to the results in figure 5.3.1.4 it is clear that there is no modification of IPI in the phosphate buffer in the absence of BV. There is clearly no formation of a signal at δ 1.10 – 1.14 ppm and the signal at δ 1.05 – 1.10 ppm, which relates to the intact IPI peptide, remains stable.

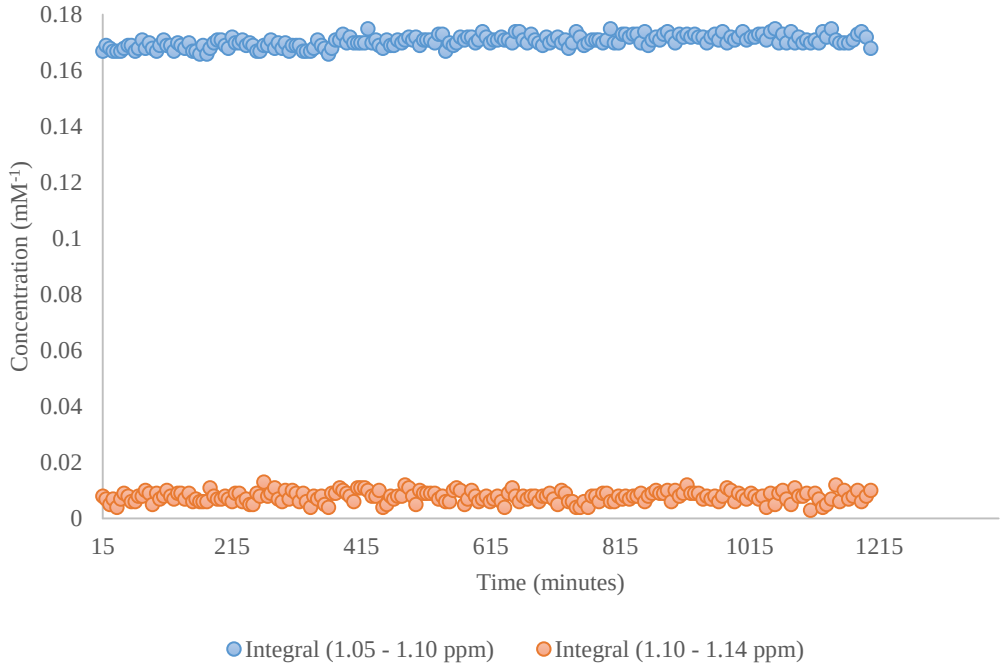

Figure 5.3.1.2: Graphical representation of the IPI control experiment. Integral 1.05 – 1.10 ppm represents protons on an amino acid residue in IPI peptide. Integral 1.10 – 1.14 ppm represents a region of spectrum where there are no signals.

The BV + IPI + buffer control experiment was carried out to see if the BV had any effect on IPI in the absence of a substrate. The ^{1}H NMR spectra of this experiment is shown in figure 5.3.1.3. There are changes in signals which can be seen in the aromatic region at δ 7.68 ppm and the aliphatic region at δ 1.1 ppm. The data in this figure mostly relates to the BV. Those signals highlighted in blue relate to the IPI peptide.

A graphical representation of this control result is shown in figure 5.3.1.4 where it is clear that there is modification of IPI in the presence of BV. From this figure it is clear that IPI is completely modified after 13.5 hours. The signal represented by δ 1.05 – 1.10 ppm relates to one of the methyl groups on the unmodified peptide and the signal represented by δ 1.10 – 1.14 ppm relates to one of the methyl groups protons on the modified peptide.

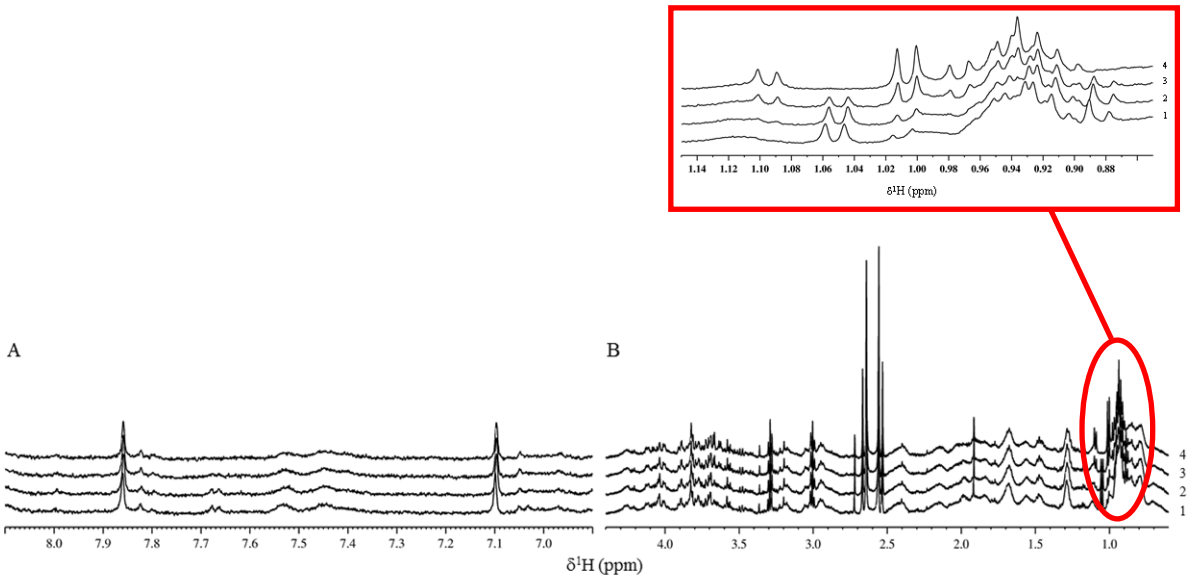

Figure 5.3.1.3: BV + IPI + buffer experiment aromatic (A) and aliphatic (B) region showing spectrum 1 (0 hours), 2 (after 1 hour), 3 (after 6 hours) and 4 (after 20.5 hours).

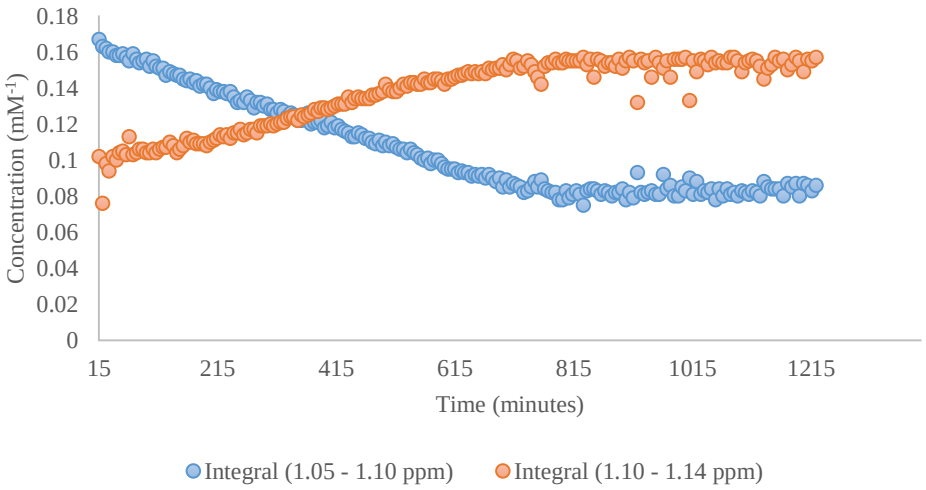

Figure 5.3.1.4: Graphical representation of the BV + IPI + buffer experiment.
Integral 1.05 – 1.10 ppm represents protons on an amino acid residue in IPI peptide.
Integral 1.10 – 1.14 ppm represents protons on product molecule.

5.3.2 IPG Controls

The results from the buffer + IPG + buffer control experiment showed that IPG is stable on its own in the potassium phosphate buffer (figure 5.3.2.1). There are no observed changes in the signals over the 15 hour period.

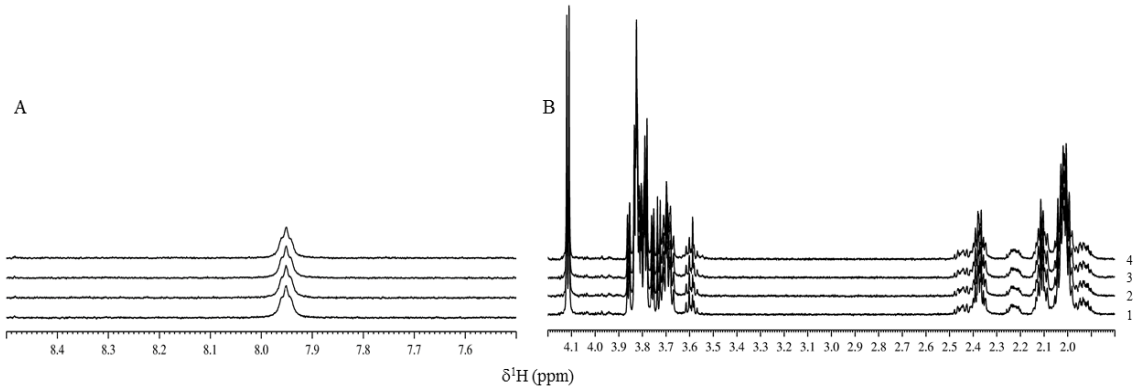

Figure 5.3.2.1: ^{1}H Buffer + IPG + buffer control aromatic (A) and aliphatic (B) regions showing spectrum 1 (0 hours), 2 (after 1 hour), 3 (after 6 hours) and 4 (after 15 hours).

Figure 5.3.2.2 shows the graphical representation of IPG in buffer control. The signal represented by δ 1.08 – 1.10 represents protons found on the isoleucine part of the IPG molecule. This signal remains constant throughout the experiment meaning it is stable. The other integral shown, which is represented by δ 3.57 – 3.59 ppm, is an area of the spectrum where there are no signals present. This was again done so that a comparison could be made to the results of the IPG peptide in the presence of BV (figure 5.3.2.4).

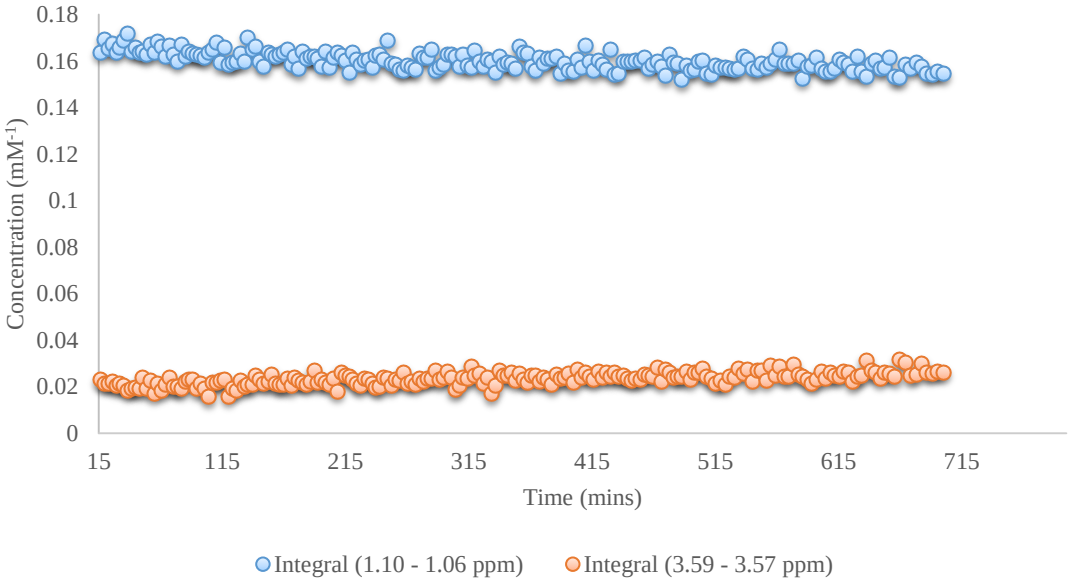

Figure 5.3.2.2: Graphical representation of the IPG in buffer control. Integral 1.10 – 1.06 ppm represents protons on an amino acid residue in IPG peptide. Integral 3.59 – 3.57 ppm represents a region of spectrum where there are no signals.

The ^{1}H NMR spectra of the BV + IPG + buffer control experiment is shown in figure 5.3.2.3. A graphical representation of this control result is shown in figure 5.3.2.4 where it is clear that there is modification of IPG in the presence of BV.

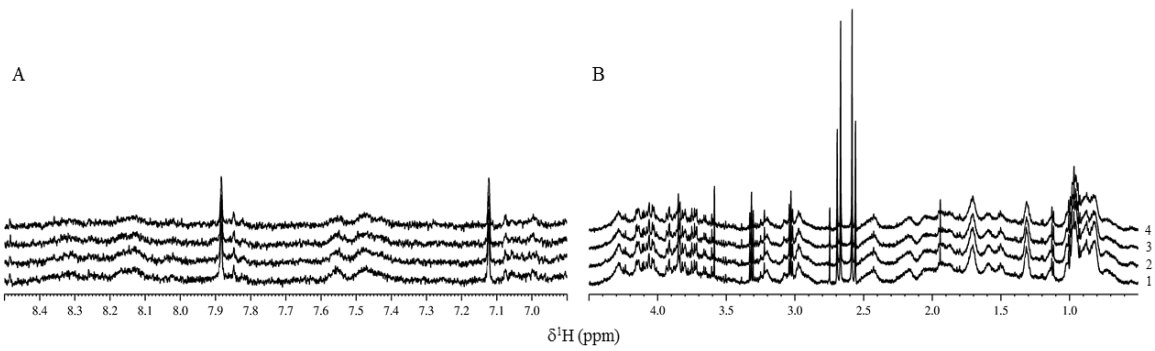

Figure 5.3.2.3: ^{1}H BV + IPG + buffer control aromatic (A) and aliphatic (B) region showing spectrum 1 (0 hours), 2 (after 1 hour), 3 (after 6 hours) and 4 (after 15 hours).

The results showed that for IPG in the presence of BV after a 30 minute incubation period, the IPG peptide has been completely modified. Therefore it was decided to look at the ^{1}H NMR data of the IPG peptide in the presence of BV during the 30 minute incubation period.

The results shown in figure 5.3.2.4 show the modification of the IPG peptide during the incubation period. It is clear that modification of the peptide stops after 22 minutes. This means that IPG is a very good substrate and therefore would not work effectively as an inhibitor. This is due to the IPG peptide being completely modified during the 30 minute BV/inhibitor incubation period. As a result of this no further work was carried out using the peptide as an inhibitor.

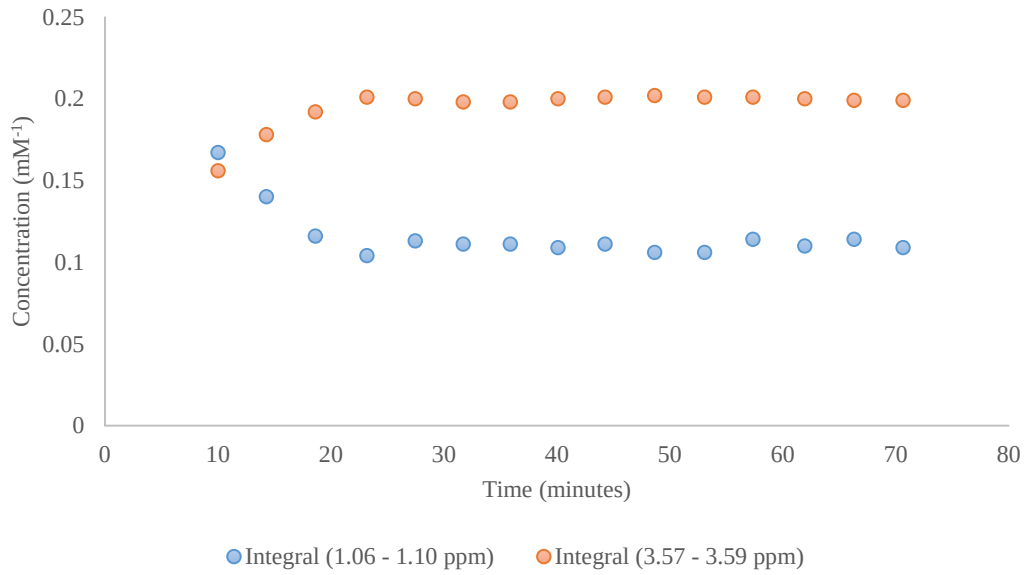

Figure 5.3.2.4: Graphical representation of IPG in the presence of BV during incubation period. Integral 1.06 – 1.10 ppm represents protons on an amino acid residue in IPG peptide. Integral 3.57 – 3.59 ppm represents protons on product molecule.

5.3.3 FPI Controls

The ^{1}H NMR spectra for the buffer + FPI + buffer control experiment show that there are no changes in the signals for the unmodified peptide (figure 5.3.3.1). This means that the peptide is stable in the potassium phosphate buffer.

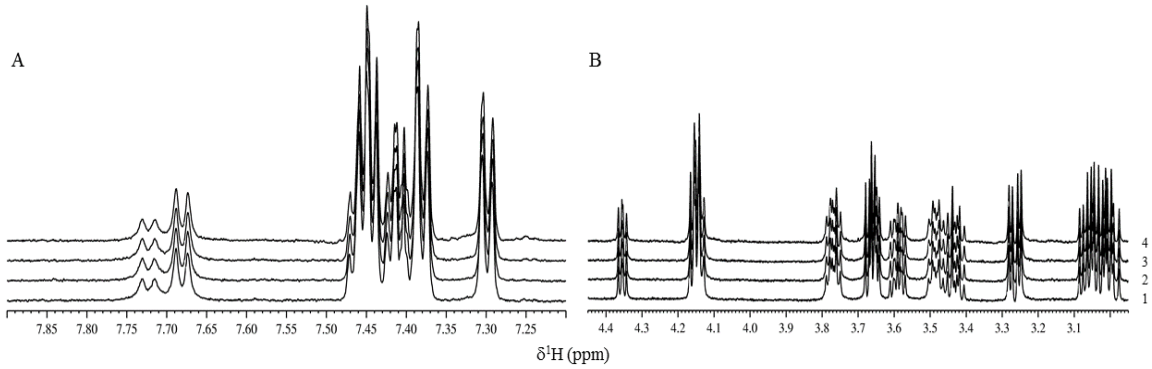

Figure 5.3.3.1: ^{1}H Buffer + FPI + buffer control aromatic (A) and aliphatic (B) regions showing spectrum 1 (0 hours), 2 (after 1 hour), 3 (after 6 hours) and 4 (after 15 hours).

The ^{1}H NMR spectra of the BV + FPI + buffer control experiment is shown in figure 5.3.3.2. These data show some changes to the signals of the unmodified peptide meaning BV is modifying FPI. A graphical representation of this control result is shown in figure 5.3.3.3 where it is clear that there is modification of FPI in the presence of BV.

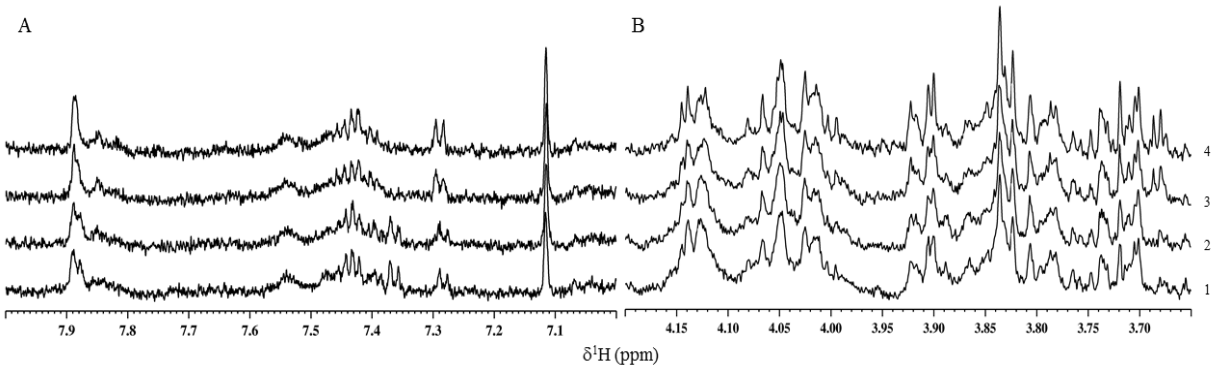

Figure 5.3.3.2: ^{1}H BV + FPI + buffer control aromatic (A) and aliphatic (B) region showing spectrum 1 (0 hours), 2 (after 1 hour), 3 (after 6 hours) and 4 (after 20.5 hours).

Figure 5.3.3.3 shows the FPI peptide in the presence of BV after a 30 minute incubation period at 37 °C along with FPI in buffer. The signals used for these two controls are the same so that a direct comparison can be made. After the incubation period the sample was put on ice and 250 µL of potassium phosphate buffer was added. This was done to mimic the experiments where a substrate would be added instead of the buffer. The results show that there is an increase in concentration of a product signal when in the presence of BV. This signal is not found in the FPI + buffer control, or in the BV hence confirming that BV is modifying the FPI peptide. The graph also shows that FPI is stable in the buffer over the reaction period meaning any changes found must be due to the BV.

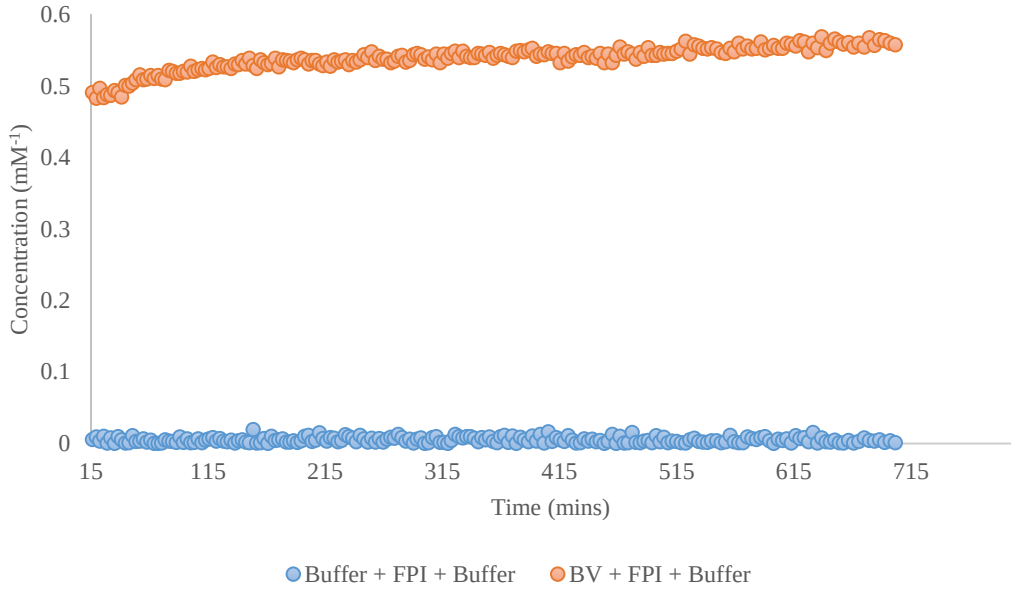

Figure 5.3.3.3: Graphical representation of FPI in buffer compared with FPI in the presence of BV after a 30 minute incubation period. The signal used was δ 3.94 – 3.98 ppm. This is the same for both experiments.

5.3.4 Substrate Controls

The ^{1}H NMR spectra for the BV + buffer + substrate controls are not shown here as similar results to these have already been reported in chapters 3 and 4 with concentration being the only difference. However a graphical representation of all the BV + buffer + substrate control experiments are presented here. The substrates show varying rates of modification when the graphical representations are compared. All controls are direct comparisons to each other as the concentration of the substrate and BV used is consistent in all experiments.

5.3.4.1 GP-X Control

Figure 5.3.4.1.1 shows the results for the BV + buffer + GP-X control. The ^{1}H signal δ 7.42 – 7.52 ppm represents one of the protons found on the ring in the methylcoumarin part of the substrate. The ^{1}H signal δ 6.86 – 6.77 ppm represents a proton on the modified DPP IV substrate. This is most likely to be a proton on the ring of the methylcoumarin part of the molecule as this chemical shift is in the aromatic region. It is clear the DPP IV substrate is completely modified by BV at *ca.* 190 minutes. The results shown in this differ from previous results in section 4.3.2. Previous results showed that the product molecule was also modified however, this is not seen here. It is possible that there is a contaminant that has inhibited the dipeptidase or this could be due to the differences in concentration of both the BV and the substrate between the two experiments.

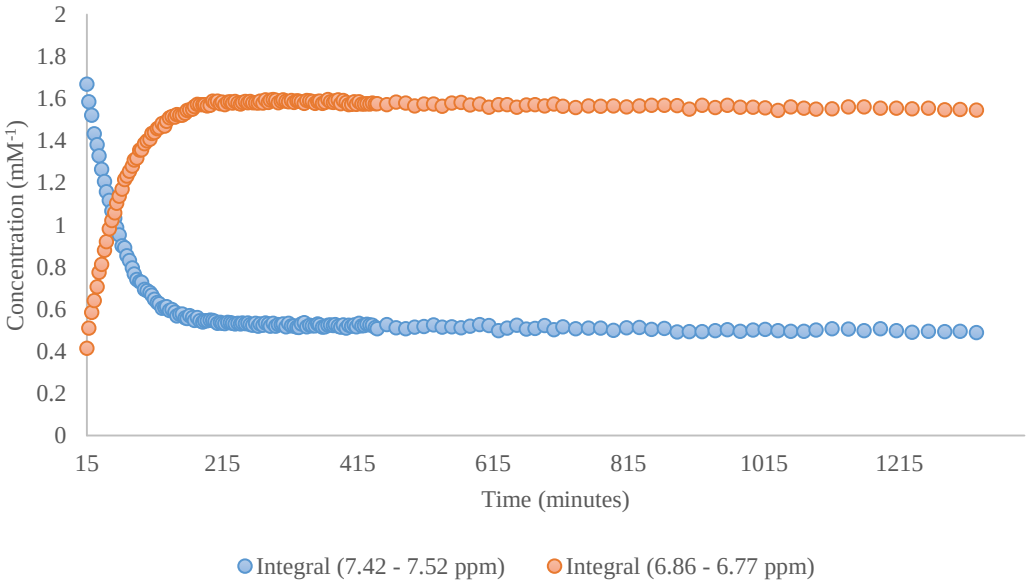

Figure 5.3.4.1.1: Graphical representation of the BV + buffer + GP-X experiment. Integral 7.42 – 7.52 ppm represents protons on the methylcoumarin part of the GP-X molecule. Integral 6.86 – 6.77 ppm represents protons on product molecule.

5.3.4.2 YGG Control

Figure 5.3.4.2.1 shows the results for the BV + buffer + YGG control. The ^{1}H signal δ 7.14 – 7.20 ppm represents two of the protons found on the ring in the tyrosine part of the YGG peptide. The ^{1}H signal δ 3.56 – 3.59 ppm represents two protons on the free glycine product (discussed in chapter 3) of the modified YGG peptide. The hydrolysis of this peptide is much slower when compared to GP-X.

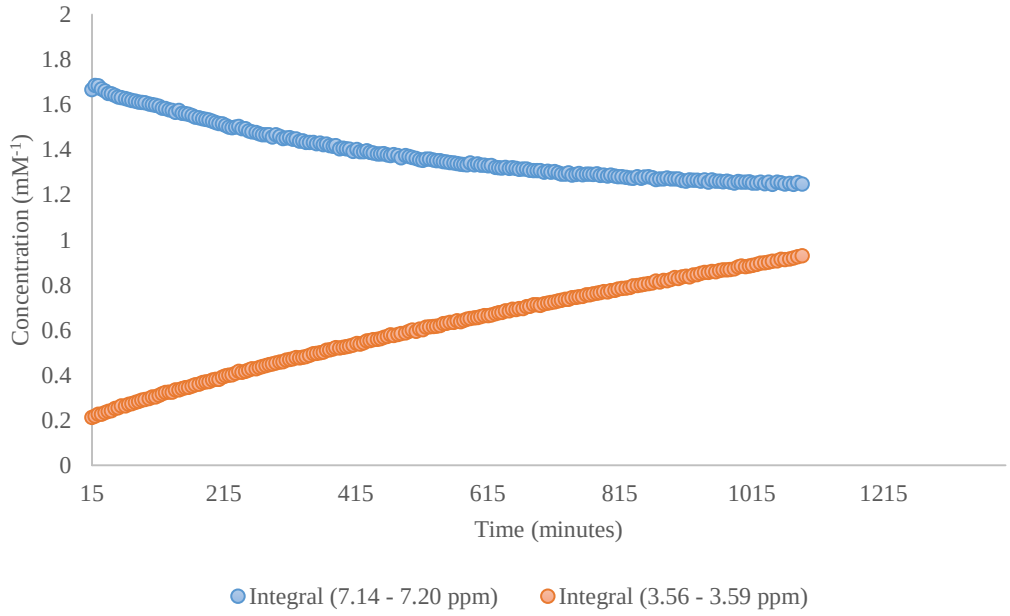

Figure 5.3.4.2.1: Graphical representation of the BV + buffer + YGG experiment. Integral 7.14 – 7.20 ppm represents equivalent protons on Y in YGG peptide. Integral 3.56 – 3.59 ppm represents protons on product molecule.

5.3.4.3 FGG Control

Figure 5.3.4.3.1 shows the results for the BV + buffer + FGG control. The ^{1}H signal δ 3.98 – 4.06 ppm represents the proton attached to the alpha carbon on the phenylalanine (F) part of the FGG peptide. The ^{1}H signal δ 3.57 – 3.59 ppm represents two protons on the free glycine product (discussed in chapter 4) of the modified FGG peptide. Hydrolysis of this peptide is slower than both GP-X and YGG with hydrolysis stopping before all of the FGG peptide is converted to FG + G.

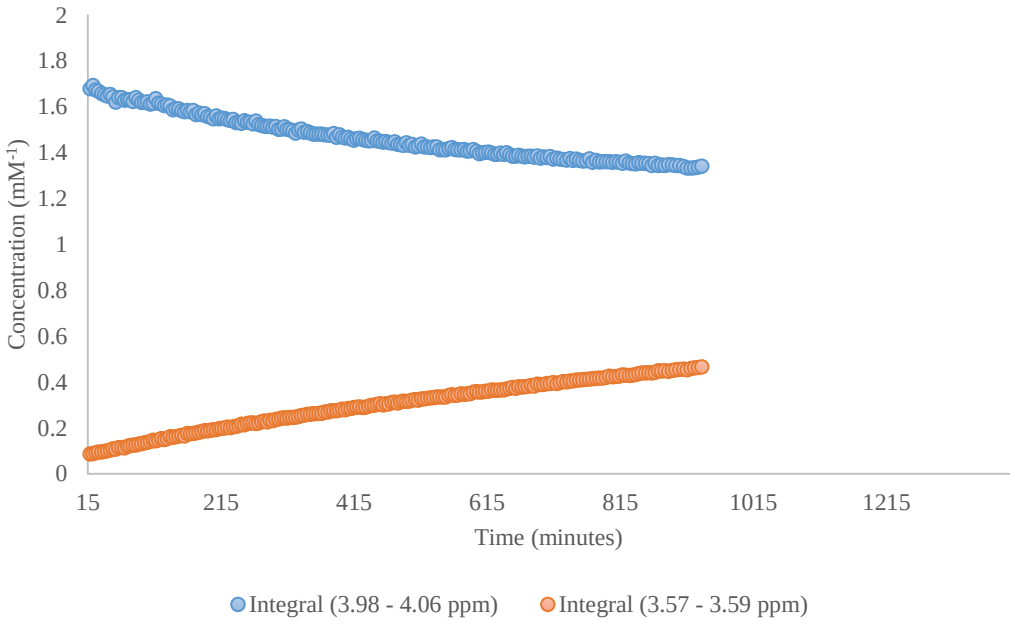

Figure 5.3.4.3.1: Graphical representation of the BV + buffer + FGG experiment. Integral 3.98 – 4.06 ppm represents protons on F in FGG peptide. Integral 3.57 – 3.59 ppm represents protons on product molecule.

5.3.4.4 YGGFM Control

Figure 5.3.4.4.1 shows the results for the BV + buffer + YGGFM control. The ^{1}H signal δ 7.14 – 7.20 ppm represents two of the protons found on the ring in the tyrosine part of the YGGFM peptide. The ^{1}H signal δ 3.72 – 3.78 ppm represents proton(s) on the product of the modified YGGFM peptide, possibly due to the Gly residue in the dipeptide YG.

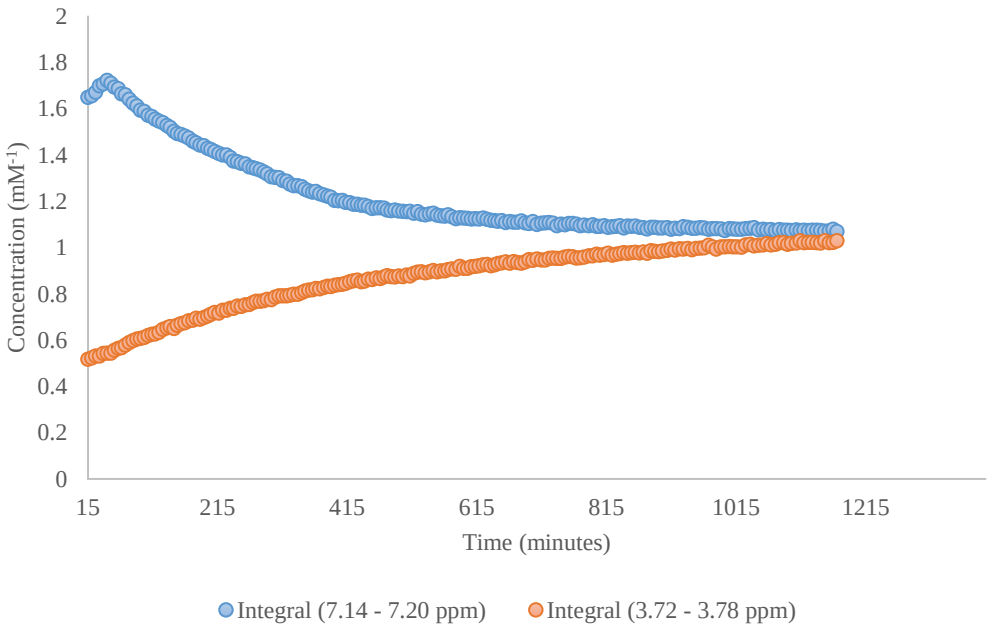

Figure 5.3.4.4.1: Graphical representation of the BV + Buffer + YGGFM experiment. Integral 7.14 – 7.20 ppm represents equivalent protons on Y in YGGFM peptide. Integral 3.72 – 3.78 ppm represents protons on product molecule.

5.3.4.5 YGGFL Control

Figure 5.3.4.5.1 shows the results for the BV + buffer + YGGFL control. The ^{1}H signal δ 7.14 – 7.21 ppm represents two of the protons found on the ring in the tyrosine part of the YGGFL peptide. The ^{1}H signal δ 3.61 – 3.66 ppm represents proton(s) on the product of the modified YGGFL peptide, possibly due to the Gly residue in the dipeptide YG.

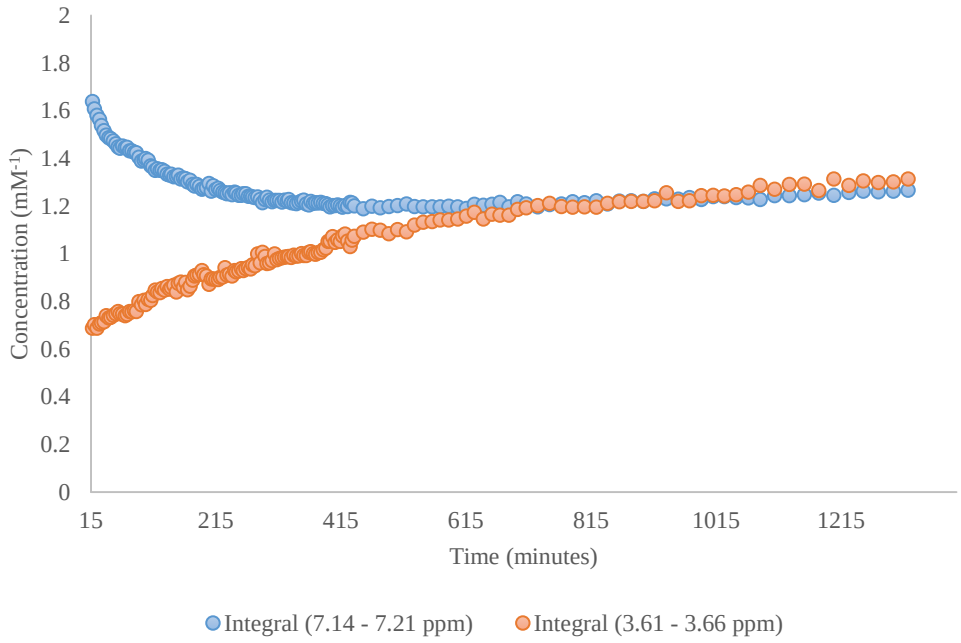

Figure 5.3.4.5.1: Graphical representation of the BV + buffer + YGGFL experiment. . Integral 7.14 – 7.21 ppm represents equivalent protons on Y in YGGFM peptide. Integral 3.61 – 3.66 ppm represents protons on product molecule.

5.3.5 Inhibitor + Substrate Controls

5.3.5.1 IPI + Substrate Controls

The IPI + substrate experiments will show if there is any interaction between IPI and the substrates in the absence of BV. An example of one of these controls is shown in figure 5.3.5.1.1 which shows the mixture of IPI with YGG. There is no modification of these peptides meaning they do not interact with each other. The rest of the results for IPI + FGG, IPI + YGGFM and IPI + YGGFL show the same results and are shown in appendix 5 (5A – 5C respectively) with the exception of IPI + GP-X. A previous experiment showed that GP-X is modified naturally on its own. The results of the mixture of IPI + GP-X substrate are shown in figure 5.3.5.1.2.

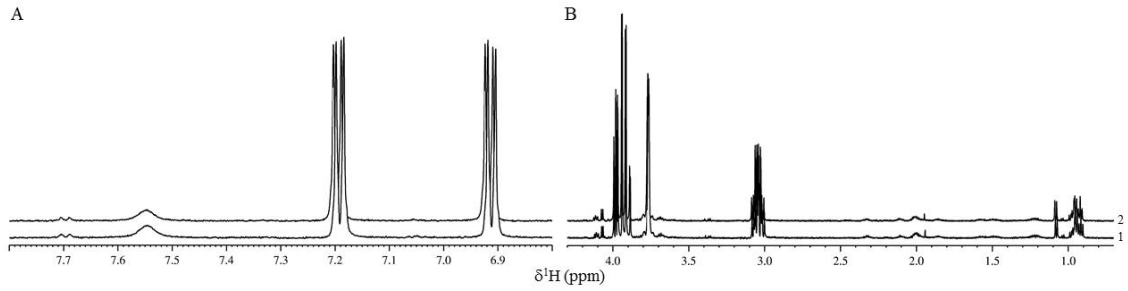

Figure 5.3.5.1.1: ^{1}H IPI + YGG control aromatic (A) and aliphatic (B) region showing spectrum 1 (0 hours), and 2 (after 7 days).

Figure 5.3.5.1.2 shows that the GP-X signals show the same changes as a previous control experiment, in which GP-X in buffer was tested. However the IPI signals remain the same in this experiment meaning that the IPI and GP-X do not react with each other.

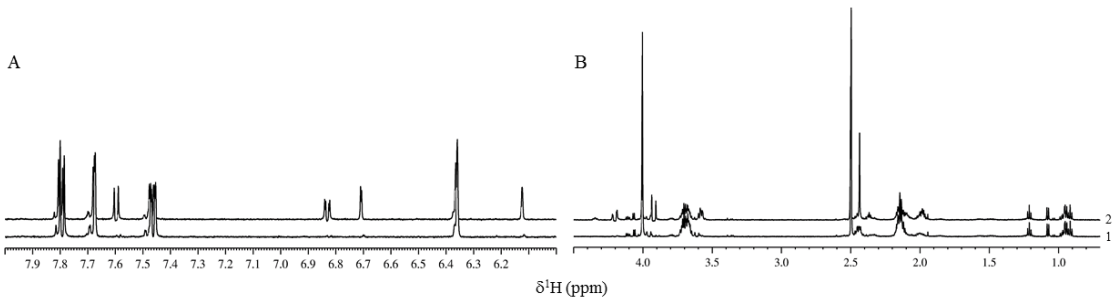

Figure 5.3.5.1.2: ^{1}H IPI + GP-X control aromatic (A) and aliphatic (B) region showing spectrum 1 (0 hours), and 2 (after 7 days).

5.3.5.2 FPI + Substrate Controls

The FPI + substrate experiments will show if there is any interaction between FPI and the substrates in the absence of BV. An example of one of these controls is shown in figure 5.3.5.2.1 which shows the mixture of FPI with YGG. There is no modification of these peptides meaning they do not react with each other. The rest of the results for FPI + FGG, FPI + YGGFM and FPI + YGGFL show the same results and are shown in appendix 5 (5D – 5F respectively) with the exception of FPI + GP-X. A previous experiment showed that GP-X is modified naturally on its own. The results of the mixture of FPI + GP-X substrate are shown in figure 5.3.5.2.2.

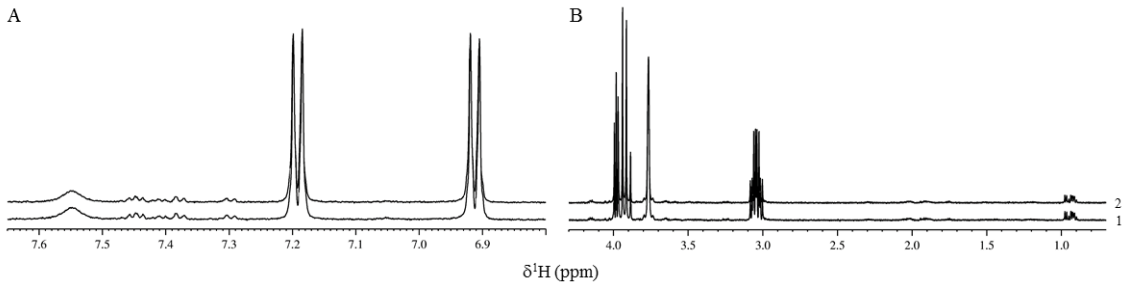

Figure 5.3.5.2.1: ^{1}H FPI + YGG control aromatic (A) and aliphatic (B) region showing spectrum 1 (0 hours), and 2 (after 7 days).

In figure 5.3.5.2.2, the GP-X signals show the same changes as a previous control experiment, in which GP-X in buffer was tested. However the FPI signals remain the same in this experiment meaning that the FPI and GP-X do not react with each other.

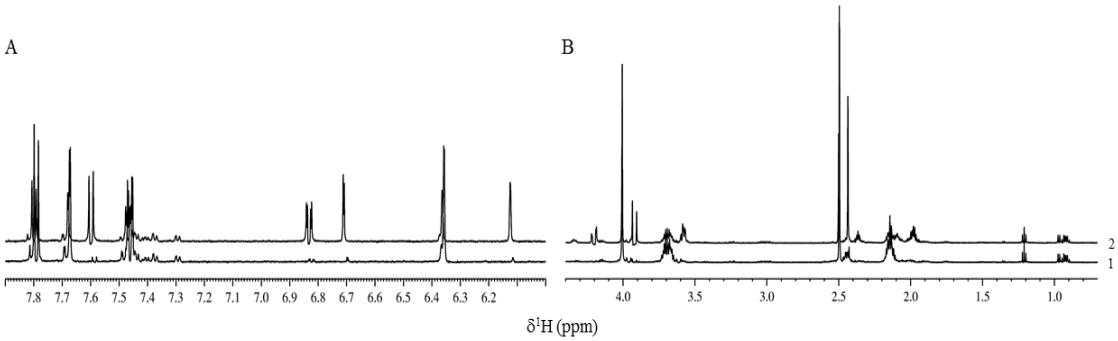

Figure 5.3.5.2.2: ^{1}H FPI + GP-X control aromatic (A) and aliphatic (B) region showing spectrum 1 (0 hours), and 2 (after 7 days).

5.3.6 Results of BV + IPI + Substrate Experiments

5.3.6.1 BV + IPI + GP-X

In figure 5.3.6.1.1 the IPI inhibitor has had an effect on the modification of GP-X. When compared to the control, where GP-X is completely modified after 200 minutes, it takes around 1200 minutes for this substrate to be completely modified in the presence of the IPI inhibitor. The signal used for this is δ 7.42 – 7.52 ppm which is a doublet that relates to a proton on the methylcoumarin part of the GP-X molecule. The same signal is used for both experiments so a direct comparison can be made. Also shown in the graph is a small increase in signal intensity at the beginning of the reaction. This could be related to shimming of the instrument or solubility. The solubility issue means that the substrate is becoming more concentrated at the beginning of the experiment, therefore showing an increase in signal intensity. This could be due to the increase in temperature.

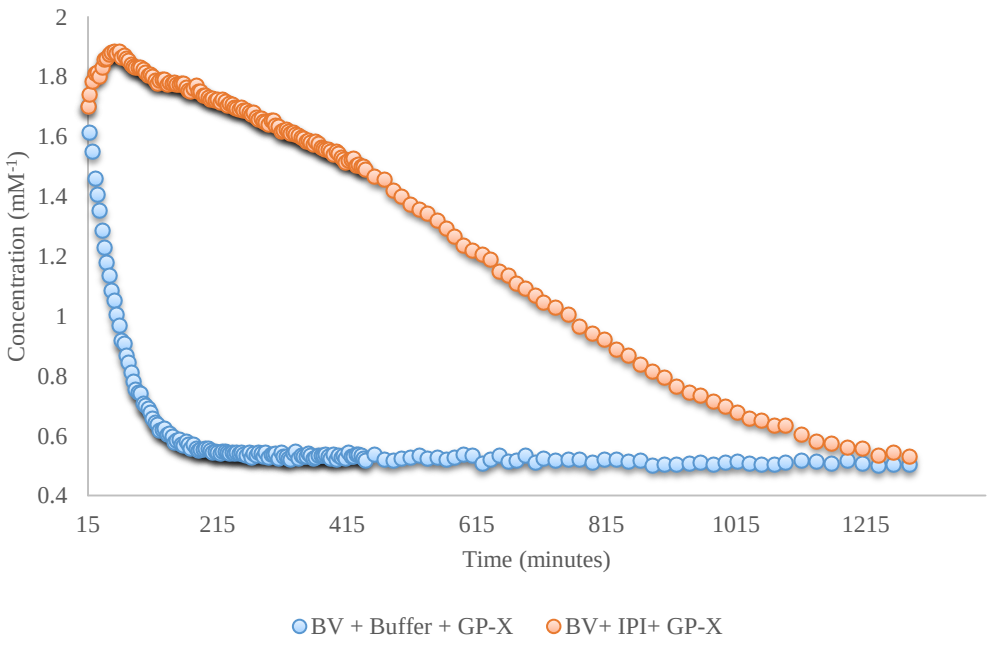

Figure 5.3.6.1.1: Graphical representation of the modification of GP-X by BV in the presence of IPI. The signal used was δ 7.42 – 7.52 ppm. This is the same for both experiments.

5.3.6.2 BV + IPI + YGG

In figure 5.3.6.2.1 the modification of the YGG peptide by BV has also been inhibited by the IPI inhibitor. There is no modification of the YGG peptide in the presence of IPI until *ca.* 800 minutes where the concentration begins to decrease. When this is compared to the control, where the modification is seen from the beginning of the reaction. The presence of IPI is affecting the ability of BV to modify the YGG peptide. The signal used for this is δ 7.14 – 7.20 ppm, which is a doublet that relates to two protons on the Y part of the YGG molecule. The same signal is used for both experiments so a direct comparison can be made.

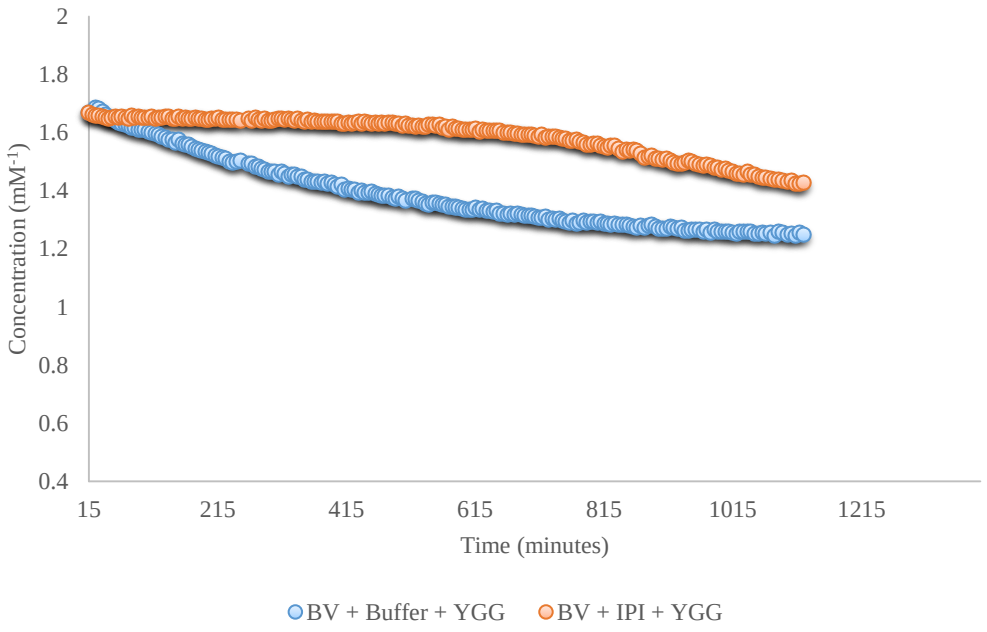

Figure 5.3.6.2.1: Graphical representation of the modification of YGG by BV in the presence of IPI. The signal used was δ 7.14 – 7.20 ppm. This is the same for both experiments.

5.3.6.3 BV + IPI + FGG

In figure 5.3.6.3.1 the modification of the FGG peptide has also been inhibited by the IPI inhibitor. There is no modification of the FGG peptide in the presence of IPI until after 500 minutes. When this is compared to the control, where the modification is seen from the beginning of the reaction, IPI is affecting the ability of BV to modify the FGG peptide. This result can also be compared to the results for the YGG peptide, which was inhibited for a longer period of time. The only difference between these two peptides is the hydroxyl on the ring of the Y amino acid. This suggests that not having the hydroxyl on the phenylalanine in the first position makes F a stronger competitor compared with Y. The signal used for this is δ 3.98 – 4.06 ppm, which is a triplet that relates to an alpha proton on the F part of the FGG molecule. The same signal is used for both experiments so a direct comparison can be made.

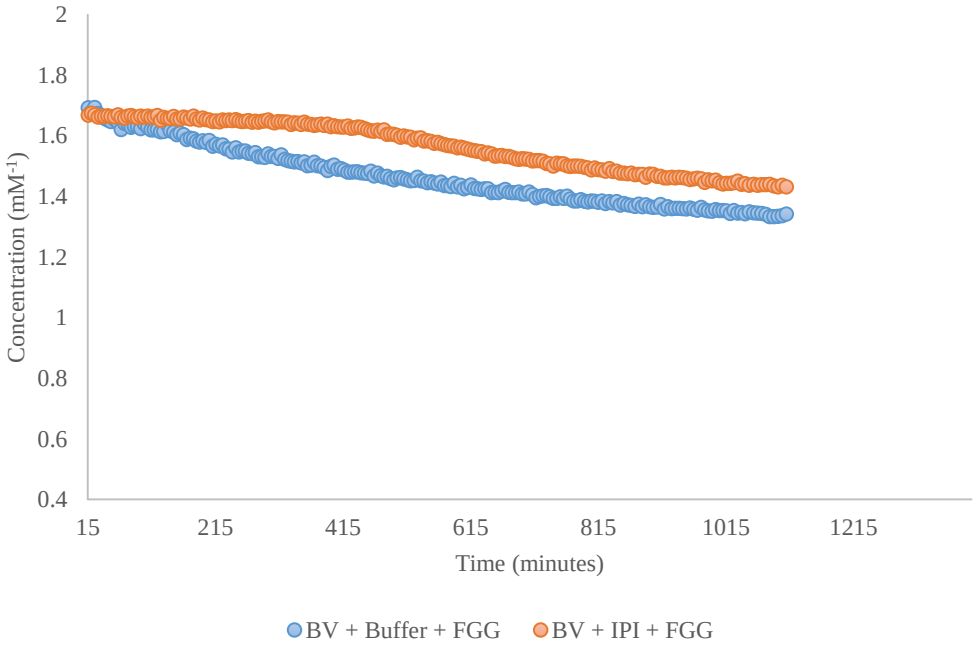

Figure 5.3.6.3.1: Graphical representation of the modification of FGG by BV in the presence of IPI. The signal used was δ 3.98 – 4.06 ppm. This is the same for both experiments.

5.3.6.4 BV + IPI + YGGFM

In figure 5.3.6.4.1 the modification of the YGGFM peptide has been inhibited by the IPI inhibitor. There are small decreases in the YGGFM concentration in the presence of IPI until after 250 minutes where this decrease in concentration becomes bigger. When this is compared to the control, where the decrease in YGGFM concentration is much bigger, IPI is affecting the ability of BV to modify the YGGFM peptide. The signal used for this is δ 7.14 – 7.20 ppm which is a doublet that relates to two protons on the Y part of the YGGFM molecule. The same signal is used for both experiments so a direct comparison can be made. The same issue is seen here as there is for the GP-X results where there is a small increase in signal intensity at the beginning of the reaction.

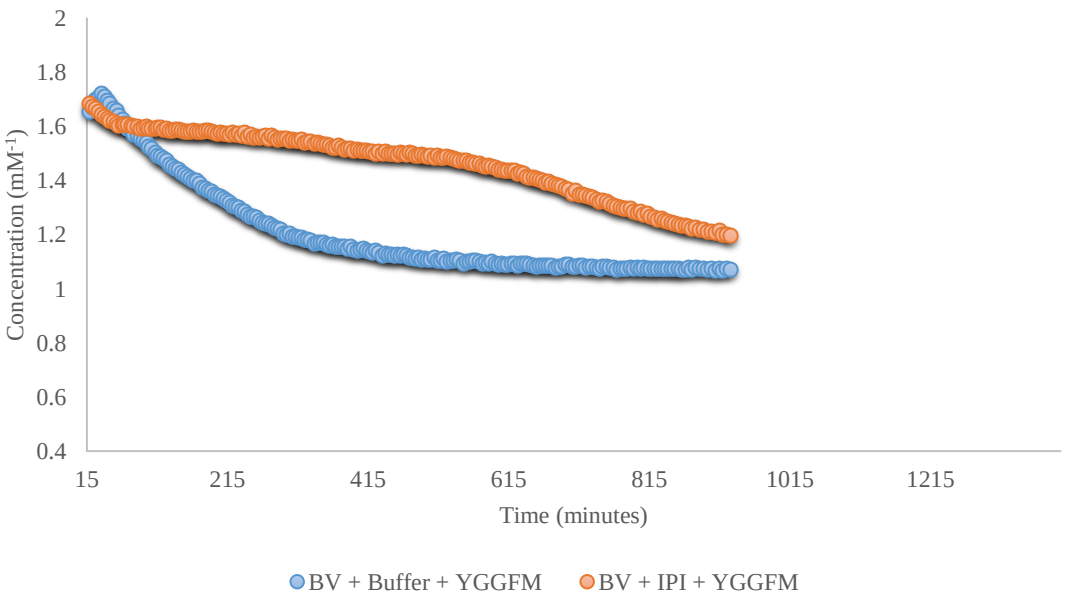

Figure 5.3.6.4.1: Graphical representation of the modification of YGGFM by BV in the presence of IPI. The signal used was δ 7.14 – 7.20 ppm. This is the same for both experiments.

5.3.6.5 BV + IPI + YGGFL

In figure 5.3.6.5.1 the modification of the YGGFL peptide has been inhibited by the IPI inhibitor. There are again small decreases in YGGFL concentration in the presence of IPI until after 1000 minutes where this decrease in concentration becomes bigger. When this is compared to the control, where the decrease in YGGFL concentration is much bigger, IPI is affecting the ability of BV to modify the YGGFL peptide. This result can be compared to the results for the YGGFM peptide which was inhibited for a shorter period of time. The difference between these two peptides is the Met/Leu amino acids at the last position in these peptides. This suggest that the YGGFM peptide is a stronger competitor compared to the YGGFL peptide. The signal used for this is δ 7.14 – 7.20 ppm which is a doublet that relates to two protons on the Y part of the YGGFL molecule. The same signal is used for both experiments so a direct comparison can be made.

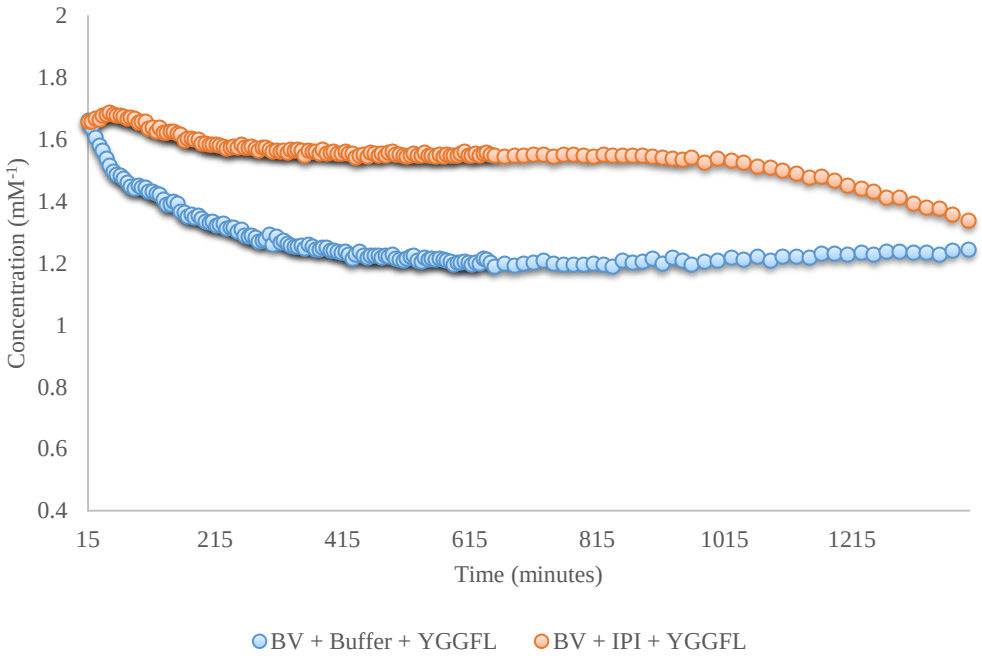

Figure 5.3.6.5.1: Graphical representation of the modification of YGGFL by BV in the presence of IPI. The signal used was δ 7.14 – 7.21 ppm. This is the same for both experiments.

The effect of inhibition by IPI is detailed in table 5.3.6.1. This table shows the amount of substrate which has been converted at 200 minutes with and without IPI present. The results show that for all of these substrates there is a decrease in conversion when in the presence of IPI. The biggest decrease is for the GP-X substrate. The % conversion of the GP-X in the presence of IPI is not shown, this is due to the small increase in signal intensity at the beginning of the experiment which could be due to solubility.

Table 5.3.6.1: Effect of inhibition

Substrate	% Breakdown at 200 mins	% Breakdown at 200 mins in presence of IPI
GP-X	67.3 %	N/A
YGG	8.2 %	1.5 %
FGG	5.5 %	1.0 %
YGGFM	19.5 %	5.7 %
YGGFL	23.5 %	5.9 %

*N/A results are due to the solubility issues.

5.3.7 Results of BV + FPI + Substrate Experiments

5.3.7.1 BV + FPI + GP-X

The results in figure 5.3.7.1.1 show the modification of GP-X in the presence of the inhibitor IPI and FPI along with a control experiment. From this graph, both the IPI and FPI appear to inhibit the modification of this substrate by BV. The IPI inhibitor appears to have a greater effect when compared with the FPI inhibitor as there is a longer duration of inhibition. It should be noted that the same signal mentioned previously is used for all three experiments.

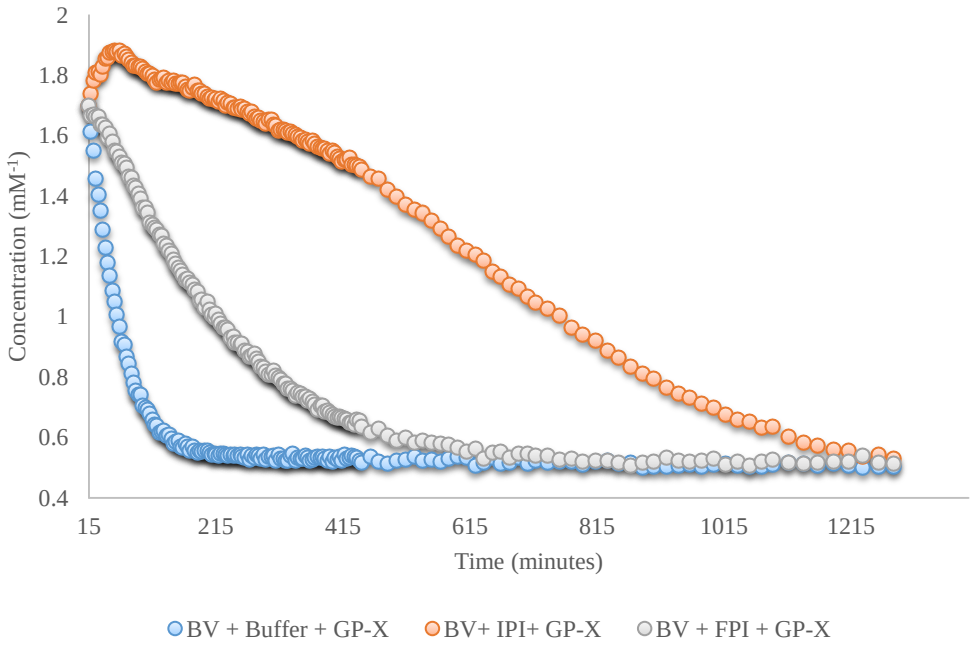

Figure 5.3.7.1.1: Graphical representation of the modification of GP-X by BV in the presence of IPI and FPI. The signal used was δ 7.42 – 7.52 ppm. This is the same for all three experiments.

5.3.7.2 BV + FPI + YGG

The results in figure 5.3.7.2.1 show the modification of the YGG model substrate in the presence of the inhibitor IPI and FPI along with a control experiment. The results for the modification of the YGG in the presence of the FPI inhibitor show that there is a small increase in the signal intensity of YGG at the beginning of this reaction (*ca.* 10 - 250 minutes). This may be due to solubility of the YGG. The peptide might be becoming more concentrated with the increase in temperature when in the probe. However, despite this solubility issue there still appears to be inhibition of the modification of the YGG peptide in the presence of both inhibitors. It is also clear that the IPI inhibitor showed stronger inhibition when compared with the FPI inhibitor. It should be noted that the same signal mentioned previously is used for all three experiments.

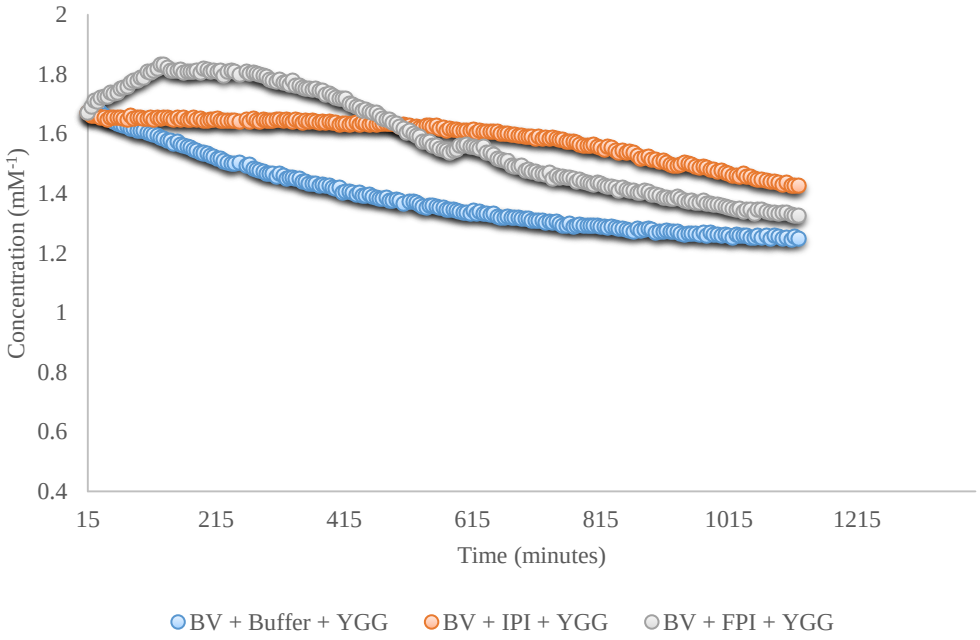

Figure 5.3.7.2.1: Graphical representation of the modification of YGG by BV in the presence of IPI and FPI. The signal used was δ 7.14 – 7.20 ppm. This is the same for all three experiments.

5.3.7.3 BV + FPI + FGG

The results in figure 5.3.7.3.1 show the modification of the FGG model substrate in the presence of the inhibitor IPI and FPI along with a control experiment. The same issue with solubility seen for the YGG peptide in the presence of FPI inhibitor is also seen here for the FGG peptide. It is also clear there is inhibition of the modification of the FGG peptide by both inhibitors. The results here show that the modification of the FGG peptide in the presence of the IPI inhibitor is completely blocked for around 450 minutes. However in the presence of the FPI inhibitor (despite the solubility issue) the modification is also blocked for around the same amount of time as with the IPI inhibitor. This shows that the inhibition of the FGG peptide by these inhibitors is almost the same. It should be noted that the same signal mentioned previously is used for all three experiments.

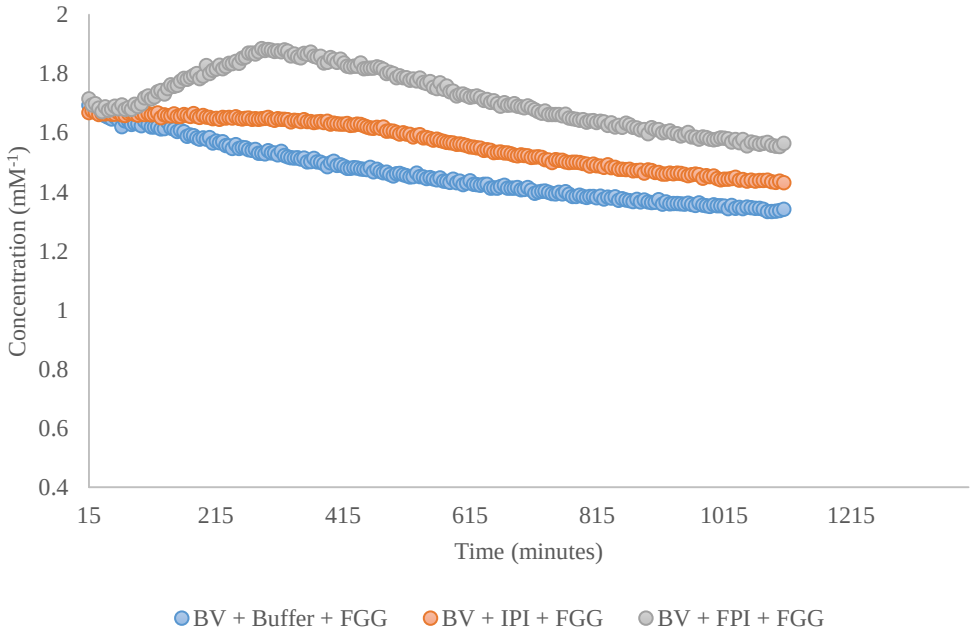

Figure 5.3.7.3.1: Graphical representation of the modification of FGG by BV in the presence of IPI and FPI. The signal used was δ 3.98 – 4.06 ppm. This is the same for all three experiments.

5.3.7.4 BV + FPI + YGGFM

The results in figure 5.3.7.4.1 show the modification of the YGGFM substrate in the presence of the inhibitor IPI and FPI along with a control experiment. The graph here clearly shows that the modification of the YGGFM substrate is inhibited. It also shows that there is only a small difference in inhibition between the presence of IPI and the presence of FPI. This can be compared to the results for the YGG peptide and the DPP IV substrate where the IPI appears to be the better inhibitor. There is also no solubility issue seen here which was noted for the YGG and FGG peptides. It should be noted that the same signal mentioned previously is used for all three experiments.

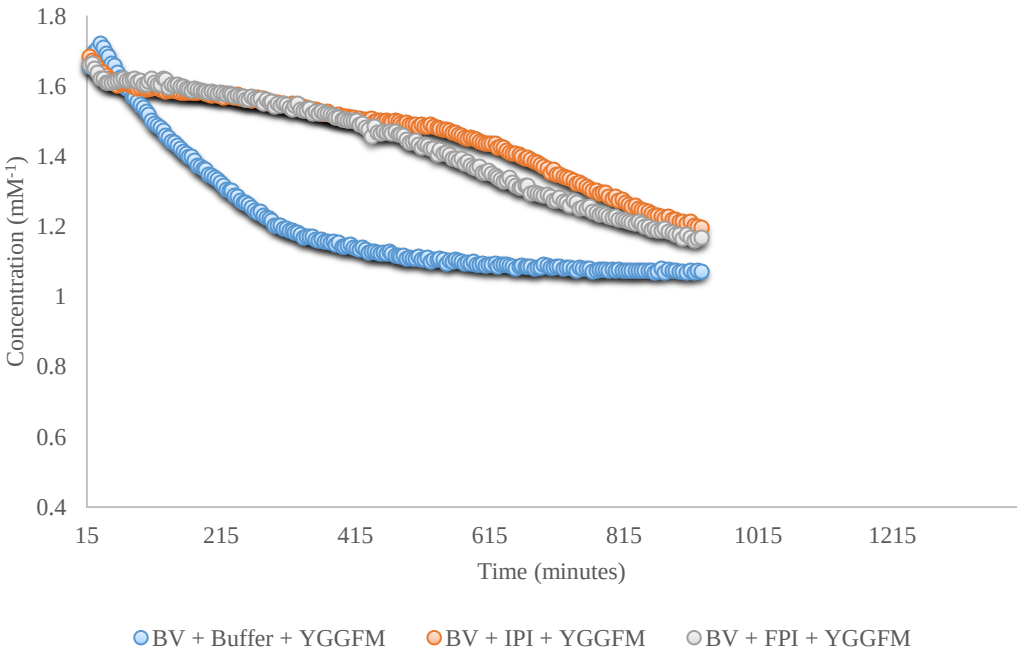

Figure 5.3.7.4.1: Graphical representation of the modification of YGGFM by BV in the presence of IPI and FPI. The signal used was δ 7.14 – 7.20 ppm. This is the same for all three experiments.

5.3.7.5 BV + FPI + YGGFL

The results in figure 5.3.7.5.1 show the modification of the YGGFL substrate in the presence of the inhibitor IPI and FPI along with a control experiment. The graph here shows that the modification of the YGGFL substrate is inhibited. The results show that the IPI inhibitor is better than the FPI inhibitor as there is a much longer duration of inhibition of the modification of the YGGFL substrate (table 5.3.7.1). Although the % conversion at 200 minutes shows that the FPI peptide is a better inhibitor, looking at the overall results the IPI peptide has a longer effect of inhibition. Comparing these results to those from the inhibition of the YGGFM modification, there is a difference between the two. The YGGFM substrate showed that in the presence of both IPI and FPI there was very similar inhibition (table 5.3.7.1). However, for the YGGFL substrate the IPI inhibitor shows much stronger inhibition. Similar to the YGGFM results there is no solubility issue seen here either. It should be noted that the same signal mentioned previously is used for all three experiments.

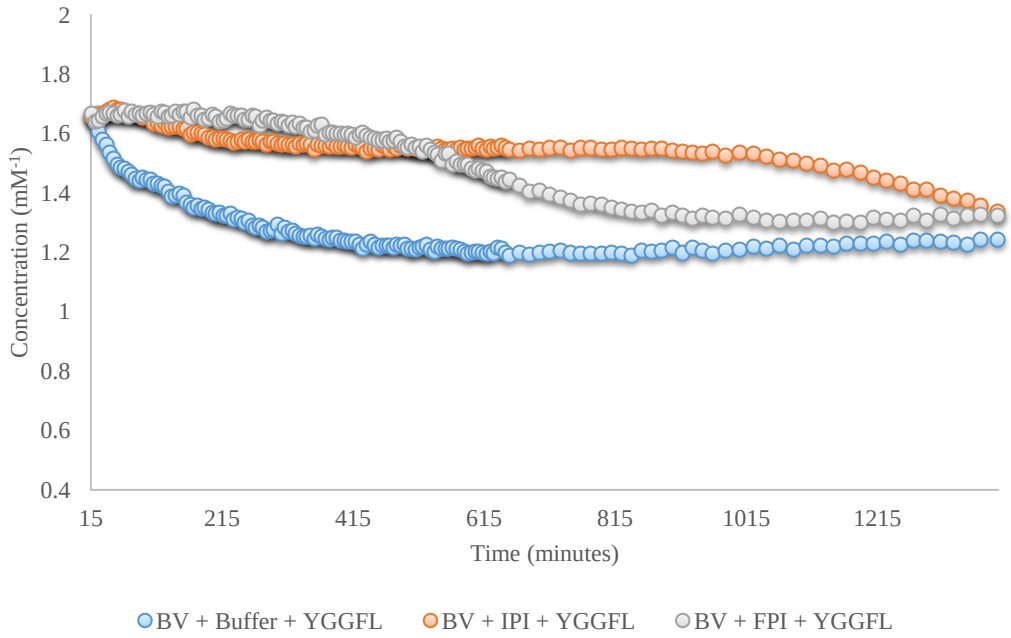

Figure 5.3.7.5.1: Graphical representation of the modification of YGGFL by BV in the presence of IPI and FPI. The signal used was δ 7.14 – 7.21 ppm. This is the same for all three experiments.

The effect of inhibition by FPI along with IPI is detailed in table 5.3.7.1. The results show that for all of these substrates there is a decrease in conversion when in the presence of either IPI or FPI. The results show that IPI has the strongest effect of inhibiting the conversion of substrates to a product by BV. As previously mentioned the % conversion for some substrates are not shown, this is due to the small increase in signal intensity at the beginning of the experiment which could be due to solubility.

Table 5.3.7.1: Effect of inhibition on enzyme activity

Substrate	% Breakdown at 200 mins	% Breakdown at 200 mins in presence of IPI	% Breakdown at 200 mins in presence of FPI
GP-X	67.3 %	N/A	38.1 %
YGG	8.2 %	1.5 %	N/A
FGG	5.5 %	1.0 %	N/A
YGGFM	19.5 %	5.7 %	5.0 %
YGGFL	23.5 %	5.9 %	1.6 %

*N/A results are due to the solubility issues.

There are no statistics shown for these experiments as they were only conducted once. Repeat experiments could not be carried out due to the time and cost of carrying out these experiments.

5.4 Summary

The results here have shown that both the IPI and FPI tripeptides inhibited the ability of BV to modify all the substrates which were tested. The IPG tripeptide tested is completely modified after 20 minutes in the presence of BV. This tripeptide was therefore not used in any further experiments. Overall the IPI inhibitor appears to be the stronger inhibitor. This is due to there being an overall lower conversion of substrate at 200 minutes when compared with the substrates in the presence of FPI (table 5.3.7.1).

Chapter 6

6.0 Discussion of results

One of the aims of this project was to develop an effective NMR method for monitoring enzyme activity. This was successfully achieved and the method allowed the enzyme reactions to be monitored in real time giving a detailed picture of the enzyme action as it took place. The successful NMR method was then applied to test for activity in BV against various defence mediators that may be released by mammals. The detection of activity in BV then led to experiments, using the established NMR method, to characterise this activity and to deduce the component responsible for this activity.

The results have shown that BV modifies several of the opioid peptides (YGGFM, YGGFL, YPWF, YPFF and YPFPGPI) along with substance P, a specific human DPP IV substrate (GP-X) and the model peptides FGG and YGG. The BV activity against these substrates was also inhibited by a specific human DPP IV enzyme inhibitor.

6.1 Quality Control

This work is part of a larger project which involves the development of a cosmetic product which contains BV. Therefore, it is important to establish the LoD/LoQ of WBV as NMR could be used as the method of determining the quality of the cosmetic product.

Cytotoxicity studies of BV were carried out using EZ-cytox Enhanced Cell Viability Assay Kit (Clements, C., unpublished work). A control was ran by incubating normal human dermal fibroblasts (NHDF) cells at 37 °C, 5% CO_2, Dulbecco's modified eagle medium (DMEM) (low glucose) added with 10% foetal bovine serum (FBS) for 24 hours. These cells were then incubated with 0.01, 0.1, 1, 5, 10 µg/mL BV for 24 and 48 hours. After incubation these cells were switched to media with no FBS. Absorbance was then measured after 2 hours of incubation. The results found that a

concentration of 5 µg/mL BV was the minimum concentration that showed cytotoxicity. Using these cytotoxic results and the NMR LoD/LoQ results; gives a window of concentrations of BV which can be used in a formulation. A range of concentrations between 0.99 µg/mL and 5 µg/mL BV can therefore be measured by NMR.

6.2 Enzyme Activity

6.2.1 Enkephalin and Nociceptin Fragments

The enkephalin peptide fragment, YGG, and the nociceptin fragment, FGG, were used as cheaper alternatives to the enkephalin peptides. Assigning the spectra for YGG and FGG provided an insight into the modification pathway for the enkephalin peptides/nociceptin.

The results of the YGG/FGG reactions showed that similar modification pathways were occurring. This was due to the formation of a singlet at around δ 3.58 ppm after 15 minutes of mixing with BV. This signal represents the two ^{1}H of the alpha carbon in free G. This meant that both of these peptides were being hydrolysed at the GG peptide bond. This was an indication that the enzyme responsible for this activity was consistent with a dipeptidyl peptidase. There is a protein found in BV, from genome sequencing, that shows significant sequence homology to the human dipeptidyl peptidase IV enzyme and it is identified as Api m 5. It is therefore possible that this protein is the enzyme responsible for the hydrolysis of the GG bond of these model peptides. It was also observed that the YG dipeptide was hydrolysed by BV forming Y and G. This means that there is also a dipeptidase enzyme present. Thus the YGG tripeptide hydrolysis pathway by BV is YGG to YG and G followed by YG to Y and G.

However, looking closely at the aromatic signals in the BV/YGG reaction, there were four different Y-derived signals present as the reaction takes place. Three of these can be attributable to YGG, YG and free Y. The appearance of the fourth Y-derived aromatic signal is unclear. It is possible there is another enzyme acting at the same

time which could be modifying the –OH on the side chain of the Y amino acid therefore resulting in the fourth Y-derived signal. The free G signal at δ 3.58 ppm is formed from the beginning of the reaction meaning the hydrolysis must firstly occur between the GG peptide bond. By comparison to the ^{1}H spectrum for GG there was no evidence observed for the formation of the dipeptide GG during this reaction.

This is an indication that the enkephalin peptides may be modified via a similar pathway to the peptide fragment, YGG. Therefore assigning the spectra in detail for both the YGGFM and YGGFL peptides to see if there is any evidence of these products being formed will be indicative of the enkephalin peptides being modified in a similar way as the peptide fragment.

6.2.2 The Enkephalin Peptides – YGGFM and YGGFL

The results for both YGGFM and YGGFL also show four Y-derived signals, similar to those obtained from the YGG peptide fragment. This suggests that BV is modifying the enkephalin peptides in a similar way to the YGG peptide. Since the discovery of the enkephalin peptides they have been widely studied. Studies have found that the enkephalin peptides are inactivated via several enzymes depending on the location of the peptides; aminopeptidase N cleaves at the YG bond, a dipeptidyl peptidase III cleaves the GG bond and neutral endopeptidase cleaves the GF bond.[116,215]

The ^{1}H spectrum for the YGG peptide (Appendix 4, 4H) showed a singlet at δ 3.76 ppm. This signal relates to the ^{1}H attached to the alpha carbon in the second glycine in the YGG peptide before reaction. The YGGFM/YGGFL results do not show the appearance of this singlet at δ 3.76 ppm during the reaction. The appearance of this signal during the BV/enkephalin reaction would indicate that YGG is being released as hydrolysis takes place. This result therefore shows that the modification of these peptides is not occurring at the GF bond to release YGG. This means that there does not appear to be a neutral endopeptidase equivalent in BV, or if there is it does not compete with DPP IV.

In the YGGFM and YGGFL reactions two doublets form at δ 7.186 and 6.906 ppm for YGGFM hydrolysis and δ 7.182 and 6.905 ppm for YGGFL hydrolysis. This can be compared to the YG spectrum which also shows two doublets at the same chemical shift region (δ 7.182 and 6.904 ppm). This result is a strong indication that the enzyme responsible is a dipeptidyl peptidase enzyme and is cleaving the enkephalin peptides at the GG peptide bond. These results also indicated that the BV may be targeting the opioid peptides so it was decided to look further into other opioid substrates.

6.2.3 Human DPP IV Substrate – GP-7-amido-4-methylcoumarin hydrobromide

GP-7-amido-4-methylcoumarin hydrobromide, referred to as GP-X is not a typical peptide like the other substrates tested as it is a peptide analogue. However it contains the dipeptide GP which, with Pro at the penultimate position, is a key characteristic for the human DPP IV enzyme. Results show that BV modified the human DPP IV substrate GP-X as the signals for the unmodified GP-X molecule disappear. This also happened in buffer however in the presence of BV this occurs at a much faster rate.

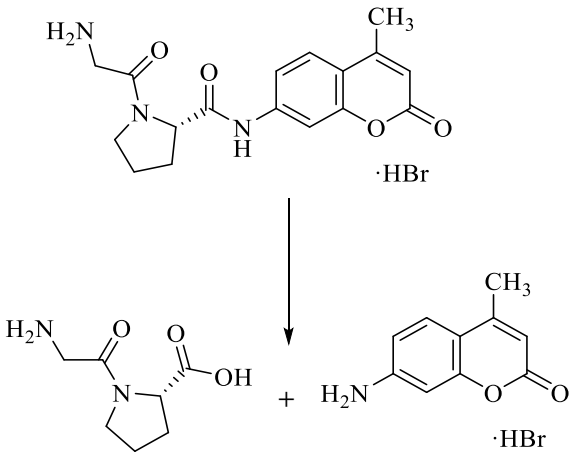

Figure 6.2.3.1: Cleavage pathway of GP-7-amido-4-methylcoumarin hydrobromide

The cleavage pathway of the DPP IV substrate is shown in figure 6.2.3.1 showing the formation of the NH_2 on the methylcoumarin degradation product. This result therefore provides more evidence for showing that the enzyme responsible for activity is consistent with the DPP IV-like enzyme.

6.3 Enzyme Inhibition

Inhibition of the BV activity by IPI in this study agrees with the results of another study. Blank *et al.* showed that IPI inhibited the BV activity against a human DPP IV substrate homologue.[57] In the Blank *et al.* study both the recombinant and native (whole BV) enzyme activity was tested for by using a different synthetic substrate (the DPP IV synthetic substrate GP-*p*-nitroanilide hydrochloride) compared to the substrates used in the current study. However the substrate homologue has the characteristic proline at the penultimate position. The inhibition of this activity was then tested in the presence of DPP IV inhibitor, diprotin A (IPI). Inhibition of activity in this study was then compared to the reported inhibition of human DPP IV enzyme. The results showed similarity to inhibition of human DPP IV. This indicated that the catalytic mechanism of human DPP IV is conserved in BV component Api m 5.

Results show the hydrolysis of the IPI (diprotin A) tripeptide by BV shows similarity with the results of another study also showing IPI being hydrolysed by the human DPP IV enzyme.[216] HPLC was used as the analytical tool in this study and showed that IPI is degraded by human DPP IV to Ile-Pro-OH and Ile (figure 6.3.1). A proline at the penultimate position is the rate limiting step for the human DPP IV enzyme. Therefore, this result is not surprising given that diprotin A has the amino acid sequence IPI. This study showed that IPI acts as a competitive inhibitor where it has a stronger specificity for the enzyme binding site over the substrates tested. To confirm if this is a competitive inhibitor for the current study further experiments would be needed. This would involve repeating the inhibitor experiments, however the concentration of IPI would be varied and the substrate concentration would be kept constant. This will have an effect on the Vmax and Km and will therefore give information on the type of inhibition.

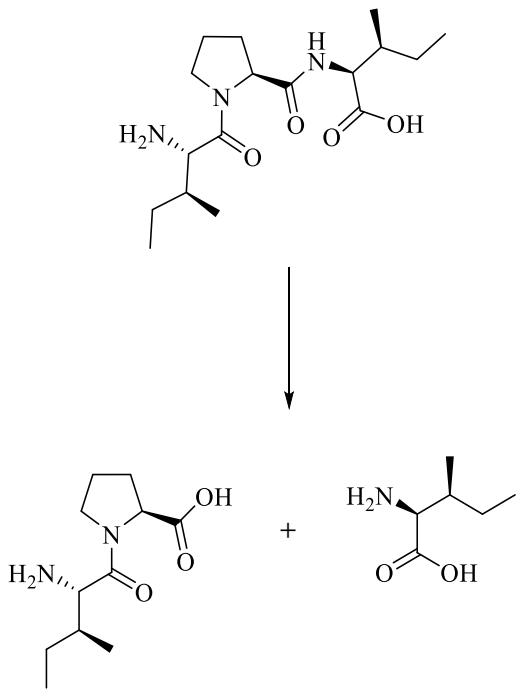

Figure 6.3.1: Cleavage pathway of IPI

Berger and Schechter devised a notation for simplifying the mapping of active sites of enzymes.[217] They divided the catalytic sites into subsites which are areas of the catalytic site which bind to only one amino acid in a substrate. The subsites (S) of the catalytic site are numbered from the point of cleavage to the N terminal S1, S2 and so on and are numbered S1', S2' and so on towards the C terminal. The amino acid residues in the substrate which occupy these subsites are labelled P1, P2 and so on towards the N terminal and P1', P2' and so on towards the C terminal, this notation is shown in figure 6.3.2. This notation will be used here to discuss the results of this study.

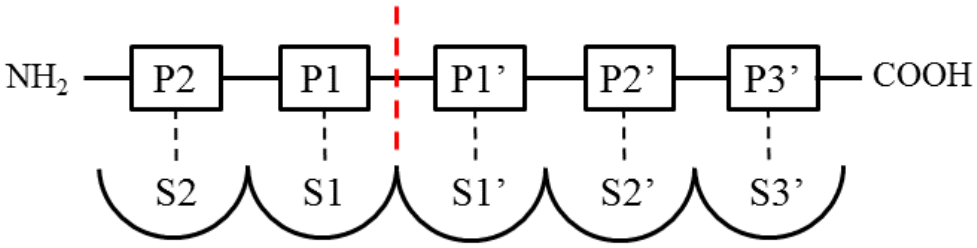

Figure 6.3.2: Enzyme-substrate complex according Berger and Schechter. The red dashed line indicates the point of cleavage.

A single amino acid substitution at the P1' position of the IPI tripeptide from Ile to Gly was made. The resulting tripeptide (IPG) was rapidly hydrolysed by the BV with no more conversion occurring after 20 minutes. A study found that binding of the P1' residue of substrates in the S1' subsite of human DPP IV was via van der Waals interactions. This is due to the flat and indistinct nature of the S1' subsite of human DPP IV.[66] The nature of this subsite means that the majority of amino acids can fit into it. This result meant that the IPG tripeptide can be described as a very good substrate, rather than an inhibitor. The flexibility of the P1' glycine residue may make this the reason that IPG is a poor inhibitor compared to the P1' isoleucine residue in IPI.

The result showing that inhibition of BV activity by FPI was not as pronounced when compared to IPI gave an insight into the catalytic subsites. A single amino acid substitution at the P2 position from Ile to Phe showed that the S2 subsite in the BV enzyme is important for inhibition. The S2 subsite of the human DPP IV is hydrophobic and composed of residues Arg125, Phe357, Tyr547, Pro550, Tyr631 and Tyr666.[66] This subsite therefore binds to hydrophobic and aromatic residues more firmly[66] making Ile and Phe both suitable residues for the P2 site in the peptide. However the result of the current study shows that Ile in the P2 position is preferred over Phe with regard to inhibition. S2 subsite residues Glu205 and Glu206, which form salt bridges with the N-terminus (NH_3^+) of inhibitors of the human DPP IV enzyme, are important for the inhibition of activity by this enzyme.[218]

A crystal structure of the human DPP IV enzyme in a complex with diprotin A (IPI) (figure 6.3.3) revealed that the low turnover for this tripeptide is due to the salt bridge interactions with both the N- and C-termini of IPI along with H-bonding resulting in the IPI tetrahedral intermediate being confined.[59] The crystal structure also revealed that the P2 and P1' Ile residues of IPI were both facing the solvent, resulting in hydrophobic interactions, suggesting that these interactions result in an unsuitable conformation for the reaction to occur optimally. Therefore it is likely that this is the mode of inhibition for the BV component Api m 5 as there is sequence homology around the catalytic site (figure 6.3.4).

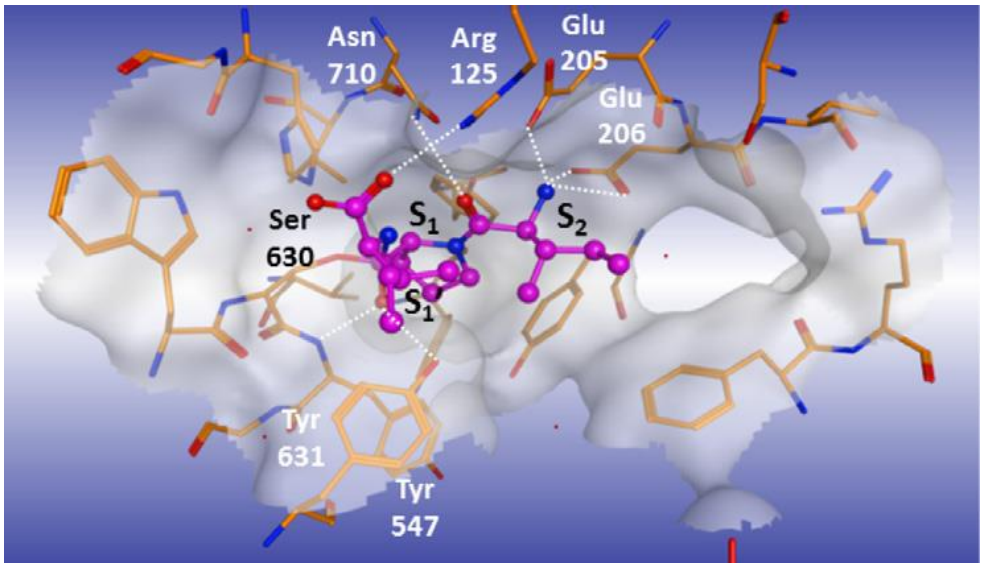

Figure 6.3.3: Co-crystal structure of DPP IV with Diprotin A showing the active site. Diprotin A is shown in magenta and DPP IV is shown in orange. Reproduced with permission.[218]

Subsites for the human DPP IV enzyme have not been defined beyond the S2 subsite. A comparison between the co-crystal structure of six different inhibitors (Sitagliptin, Vildagliptin, Saxagliptin, Alogliptin, Linagliptin and Teneligliptin) with the human DPP IV enzyme was carried out.[218] This comparison has revealed that an increase in inhibition can be achieved by an interaction with a subsite beyond the S2 subsite which has been called the S2 extensive subsite. This S2 extensive subsite is beyond the S2

subsite and does not play a role in substrate binding. Val207, Ser209, Phe357 and Arg358 are the residues which make the S2 extensive subsite. Following the results of this study the authors have suggested a classification system for the inhibitors of the human DPP IV enzyme according to the subsites' interaction with the inhibitor. Although none of these inhibitors were tested against BV it is possible that they are able to inhibit BV activity. Obtaining the crystal structure of BV Api m 5 with diprotin A is therefore an important experiment to carry out. The information gained from this experiment would give a deeper insight into the BV enzyme subsites and could help with the development of better inhibitors.

The results in this current study are the first to show the inhibition of BV enzyme Api m 5 modification of opioid peptides. This could have potential therapeutic benefits. Inhibited BV may have pain relieving properties as it could be used to stimulate the release of opioid peptides such as endomorphin I and II along with met- and leu-enkephalin. Overall the result showing that BV activity was inhibited by human DPP IV inhibitor is evidence that the enzyme responsible for activity in BV is DPP IV-like.

Figure 6.3.4: Sequence alignment of human DPP IV enzyme (P27487 DPP4_HUMAN) and BV component Api m 5 (B2D0J4 VDPP4_APIME). The active site is highlighted in red.

6.4 Substrate Specificity

Despite the difference in concentration ratios, the results show that YPWF is modified the quickest, with FGG being modified the slowest. As the YPWF peptide is modified quicker than the YPFF this suggests that the BV peptidase binds to the W residue with higher affinity compared to the F residue.

Entry of substrates through the β-propeller tunnel and exit through the side opening (figure 1.0.2.6.3) in the human DPP IV enzyme explained the high specificity of this substrate. As BV component Api m 5 is only similar to human DPP IV around the catalytic site (figure 6.3.4) it is possible that the substrate access and product exit is different from the human DPP IV enzyme. However, given the high substrate selectivity it is also possible that Api m 5 has similar routes of entry and exit to the catalytic site. This also highlights the need to deduce the crystal structure of Api m 5.

6.5 Identification of Enzyme

As the BV component Api m 5 shows sequence homology to the human DPP IV enzyme around the catalytic site[57] it can assumed that the activity of the BV component Api m 5 will be similar to the human enzyme. These residues are also present in the Api m 5 sequence when compared with the sequence of the human DPP IV enzyme (figure 6.3.4). However further studies will be required to establish the specific activity of the BV enzyme. The 3D structure of the human DPP IV enzyme could be used to help model the crystal structure of BV component Api m 5.

The results in this study have shown that BV is targeting the opioid peptides and is hydrolysing the substrates by cleaving dipeptides from the N-terminus. Cleavage of dipeptides from the N-terminus with Pro or Ala at the penultimate position is characteristic of the human DPP IV enzyme. The human DPP IV enzyme is known to hydrolyse the substance P peptide (table 6.5.1).[30,219]

Table 6.5.1: Comparison of enzyme substrate specificity

Substrate	Amino Acid Sequence	Human DPP III	Human DPP IV	BV
Endomorphin I	YPWF	✓	✓	✓
Endomorphin II	YPFF	✓	✓	✓
Substance P	RPKPQQFFGLM	×	✓	✓
Gly-Pro-7-amido-4-methylcoumarin hydrobromide	GP-X	×	✓	✓
Leu-enkephalin	YGGFL	✓	×	✓
Casomorphin 1-7	YPFPGPI	×	✓	✓
Met-enkephalin	YGGFM	✓	×	✓
Angiotensin II	DRVYIHPF	✓	×	×
Bradykinin	RPPGFSPFR	×	×	×
Epinephrine	N/A	×	×	×
Cortisol	N/A	×	×	×

According to the BRENDA database cortisol and epinephrine are not substrates for DPP III/IV.

Püschel *et al.* identified that substance P hydrolysis by human DPP IV produces the two dipeptides RP and KP.[219] Given that the results from the enkephalin hydrolysis indicate that a DPP was involved, it is likely that the same enzyme is involved in the substance P hydrolysis. A full spectral assignment of substance P was not deduced. However, evidence from other results indicate an enzyme similar to human DPP IV in BV is responsible for hydrolysis. Therefore it is likely that hydrolysis of substance P by BV occurs by this BV component. It can therefore be inferred that substance P would firstly be hydrolysed at the Pro2-Lys3 bond followed by the Pro4-Gln5 bond to release the dipeptides RP and KP respectively.

Contradictory to the result of BV hydrolysing substance P is that BV hydrolysed both the enkephalin peptides, which the human DPP IV enzyme is not known to hydrolyse. Another dipeptidyl peptidase (DPP III) enzyme is responsible for the hydrolysis of these opioid peptides in humans (table 6.5.1).

The human DPP III enzyme (sometimes referred to as Enkephalinase B)[220] belongs to the M49 metalloproteinase family which relies on a zinc ion for activity.[122] The human DPP III enzyme also hydrolyses dipeptides from the N termini of peptides.[122,220] Human DPP III also hydrolyses the endomorphin peptides.[122]

Human DPP III (EC 3.4.14.4) enzyme is composed of 737 amino acids.[220] The ribbon structure for this enzyme has been deduced and is shown in figure 6.5.1. There is a large cleft which separates two lobes, with the lower lobe being predominately composed of α-helices, which is also where the zinc binding site is found. The upper lobe has both α and β folds along with a core which is composed of a 5-stranded β-barrel.[122]

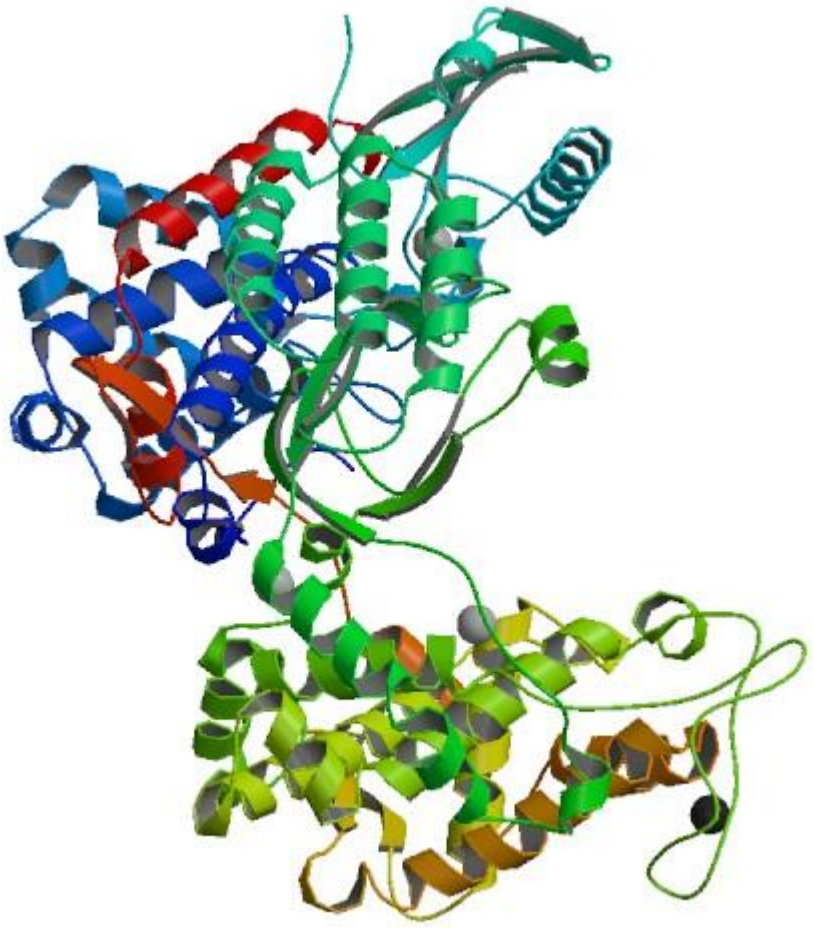

Figure 6.5.1: Ribbon structure of human DPP III enzyme, this structure was obtained at a resolution of 1.9 Å. The structure was taken from the RCSB protein data bank.[221] The different colours represent the different secondary folds within the protein. Zinc ion is shown as grey ball.

Human DPP III contains a unique conserved zinc binding motif, 450-HELLGH-455, which follows the characteristic HEXXGH motif for the M49 metalloproteinase family.[122,220] The His450 and His455 residues of this conserved motif are involved in the coordination of the zinc ion (figure 6.5.2). There is another conserved motif, 507-EECRAE-512, where the Glu508 residue in this motif is also involved in coordination of the zinc ion.[121,122] Along with residues His450, His455 and Glu508, there is a water molecule involved in forming the tetrahedral complex with the zinc ion for catalysis.[121]

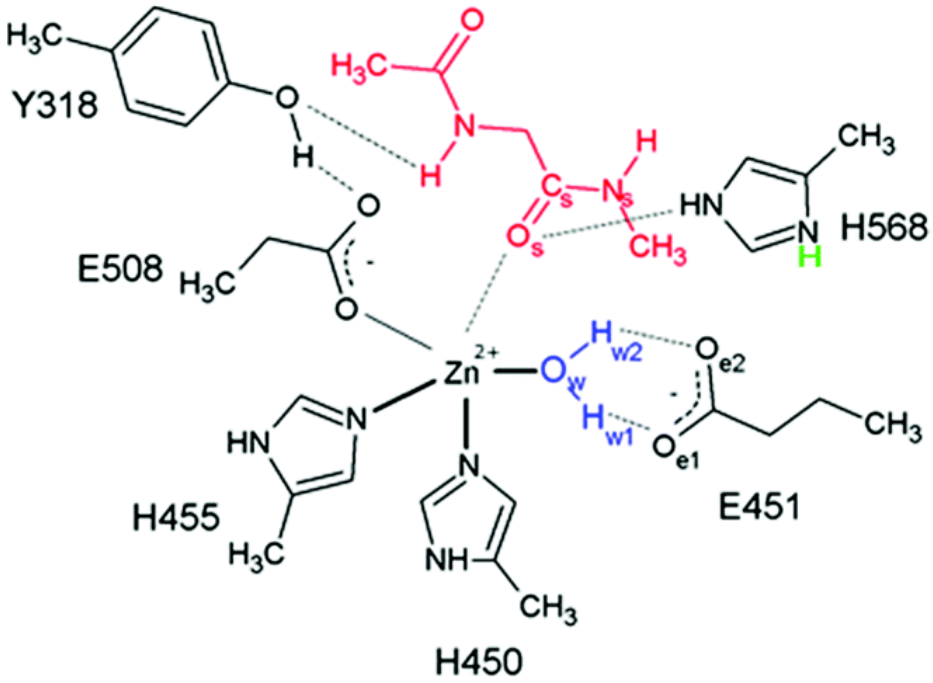

Figure 6.5.2: DPP III active site. Water is shown in blue and substrate (CH_3CO–Gly–$NHCH_3$) is shown in red. Black dashed lines represent electrostatic interactions. His568 is protonated. Reproduced with permission from RSC (Published by the PCCP Owner Societies).[222]

Human DPP III has a different catalytic mechanism when compared to the human DPP IV enzyme as it relies on a metal ion for catalysis whereas the DPP IV enzyme has a catalytic triad for catalysis. The mechanism for the DPP III enzyme begins with deprotonation of the water molecule by Glu451. Following deprotonation of the water molecule the carbonyl carbon of the scissile bond is attacked forming an oxyanion which is stabilised by His568.[122] This is known as the water mechanism and is how the human DPP III enzyme hydrolyses met- and leu-enkephalin. However, a second mechanism has been proposed for hydrolysis of endomorphin I and endomorphin II, which has been named the anhydride mechanism. This is due to the Pro2 residue in these peptides being closer in distance to coordinate with the zinc ion meaning the Glu451 residue can attack the scissile bond directly.[122]

Studies on the human DPP III enzyme revealed that there are large scale conformational changes which occur upon substrate binding which has been described as "protein closure".[220,223,224] Results also revealed that residue Asp372 plays an important role in this conformational change.[223] The substrate binding to human DPP III is an entropy driven process resulting in bulk release of water molecules from the cleft.[220] The "protein closure" of human DPP III is thought to contribute to the wide substrate specificity of this enzyme.[220,223] Human DPP III subsites are fairly hydrophobic and deep which also contributes to the wide specificity of this enzyme.[220] This is in contrast to the human DPP IV enzyme where the small nature of the S1 subsite along with its hydrophobicity (due to residues Val711, Val656, Tyr662, Tyr666, Trp659 and Tyr631) restricts the P1 position to either Pro, Gly or Ala residues.[59,225]

A bee sting in mammals, in particular humans, penetrate the skin. It is therefore important to consider the presence of certain biomolecules which are present in the skin and would come into contact with the BV. A study carried out by Slominski *et al.* looked at the expression of the pro-enkephalin (PENK) gene in human skin.[226] This gene is processed to produce both met- and leu-enkephalin. This study found that there was expression of the PENK gene/protein most significantly in fibroblasts and keratinocytes of skin and cultured cells. Results from mass spectrometry confirmed the presence of both YGGFM and YGGFL in the skin. This study also looked at the regulation of the PENK expression in the skin in the presence of a stressful stimulus (ultraviolet B (UVB)) and during a pathological condition (psoriasis). The observed results showed that PENK was upregulated during stress and changed during a pathological condition. This suggested a role for the enkephalin peptides in playing a part in the protective barrier of the skin and in helping to control homeostasis. A bee sting would be considered a stressful stimulus to humans and would therefore interrupt homeostasis. Slominski *et al.* showed that it is possible the expression of PENK and subsequent release of the enkephalin peptides might be increased during a bee sting. The results showing that BV hydrolyses both enkephalin peptides suggest that the BV has evolved to overcome these defence mechanisms in humans.

The results show that BV hydrolyses substrates which are hydrolysed in humans by two different enzymes with different catalytic mechanisms. This shows that although the BV enzyme (Api m 5) is structurally similar to the human DPP IV (32 % sequence homology) at the catalytic site, the enzyme has evolved to allow substrates, which are a target for human DPP III, to bind to the enzyme.

The human DPP IV enzyme is unable to hydrolyse P-P bonds.[60] Therefore the results showing that BV does not hydrolyse bradykinin (table 6.5.1) provides more evidence that the enzyme responsible for the activity found in BV is like DPP IV. This is because the first three amino acids in the bradykinin sequence are RPP which human DPP IV would not be able to cleave. Proline has two conformations (cis or trans) and therefore having two proline residues next to each other in a peptide could produce a conformation which may not be able to react with the enzyme. The S1' subsite of the human DPP IV enzyme has also been described as flat and non-distinct which could also be why this enzyme cannot hydrolyse P-P bonds.

Together these results show that BV component Api m 5 shows enzyme similarity to both the human DPP III and DPP IV enzymes. This conclusion was made due to the knowledge that the enkephalin peptides are hydrolysed by human DPP III, the endomorphin peptides are hydrolysed by human DPP III and DPP IV, and substance P is hydrolysed by human DPP IV. The BV component Api m 5 is more like human DPP IV due to the similarity around the catalytic site (figure 6.3.3). However, it is able to hydrolyse substrates which are a target for the human DPP III enzyme. This makes the BV enzyme different from the human DPP IV enzyme. These results also suggest that BV is specifically targeting the opioid peptides within a mammal.

General Conclusions

The substrate screening study against BV showed that there was activity against only a few of the substrates tested. This indicated that the enzyme present was targeting peptides involved in pain perception and led to experiments using other substrates involved in pain perception. To summarise, the following are substrates that BV modified:

- Endomorphin I (YPWF)
- Endomorphin II (YPFF)
- Substance P (RPKPQQFFGLM)
- Casomorphin 1-7 (YPFPGPI)
- Met-enkephalin (YGGFM)
- Leu-enkephalin (YGGFL)
- YGG
- FGG

BV also modified the human DPP IV specific substrate (GP-7-amido-4-methylcoumarin hydrobromide). This modification gave further evidence that the DPP IV-like enzyme found in BV was responsible for the modification of the other substrates tested.

The substrate which was hydrolysed most rapidly was endomorphin I, closely followed by endomorphin II. This showed that having a proline residue in the P1' position resulted in the substrate being hydrolysed more rapidly when compared with glycine in this position (the enkephalin peptides).

Diprotin A (a DPP IV specific inhibitor) also proved to be effective at slowing the degradation of substrates for BV. Results also showed that the inhibitor itself is slowly broken down by BV meaning it acts as a competitive inhibitor. This leads to the conclusion that the DPP IV-like enzyme in BV is responsible for the observed biological action of BV.

BV showed similar enzyme specificity to both human DPP III and DPP IV. However, structurally it is most similar to the human DPP IV catalytic site (due to sequence similarity). Therefore, the conclusion made is that BV component Api m 5 is a DPP IV-like enzyme responsible for the biological activity in humans. This is the first report of the action for this enzyme showing that it targets opioid peptides.

In mammals bee stings cause pain[227] as a distraction. Therefore, these results are logical. One of the ways in which BV can cause pain is that it contains the enzyme PLA_2 which attacks cell membranes by cleaving the phospholipids and releasing arachidonic acid.[44] Arachidonic acid, an eicosanoid, can then be metabolised by cyclooxygenase enzymes to form prostaglandin G_2 (PGG_2). This is converted to prostaglandin H_2 (PGH_2) by peroxidase where PGH_2 can then be converted to either prostaglandin or thromboxane by prostaglandin synthase or thromboxane synthase respectively.[228] Prostaglandins are involved in inflammation and also sensitising neurons to pain.[229] The results of this current study showing that BV inactivates several of the opioid peptides which are released to dull pain is therefore to prolong the pain caused by other components of the venom.

Collaborative Work

As previously mentioned this work is part of a larger project. There is a collaboration between Strathclyde University (both Pure and Applied Chemistry and Strathclyde Institute of Pharmacy and Biomedical Sciences departments) and London College of Fashion (LCF). The aim was to develop a cosmetic formulation which incorporates BV for the European market. Therefore, an NMR method can be used for checking the quality of the formulations and the stability of the BV within a formulation. This would ensure that the quality of the cosmetic product produced is consistent and reliable. As the work discussed in this thesis has been used for a patent application there are no publications. However, attached to this thesis are three published papers from additional work carried out as part of the larger project.

Purification of WBV was carried out by PhD student Jonans Tusiimire from the Strathclyde Institute of Pharmacy and Biomedical Sciences department. NMR was then used to establish the quality of a particular purified WBV fraction (discussed in paper 1). Experiments also carried out by Jonans Tusiimire indicated that a particular components of purified BV had activity. However, this component could not be identified by mass spectrometry. Therefore, the component was analysed using NMR to identify it (discussed in paper 2). The NMR method established for paper 1 was then used to test the purity of the melittin used in paper 3 and 4. For electronic copy of this thesis the reference links to these papers are shown below.

1. An LCMS method for the assay of melittin in cosmetic formulations containing bee venom. J. Tusiimire, J. Wallace, M. Dufton, J. Parkinson, C.J. Clements, L. Young, J.K. Park, J.W. Jeon and D.G. Watson. Analytical and Bioanalytical Chemistry. Volume 407, 2015.
2. Effect of Bee Venom and Its Fractions on the Release of Pro-Inflammatory Cytokines in PMA-Differentiated U937 Cells Co-Stimulated with LPS. J. Tusiimire, J. Wallace, N. Woods, M. Dufton, J. Parkinson, G. Abbott, C.J. Clements, L. Young, J.K. Park, J.W. Jeon, V.A. Ferro and D.G. Watson. Vaccines. Volume 4, 2016.

3. Metabolomic Profiling of the Effects of Melittin on Cisplatin Resistant and Cisplatin Sensitive Ovarian Cancer Cells Using Mass Spectrometry and Biolog Microarray Technology. S. Alonezi, J. Tusiimire, J. Wallace, M. Dufton, J. Parkinson, C.J. Clements, L. Young, J.K. Park, J.W. Jeon, V.A. Ferro and D.G. Watson. Metabolites, 2016.
4. Metabolomic Profiling of the Synergistic Effects of Melittin in Combination with Cisplatin on Ovarian Cancer Cells. S. Alonezi, J. Tusiimire, J. Wallace, M. Dufton, J. Parkinson, C.J. Clements, L. Young, J.K. Park, J.W. Jeon, V.A. Ferro and D.G. Watson. Metabolites, 2017.

Future Work

There is a delay associated with collecting the first spectrum after the point of mixing when carrying out these experiments. This is due to the time it takes to transfer the tube into the probe and lock and shim the sample. Therefore this results in the first 10 to 15 minutes of the reaction unrecorded. As a result there is a need to develop new technology which can tackle this issue.

To further investigate the characterisation of the enzyme in BV, other human DPP IV inhibitors such as P32/98 and diprotin B (VPL) could be used. The small model peptide used, YGG, may also act as an inhibitor so this would be another experiment to carry out. Modifications could be made to the diprotin A and B tripeptides in the hope of discovering a better inhibitor. These experiments were not carried out due to cost and time constraints.

Obtaining the crystal structure of the BV Api m 5 component would be a very useful result. This could provide an insight into the catalytic site by providing detailed information about the catalytic subsites such as the residues which make these subsites. This information would therefore help with the development of better inhibitors.

Inhibitor kinetic experiments could also be carried out for the IPI and FPI inhibitors to show the mode of inhibition along with how well the inhibitor binds to the enzyme. This can be done by varying the concentration of the inhibitor and keeping the substrate concentration constant. This will produce a Lineweaver-Burk plot similar to the substrate kinetic experiments. These experiments could not be carried out due to the cost associated with these peptides.

There could also be more analysis on the other opioid peptides (endomorphin I & II and casomorphin 1-7) along with the DPP IV substrate to obtain the kinetic values, to look at the inhibition of these substrates (similarly to the substrates already studied) and work out the pathway by which BV is modifying these peptides. This would give more information about the BV enzyme characteristics.

For more insight into which substrate is the main target of the enzyme, experiments could be carried out by using combinations of peptides. This could be done by

combining leu- and met- enkephalin to see which one is more competitive for the enzyme pocket, similar experiments can also be carried out for the endomorphin peptides.

Additionally this NMR method could be used to look at the relative reactions going on at the same time as peptidase activity (such as hyaluronidase or phospholipase A_2). This will give insight into the biochemical pathway of these enzymes along with the enzyme kinetics. Preliminary experiments have been carried out for the hyaluronidase enzyme and the results are shown in appendix 6.

References

(1) Debevec, A. H.; Cardinal, S.; Danforth, B. N. *Zool. Scr.* **2012**, *41* (5), 527–535.

(2) Fitzgerald, K. T.; Flood, A. A. *Clin. Tech. Small Anim. Pract.* **2006**, *21* (4), 194–204.

(3) Warpinski, J. R.; Bush, R. K. *J. Wilderness Med.* **1990**, *1*, 249–257.

(4) Vetter, R. S.; Visscher, P. K. *Int. J. Dermatol.* **1998**, *37*, 481–496.

(5) Consortium, H. G. S. *Nature* **2006**, *443* (7114), 931–949.

(6) Solomon, C. G.; Casale, T. B.; Burks, A. W. *N. Engl. J. Med.* **2014**, *370* (15), 1432–1439.

(7) Page Jr, R. E.; Y-S Peng, C. *Exp. Gerontol.* **2001**, *36* (36), 695–711.

(8) Klowden, M. J. *Physiological Systems in Insects*, Third.; Academic Press, 2013.

(9) Vilmos, P.; Kurucz, E. *Immunol. Lett.* **1998**, *62* (2), 59–66.

(10) Zhou, J.; Zhao, J.; Zhang, S.; Shen, J.; Qi, Y.; Xue, X.; Li, Y.; Wu, L.; Zhang, J.; Chen, F.; Chen, L. *Anal. Biochem.* **2010**, *404* (2), 171–178.

(11) Chen, J.; Lariviere, W. R. *Prog. Neurobiol.* **2010**, *92* (2), 151–183.

(12) Visscher, P. K.; Vetter, R. S.; Camazine, S. *Lancet* **1996**, *348* (9023), 301–302.

(13) Son, D. J.; Lee, J. W.; Lee, Y. H.; Song, H. S.; Lee, C. K.; Hong, J. T. *Pharmacol. Ther.* **2007**, *115* (2), 246–270.

(14) Baracchi, D.; Francese, S.; Turillazzi, S. *Toxicon* **2011**, *58* (6–7), 550–557.

(15) Pankiw, T. *Apidologie* **2004**, *35*, 217–226.

(16) Van Halteren, H. K.; Van Der Linden, P. W. G.; Burgers, S. a.; Bartelink, A. K. M. *J. Allergy Clin. Immunol.* **1996**, *97* (5), 1058–1063.

(17) Smith, M. L. *PeerJ* **2014**, *2*, e338.

(18) Golden, D. B. K. *Immunol. Allergy Clin. North Am.* **2007**, *27* (2), 261–72, vii.

(19) Baldo, B. A.; Pham, N. H. *Drug allergy: Clinical aspects, diagnosis, mechanisms, structure-activity relationships*; Springer, 2013.

(20) Akdis, C. A.; Blesken, T.; Akdis, M.; Alkan, S. S.; Wüthrich, B.; Heusser, C. H.; Blaser, K. *J. Allergy Clin. Immunol.* **1997**, *99* (3), 345–353.

(21) Stuhlmeier, K. M. *J. Immunol.* **2007**, *179* (1), 655–664.

(22) Allergen nomenclature - WHO/IUIS Allergen Nomenclature sub-committee http://www.allergen.org/search.php?allergenname=&allergensource=bee+venom&TaxSource=Animalia+Arthropoda&TaxOrder=&foodallerg=all&bioname= (accessed Apr 14, 2016).

(23) Amdam, G. V; Rueppell, O.; Fondrk, M. K.; Jr, R. E. P.; Mindy, C. *Exp. Gerontol.* **2013**, *44* (0), 467–471.

(24) BRENDA http://www.brenda-enzymes.org/ (accessed Jan 18, 2017).

(25) Orsolic, N. *Cancer Metastasis Rev.* **2012**, *31* (1–2), 173–194.

(26) Fenton, A. W.; West, P. R.; Odell, G. V.; Hudiburg, S. M.; Ownby, C. L.; Mills, J. N.; Scroggins, B. T.; Shannon, S. B. *Toxicon* **1995**, *33* (6), 763–770.

(27) Raghuraman, H.; Chattopadhyay, A. *Biosci. Rep.* **2007**, *27* (4–5), 189–223.

(28) Melittin http://www.rcsb.org/pdb/explore.do?structureId=2mlt (accessed Jun 1, 2016).

(29) Suchanek, G.; Kreil, G.; Hermodson, M. a. *Proc. Natl. Acad. Sci. U. S. A.* **1978**, *75* (2), 701–704.

(30) Kreil, G.; Haiml, L.; Suchanek, G. *Eur. J. Biochem.* **1980**, *111* (1), 49–58.

(31) Sciani, J. M.; Marques-Porto, R.; Lourenco Junior, A.; Orsi Rde, O.; Ferreira Junior, R. S.; Barraviera, B.; Pimenta, D. C. *Peptides* **2010**, *31* (8), 1473–1479.

(32) Terwilliger, T. C.; Eisenberg, D. *J. Biol. Chem.* **1982**, *257* (11), 6016–6022.

(33) Talbot, J. C.; Dufourcq, J.; de Bony, J.; Faucon, J. F.; Lussan, C. *FEBS Lett.* **1979**, *102* (1), 191–193.

(34) Chen, L. Y.; Cheng, C. W.; Lin, J. J.; Chen, W. Y. *Anal. Biochem.* **2007**, *367* (1), 49–55.

(35) Yang, L.; Harroun, T. a; Weiss, T. M.; Ding, L.; Huang, H. W. *Biophys. J.* **2001**, *81* (3), 1475–1485.

(36) Sengupta, D.; Leontiadou, H.; Mark, A. E.; Marrink, S. J. *Biochim. Biophys. Acta - Biomembr.* **2008**, *1778* (10), 2308–2317.

(37) Vogel, H.; Jähnig, F. *Biophys. J.* **1986**, *50* (4), 573–582.

(38) Monti, M. C.; Casapullo, A.; Santomauro, C.; D'Auria, M. V; Riccio, R.; Gomez-Paloma, L. *Chembiochem* **2006**, *7* (6), 971–980.

(39) Wilton, D. C. *Eur. J. Lipid Sci. Technol.* **2005**, *107* (3), 193–205.

(40) Gijón, M. A.; Leslie, C. C. *J. Leukoc. Biol.* **1999**, *65* (3), 330–336.

(41) Balsinde, J.; Winstead, M. V.; Dennis, E. A. *FEBS Letters*. 2002, pp 2–6.

(42) RSC http://www.rsc.org/Education/Teachers/Resources/cfb/cells.htm (accessed Apr 20, 2016).

(43) Schaloske, R. H.; Dennis, E. A. *Biochimica et Biophysica Acta*. 2006, pp 1246–1259.

(44) Scott, D. L.; Otwinowski, Z.; Gelb, M. H.; Sigler, P. B. *Science* **1990**, *250*, 1563–1566.

(45) Kuchler, K.; Gmachl, M.; Sippl, M. J.; Kreil, G. *Eur. J. Biochem.* **1989**, *184*, 249–254.

(46) Annand, R. R.; Kontoyianni, M.; Penzotti, J. E.; Dudler, T.; Lybrand, T. P.; Gelb, M. H. *Biochemistry* **1996**, *35* (14), 4591–4601.

(47) Crystal Structure of Bee Venom Phospholipase A2 in a complex with a transition-state analogue http://www.rcsb.org/pdb/explore/explore.do?structureId=1POC (accessed Jun 1, 2016).

(48) El-Safory, N. S.; Fazary, A. E.; Lee, C. K. *Carbohydr. Polym.* **2010**, *81* (2),

165–181.

(49) Marković-Housley, Z.; Miglierini, G.; Soldatova, L.; Rizkallah, P. J.; Müller, U.; Schirmer, T. *Structure* **2000**, *8* (10), 1025–1035.

(50) Girish, K. S.; Kemparaju, K. *Life Sci.* **2007**, *80* (21), 1921–1943.

(51) Baumann, L. *J. Pathol.* **2007**, *211* (2), 241–251.

(52) Burdick, J. A.; Prestwich, G. D. *Adv. Mater.* **2011**, *23* (12), H41-56.

(53) Crystal Structure (monoclinic) of Bee Venom Hyaluronidase http://www.rcsb.org/pdb/explore.do?structureId=1fcq (accessed Jun 1, 2016).

(54) Padavattan, S.; Schirmer, T.; Schmidt, M.; Akdis, C.; Valenta, R.; Mittermann, I.; Soldatova, L.; Slater, J.; Mueller, U.; Markovic-Housley, Z. *J. Mol. Biol.* **2007**, *368* (3), 742–752.

(55) Ziai, M. R.; Russek, S.; Wang, H. C.; Beer, B.; Blume, A. J. *J. Pharm. Pharmacol.* **1990**, *42* (7), 457–461.

(56) Gauldie, J.; Hanson, J. M.; Shipolini, R. a; Vernon, C. a. *Eur. J. Biochem.* **1978**, *83* (2), 405–410.

(57) Blank, S.; Seismann, H.; Bockisch, B.; Braren, I.; Cifuentes, L.; McIntyre, M.; Ruhl, D.; Ring, J.; Bredehorst, R.; Ollert, M. W.; Grunwald, T.; Spillner, E. *J. Immunol.* **2010**, *184* (9), 5403–5413.

(58) Ohnuma, K.; Dang, N. H.; Morimoto, C. *Trends Immunol.* **2008**, *29* (6), 295–301.

(59) Thoma, R.; Loffler, B.; Stihle, M.; Huber, W.; Ruf, A.; Hennig, M. *Structure* **2003**, *11* (8), 947–959.

(60) Mentlein, R. *Regul. Pept.* **1999**, *85* (1), 9–24.

(61) Drucker, D. J. *Diabetes Care* **2007**, *30* (6), 1335–1343.

(62) Mulvihill, E. E.; Drucker, D. J. *Endocr. Rev.* **2014**, *35* (6), 992–1019.

(63) Boonacker, E.; Van Noorden, C. J. *Eur. J. Cell Biol.* **2003**, *82* (2), 53–73.

(64) Crystal structure of human Dipeptidyl Peptidase IV (DPP-IV) http://www.rcsb.org/pdb/explore.do?structureId=1nu6 (accessed Jun 1, 2016).

(65) Engel, M.; Hoffmann, T.; Wagner, L.; Wermann, M.; Heiser, U.; Kiefersauer, R.; Huber, R.; Bode, W.; Demuth, H.-U.; Brandstetter, H. *Proc. Natl. Acad. Sci. U. S. A.* **2003**, *100* (9), 5063–5068.

(66) Aertgeerts, K.; Ye, S.; Tennant, M. G.; Kraus, M. L.; Rogers, J.; Sang, B.; Skene, R. J.; Webb, D. R.; Prasad, G. S. *Protein Sci.* **2004**, *13* (2), 412–421.

(67) Bjelke, J. R.; Christensen, J.; Branner, S.; Wagtmann, N.; Olsen, C.; Kanstrup, A. B.; Rasmussen, H. B. *J. Biol. Chem.* **2004**, *279* (33), 34691–34697.

(68) Abbott, C. A.; McCaughan, G. W.; Gorrell, M. D. *FEBS Lett.* **1999**, *458* (3), 278–284.

(69) Samy, R. P.; Gopalakrishnakone, P.; Thwin, M. M.; Chow, T. K. V; Bow, H.; Yap, E. H.; Thong, T. W. J. *J. Appl. Microbiol.* **2007**, *102* (3), 650–659.

(70) Peiren, N.; de Graaf, D. C.; Vanrobaeys, F.; Danneels, E. L.; Devreese, B.; Van Beeumen, J.; Jacobs, F. J. *Toxicon* **2008**, *52* (1), 72–83.

(71) Kini, R. M. *Biochem. J.* **2006**, *397* (3), 377–387.

(72) Camargo, A. C. M.; Ianzer, D.; Guerreiro, J. R.; Serrano, S. M. T. *Toxicon* **2012**, *59* (4), 516–523.

(73) Chen, Y. H.; Liou, R. F.; Hu, C.; Juan, C. C.; Yang, J. T. *Mol. Cell. Biochem.* **1987**, *73* (1), 69–76.

(74) Fletcher, J. E.; Jiang, M. S. *Toxicon* **1993**, *31* (6), 669–695.

(75) Caccin, P.; Pellegatti, P.; Fernandez, J.; Vono, M.; Cintra-Francischinelli, M.; Lomonte, B.; Gutierrez, J. M.; Di Virgilio, F.; Montecucco, C. *Biochem. Biophys. Res. Commun.* **2013**, *430* (4), 1289–1293.

(76) Ranawaka, U. K.; Lalloo, D. G.; de Silva, H. J. *PLoS Negl. Trop. Dis.* **2013**, *7* (10).

(77) Du, X. Y.; Clemetson, K. J. *Toxicon* **2002**, *40* (6), 659–665.

(78) Costa, T. R.; Burin, S. M.; Menaldo, D. L.; de Castro, F. A.; Sampaio, S. V. *J. Venom. Anim. Toxins Incl. Trop. Dis.* **2014**, *20*, 23.

(79) Gutiérrez, J. M.; Rucavado, A. *Biochimie* **2000**, *82* (9–10), 841–850.

(80) Koh, C. Y.; Kini, R. M. *Toxicon* **2012**, *59* (4), 497–506.

(81) Langton, A. K.; Sherratt, M. J.; Griffiths, C. E.; Watson, R. E. *Int. J. Cosmet. Sci.* **2010**, *32* (5), 330–339.

(82) Menon, G. K. *Adv. Drug Deliv. Rev.* **2002**, *54 Suppl 1*, S3-17.

(83) Breitkreutz, D.; Mirancea, N.; Nischt, R. *Histochem. Cell Biol.* **2009**, *132* (1), 1–10.

(84) Pathan, I. B.; Setty, C. M. *Trop. J. Pharm. Res.* **2009**, *8* (2), 173–179.

(85) Zhao, Z.-L.; Zhao, H.-P.; Ma, G.-J.; Wu, C.-W.; Yang, K.; Feng, X.-Q. *Biol. Open* **2015**, *4* (7), 921–928.

(86) Boulais, N.; Misery, L. *Eur. J. Dermatology* **2008**, *18* (2), 119–127.

(87) Denning, M. F. *Int. J. Biochem. Cell Biol.* **2004**, *36* (7), 1141–1146.

(88) Proksch, E.; Brandner, J. M.; Jensen, J. M. *Exp. Dermatol.* **2008**, *17* (12), 1063–1072.

(89) Harding, C. R. *Dermatol. Ther.* **2004**, *17 Suppl 1*, 6–15.

(90) Madison, K. C. *J. Invest. Dermatol.* **2003**, *121* (2), 231–241.

(91) Wertz, P. W. *Acta Dermato-Venereologica, Suppl.* **2000**, *208*, 7–11.

(92) Bosman, F. T.; Stamenkovic, I. *J. Pathol.* **2003**, *200* (4), 423–428.

(93) Kuivaniemi, H.; Tromp, G.; Prockop, D. J. *Hum. Mutat.* **1997**, *9*, 300–315.

(94) Sherman, V. R.; Yang, W.; Meyers, M. A. *Journal of the Mechanical Behavior of Biomedical Materials*. 2015, pp 22–50.

(95) Uitto, J. *J. Invest. Dermatol.* **1979**, *72* (1), 1–10.

(96) Ashworth, J. L.; Murphy, G.; Rock, M. J.; Sherratt, M. J.; Shapiro, S. D.;

Shuttleworth, C. A.; Kielty, C. M. *Biochem. J.* **1999**, *340 (Pt 1*, 171–181.

(97) Stratakis, C. A.; Chrousos, G. P. *Ann. N. Y. Acad. Sci.* **1995**, *771*, 1–18.

(98) Young, E. A.; Abelson, J.; Lightman, S. L. *Front. Neuroendocrinol.* **2004**, *25* (2), 69–76.

(99) Fuller, M. D.; Emrick, M. A.; Sadilek, M.; Scheuer, T.; Catterall, W. A. *Sci. Signal.* **2010**, *3* (141), ra70.

(100) Rang, H. P. .; Dale, M. M. .; Ritter, J. M. .; Flower, R. J. *Rang and Dale's Pharmacology*, 6th ed.; Churchill Livingstone Elsevier, 2007.

(101) Murphy, K.; Travers, P.; Walport, M. *Janeway's Immunobiology*, 7th ed.; Garland Science, Taylor & Francis Group, LLC., 2008.

(102) Pradhan, T.; Jung, H. S.; Jang, J. H.; Kim, T. W.; Kang, C.; Kim, J. S. *Chem. Soc. Rev.* **2014**, 4684–4713.

(103) Joh, T. H.; Hwang, O. *Ann. N. Y. Acad. Sci.* **1962**, *342*, 342–350.

(104) Insel, P. A. *N. Engl. J. Med.* **1996**, *334* (9), 580–585.

(105) Bylund, D. B.; Eikenberg, D. C.; Hieble, J. P.; Langer, S. Z.; Lefkowitz, R. J.; Minneman, K. P.; Molinoff, P. B.; Ruffolo, R. R.; Trendelenburg, U. *Pharmacol. Rev.* **1994**, *46* (2), 121–136.

(106) Kvetnansky, R.; Sabban, E. L.; Palkovits, M. *Physiol. Rev.* **2009**, *89* (2), 535–606.

(107) Rhen, T.; Cidlowski, J. A. *N. Engl. J. Med.* **2005**, *353* (16), 1711–1723.

(108) Dickerson, S. S.; Kemeny, M. E. *Psychol. Bull.* **2004**, *130* (3), 355–391.

(109) Pruessner, J. C.; Hellhammer, D. H.; Kirschbaum, C. *Pers. Individ. Dif.* **1999**, *27* (3), 477–489.

(110) Oakley, R. H.; Cidlowski, J. A. *J. Biol. Chem.* **2010**, *286* (5), 3177–3184.

(111) Tomlinson, J. W.; Walker, E. A.; Bujalska, I. J.; Draper, N.; Lavery, G. G.; Cooper, M. S.; Hewison, M.; Stewart, P. M. *Endocr. Rev.* **2004**, *25* (5), 831–

866.

(112) Le Merrer, J.; Becker, J. A. J.; Befort, K.; Kieffer, B. L. *Physiol. Rev.* **2009**, *89* (4), 1379–1412.

(113) Fichna, J.; Janecka, A.; Costentin, J.; Do Rego, J. C. *Pharmacol. Rev.* **2007**, *59* (1), 88–123.

(114) Koneru, A.; Satyanarayana, S.; Rizman, S. *Glob. J. Pharmacol.* **2009**, *3* (3), 149–153.

(115) Davies, J.; Dray, A. *Br. J. Pharmacol.* **1978**, *63*, 87–96.

(116) Hersh, L. B. *Mol. Cell. Biochem.* **1982**, *43* (23), 35–43.

(117) Venturelli, F.; Roscetti, G.; Possenti, R.; Vita, F.; Roda, G. *Neurochem. Res.* **1985**, *10* (3), 333–342.

(118) Roscetti, G.; Possenti, R.; Bassano, E.; Roda, G. *Neurochem. Res.* **1985**, *10* (10), 1393–1404.

(119) Xu, Y.; Wellner, D.; Scheinberg, D. A. *Biochem. Biophys. Res. Commun.* **1995**, *208* (2), 664–674.

(120) Erdös, E.; Skidgel, R. *FASEB J.* **1989**, *3*, 145–151.

(121) Baral, P. K.; Jajcanin-Jozic, N.; Deller, S.; Macheroux, P.; Abramic, M.; Gruber, K. *J. Biol. Chem.* **2008**, *283* (32), 22316–22324.

(122) Kumar, P.; Reithofer, V.; Reisinger, M.; Wallner, S.; Pavkov-Keller, T.; Macheroux, P.; Gruber, K. *Sci. Rep.* **2016**, *6*, 23787.

(123) Prajapati, S. C.; Chauhan, S. S. *FEBS J.* **2011**, *278* (18), 3256–3276.

(124) Kaplan, A. P.; Joseph, K.; Silverberg, M. *J. Allergy Clin. Immunol.* **2002**, *109* (2), 195–209.

(125) Regoli, D.; Nsa Allogho, S.; Rizzi, A.; Gobeil, F. J. *Eur. J. Pharmacol.* **1998**, *348*, 1–10.

(126) Petho, G.; Reeh, P. W. *Physiol. Rev.* **2012**, *92* (4), 1699–1775.

(127) Manning, D. C.; Raja, S. N.; Meyer, R. A.; Campbell, J. N. *Clin. Pharmacol. Ther.* **1991**, *50* (6), 721–729.

(128) Taubman, M. B. *Circ. Res.* **2003**, *92* (1), 9–11.

(129) Dostal, D. E.; Baker, K. M. *Circ. Res.* **1999**, *85* (7), 643–650.

(130) Savoia, C.; Burger, D.; Nishigaki, N.; Montezano, A.; Touyz, R. M. *Expert Rev. Mol. Med.* **2011**, *13*, e11.

(131) Atlas, S. A. *J. Manag. Care Pharm.* **2007**, *13* (8 Suppl B), 9–20.

(132) Harrison, S.; Geppetti, P. *Int. J. Biochem. Cell Biol.* **2001**, *33* (6), 555–576.

(133) Krause, J. E.; Takeda, Y.; Hershey, A. D. *J. Invest. Dermatol.* **1992**, *98* (6 Suppl), 2S–7S.

(134) Ebner, K.; Singewald, N. *Amino Acids* **2006**, *31* (3), 251–272.

(135) Matsas, R.; Kenny, A. J.; Turner, A. J. *Biochem. J.* **1984**, *223*, 433–440.

(136) Probert, L.; Hanley, M. R. *Neurosci. Lett.* **1987**, *78* (2), 132–137.

(137) Cascieri, M. A.; Bull, H. G.; Mumford, R. A.; Patchett, A. A.; Thornberry, N. A.; Liang, T. *Mol. Pharmacol.* **1984**, *25* (2), 287–293.

(138) Heymann, E.; Mentlein, R. *FEBS Lett.* **1978**, *91* (2), 360–364.

(139) Kalwant, S.; Porter, A. G. *Biochem. J.* **1991**, *276*, 237–244.

(140) Kageyama, T. *Eur J Biochem* **1993**, *216* (3), 717–728.

(141) Cho, S. Y.; Shim, S. R.; Rhee, H. Y.; Park, H. J.; Jung, W. S.; Moon, S. K.; Park, J. M.; Ko, C. N.; Cho, K. H.; Park, S. U. *Park. Relat. Disord.* **2012**, *18* (8), 948–952.

(142) Park, H. J.; Lee, S. H.; Son, D. J.; Oh, K. W.; Kim, K. H.; Song, H. S.; Kim, G. J.; Oh, G. T.; Yoon, D. Y.; Hong, J. T. *Arthritis Rheum.* **2004**, *50* (11), 3504–3515.

(143) Lee, J. D.; Park, H. J.; Chae, Y.; Lim, S. *Evidence-based Complement. Altern. Med.* **2005**, *2* (1), 79–84.

(144) McInnes, I. B.; Schett, G. *N. Engl. J. Med.* **2011**, *365* (23), 2205–2219.

(145) Hunter, D. J.; Felson, D. T. *BMJ* **2006**, *332*, 639–642.

(146) Khanna, D.; Sethi, G.; Ahn, K. S.; Pandey, M. K.; Kunnumakkara, A. B.; Sung, B.; Aggarwal, A.; Aggarwal, B. B. *Curr. Opin. Pharmacol.* **2007**, *7* (3), 344–351.

(147) Moon, D. O.; Park, S. Y.; Lee, K. J.; Heo, M. S.; Kim, K. C.; Kim, M. O.; Lee, J. D.; Choi, Y. H.; Kim, G. Y. *Int. Immunopharmacol.* **2007**, *7* (8), 1092–1101.

(148) Orsolic, N.; Sver, L.; Verstovsek, S.; Terzic, S.; Basic, I. *Toxicon* **2003**, *41* (7), 861–870.

(149) Jo, M.; Park, M. H.; Kollipara, P. S.; An, B. J.; Song, H. S.; Han, S. B.; Kim, J. H.; Song, M. J.; Hong, J. T. *Toxicol. Appl. Pharmacol.* **2012**, *258* (1), 72–81.

(150) Maurice, N.; Deltheil, T.; Melon, C.; Degos, B.; Mourre, C.; Amalric, M.; Goff, L. K. Le. *PLoS One* **2015**, *10* (11).

(151) Chung, E. S.; Kim, H.; Lee, G.; Park, S.; Kim, H.; Bae, H. *Brain. Behav. Immun.* **2012**, *26* (8), 1322–1330.

(152) Dauer, W.; Przedborski, S. *Neuron* **2003**, *39* (6), 889–909.

(153) Alvarez-Fischer, D.; Noelker, C.; Vulinović, F.; Grünewald, A.; Chevarin, C.; Klein, C.; Oertel, W. H.; Hirsch, E. C.; Michel, P. P.; Hartmann, A. *PLoS One* **2013**, *8* (4).

(154) Rodial http://www.rodial.co.uk/skincare/products/moisturisers/bee-venom-moisturiser-4 (accessed Jul 13, 2016).

(155) Manuka Doctor http://www.manukadoctor.co.uk/apinourish.html (accessed Jul 13, 2016).

(156) Han, S. M.; Hong, I. P.; Woo, S. O.; Chun, S. N.; Park, K. K.; Nicholls, Y. M.; Pak, S. C. *Clin. Interv. Aging* **2015**, *10*, 1587–1592.

(157) Gladden, L. F. *Chem. Eng. Sci.* **1994**, *49* (20), 3339–3408.

(158) Hore, P. J. *Nuclear Magnetic Resonance*; Oxford University Press, 1995.

(159) Deihl, B.; Holzgrabe, U.; Wawer, I. *NMR Spectroscopy in Pharmaceutical Analysis* ; Elsevier, 2008.

(160) Veeman, W. S. *Geoderma* **1997**, *80*, 225–242.

(161) Freeman, R. *Magnetic Resonance in Chemistry and Medicine*; Oxford University Press, 2003.

(162) Levitt, M. H. *Spin Dynamics - Basics of Nuclear Magnetic Resonance*, Second Edi.; John Wiley & Sons Ltd, 2007.

(163) Claridge, T. D. W. *High-Resolution NMR Techniques in Organic Chemsitry*; Elsevier Science Ltd, 1999; Vol. 19.

(164) De Graaf, R. A. *In Vivo NMR Spectroscopy: Principles and Techniques.*, 2nd ed.; John Wiley and Sons Ltd., 2007.

(165) Cavanagh, J.; Fairbrother, W. J.; Palmer III, A. G.; Rance, M.; Skelton, N. J. *Protein NMR Spectroscopy: Principles and Practise*, Second.; Elsevier, 2007.

(166) Khajeh, M.; Bernstein, M. A.; Morris, G. A. *Magn. Reson. Chem.* **2010**, *48* (7), 516–522.

(167) Foley, D. A.; Doecke, C. W.; Buser, J. Y.; Merritt, J. M.; Murphy, L.; Kissane, M.; Collins, S. G.; Maguire, A. R.; Kaerner, A. *J. Org. Chem.* **2011**, *76* (23), 9630–9640.

(168) Foley, D. A.; Bez, E.; Codina, A.; Colson, K. L.; Fey, M.; Krull, R.; Piroli, D.; Zell, M. T.; Marquez, B. L. *Anal. Chem.* **2014**, *86* (24), 12008–12013.

(169) MestreLab http://mestrelab.com/software/mnova/nmr/ (accessed Feb 15, 2016).

(170) InsightMR https://www.bruker.com/products/mr/nmr/nmr-software/software/insightmr/overview.html (accessed Feb 15, 2016).

(171) Hwang, T. L.; Shaka, A. J. *J. Magn. Reson. Ser. A* **1995**, *112* (2), 275–279.

(172) Holzer, P. *Am. J. Gastroenterol. Suppl.* **2014**, *2* (1), 9–16.

(173) Trigo, J. M.; Martin-García, E.; Berrendero, F.; Robledo, P.; Maldonado, R. *Drug Alcohol Depend.* **2010**, *108*, 183–194.

(174) Pradhan, A. A.; Smith, M. L.; Kieffer, B. L.; Evans, C. J. *Br. J. Pharmacol.* **2012**, *167* (5), 960–969.

(175) Thompson, A. A.; Liu, W.; Chun, E.; Katritch, V.; Wu, H.; Vardy, E.; Huang, X.-P.; Trapella, C.; Guerrini, R.; Calo, G.; Roth, B. L.; Cherezov, V.; Stevens, R. C. *Nature* **2012**, *485* (7398), 395–399.

(176) Feng, Y.; He, X.; Yang, Y.; Chao, D.; Lazarus, L. H.; Xia, Y. *Curr. Drug Targets* **2012**, *13* (2), 230–246.

(177) Horvath, G. *Pharmacol. Ther.* **2000**, *88* (2000), 437–463.

(178) Lin, X.; Yang, D. J.; Cai, W. Q.; Zhao, Q. Y.; Gao, Y. F.; Chen, Q.; Wang, R. *Biochim. Biophys. Acta* **2003**, *1639* (3), 195–202.

(179) Przewłocki, R.; Przewłocka, B. *Eur. J. Pharmacol.* **2001**, *429* (1–3), 79–91.

(180) Janecka, A.; Staniszewska, R.; Gach, K.; Fichna, J. *Peptides* **2008**, *29* (11), 2066–2073.

(181) Tomboly, C.; Peter, A.; Toth, G. *Peptides* **2002**, *23* (9), 1573–1580.

(182) Péter, A.; Tóth, G.; Tömböly, C.; Laus, G.; Tourwè, D. *J. Chromatogr. A* **1999**, *846* (1–2), 39–48.

(183) Janecka, A.; Staniszewska, R.; Gach, K.; Fichna, J. *Peptides* **2008**, *29* (11), 2066–2073.

(184) Dishman, R. K.; O'Connor, P. J. *Ment. Health Phys. Act.* **2009**, *2* (1), 4–9.

(185) Dalayeun, J. F.; Norès, J. M.; Bergal, S. *Biomed. Pharmacother.* **1993**, *47* (8), 311–320.

(186) Roth-Deri, I.; Green-Sadan, T.; Yadid, G. *Prog. Neurobiol.* **2008**, *86* (1), 1–21.

(187) Sandin, J.; Nylander, I.; Silberring, J. *Regul. Pept.* **1998**, *73* (1), 67–72.

(188) Reed, B.; Bidlack, J. M.; Chait, B. T.; Kreek, M. J. *J. Neuroendocrinol.* **2008**, *20* (5), 606–616.

(189) Schwarzer, C. *Pharmacol. Ther.* **2009**, *123* (3), 353–370.

(190) Knoll, A. T.; Carlezon, W. A. *Brain Res.* **2010**, *1314*, 56–73.

(191) Shippenberg, T. S.; Zapata, A.; Chefer, V. I. *Pharmacol. Ther.* **2007**, *116* (2), 306–321.

(192) Safavi, A.; Hersh, L. B. *J. Neurochem.* **1995**, *65*, 389–395.

(193) Vickers, C.; Hales, P.; Kaushik, V.; Dick, L.; Gavin, J.; Tang, J.; Godbout, K.; Parsons, T.; Baronas, E.; Hsieh, F.; Acton, S.; Patane, M.; Nichols, A.; Tummino, P. *J. Biol. Chem.* **2002**, *277* (17), 14838–14843.

(194) Silberring, J.; Castello, M. E.; Nyberg, F. *J. Biol. Chem.* **1992**, *267* (30), 21324–21328.

(195) Tan-No, K.; Taira, A.; Sakurada, T.; Inoue, M.; Sakurada, S.; Tadano, T.; Sato, T.; Sakurada, C.; Nylander, I.; Silberring, J.; Terenius, L.; Kisara, K. *Eur. J. Pharmacol.* **1996**, *314* (1–2), 61–67.

(196) Bruijnzeel, A. W. *Brain Res. Rev.* **2009**, *62* (1), 127–146.

(197) Mogil, J. S.; Pasternak, G. W. *Pharmacol. Rev.* **2001**, *53* (3), 381–415.

(198) Meunier, J. C. *Eur. J. Pharmacol.* **1997**, *340* (1), 1–15.

(199) Mogil, J. S.; Grisel, J. E.; Zhangs, G.; Belknap, J. K.; Grandy, D. K. *Neurosci. Lett.* **1996**, *214*, 131–134.

(200) Gintzler, A. R.; Adapa, I. D.; Toll, L.; Medina, V. M.; Wang, L. *Eur. J. Pharmacol.* **1997**, *325* (1), 29–34.

(201) Darland, T.; Heinricher, M. M.; Grandy, D. K. *Trends Neurosci.* **1998**, *21* (5), 215–221.

(202) Montiel, J. L.; Cornille, F.; Roques, B. P.; Noble, F. *J. Neurochem.* **1997**, *68* (1), 354–361.

(203) Meisel, H. *Int. Dairy J.* **1998**, *8* (5–6), 363–373.

(204) Teschemacher, H. *Curr. Pharm. Des.* **2003**, *9*, 1331–1344.

(205) Meisel, H.; FitzGerald, R. J. *Br. J. Nutr.* **2000**, *84 Suppl 1*, S27–S31.

(206) Silva, S. V.; Malcata, F. X. *Int. Dairy J.* **2005**, *15* (1), 1–15.

(207) Kreil, G.; Umbach, M.; Brantl, V.; Teschemacher, H. *Life Sci* **1983**, *33 Suppl 1*, 137–140.

(208) Jarmołowska, B.; Bielikowicz, K.; Iwan, M.; Sidor, K.; Kostyra, E.; Kaczmarski, M. *Peptides* **2007**, *28* (3), 678–682.

(209) Meisel, H. *Livest. Prod. Sci.* **1997**, *50* (1–2), 125–138.

(210) Fromm, H. J.; Hargrove, M. *Essentials of Biochemistry*, First.; Springer Berlin Heidelberg, 2012.

(211) Adams, R. W.; Holroyd, C. M.; Aguilar, J. A.; Nilsson, M.; Morris, G. A. *Chem Commun* **2013**, *49* (4), 358–360.

(212) Buxbaum, E. *Fundamentals of Protein Structure and Function*; 2007.

(213) Mucha, A.; Drag, M.; Dalton, J. P.; Kafarski, P. *Biochimie* **2010**, *92* (11), 1509–1529.

(214) Sakurada, C.; Sakurada, S.; Hayashi, T.; Katsuyama, S.; Tan-No, K.; Sakurada, T. *Biochem. Pharmacol.* **2003**, *66* (4), 653–661.

(215) Schwartz, J. C.; Malfroy, B.; De La Baume, S. *Life Sci.* **1981**, *29* (17), 1715–1740.

(216) Rahfeld, J.; Schierhorn, M.; Hartrodt, B.; Neubert, K.; Heins, J. *Biochim. Biophys. Acta* **1991**, *1076* (2), 314–316.

(217) Berger, A.; Schechter, I. *Philos. Trans. R. Soc. Lond. B. Biol. Sci.* **1970**, *257* (813), 249–264.

(218) Nabeno, M.; Akahoshi, F.; Kishida, H.; Miyaguchi, I.; Tanaka, Y.; Ishii, S.; Kadowaki, T. *Biochem. Biophys. Res. Commun.* **2013**, *434* (2), 191–196.

(219) Püschel, G.; Mentlein, R.; Heymann, E. *Eur. J. Biochem.* **1982**, *126* (2), 359–365.

(220) Bezerra, G. a; Dobrovetsky, E.; Viertlmayr, R.; Dong, A.; Binter, A.; Abramic, M.; Macheroux, P.; Dhe-Paganon, S.; Gruber, K. *Proc. Natl. Acad. Sci. U. S. A.*

2012, *109* (17), 6525–6530.

(221) Crystal structure of human Dipeptidyl Peptidase III http://www.rcsb.org/pdb/explore.do?structureId=3fvy (accessed Nov 3, 2016).

(222) Tomić, A.; Kovačević, B.; Tomić, S. *Phys. Chem. Chem. Phys.* **2016**, *18* (39), 27245–27256.

(223) Tomić, A.; González, M.; Tomić, S. *J. Chem. Inf. Model.* **2012**, *52* (6), 1583–1594.

(224) Tomić, A.; Tomić, S. *Dalt. Trans.* **2014**, *43* (41), 15503–15514.

(225) Soisson, S. M.; Patel, S. B.; Abeywickrema, P. D.; Byrne, N. J.; Diehl, R. E.; Hall, D. L.; Ford, R. E.; Reid, J. C.; Rickert, K. W.; Shipman, J. M.; Sharma, S.; Lumb, K. J. *BMC Struct. Biol.* **2010**, *10* (1), 16.

(226) Slominski, A. T.; Zmijewski, M. A.; Zbytek, B.; Brozyna, A. A.; Granese, J.; Pisarchik, A.; Szczesniewski, A.; Tobin, D. J. *J Invest Dermatol* **2011**, *131* (3), 613–622.

(227) de Graaf, D. C.; Aerts, M.; Danneels, E.; Devreese, B. *J. Proteomics* **2009**, *72* (2), 145–154.

(228) Williams, C. S.; Mann, M.; DuBois, R. N. *Oncogene* **1999**, *18* (55), 7908–7916.

(229) Ricciotti, E.; Fitzgerald, G. A. *Arterioscler. Thromb. Vasc. Biol.* **2011**, *31* (5), 986–1000.

Appendix 1

```
;zgesgp_k
;avance-version (02/05/31)
;1D sequence
;water suppression using excitation sculpting with gradients
;T.-L. Hwang & A.J. Shaka, J. Magn. Reson.,
;   Series A 112 275-279 (1995)
;
;Used for delaying acquistion i.e. for kinetics  JAP 07-11-08
;
;$CLASS=HighRes
;$DIM=1D
;$TYPE=
;$SUBTYPE=
;$COMMENT=


;$OWNER=Administrator
prosol relations=<triple>


#include <Avance.incl>
#include <Grad.incl>

"acqt0=-p1*2/3.1416"    /*Timing correction to prevent baseline smile/curvature*/

"p2=p1*2"               /*p2 is the 1H 180 degree pulse at power level pl1*/
"d12=20u"               /* d12 is a housekeeping delay to allow events to occur during it */


1 ze                     /* zero memory */
  d20                    /* pre-acquisition delay */
2 30m                    /* Start of internal loop with 30 ms housekeeping delay */
  d12 pl1:f1 BLKGRAD     /* d12 delay; pl1:f1 sets default high power on r.f. channel 1; BLKGRAD
                            blanks the gradient amplifier */
  d1                     /* d1 is a relaxation delay – should be 1-5 * T1 value */
  p1 ph1                 /* p1 – pulse length on channel 1 with phase value ph1 read from table
*/

  50u UNBLKGRAD          /* 50 us housekeeping delay to allow gradient amp unblanking */
****************************************************************************
***
FIRST PULSED FIELD GRADIENT SPIN-ECHO (PFGSE)
****************************************************************************
***
  p16:gp1                /* p16 is a delay associated with gradient application; gp1 is strength of
                            gradient 1 as a percentage of the actual gradient strength in gauss/cm
–
                            max = 54 G/cm; gradient is applied with a gradient shape gpnam */
  d16 pl0:f1             /* d16 is a gradient recovery delay;
                           set default power level pl0 = 120 dB on f1 no power – for protection of
                           probe */
```

```
  (p12:sp1 ph2:r):f1      /* apply a lower power (sp1), long shaped pulse during period p12 –
                             narrow band excitation – i.e. selective for narrow frequency range;
                             pulse applied with phase value ph2 on channel f1; r makes it possible
to
                             finely control the pulse phase */
  4u                      /* housekeeping delay of 4 us */
  d12 pl1:f1              /* housekeeping delay to allow power switching back to high power */

  p2 ph3                  /* 180 degree pulse with phase ph3 */

  4u                      /* housekeeping delay – 4 us */
  p16:gp1                 /* repeat same gradient pulse */
  d16                     /* gradient recovery delay */
************************************************************************************
***
************************************************************************************
***
SECOND PFGSE (HENCE DPFGSE – Double PFGSE)
************************************************************************************
***
  50u
  p16:gp2
  d16 pl0:f1
  (p12:sp1 ph4:r):f1
  4u
  d12 pl1:f1

  p2 ph5

  4u
  p16:gp2
  d16
************************************************************************************
***
************************************************************************************
**
ACQUISITION OF DATA
************************************************************************************
***
go=2 ph31                 /*Open receiver, acquire FID and loop to line 2 in program for ns scans
*/
  30m mc #0 to 2 F0(zd) /* Write data to disc */
  4u BLKGRAD              /* Blank Gradient Amp during 4 us delay */
Exit                      /* Stop */

******************************
PHASE TABLE
******************************
ph1=0
ph2=0 1
ph3=2 3
ph4=0 0 1 1
ph5=2 2 3 3
ph31=0 2 2 0
```

```
*****************************
COMMENTS AND ADVICE
*****************************
;pl0 : 120dB
;pl1 : f1 channel - power level for pulse (default)
;sp1 : f1 channel - shaped pulse 180 degree
;p1 : f1 channel -  90 degree high power pulse
;p2 : f1 channel - 180 degree high power pulse
;p12: f1 channel - 180 degree shaped pulse (Squa100.1000)   [2 msec]
;p16: homospoil/gradient pulse
;d1 : relaxation delay; 1-5 * T1
;d12: delay for power switching                    [20 usec]
;d16: delay for homospoil/gradient recovery
;d20: Preacquisition delay
;NS: 8 * n, total number of scans: NS * TD0
;DS: 4


;use gradient ratio:    gp 1 : gp 2
;                       31 :   11

;for z-only gradients:
;gpz1: 31%
;gpz2: 11%

;use gradient files:
;gpnam1: SINE.100
;gpnam2: SINE.100



;$Id: zgesgp,v 1.5 2005/11/10 12:17:01 ber Exp $
```

Pulse programme. Writing in red indicates annotation.

Appendix 2

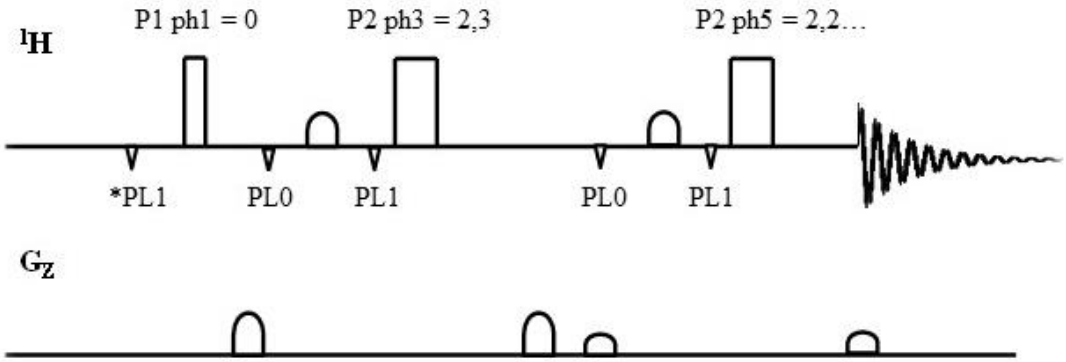

Diagram showing the pulse programme described in appendix 1. *Power switching event.

Appendix 3

```
/*** ^^A -*-C++-*- ********************************************/
/* au_zg_ts 10.10.1990 */
/*************************************************************/
/* Short Description : */
/* General AU program for data acquisition. */
/*************************************************************/
/* Keywords : */
/* zg */
/*************************************************************/
/* Description/Usage : */
/* General AU program for data acquisition. */
/* First a new topshim is carried out          */
/*  an rga is then done, then the acquisition is started. */
/*************************************************************/
/* Author(s) : */
/* Name : Peter Dvortsak */
/* Organisation : Bruker Analytik */
/* Email : peter.dvortsak@bruker.de */
/*************************************************************/
/* Name Date Modification: */
/* pdv 901010 created */
/*************************************************************/
/*
$Id: au_zg,v 1.5 2000/07/12 11:39:39 gsc Exp $
*/

GETCURDATA       /* calls up parameters */
XAU("tbishim","") /* shimming of sample */
ZG               /* data is acquired */
QUIT             /* stop */
```

Automation Programme. Writing in red indicates annotation.

Appendix 4

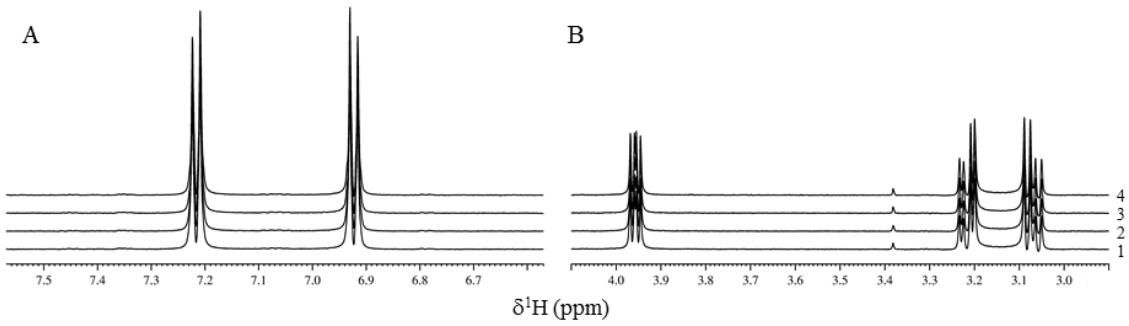

4A: ^{1}H Tyrosine control aromatic (A) and aliphatic (B) region showing spectrum 1 (0 hours), 2 (after 1 hour), 3 (after 6 hours) and 4 (after 12.5 hours).

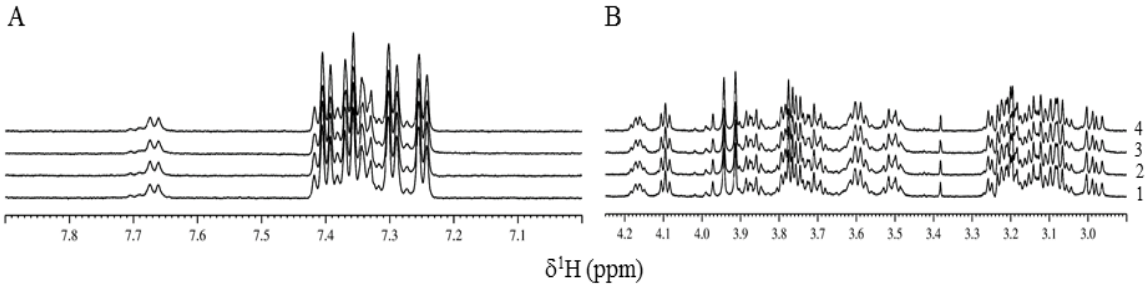

4B: ^{1}H Bradykinin control aromatic (A) and aliphatic (B) region showing spectrum 1 (0 hours), 2 (after 1 hour), 3 (after 6 hours) and 4 (after 12.5 hours).

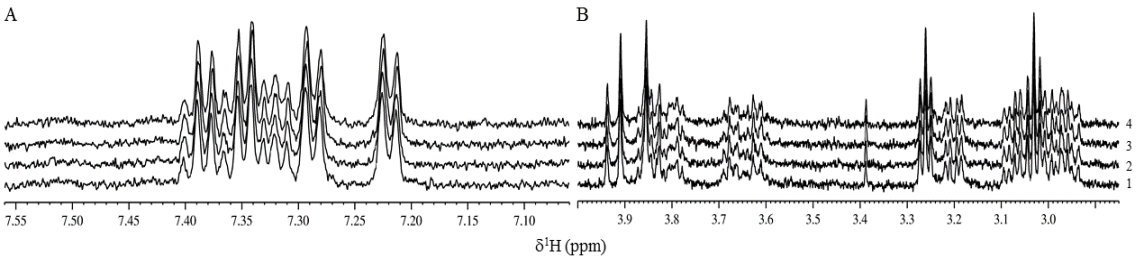

4C: ^{1}H Substance P control aromatic (A) and aliphatic (B) region showing spectrum 1 (0 hours), 2 (after 1 hour), 3 (after 6 hours) and 4 (after 15 hours).

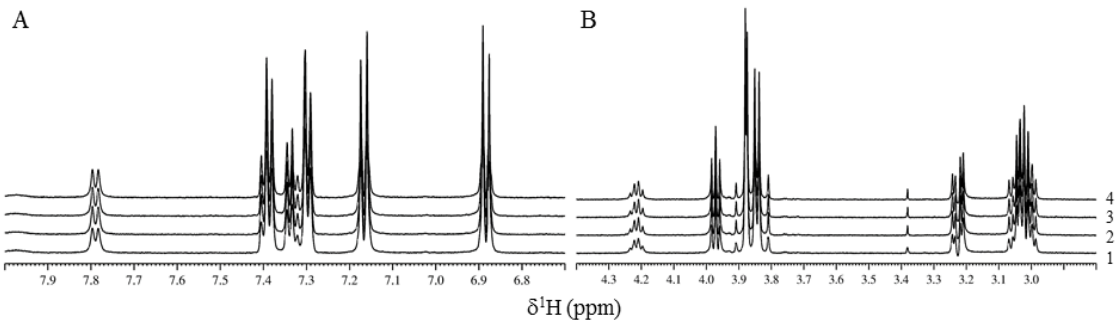

4D: ^{1}H Leu-enkephalin control aromatic (A) and aliphatic (B) region showing spectrum 1 (0 hours), 2 (after 1 hour), 3 (after 6 hours) and 4 (after 12.5 hours).

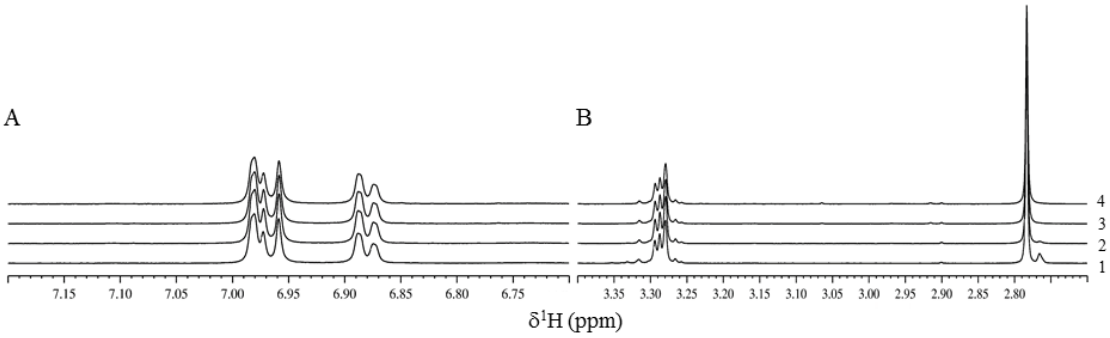

4E: ^{1}H Epinephrine control aromatic (A) and aliphatic (B) region showing spectrum 1 (0 hours), 2 (after 1 hour), 3 (after 6 hours) and 4 (after 12.5 hours).

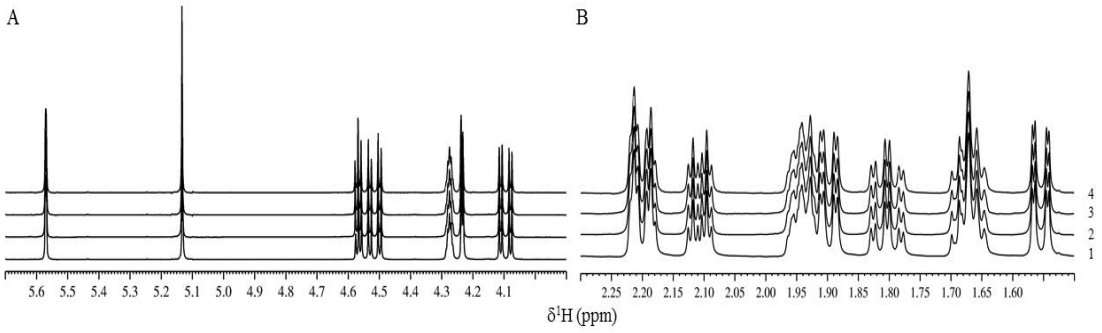

4F: ^{1}H Cortisol control high aliphatic (A) and low aliphatic (B) region showing spectrum 1 (0 hours), 2 (after 1 hour), 3 (after 6 hours) and 4 (after 12.5 hours).

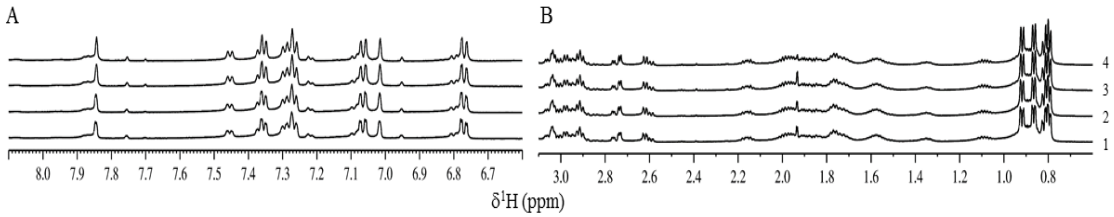

4G: ^{1}H Angiotensin II control aromatic (A) and aliphatic (B) region showing spectrum 1 (0 hours), 2 (after 1 hour), 3 (after 6 hours) and 4 (after 12.5 hours).

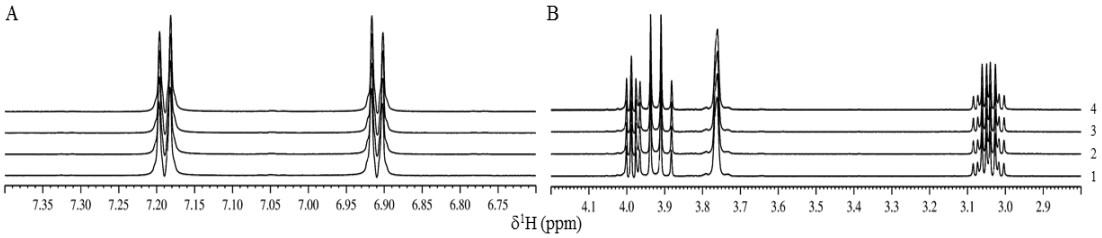

4H: ^{1}H YGG control aromatic (A) and aliphatic (B) region showing spectrum 1 (0 hours), 2 (after 1 hour), 3 (after 6 hours) and 4 (after 12.5 hours).

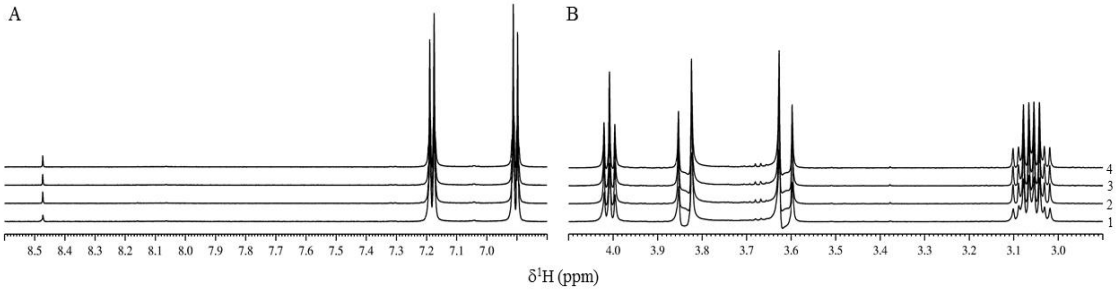

4I: ^{1}H YG control aromatic (A) and aliphatic (B) region showing spectrum 1 (0 hours), 2 (after 1 hour), 3 (after 2.5 hours) and 4 (after 5 hours).

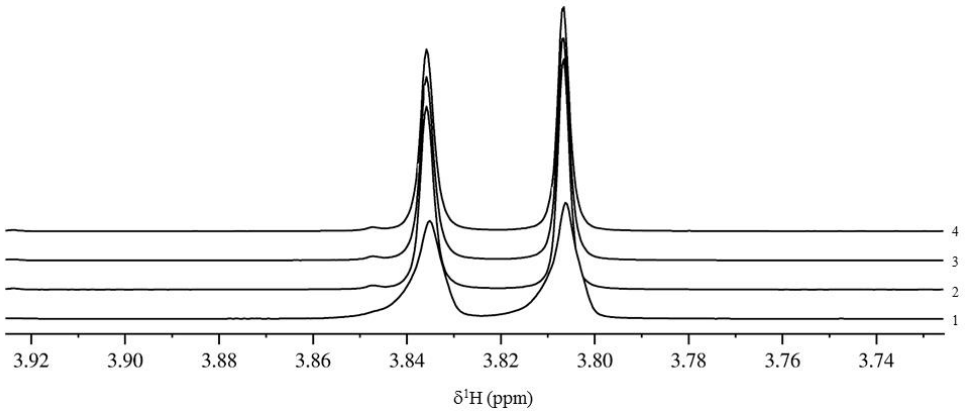

4J: ^{1}H GG control showing spectrum 1 (0 hours), 2 (after 1 hour), 3 (after 2.5 hours) and 4 (after 5 hours).

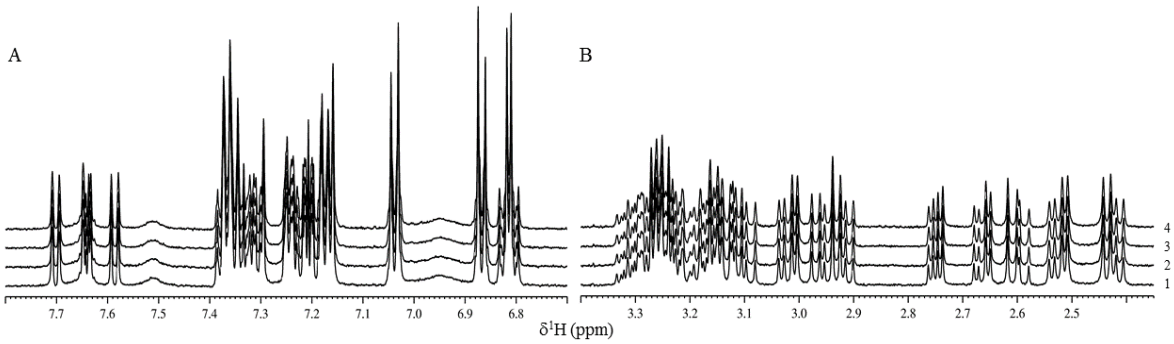

4K: ^{1}H Endomorphin I control aromatic (A) and aliphatic (B) region showing spectrum 1 (0 hours), 2 (after 1 hour), 3 (after 6 hours) and 4 (after 15 hours).

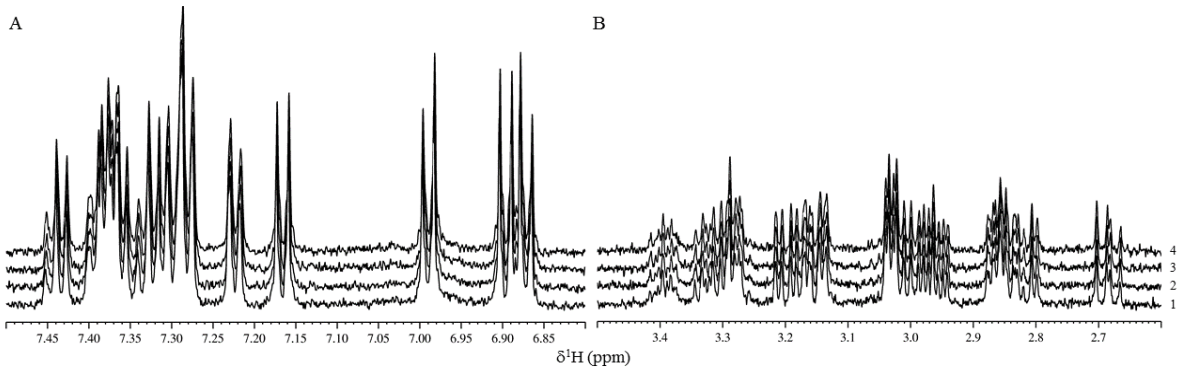

4L: ^{1}H Endomorphin II control aromatic (A) and aliphatic (B) region showing spectrum 1 (0 hours), 2 (after 1 hour), 3 (after 6 hours) and 4 (after 15 hours).

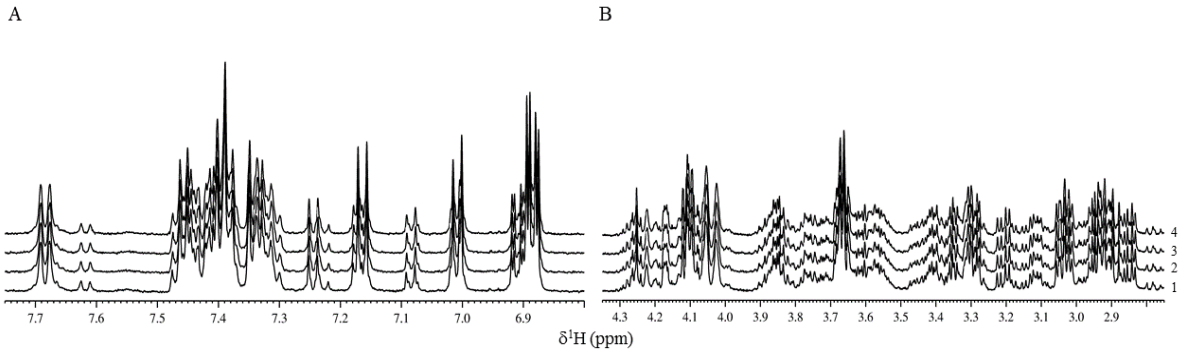

4M: ^{1}H Casomorphin control aromatic (A) and aliphatic (B) region showing spectrum 1 (0 hours), 2 (after 1 hour), 3 (after 6 hours) and 4 (after 15 hours).

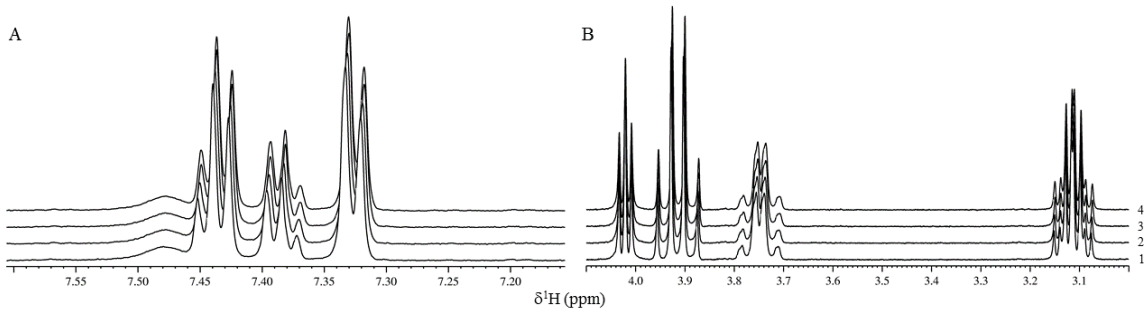

4N: ^{1}H FGG Control aromatic (A) and aliphatic (B) region showing spectrum 1 (0 hours), 2 (after 1 hour), 3 (after 6 hours) and 4 (after 18 hours).

Appendix 5

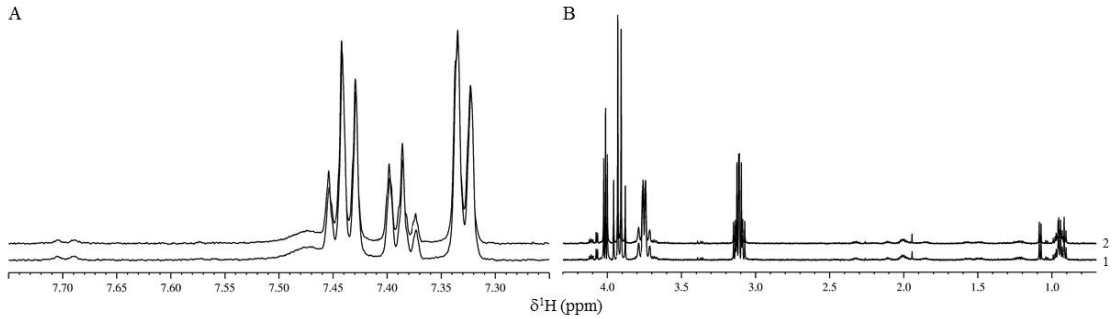

5A: ^{1}H IPI + FGG control aromatic (A) and aliphatic (B) region showing spectrum 1 (0 hours), and 2 (after 7 days).

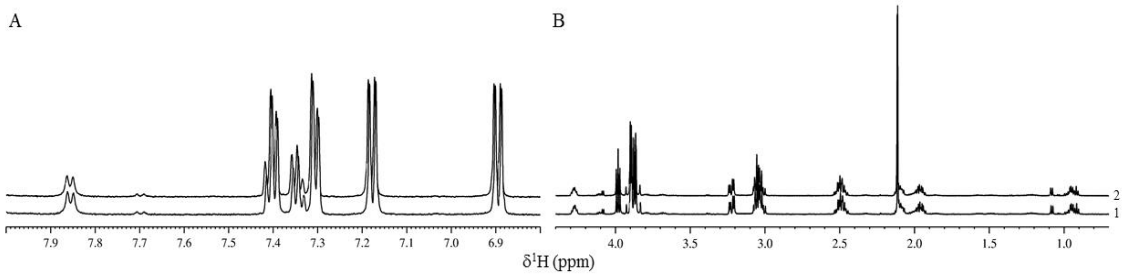

5B: ^{1}H IPI + YGGFM control aromatic (A) and aliphatic (B) region showing spectrum 1 (0 hours), and 2 (after 7 days).

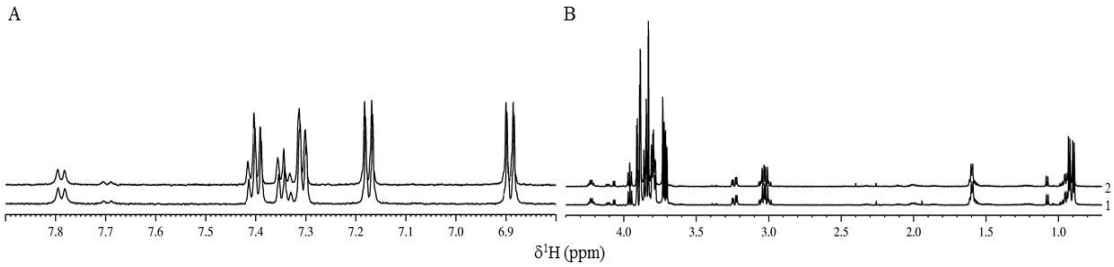

5C: ^{1}H IPI + YGGFL control aromatic (A) and aliphatic (B) region showing spectrum 1 (0 hours), and 2 (after 7 days).

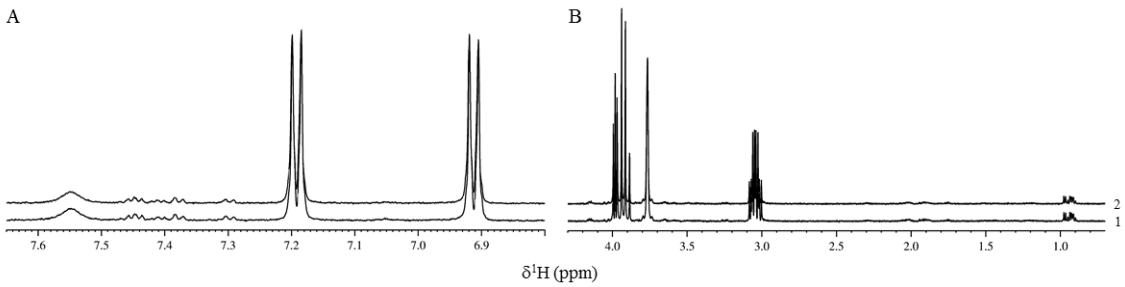

5D: ^{1}H FPI + YGG control aromatic (A) and aliphatic (B) region showing spectrum 1 (0 hours), and 2 (after 7 days).

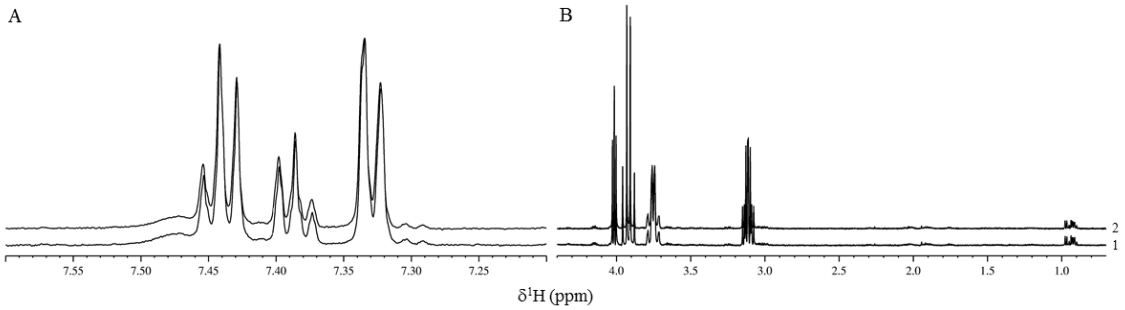

5E: ^{1}H FPI + FGG control aromatic (A) and aliphatic (B) region showing spectrum 1 (0 hours), and 2 (after 7 days).

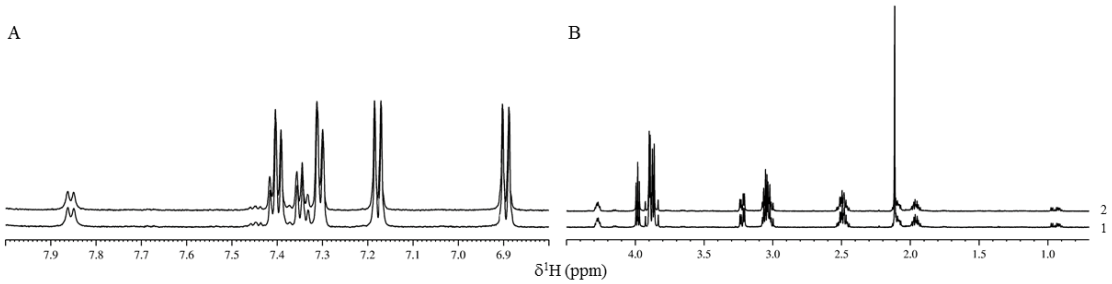

5F: ^{1}H FPI + YGGFM control aromatic (A) and aliphatic (B) region showing spectrum 1 (0 hours), and 2 (after 7 days).

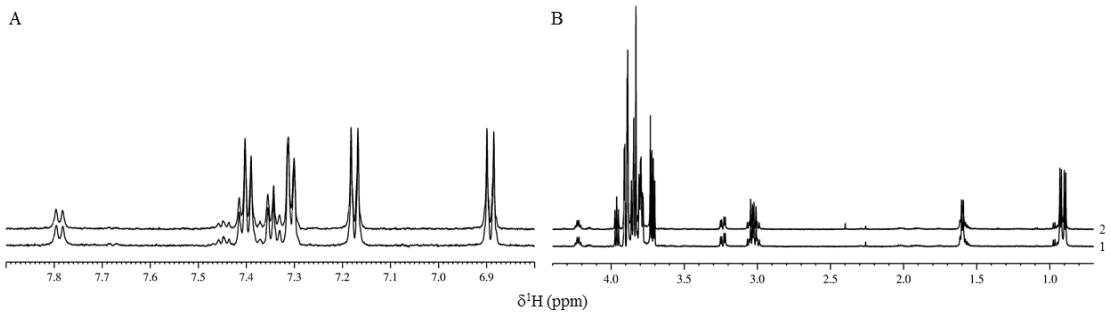

5G: ^{1}H FPI + YGGFL control aromatic (A) and aliphatic (B) region showing spectrum 1 (0 hours), and 2 (after 7 days).

Appendix 6

It is well known from the literature that hyaluronidase is an enzyme found in BV. This enzyme is known as the 'spreading factor' in BV. It acts by hydrolysing hyaluronic acid (HA) causing the collapse of the cell structure.[52] It was therefore decided to look at the kinetics of this enzyme using the same method previously applied for another enzyme found in BV.

Method

For the enzyme kinetic experiments the concentration of BV was kept constant and the substrate concentration was varied. The details of the solutions used for the enzyme kinetic experiments are shown in table 1. The kinetic experiment reactions were only run for *ca.* 2 hours to obtain the initial reaction velocity. Substrate solutions were always sonicated at 37 °C for 15 minutes beforehand to ensure they were fully dissolved and degassed. The kinetic values to be obtained are the Vmax and Km. Km is the substrate concentration at which the reaction rate is half of Vmax and Vmax is the maximal rate of the reaction. From the point of mixing the substrate with the BV and transferring the mixture into the NMR probe there is a delay of approximately 10 to 15 minutes. This means that capturing the very beginning of the reaction was lost due to this delay. The results shown here are therefore less accurate than if a stop flow method for the NMR was used. The results will, however, still give a good indication of the enzyme behaviour.

Table 1: Solution mixing details for HA kinetic experiments

Stock Substrate Concentration (mg/mL)	Final Substrate Concentration (mg/mL)	Stock BV Concentration (mg/mL)	Final BV Concentration (mg/mL)
5	1.23	5.04	1.26
2.5	0.63	5.04	1.26
1	0.25	5.04	1.26
0.5	0.125	5.04	1.26

Results

The results of the HA control in phosphate buffer are shown in figure 1. The results showed that HA is stable over the 15 hour period.

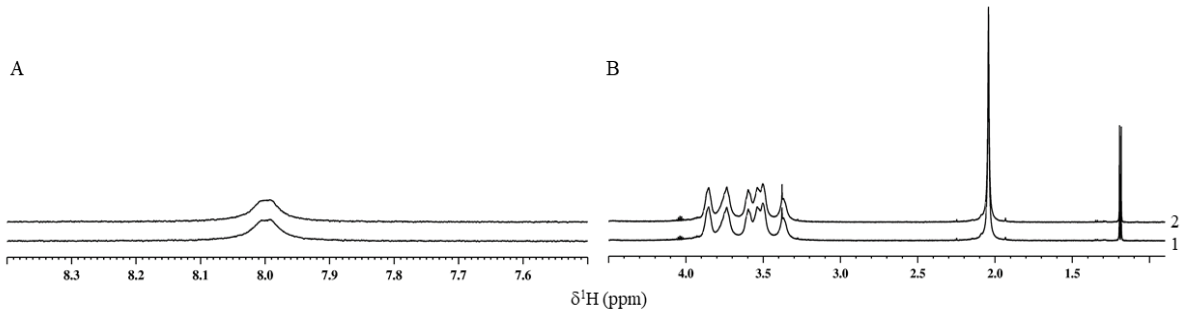

Figure 1: ^{1}H HA control aromatic (A) and aliphatic (B) region showing spectrum 1 (0 hours) and 2 (after 15 hours).

The results of the HA in the presence of BV are shown in figure 2. The results showed that HA is modified by BV over the 15 hour period. There are changes in the signals in both the aromatic and aliphatic regions of the NMR spectrum.

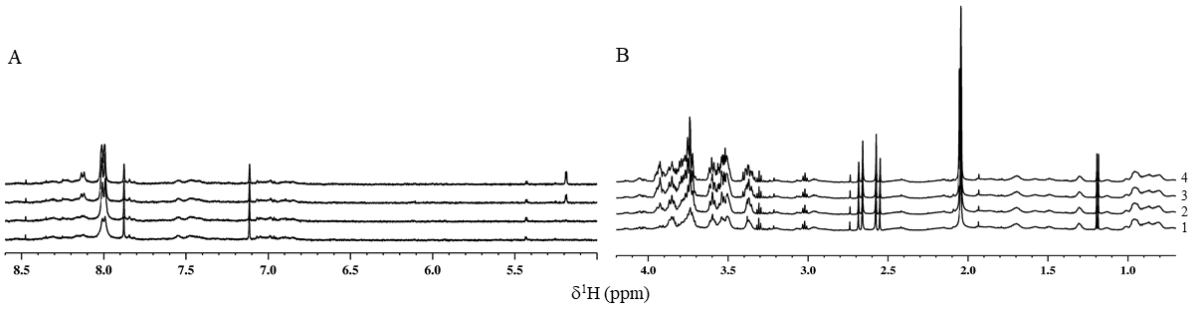

Figure 2: ^{1}H BV + HA aromatic (A) and aliphatic (B) region showing spectrum 1 (0 hours), 2 (after 1 hour), 3 (after 6 hours) and 4 (after 15 hours).

The results of the kinetic experiment are shown in figure 3. The results show that the Vmax is 8.23 µg/mL/min^{-1} and the Km is 0.49 mg/mL. Some of the points sit off the line of best fit, this is possibility due to solubility of the HA. As this reaction is quick and it takes around 5 – 10 minutes to obtain the first NMR spectrum these results will be slightly inaccurate. This highlights the need to establish a method for obtaining an NMR mixture from the point of mixing.

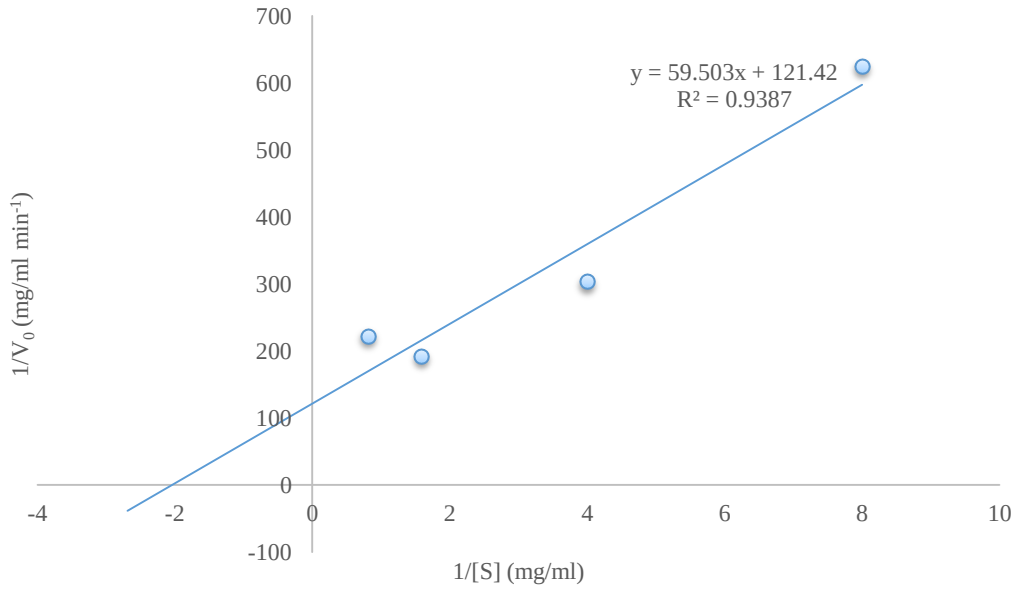

Figure 3: Lineweaver-Burk Plot for the BV + HA reaction

Appendix 7

Table 7A: Amino acid coding

Amino Acid	Three letter code	Single letter code
Arginine	Arg	R
Lysine	Lys	K
Aspartic Acid	Asp	D
Glutamic Acid	Glu	E
Glutamine	Gln	Q
Asparagine	Asn	N
Histidine	His	H
Serine	Ser	S
Threonine	Thr	T
Tyrosine	Tyr	Y
Cysteine	Cys	C
Methionine	Met	M
Tryptophan	Trp	W
Alanine	Ala	A
Isoleucine	Ile	I
Leucine	Leu	L
Phenylalanine	Phe	F
Valine	Val	V
Proline	Pro	P
Glycine	Gly	G

Anal Bioanal Chem
DOI 10.1007/s00216-015-8578-5

RESEARCH PAPER

An LCMS method for the assay of melittin in cosmetic formulations containing bee venom

Jonans Tusiimire · Jennifer Wallace · Mark Dufton · John Parkinson · Carol J. Clements · Louise Young · Jin Kyu Park · Jong Woon Jeon · David G. Watson

Received: 7 December 2014 / Revised: 12 February 2015 / Accepted: 18 February 2015

Abstract There is a growing interest in the potential of bee venom in cosmetics as a rejuvenating agent. Products currently on the market do not specify exactly their content of bee venom (BV). Therefore, we developed a method for the detection and quantification of melittin, as a marker of bee venom content, in selected commercial creams which contained BV according to their marketing claims, in order to gauge the relative quality of such formulations. A quantitative method was achieved following a rigorous extraction procedure involving sonication, liquid-liquid extraction and solid phase extraction since carryover of excipients was found to cause a rapid deterioration in the chromatographic performance. The method employed a standard additions approach using, as spiking standard, purified melittin isolated from bee venom and standardised by quantitative NMR. The aqueous extracts of the spiked creams were analysed by reversed phase LCMS on an LTQ Orbitrap mass spectrometer. The purity of the melittin spiking standard was determined to be 96.0 %. The lowest measured mean melittin content in the creams was 3.19 ppm (±1.58 ppm 95 % CI) while the highest was 37.21 ppm (±2.01 ppm 95 % CI). The method showed adequate linearity ($R^2 \geq 0.98$) and a recovery of 87.7–102.2 % from a spiked blank cream. An assay precision of <20 % RSD was achieved for all but one sample where the RSD value was 27.5 %. The method was sensitive enough for use in routine assay of BV-containing cosmetic creams. Differences in the melittin content of the commercial products assayed were nearly tenfold.

Keywords Melittin · Bee venom · Extraction · LCMS · Creams · Cosmetics · Quantitative NMR

Introduction

The venom of *Apis meliffera* (honey bee) and its components are increasingly being used as primary ingredients in various cosmetic formulations including skin creams, balms, face masks and serums. Cosmetics are some of the most widely used consumer goods [1], with the market annually generating billions of pounds worldwide [2], and so their testing must be thorough in view of their widespread usage. Although the separate testing of constituents may not necessarily indicate properties of the final formulation, appropriate methods are needed for the routine assay, stability monitoring and quality control of primary ingredients in order to set a quality standard for a particular product even though there is no prescribed content for BV in such creams [3].

A. meliffera venom contains various ingredients ranging from relatively low molecular weight (MW) amines, such as histamine (MW ~111), to relatively large-sized proteins such as phospholipase (MW ~16,000) and hyaluronidase (MW ~53,000) enzymes. Melittin (MW ~2,800) is the main constituent of the venom, constituting approximately 45–60 % of the bulk venom material and is a 26-amino acid peptide [4]. The other components are the peptides apamine, mast cell

J. Tusiimire · C. J. Clements · L. Young · D. G. Watson (✉)
Strathclyde Institute of Pharmacy and Biomedical Sciences, University of Strathclyde, 161 Cathedral Street, Glasgow G4 0RE, UK
e-mail: D.G.Watson@strath.ac.uk

J. Wallace · M. Dufton · J. Parkinson
Department of Pure and Applied Chemistry, University of Strathclyde, 295 Cathedral Street, Glasgow G1 1XL, UK

J. K. Park · J. W. Jeon
Wissen Company, 410 Bio Venture Town, Yuseong Daero 1662, 305, Dae Jeon, South Korea

Published online: 08 March 2015

degranulating peptide (MCDP), secapin, adolapin and apidaecin [3, 5, 6]. Both phospholipase (api m1) and hyaluronidase (api m3) are classified as major allergens according to the International Union of Immunological Societies (IUIS) [7]. The other bee venom allergens include dipeptidyl dipeptidase IV (api m5), serine carboxypeptidase (api m9), CUB serine protease (api m7) and vitellogenin (api m12) among others. A host of other ingredients including amino acids, carbohydrates, amines and lipids have also been described [6, 8, 9]. The presence of ionisable free primary amino and the highly basic guanidino groups (on lysine and arginine, respectively), in addition to polar amido (on N-terminal glycine and both C-terminal glutamines) and hydroxyl (on threonine and serine residues) groups in melittin reduces its retention on a hydrophobic C18-type column, particularly when ionised in an acidic medium (0.1 % *v*/*v* formic acid). However, due to the presence of valine (2), leucine (4) and isoleucine (3) residues (all with non-polar side chains) in its amino acid sequence, the molecule is retained long enough for analysis by a reversed phase method.

Recent advances in cosmetic analysis have focused on developing new methods for determining cosmetic preservatives, fragrance allergens and plasticizers such as phthalates, using chromatographic and mass spectrometry techniques [10]. New methods become more necessary when new ingredients are used in formulations for general use. Thus, although bee venom-based products have been on the European markets for quite some time (such as Forapin in Germany, Virapin in Slovakia, Apiven in France, Melivenon in Bulgaria and Apifor in Russia) [11], these have been available more as topical medications rather than as general use consumer products in the wider international market. Products designed to fit the latter category (e.g. the Manuka cosmetics range) have only recently appeared on the EU markets. These products are being marketed as containing "purified bee venom" or "bee venom extracts" (e.g. 10 Natural Effects Bee Venom Essence by Laboratorios DIET Esthetic S.A.) without further specification. Despite this growing use of bee venom, the current literature does not report a sufficient number of studies showing how to assess the composition of cosmetics in general [2], let alone the bee venom content in these products.

Analysis of cosmetic products may be considered as relating to that of non-oral semi-solid dosage forms (which include ointments, gels, creams and pastes) in pharmaceutical formulations and whose sample preparation methods for analysis have been previously reviewed [12]. It would appear from The Cosmetic, Toiletry and Perfumery Association (CTPA) [13] that the main difference, at least in practical terms, between a cosmetic product and its corresponding pharmaceutical counterpart is the purpose of application and composition. Both cosmetics and topical pharmaceutical products have common sites of application although the former tend to be more complex in composition.

Directive 93/35/EEC, the Sixth Amendment to the original Cosmetic Directive of 1976, incorporates the following definition of a cosmetic product:

> A "cosmetic product" shall mean any substance or mixture intended to be placed in contact with the various external parts of the human body (epidermis, hair system, nails, lips and external genital organs) or with the teeth and the mucous membranes of the oral cavity with a view exclusively or mainly to cleaning them, perfuming them, changing their appearance and/or correcting body odours and/or protecting them or keeping them in good condition.

Cosmetics are not expected to contain substances with therapeutic action, but are instead only formulated for topical applications exerting local effects. Thus, the level of emphasis placed on exact proportions of their chemical constituents (i.e. content uniformity) is lower than for pharmaceutical products. In addition, the control of how many constituents there are in a single formulation (complexity), component compatibility and susceptibility to degradation, and the general requirement for standardisation is also lower than for pharmaceuticals. Even the labelling requirement does not expect the manufacturer to specify quantities of ingredients while "top secret" ones are not even included on the label [14]. A cosmetic product tends to be considered acceptable as long as it does not contain banned substances (or restricted substances beyond allowed limits), is nontoxic, does not make unjustified marketing claims and generally satisfies the customer's needs.

Although current legislation does not require full profiling of all constituents in a cosmetic product, but only focuses on controlling restricted or banned ingredients [15], it is likely that such requirements will be invoked in the future as technologies advance, and new molecules or formulations, such as nanoparticles, become more commonly available.

Thus in order to meet current and anticipated formulation and regulatory requirements for bee venom formulated skin products, it is important to be able to detect, quantify and control the amount of active bee venom material. Since bee venom is only present in small amounts in creams, the current work focussed on developing a reliable sample preparation and clean-up procedure in order to isolate melittin, the most abundant marker compound for the presence of bee venom, from the formulation excipients with subsequent analysis of the extracts by LCMS using a standard additions technique. For an analytical method based on an efficient separation technique such as reversed phase HPLC and highly selective and sensitive detection systems such as Orbitrap mass spectrometry [16], one would ideally not have to worry much about coeluting compounds in the extract solution [17]. However, because cosmetic products are generally very complex in composition [12], with most of the ingredient structures

unknown but likely to be comprised of varying proportions of lipophilic and hydrophilic materials, the whole process of analytical method development may become unpredictable even when employing some of the latest highly selective analytical devices. At the very least, in order to protect the analytical column and detection system, there is a need to attempt to selectively extract and concentrate the analyte of interest from the matrix of the complex product. This paper reports a method based on liquid-liquid extraction in a ternary solvent system followed by solid phase extraction (SPE) on a reversed phase (C18) cartridges to obtain relatively clean samples for analysis of melittin, which gives an indication of bee venom content, in bee venom-containing cosmetics by LCMS.

Materials and methods

Study samples

Six commercial cosmetics which were stated to contain bee venom were analysed. Throughout the experiments, the samples were stored in a cool, dry environment and away from direct sunlight as recommended by the manufacturers. Prepared solutions for analysis were run immediately to avoid any sample degradation.

Solvents and chemicals

HPLC-grade acetonitrile and methanol were purchased from Fisher Scientific, UK, while chloroform was from Sigma-Aldrich Ltd, UK. Deionised purified water was produced in the lab using a Direct-Q 3 Millipore Ultrapure water purification system (Millipore, UK). AnalaR-grade formic acid (BDH-Merck, UK) was used as a pH modifier. D_2O was obtained from Sigma-Aldrich, Dorset, UK. Crude bee venom from which melittin was purified was supplied by Wissen Co., Seoul, S. Korea.

Instrumentation and consumables

The syringes and filters were obtained from Fisher Scientific, UK. The following equipment were also used: a micro-centrifuge, a vortex mixer, an ultrasonic bath (Fisher Scientific, UK) and automatic pipettes (Gilson, Anachem, UK). The Reveleris® Flash Chromatography was supplied by Alltech, UK. The Reveleris system uses two variable wavelengths and evaporative light scattering (ELSD) detectors to detect both chromophoric and non-chromophoric compounds in a single run. The LCMS system consisted of a Surveyor pump connected to a LTQ Orbitrap (Thermo Fisher, Hemel Hempstead, UK). The HPLC column used was a reversed phase ACE 3 C18 column; 150×3.0 mm, 3 μm, supplied from Hichrom, Reading, UK. For sample purification of melittin, a reversed phase semi-prep HPLC column (250 mm length×10 mm I.D., 5 μm particle size), supplied by HiChrom Ltd, UK, was used.

LCMS

Final diluted and filtered sample solutions were run on the LCMS under these conditions. Mobile phases consisted of 0.1 % *w*/*v* formic acid in water (A) and 0.1 % formic acid in acetonitrile (B). The solvent gradient used was 20–70 % B (from 0 to 10 min), 70 % (10–16 min), 70–20 % (16–20 min) and finally 20 % (20–25 min) at a flow rate 0.3 mL/min. Injection volume was 10 μL. The ESI interface was employed in positive ionisation mode for detection of $[M+H]^+$ ions, with a spray voltage of capillary and cone at 4.5 and 35 kV, respectively. The sheath and auxiliary gas flow rates were 50 and 15 arbitrary units, ion transfer capillary temperature was set at 275 °C and full scan data were collected between *m*/*z* 100–2,000. The data was collected and processed using Xcalibur 2.1.0 software (Thermo Fisher Scientific, UK).

Melittin isolation from bee venom

The melittin used in the spiking standard solution was prepared by medium pressure liquid chromatographic (MPLC) fractionation of a bee venom sample on a Reveleris Flash chromatography system. Approximately 800 mg of bee venom sample was mixed with 3 g of purified silica (Celite) in a dry-loading cartridge prior to the fractionation. The column used was prepared by packing an empty 20 g Easyvarioflash D24 cartridge (VWR International, UK) with ca 13 g of Polymeric Retain PEP for SPE (Thermo Scientific, UK). The mobile phases used were water (solvent A) and acetonitrile (solvent B) under the following gradient conditions: 0–10 min (0 % B), 10–20 min (20 % B), 20–30 min (50 % B), 30–60 min (60 % B) and 60–70 min (100 % B) at a flow rate of 12 mL/min. The melittin peak eluted between 22 and 28 min. Following LCMS analysis on the Orbitrap, similar fractions were pooled together and further purification of the melittin fraction was achieved by semi-preparative HLPC using a Thermo Separations P2000 pump and ACE C18 column (250 mm length×10 mm I.D., 5 μm particle size; HiChrom Ltd, UK). To this end, aliquots of the pooled melittin fractions from MPLC (100 μL of a 0.1 g/mL aqueous solution) were injected onto the HPLC column. The injected samples were eluted with water/acetonitrile (60:40) at a flow rate of 5 mL/min. The dual UV detector was set at wavelengths 220 and 295 nm, and data was collected using the ChromQuest software. The melittin peak was collected and lyophilised.

Melittin purity measurement by NMR

A solution of the melittin spiking standard was made by dissolving 14.23 mg of the sample in 1 mL of D_2O to give a final

concentration of 5.0 mM. A portion of exactly 600 μL of this solution was then taken for NMR analysis. After this, 30 μL of a 50 mM solution of MeOH in D_2O was then spiked into the melittin sample to give a final methanol concentration of ca 2.5 mM. The samples were each run in triplicate at 310 K for 16 scans with a pre-saturation pulse programme which had a long recovery time (D1=58 s) and a short pre-saturation time (D2=2 s). This long recovery time allowed for all the resonances to be fully detected. One dimensional ^{1}H NMR data were acquired under Topspin (version 2.1, Bruker Biospin, Karlsruhe) using a method analogous to that previously described by Evstigneev et al. [18]. A Bruker AVANCE III 600 NMR spectrometer operated at a proton resonance frequency of 600.13 MHz was equipped with a TBI [^{1}H, ^{13}C, ^{31}P–^{15}N]-z triple resonance probe head fitted with an actively shielded gradient coil for delivery of pulsed-field gradients.

Assay method

A sample of cream (ca 1 g) was weighed into a 20-mL glass vial and dispersed in 10 mL of methanol-chloroform (1:2) mixture. The mixture was then sonicated, with intermittent shaking, for 30 min in an ultrasonic bath until homogenous. A portion (1 mL) of the extraction solvent was pipetted and transferred into a 2-mL centrifuge tube and spiked with a known quantity of melittin standard reconstituted in 0.1 % *v*/*v* formic acid, and then made up to 2 mL with 0.1 % *v*/*v* formic acid. The mixture was then shaken on a vortex mixer for about 2–3 min to allow complete mixing. Thereafter, it was centrifuged at 6,000 rpm for 15 min upon which the supernatant was transferred into a separate vial for SPE. SPE was performed on Strata C18, 100 mg/mL packed columns (Phenomenex, UK). The sample was loaded onto the SPE column and washed with 1 mL of 30/70 (acetonitrile/water) and then eluted with 1 mL of 50/50 (acetonitrile/water). Final eluted solutions were run on the LCMS according to the method described earlier. Peak area was obtained by integrating extracted ion chromatograms of the abundant +4 (*m*/*z* 712.45±0.01) and +5 (570.16±0.01) melittin ions [17] using the XCalibur software.

Calibration with standard additions

Sample extracts were spiked with aliquots of 0.1 mg/mL of a freshly prepared standard spike solution of melittin. Spike weights of 0.0, 2.5, 5.0, 7.5, 10.0, 12.5 and 15.0 μg of melittin corresponded to 0, 25, 50, 75, 100, 125 and 150 μL of the spiking standard solution. Following the spiking, samples were gently vortexed and mixed thoroughly before liquid-liquid extraction by centrifugation and later solid phase extraction. A calibration curve of analyte response versus amount of spiked standard melittin was then constructed using the unspiked sample as the lowest point on the curve. From this curve, the content of melittin in each cream sample was then determined by extrapolating the line to meet the concentration (horizontal) axis.

Results

Melittin purity determination

The NMR spectra obtained showed clear distinction at σ3.4 ppm chemical shift between melittin spiking standard and that of its solution after spiking with pure methanol internal standard (Fig. 1). The methyl protons in methanol overlapped with some unidentified protons in melittin and thus they could not be integrated independently. However, the aromatic region of melittin clearly showed the 5 protons corresponding to the single tryptophan residue in melittin. Integrating this reference region to 5 protons, the rest of the standard melittin spectrum integrated to 174 protons—representing the other non-exchangeable protons in melittin. In addition, the methanol-spiked standard solution integrated to 174 protons plus the contribution from the extra 3 non-exchangeable protons from methanol.

The purity of the standard melittin was calculated by using the formula proposed by Malz and Jancke [19] given as:

$$p_x = \frac{I_X\, N_{\mathrm{std}}\, M_x\, m_{\mathrm{std}}}{I_{\mathrm{std}}\, N_x\, M_{\mathrm{std}}\, m_x} P_{\mathrm{std}} \qquad (1)$$

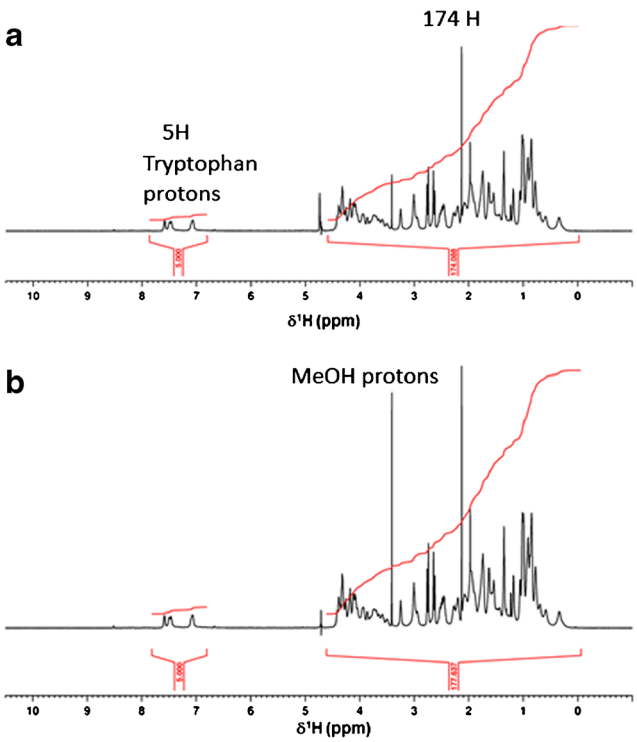

Fig. 1 Proton NMR spectra of melittin (**A**) and melittin+methanol (**B**)

where I, N, M, m and P represent magnitude of signal response (area integral), number of resonant nuclei (protons), molar mass, sample weight and purity of the unknown and standard compounds, respectively.

For this experiment, the following values apply for the unknown sample (melittin) and internal standard (methanol) (Table 1). Although melittin has 229 protons in total, 50 of them are exchangeable with deuterium atoms from the D_2O used as solvent so that the resonant ones are only 179.

Substituting the values in Table 1 into Eq. 1 above gives P_x, the purity of melittin, as 96.0 %. Since the mass spectrum of the melittin spiking solution showed only a single peak representing melittin, it is likely that any impurity present might be due to water or counter anions associated with the basic side chains in melittin. Figure 2 shows a chromatogram obtained for 10 μg/mL of melittin standard.

Mean melittin content in creams

The Table 2 shows a summary of results obtained after assay of six samples of each cream on three separate occasions. Each analysis was conducted by running seven spiked 1 mL aliquots of extract, each prepared from 1 g of cream, on the LCMS and using the melittin peak areas obtained to plot a straight line from which the content in the un-spiked extract was estimated by extrapolation of the standard additions plot.

Assay precision

Analytical precision was determined both between and within runs. Inter-assay precision was checked by testing, on three separate occasions, each of the cream samples using the developed method and then calculating the relative standard deviation (Table 2). The calculated between-run precisions were found to be less than 20 % except for product F where the RSD was 27.5 % perhaps due to the melittin content being close to the limit of quantification of the method. The between sample variations could also be due to variation in the uniformity of content within the creams rather than the analytical precision of the method.

Table 1 Values used in the calculation of melittin purity

Parameter	Internal standard (methanol)	Unknown (melittin)
Signal response (I)	3 (177 less 174)	174
Number of resonant nuclei (N)	3	174 (179 less 5 of Trp)
Molecular weight (M)	32.04	2,846.46
Sample weight in mg (m)	0.09649	8.9649
Purity % (P)	99.9	P_x

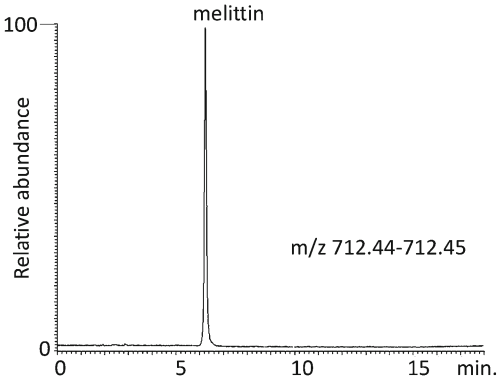

Fig. 2 The chromatogram of the melittin spiking standard

Intra-assay precision was calculated using Eq. 2 below, as previously described by Bruce and Gill [20], to calculate the standard error (s_c) in the concentration (c_x) of the assay mixture obtained by extrapolation of the linear regression standard additions plot.

$$s_c^2 = \frac{s_y^2}{m^2}\left(\frac{1}{N} + \frac{\bar{y}^2}{m^2 S_{xx}}\right) \quad (2)$$

where s_y is the standard deviation around the regression line (standard deviation of the residuals), m is the slope of the regression line, N is the number of samples for each plot, $\bar{y}$ is the response mean and S_{xx} is the corrected sum of squares of the independent variable (spiked concentration).

Table 3 shows the margin of error (precision) estimates calculated for each assay using the equation above and the 95 % confidence intervals for the determined melittin content in the cosmetic products assayed.

From Table 3, it can be seen that the margin of error was, unsurprisingly, high for products whose melittin content was below 10 ppm (A, B and F). However, for the rest of the products, the margin of error was well below the 10 % threshold set for mass fraction of ≥1,000 μg kg^{-1} in accordance with CD2002/657/EC [21], although the direct application of this standard in a standard additions technique does not seem feasible given the complexity of the sample, nor has it been reported previously. The observed degradation of precision is expected in standard additions procedures as described by Ellison and Thompson [22], although such variations are also expected to arise from the detailed extraction procedures required for this type of formulation [12, 23]. Table 4 summarises the equations of the lines obtained for the standard addition curves prepared for each of the samples analysed.

Recovery, specificity and linearity

Since no appropriately matched matrix samples were available, extraction recovery of the method was determined using

Table 2 Triplicate assays of commercial facial creams claimed to contain unstated amounts of bee venom. The values represent complete assays performed on three separate occasions using a seven-point standard additions technique

Samples	Assay of melittin content (in ppm)				Retention time	Linearity
	I	II	III	Mean (RSD, %)	Mean (RSD, %)	Mean R^2 (RSD, %)
A	3.90	4.21	5.42	4.51 (17.8)	6.29 (0.56)	0.989 (0.35)
B	4.37	3.98	3.51	3.95 (10.8)	6.26 (0.88)	0.985 (0.60)
C	36.60	37.21	32.55	35.45 (7.1)	6.36 (0.55)	0.979 (0.18)
D	15.53	17.03	14.45	15.61 (8.9)	6.35 (0.24)	0.992 (0.35)
E	32.59	35.06	34.55	34.07 (3.8)	6.37 (0.24)	0.990 (0.54)
F	3.19	5.62	4.45	4.42 (27.5)	6.69 (0.09)	0.981 (0.82)

a spiked base cream (Nivea) because it was expected to offer comparable extraction challenges to those exhibited by the samples assayed. The blank cream samples were fortified at 5.0, 10.0 and 15.0 μg per 100 mg with melittin and assayed in triplicate. The peak areas obtained were compared to those of external standards prepared in triplicate at the mid-point of the expected concentration range (10.0 μg/mL). The mean recovery obtained was 94.0 % (range, 87.7–102.2 %) with a coefficient of variation (RSD) of 4.6 % (Tables 5 and 6).

Specificity of detection was accomplished by using extracted ion chromatograms for the melittin molecule using two of its abundant ions its mass spectrum (Fig. 3), filtering within a tight range of *m*/*z* 712.445±0.005 and 570.165±0.005. This was further confirmed by looking at the ion spectrum of the peak within the retention time range of the melittin standard. No other compounds from the samples appeared in the chromatogram at the retention time of melittin under these conditions. This was further confirmed by running blank samples.

Linearity of the response was evaluated by using a spiked blank matrix at six calibration points i.e. 2.5, 5.0, 7.5, 10.0, 12.5 and 15.0 μg/mL and then carrying out a linear regression analysis of the analyte peak areas obtained versus concentration. The method showed good linearity in the analytical range with correlation coefficient (R^2)≥0.99. Standard melittin peaks were stable with a retention time mean 6.26 min (RSD≤1.0 %). The mean chromatographic efficiency for the melittin was calculated at ~75,000 plates/m. The limits of detection (LOD) and quantification (LOQ) of melittin in the spiking solution, determined according to ICH guidelines [24], were 50 and 150 ng/mL, respectively.

Table 3 Intra-assay precision estimates at 95 % confidence level (p=0.05, df=5). The t value for a two-tailed t test is ±2.5706 from the Student t table. The 95 % confidence interval was calculated as (95 % CI=tsc) as described in [20]

Product	Run	Assay (ppm)	Standard error (s_c)	Margin of error (%)	±95 % CI (±ts$_c$) (ppm)	Lower CI (ppm)	Upper CI (ppm)
A	1	3.90	0.3952	26.05	1.0159	2.88	4.92
	2	4.21	0.4173	25.48	1.0727	3.14	5.28
	3	5.42	0.5270	25.00	1.3548	4.07	6.77
B	1	4.37	0.4683	27.54	1.2037	3.17	5.57
	2	3.98	0.4447	28.72	1.1431	2.84	5.12
	3	3.51	0.6230	45.63	1.6015	1.91	5.11
C	1	36.60	0.7662	5.38	1.9697	34.63	38.57
	2	37.21	0.7817	5.40	2.0094	35.20	39.22
	3	32.55	0.8060	6.37	2.0720	30.48	34.62
D	1	15.53	0.3310	5.48	0.8509	14.68	16.38
	2	17.03	0.3656	5.52	0.9398	16.09	17.97
	3	14.25	0.4927	8.89	1.2664	12.98	15.52
E	1	32.59	0.6143	4.85	1.5790	31.01	34.17
	2	35.06	0.4388	3.22	1.1281	33.93	36.19
	3	34.55	0.4624	3.44	1.1885	33.36	35.74
F	1	3.19	0.6138	49.46	1.5778	1.61	4.77
	2	5.62	0.4211	19.26	1.0826	4.54	6.70
	3	4.45	0.6801	39.28	1.7481	2.70	6.20

Table 4 Summary of the equations of calibration curves (in the form of y=mx+c) obtained during the assay of the six creams (A–F)

Samples	Slope, m (μg^{-1})	y-intercept, c	|x-intercept| (μg)	Linearity, R^2
A	82,462.4629	32,135.2843	0.3897	0.9911
	82,367.8220	34,708.6236	0.4214	0.9902
	79,832.8949	43,257.5386	0.5419	0.9847
B	85,601.1771	37,387.7843	0.4368	0.9877
	83,035.3569	33,012.0036	0.3976	0.9888
	85,052.6091	29,889.6814	0.3514	0.9781
C	6,567.3226	24,035.9279	3.6599	0.9807
	6,513.4514	24,235.4514	3.7208	0.9802
	6,970.9136	22,688.1725	3.2547	0.9774
D	89,737.9669	139,404.2871	1.5535	0.9949
	86,782.1707	147,767.1025	1.7027	0.9929
	76,890.2507	109,605.3996	1.4255	0.9885
E	65,242.3570	212,602.9011	3.2587	0.9868
	62,561.6680	219,322.2243	3.5057	0.9935
	63,100.6986	218,032.7721	3.4553	0.9927
F	339,024.0249	108,079.3764	0.3188	0.9786
	322,348.3874	181,137.1043	0.5619	0.9902
	359,450.2041	159,968.0232	0.4450	0.9744

Table 5 Recovery data obtained using a blank cream fortified at three different levels of 5, 10 and 15 μg per mL of extract containing 100 mg cream

Replicates	Fortification level (μg per 100 mg)	Peak area	RT (min)	Recovery (%)	Mean area (%)	RSD (%)
1	5.0	425,882	6.22	87.7	95.1	7.7
2	5.0	463,353	6.24	95.4		
3	5.0	496,710	6.25	102.2		
1	10.0	918,056	6.24	94.5	92.4	2.2
2	10.0	896,992	6.25	92.3		
3	10.0	877,902	6.24	90.3		
1	15.0	1,413,491	6.24	97.0	94.5	3.7
2	15.0	1,398,745	6.26	96.0		
3	15.0	1,318,737	6.27	90.5		
Overall mean			6.25	94.0		4.6

Discussion

The standard additions method is used to eliminate matrix effects in samples that would lead to biased results during analysis [25]. This is particularly likely to occur with trace amounts of a chemically complex moiety such as melittin in the complex cream matrix. It has been proposed that the method of standard additions solves a particular type of matrix effect (called the rotational effect), but not translational effects—which must be separately dealt with [22]. In the method of standard additions, known quantities of the analyte being assayed are spiked into a sample containing the analyte at increasing concentrations, starting from zero, and then extracted. Final solutions are subsequently analysed and the peak areas obtained are plotted against the spiked volumes or concentration of spiked samples. Provided that the area response is directly proportional to concentration, a straight line is obtained. This straight line crosses the response (vertical) axis at the response value of the un-spiked sample; extrapolating this straight line to the concentration (horizontal) axis gives, numerically, the weight of analyte in the un-spiked sample (Fig. 4). The main advantage of using standard additions is that there is no need for complete extraction of analyte from matrix provided all the samples have been subjected to exactly the same extraction process. It is important that the samples

Table 6 Peak areas of standard melittin assayed at 10 μg/mL

Replicates	Concentration (μg/mL)	Peak area	RT (min)	Mean area	Precision (RSD, %)
1	10.0	978,938	6.24	971,682.3	0.79
2	10.0	963,628	6.24		
3	10.0	972,481	6.25		

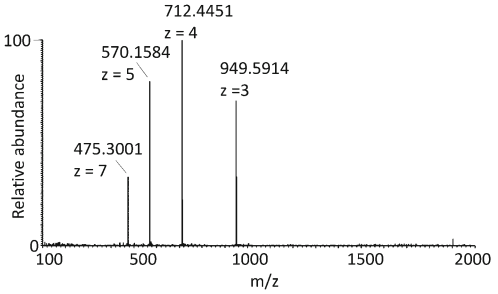

Fig. 3 The mass spectrum of melittin. Melittin molecules can acquire up to six positive charges during electrospray ionisation (ESI) in the mass spectrometer. The most abundant ions in the spectrum are *m/z*: 712.45 (+4) and 570.16 (+5) species

are not spiked to levels exceeding linearity limits of the analyte response. The amount of standard added depends on the approximate concentration of the un-spiked samples. Ideally, samples should be spiked at any evenly spaced concentrations of standard solutions within the linear range, although it has been recommended that spiked concentrations should be at least four times the concentration of analyte [22].

In this experiment, initial analyses had given us varying composition of melittin in the creams ranging from approximately 5 to 100 ppm (μg/g). This translates to a melittin content of about 0.5–10 μg per 100 mg of the cream. Thus in this work, the samples were spiked with the melittin standard at 0, 25, 50, 75, 100, 125 and 150 μg per 100 mg. These spiking levels conform to the sequence $x_1 \approx x_0$, $x_2 = 2x_1$,.... $x_p = px_1$ (x being analyte amount) which is generally acceptable [25]. The levels are nevertheless slightly below those recommended by Ellison and Thompson (2008) where at least five times the expected concentration of analyte should be used with repetitive measurements, if necessary, to improve precision [22]. Clearly, the latter approach also reduces the total amount of sample preparation time required. Based on results obtained and observations made during this assay, it is quite clear that the extraction and determination of melittin in the creams is a complex and laborious process which might introduce some errors depending on the degree of control of extraction conditions. The liquid layers formed after solvent extraction

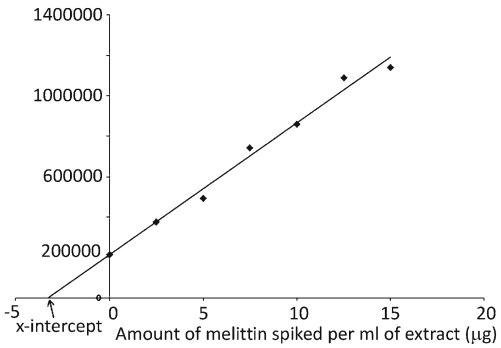

Fig. 4 Sample calibration plot representing cream sample E. The plot represents data obtained with replicate 1. The values of m, c and R^2 for this assay are 65,242.4, 212,602.9 and 0.9868, respectively

centrifugation were quite distinctly separated, but with a white precipitate forming at the liquid-liquid interface for three of the samples analysed (C, E and F). This was thought to be possibly due to lignin from the herbal components stated to be present in these products. Our preliminary liquid-liquid extraction (LLE) extracts without SPE had exhibited poor compatibility with the reversed phase analytical column leading to significant peak distortions. This was understood to arise from matrix interferents that probably suppressed melittin ionisation or its ability to chromatograph properly leading to poor chromatographic efficiency as peaks became broader and noisier, especially at spiked analyte concentrations $\leq$2.5 μg/mL. Extraction with either aqueous or organic solvent alone proved inadequate as this led to incomplete dispersion of the creams. Ideally, a good SPE method should achieve strong enough retention of an analyte on the column during sample loading and washing steps so that it can be concentrated and eluted in a more controlled manner to obtain relatively clean fractions [26]. The initial lack of adequate retention of melittin on the SPE cartridge was found to be associated with fast loading under vacuum. Allowing the sample to load slowly, freely under gravity, overcame this problem. Attempts at preventing early breakthroughs by using high pH (at which the melittin was less ionised) during LLE proved fruitless due to low extraction recovery. This observation concerning the role of low pH (with formic acid) in the extraction of melittin from the cream might have been expected since a basic amphiphilic peptide such as melittin needs to be ionised in order to effectively partition into the aqueous layer that was analysed in this assay. Complete elimination of formic acid thus prevents such ionisation leading to insufficient extraction.

Aqueous solutions of whole bee venom demonstrated gradual degradation of melittin within the ^{21}Lysine-^{22}Arginine-^{23}Lysine-^{24}Arginine region of the amino acid sequence under sterile conditions at room temperature (data not shown). Zhou et al. have previously reported a similar behaviour in pure melittin and apamin aqueous samples as well as in aqueous crude bee venom extracts [17]. We have observed here that purified melittin degrades comparatively much more slowly than when it is in the crude venom. The observed activity appears to be enzyme catalysed and the enzyme involved seems to be trypsin-like. It is probable that the observed activity is due to a serine carboxypeptidase already identified in bee venom as an allergen through genome analysis. That would mean that our method of purification of melittin either removes or denatures this peptidase activity. Currently, we cannot confirm if such degradation does occur in the formulated products and, if it does, the extent of such degradation. Thus, the results of this assay can only confirm the melittin content of the creams at the time of analysis which may differ from the original amount incorporated.

Conclusion

A reversed phase LCMS method was developed for the assay of melittin in six commercially available creams containing unspecified amounts of purified bee venom. Given that the proportions of bee venom in the products were not specified, it is not possible to comment on how well the products conform to a label claim. Extraction recovery suggests the accuracy of our assay method to be acceptable, although the blank matrix was an entirely different cream altogether, but with no bee venom in it. This might have biased the results of extraction recovery since this can vary across different blank matrices. Nevertheless there, certainly, is significant variation in the amount of melittin measured in the creams which ranged between 3.2 and 37.2 ppm, which is more than tenfold but with satisfactory intra and inter- assay precisions. Production of a good quality product requires adequate quality control for the finished product. The chemical and physical stability of bee venom in cream matrices would require careful assessment and this is something which we are now able to do.

Acknowledgments We thank the Korean Government KIAT scheme and Wissen Co. for the support for the work.

References

1. Gagliardi L, De Orsi D, Dorato S (2007) General review of official methods of analysis for cosmetics in different countries. In: Salvador A, Chisvert A (eds) Analysis of Cosmetic Products. Elsevier, Amsterdam, pp 45–71
2. Gao W, Gray N, Heaton J, Smith NW, Jia Y et al (2012) UV gradient combined with principal component analysis: highly sensitive and specific high performance liquid chromatography analysis of cosmetic creams. J Chromatogr A 1228:324–328
3. Kokot ZJ, Matysiak J (2009) Simultaneous determination of major constituents of honeybee venom by LC-DAD. Chromatographia 69: 1401–1405
4. Terwilliger TC, Eisenberg D (1982) The structure of melittin. I. Structure determination and partial refinement. J Biol Chem 257: 6010–6015
5. Van Vaerenbergh M, Cardoen D, Formesyn EM, Brunain M, Van Driessche G et al (2013) Extending the honey bee venome with the antimicrobial peptide apidaecin and a protein resembling wasp antigen 5. Insect Mol Biol 22:199–210
6. Chen J, Lariviere WR (2010) The nociceptive and anti-nociceptive effects of bee venom injection and therapy: a double-edged sword. Prog Neurobiol 92:151–183
7. WHO/IUIS (2014) Allergen Nomenclature. www.allergen.org: Allergen Nomenclature Sub-Committee
8. Orsolic N (2012) Bee venom in cancer therapy. Cancer Metastasis Rev 31:173–194
9. Ferreira Junior RS, Sciani JM, Marques-Porto R, Lourenco Junior A, Orsi RO et al (2010) Africanized honey bee (*Apis mellifera*) venom profiling: seasonal variation of melittin and phospholipase A(2) levels. Toxicon 56:355–362
10. Alvarez-Rivera G, Lores M, Llompart M, Garcia-Jares C (2013) Cosmetics and toiletries: chromatography. Reference Module in

Chemistry, Molecular Sciences and Chemical Engineering: Elsevier, Waltham
11. Matysiak J, Schmelzer CEH, Neubert RHH, Kokot ZJ (2011) Characterization of honeybee venom by MALDI-TOF and nanoESI-QqTOF mass spectrometry. J Pharm Biomed Anal 54: 273–278
12. Bu X, Chandran S, Spirig J, Wang Q (2011) Sample preparation for selected nonsolid dosage forms. In: Nickerson B, editor. Sample preparation of pharmaceutical dosage forms: challenges and strategies for sample preparation and extraction: American Association of Pharmaceutical Scientists. pp 179–210
13. CTPA (2013) How are cosmetics regulated? Definition of a cosmetic. CTPA Website: CTPA
14. Llompart M, Celeiro M, Pablo Lamas J, Sanchez-Prado L, Lores M et al (2013) Analysis of plasticizers and synthetic musks in cosmetic and personal care products by matrix solid-phase dispersion gas chromatography–mass spectrometry. J Chromatogr A 1293:10–19
15. Tullo C (2013) Consumer protection: the cosmetic products enforcement regulations 2013. In: Kingdom PotU, editor. 20131478. United Kingdom: The Stationery Office Limited. pp 1–28
16. Denisov E, Damoc E, Lange O, Makarov A (2012) Orbitrap mass spectrometry with resolving powers above 1,000,000. Int J Mass Spectrom 325:80–85
17. Zhou J, Zhao J, Zhang S, Shen J, Qi Y et al (2010) Quantification of melittin and apamin in bee venom lyophilized powder from *Apis mellifera* by liquid chromatography-diode array detector-tandem mass spectrometry. Anal Biochem 404:171–178
18. Evstigneev MP, Parkinson JA, Lantushenko AO, Kostjukov VV, Pahomov VI (2010) Hexamer oligonucleotide topology and assembly under solution phase NMR and theoretical modeling scrutiny. Biopolymers 93:1023–1038
19. Malz F, Jancke H (2005) Validation of quantitative NMR. J Pharm Biomed Anal 38:813–823
20. Bruce GR, Gill PS (1999) Estimates of precision in a standard additions analysis. J Chem Educ 76:805
21. Communities TCotE (2002) Commission Decision 2002/657/EC. In: Union E, editor. L221/8. 17 August 2002: Official Journal of the European Communities
22. Ellison SL, Thompson M (2008) Standard additions: myth and reality. Analyst 133:992–997
23. Bishop JE, Kou D, Manius G, Chokshi PH (2011) Sample preparation method validation. In: Nickerson B, editor. Sample preparation of pharmaceutical dosage forms: challenges and strategies for sample preparation and extraction. 1 ed: American Association of Pharmaceutical Scientists. pp. 233–251
24. ICH (1996) Validation of analytical procedures: methodology, ICH Topic Q2B (CPMP/ICH/281/95). The European Agency for the Evaluation of Medicinal Products
25. Danzer K, Currie LA (1998) Guidelines for calibration in analytical chemistry—Part 1. Fundamentals and single component calibration (IUPAC recommendations 1998). Pure And Appl Chemistry 70:993–1014
26. Moldoveanu S, David V (2015) Chapter 7—Solid-phase extraction. In: David SM (ed) Modern sample preparation for chromatography. Elsevier, Amsterdam, pp 191–286

Effect of Bee Venom and Its Fractions on the Release of Pro-Inflammatory Cytokines in PMA-Differentiated U937 Cells Co-Stimulated with LPS

Article *in* Vaccines · April 2016

DOI: 10.3390/vaccines4020011

12 authors, including:

John A Parkinson

University of Strathclyde

169 PUBLICATIONS **3,994** CITATIONS

SEE PROFILE

Carol Clements

University of Strathclyde

36 PUBLICATIONS **202** CITATIONS

SEE PROFILE

Louise Young

University of Strathclyde

28 PUBLICATIONS **341** CITATIONS

SEE PROFILE

Valerie A Ferro

University of Strathclyde

76 PUBLICATIONS **927** CITATIONS

SEE PROFILE

vaccines

MDPI

Article

Effect of Bee Venom and Its Fractions on the Release of Pro-Inflammatory Cytokines in PMA-Differentiated U937 Cells Co-Stimulated with LPS

Jonans Tusiimire [1], Jennifer Wallace [2], Nicola Woods [1], Mark J. Dufton [2], John A. Parkinson [2], Grainne Abbott [1], Carol J. Clements [1], Louise Young [1], Jin Kyu Park [3], Jong Woon Jeon [3], Valerie A. Ferro [1] and David G. Watson [1,*]

1 Strathclyde Institute of Pharmacy and Biomedical Sciences, University of Strathclyde, 161 Cathedral Street, Glasgow G4 0RE, U.K.; jonans.tusiimire@strath.ac.uk (J.T.); nicola.woods@strath.ac.uk (N.W.); grainne.abbott@strath.ac.uk (G.A.); c.j.clements@strath.ac.uk (C.J.C.); Louise.c.young@strath.ac.uk (L.Y.); v.a.ferro@strath.ac.uk (V.A.F.)

2 WestCHEM Department of Pure and Applied Chemistry, University of Strathclyde, 295 Cathedral Street, Glasgow G1 1XL, U.K.; jennifer.wallace.101@strath.ac.uk (J.W.); mark.dufton@strath.ac.uk (M.J.D.); john.parkinson@strath.ac.uk (J.A.P.)

3 #204, Beesen Co. Ltd., Bio Venture Town, Yuseong Daero 1662, 34054 Dae Jeon, Korea; jkypark@live.co.kr (J.K.P.); confessor@hanmail.net (J.W.J.)

* Correspondence: d.g.watson@strath.ac.uk; Tel.: +44-141-548-2651; Fax: +44-141-552-6443

Academic Editor: Diane M. Harper
Received: 2 March 2016; Accepted: 13 April 2016; Published: 19 April 2016

Abstract: The venom of *Apis mellifera* (honey bee) has been reported to play a role in immunotherapy, but existing evidence to support its immuno-modulatory claims is insufficient. Four fractions from whole bee venom (BV) were separated using medium pressure liquid chromatography. Their ability to induce the production of cytokines TNFα, IL-1β and IL-6 in phorbol-12-myristate-13-acetate (PMA)-treated U937 cells was assessed. The levels of the three cytokines produced by stimulation with the four fractions and crude BV without LPS were not significantly different from negative control values. However, co-stimulation of the cells with LPS and Fraction 4 (F-4) induced a 1.6-fold increase in TNF-α level ($p < 0.05$) compared to LPS alone. Likewise, LPS-induced IL-1β production was significantly synergised in the presence of F-1 (nine-fold), F-2 (six-fold), F-3 (four-fold) and F-4 (two-fold) fractions, but was only slightly enhanced with crude BV (1.5-fold) relative to LPS. Furthermore, the LPS-stimulated production of IL-6 was not significantly increased in cells co-treated with F-2 and F-3, but the organic fraction (F-4) showed an inhibitory effect ($p < 0.05$) on IL-6 production. The latter was elucidated by NMR spectroscopy and found to contain(*Z*)-9-eicosen-1-ol. The effects observed with the purified BV fractions were more marked than those obtained with the crude sample.

Keywords: bee venom; pro-inflammatory cytokines; LPS stimulation; U937 cells; PMA differentiated; ELISA; (*Z*)-9-eicosen-1-ol; *Apis mellifera*

1. Introduction

Bee venom (BV) is mainly used as a defence tool by the honey bee, and its primary function is to inflict pain on any intruders into the hive [1]. Despite its pain-causing effects, the main reported human administration uses relate to pain relief in conditions, such as arthritis and rheumatism [2,3], tendonitis, multiple sclerosis, wounds and gout [4–6]. The chemical composition of BV is complex, but the primary ingredients are bioactive peptides, proteins and several other biomolecules [6–10].

The principal component is a 26-amino acid haemolytic peptide, melittin, which accounts for about 50%–60% of the venom by dry weight and is responsible for most of the observed effects [9,11,12].

BV components have been reported to possess various and, sometimes, conflicting immune-related effects. Available evidence suggests that apamin [13], histamine [14], mast cell degranulating (MCD) peptide [15,16] and phospholipase A_2 (PLA_2) [17] significantly increase the inflammatory response. The small neurotoxic peptide apamin (MW 2.0 kDa) is a Ca^{2+}-activated K^+-channel blocker, which has been reported to increase murine T-cell proliferation [13]. However, it has also been reported to inhibit histamine release in lung tissues, suggesting that it could decrease allergic airway inflammation through mast cell stabilisation [18]. Park *et al.* (2004) also demonstrated that histamine increased the production of IL-6 in nasal fibroblasts and induced nuclear factor kappa B (NF-κB) [14], a transcriptional factor for many pro-inflammatory genes [19]. On the other hand, MCD peptide was reported to inhibit histamine release from mast cells [15] by binding, in a dose-related manner, to mast cell receptors, thereby partially inhibiting IgE binding to these receptors [20]. Similarly, PLA_2 was shown to activate T-cells via its action on phospho-diacylglycerides to form small neoantigenic factors *in vivo*, in a process dependent on antigen presentation by CD1a proteins [17].

Conversely, some components of BV have been reported to possess anti-inflammatory actions. For instance, the basic polypeptide adolapin (MW 11.5 kDa) was reported to possess anti-inflammatory and analgesic activities in carrageenan-, prostaglandin- and adjuvant-induced rat oedema and adjuvant polyarthritis [21]. These effects were attributed to the inhibition of prostaglandin synthesis, via cyclooxygenase inhibition, as well as through central mechanisms [21]. Adolapin was also shown to inhibit the activity of BV PLA_2 and human lipoxygenase from platelets and possessed antipyretic effects [22].

Past reports on immuno-modulating effects of the main bee venom peptide melittin are rather contradictory. For instance, whereas Bramwell *et al.* (2003) reported dose-dependent mucosal adjuvant action of intranasal melittin co-administered with tetanus and diphtheria toxoids in mice [23], a number of other studies have reported its "neutralising" effects on LPS in murine macrophage cell lines [24,25]. The adjuvant effects of melittin were linked to its enhancement of vaccine absorption across the mucosal lining, which led to higher antibody (IgG) titres than those of either component alone [23]. On the other hand, its antagonistic effects on LPS were linked to inhibition of NF-κB binding to DNA [24] and phosphorylation of IκB kinase [25], respectively. In addition, treatment of LPS-stimulated BV2 immortalized murine microglial cells with BV or melittin, decreased the expression of pro-inflammatory cytokines (IL-1β, IL-6 and TNF-α) and inhibited inducible nitric oxide synthase (iNOS) production and nitric oxide (NO) expression, as was the expression of cyclooxygenase-2 (COX-2) and prostaglandin E_2 (PGE_2) production [26,27]. These anti-inflammatory effects were linked mainly to the leucine zipper sequence in melittin, which contains two leucine residues, since Leu-Ala substitution in this sequence progressively reduced this neutralising effect [27]. Jang *et al.* (2005) also reported anti-inflammatory effects of BV in RAW 264.7 macrophages that were attributed to a downregulation of iNOS, COX-2, NF-κB and mitogen-activated protein kinases (MAPKs) [28]. In addition, Park *et al.* (2004) also reported that BV and melittin decreased carrageenan-induced oedema and adjuvant-induced arthritis in rat models consistent with their inhibitory effects on LPS-induced expression of COX-2, cytosolic PLA_2 and iNOS and on the generation of PGE_2 and NO [24]. BV and melittin also prevented LPS-induced transcriptional and DNA binding activity of NF-κB via inhibition of IκB release [2].

Since upregulation of most pro-inflammatory genes (e.g., cytokines and chemokines) relies on activation of NF-κB [19], inactivation of the latter by BV or its components would be a key mechanism for exerting anti-inflammatory effects [29]. However, in a previous study, no significant inactivation of IL-1β-induced NF-κB was observed in fibroblast-like synoviocytes from rheumatoid arthritis patients, as well as in dermal fibroblasts and red blood cells from healthy volunteers, after treatment with BV and melittin [30]. In addition, there was no effect on the phosphorylation or degradation of IκB, and even at high concentrations, BV and melittin had no effect on NF-κB-p50-DNA interactions. Instead,

significant increases in mRNA levels of several pro-inflammatory genes (including COX-2, IL-1β, TNF-α) and large quantities of oxygen radicals were observed following exposure to BV or melittin [30]. This suggested that melittin alone and BV as a whole are pro- rather than anti-inflammatory.

In the current study, the effects of BV and its fractions on the production of cytokines TNF-α, IL-1β and IL-6 were investigated in PMA-treated U937 cells. The latter belong to a monocytic differentiation lineage derived from malignant cells of a patient with generalised histiocytic lymphoma [31], and their differentiation with PMA, a potent tumour promoting agent [32], is known to impart functional properties typical of macrophages [32–34]. The presence of synergy between BV and LPS, a standard antigen, in inducing the production of the pro-inflammatory mediators would suggest the potential application of BV as a source of immuno-modulating agents for use as vaccine adjuvants.

2. Materials and Methods

2.1. Cell Culture

U937 cell cultures (obtained from ECACC, Porton Down, Salisbury, UK) were seeded at 3×10^5 cells/mL in RPMI-1640 (Lonza, Verviers, Belgium) supplemented with 2 mM L-glutamine (Life Tech, Paisley, UK), 100 IU/100 µg/mL penicillin/streptomycin (Life Tech, Paisley, UK) and 10% (*v*/*v*) foetal bovine serum (FBS) (Sigma-Aldrich, Dorset, UK). Cells were subcultured every 2–4 days and maintained at 37 °C in a humidified atmosphere of 5% CO_2.

2.2. Test Sample Isolation, Preparation and Analysis

Crude BV (supplied lyophilized by Beesen Co. Ltd., Dae Jeon, Korea) was prepared for bioassay by dissolving 10 mg in 1 mL of dimethyl sulphoxide (DMSO, Sigma-Aldrich) followed by filtration through a 0.2-µm filter (Millex®, Sigma-Aldrich). The venom fractions F-1–F-4 were isolated from 800 mg of crude BV by reversed phase medium pressure liquid chromatography (MPLC) on a Reveleris® iES flash chromatography system (Grace Davison Discovery Sciences, Carnforth, UK) with dual UV (λ = 220/280 nm) and evaporative light scattering (ELSD) detection. The sample was mixed with 3 g of Celite® before loading it into a dry-loading cartridge. The column used was an Easyvarioflash D24 cartridge (VWR International, Lutterworth, UK) packed with *ca.* 13 g of Polymeric Retain PEP for SPE (Thermo Scientific, Paisley, U.K.), as previously described [35]. Fraction F-1 was eluted with 100% water and F-4 with 100% acetonitrile (Sigma-Aldrich), both solvents being of HPLC grade. Fractions F-2 and F-3 were eluted in water/acetonitrile mixtures of 80/20% and 50/50%, respectively. The resulting purified fractions were freeze-dried and stored at −30 °C until required for the assay. Samples for bioassays were reconstituted at 10 mg/mL in DMSO. Liquid chromatography-mass spectrometry (LC-MS) analysis of the freeze-dried fractions was carried out. The samples were reconstituted in water (F-1, F-2 and F-3) or acetonitrile:water (1:1) (F-4) to achieve concentrations of 0.1 mg/mL in each case, and 10-µL aliquots were injected into a Finnigan Surveyor HPLC system interfaced to an Orbitrap Mass Spectrometer (Thermo Fisher Scientific, Bremen, Germany). All of the samples were analysed using an ACE 3 C18 column (150 × 3.0 mm, 3 µm particle size) supplied by Hichrom Ltd. (Reading, UK). The mobile phase consisted of 0.1% formic acid in water (A) and 0.1% formic acid in acetonitrile (B) at a flow rate of 0.3 mL/min. The gradient used for F-1 to F-3 was 20%–70% B from 0–10 min, 6 min hold at 70% B, then return to 20% B over 4 min, followed by 5 min re-equilibration. In the case of F-4, an initial 5-min isocratic profile at 50% B was followed by a 1-min ramp to 95% B, held there for 8 min, before a 1-min return to 50% B and re-equilibration for 4 min. Full scan spectra were obtained within m/z 100–2000 in the positive ESI mode for all samples, except F-4, which was detected in the m/z range 200–1200 in the negative ESI mode. For MS/MS of F-4, collision-induced dissociation (CID) of the $[M - H]^-$ parental ion was carried out at a normalised collisional energy of 35.0 V, and the product ion scan was made in the m/z rage of 200–700, also in the negative ESI mode. The spray needle voltages were set at 4.5 and −3.5 kV in positive and negative ESI modes, respectively. The sheath and auxiliary gas flow rates were

50 and 15 arbitrary units, respectively, while ion transfer capillary temperature was set at 275 °C. All data were collected and processed using XCalibur software (version 2.1.0, Thermo Fisher Scientific, Bremen, Germany).

2.3. Cytotoxicity Assay

U937 cells were seeded at 2.25×10^4 cells/well in 96-well plates (Corning®, Sigma-Aldrich) and incubated in the presence and absence of BV or its fractions at final concentrations ranging from 100 μg/mL–3 ng/mL ($n = 3$). Triton X at 1% (v/v) served as a positive control. The plate was then incubated at 37 °C and 5% CO_2 in a humidified atmosphere for 48 h. After incubation, Alamar® Blue (AbD Serotec®, Kidlington, U.K.) was added at a final concentration of 10% in a total assay volume of 100 μL per well and the plate incubated for a further 6 h. Fluorescence readings of the plate were taken using a Perkin Elmer Wallac Victor^2 1420 Multilabel Counter ($\lambda_{Ex/EM}$: 560/590 nm). All readings were corrected for background by subtracting the mean fluorescence of the Triton X wells. Cell viability was then calculated for each well as a percentage of fluorescence readings in the presence of test sample relative to the mean value of the negative controls. The resulting data were analysed with GraphPad Prism for Windows (version 4.03, GraphPad Software, San Diego, CA, USA, www.graphpad.com) to obtain dose-response curves for each sample and their corresponding mean inhibitory concentration (IC_{50}) values.

2.4. Induction of Cell Differentiation

U937 cells were seeded at 4.5×10^4 cells/well in a volume of 450 μL in 24-well tissue culture plates (Corning®, Sigma-Aldrich) ($n = 3$) in media containing 60 ng/mL PMA (Sigma-Aldrich). A control well containing cells in media without PMA was also included. The cells were then incubated in a humidified atmosphere at 37 °C and 5% CO_2 for 48 h. Micrographs of the cells were taken after 24 and 48 h for evidence of differentiation.

2.5. Stimulation of Cytokine Release

After 48 h of differentiation, the media were aspirated and replaced with fresh media, without PMA, and the cells incubated for a further 24 h. At this point, samples of BV or fractions, with or without *Escherichia coli* (*E. coli*) LPS (Sigma-Aldrich), were then added from a separate sample dilution plate prepared using 10 mg/mL stock solutions (Table S1 in the Supplementary Materials). The final concentrations of the samples on the cell culture plate were 100 μg/mL (F-1 and F-2), 12 μg/mL (F-3 and BV) and 120 μg/mL (F-4), respectively. The final LPS concentration in the LPS-containing samples was 1 μg/mL.

2.6. Assessment of Cytokine Release

Three ELISA kits from R&D Systems (Abingdon, U.K.) were used to assess the release of interleukin (IL)-1β/IL-1F-2, IL-6 and tumour necrosis factor (TNF)-α from LPS-stimulated and non-stimulated U937 cells. The ELISA assay was carried out according to the kit manufacturer's instructions, except that the colour substrate used (3,3'5,5'-tetramethylbenzidine, TMB) was from Sigma-Aldrich (Dorset, U.K.) and came as ready for use. The reaction was stopped with 2 N sulphuric acid (H_2SO_4) and the plate was read immediately at a 450-nm wavelength using a SpectraMax Pro 5 (Wokingham, U.K.) with wavelength correction by subtracting readings taken at 570 nm.

2.7. Data Analysis

Standard calibration curves were plotted by fitting the optical density data of TNF-α, IL-1β and IL-6 to 4-parameter logistic (4-PL) regression curves (Table S2 and Figures S1–S9 in the Supplementary

Materials). Each of these standards was prepared in duplicate at each of the concentrations in the ranges recommended by the manufacturer. The 4-PL regression equation is given by:

$$y = d + \frac{a - d}{1 + \left(\frac{x}{c}\right)^b} \quad (1)$$

where y is the response value (*i.e.*, measured optical density), x is the concentration (in pg/mL) and a, b, c and d are constants. The regression analysis also computes the R^2 value, which gives an indication of how best the fitted curve agrees with the data. From Equation (1), the unknown concentration, x, of a sample of optical density, y, can be calculated according to:

$$x = c\left(\frac{a - d}{y - d} - 1\right)^{\frac{1}{b}} \quad (2)$$

Using Equation (2), the concentrations of TNF-α, IL-1β and IL-6 induced by each of the samples assayed (with and without LPS) were calculated and expressed as ratios of the mean cytokine level induced by LPS (positive control), assayed in triplicate (n = 3). The resulting data were then analysed with GraphPad Prism to obtain bar graphs whose statistical significances were tested at the 95% confidence level (CI) relative to the mean positive control ratio of 1.0.

2.8. NMR Spectroscopy

NMR spectroscopy was carried out on 7.4 mg of BV fraction F-4 dissolved in 600 μL DMSO-d_6. NMR data were acquired with a Bruker AVANCE II$^+$ NMR spectrometer (Bruker Biospin GmbH, Rheinstetten, Germany) equipped with a 14.1 T Ultrashield^{TM} superconducting magnet operating at a ^{1}H resonance frequency of 600.13 MHz under TopSpin (version 2.1, Bruker Biospin GmbH, Rheinstetten, Germany) running in a Microsoft Windows environment. All data were acquired using a BBO-z-atm probe head operating at ambient temperature (298 K) regulated by means of a BCU-05 chiller unit.

1D ^{1}H-NMR spectra were acquired with 16 transients over a frequency width of 7.2 kHz (12.0 ppm) centred at a frequency offset of 5.0 ppm into 32 K data points for an acquisition time of 2.27 s using a 30-degree radio frequency (r.f.) pulse and a recycle delay of 2.0 s.

1D ^{13}C-{^{1}H} NMR spectra were acquired with 1024 transients over a frequency width of 33.33 kHz (220.8 ppm) centred at a frequency offset of 100.0 ppm into 32 K data points for an acquisition time of 491.5 ms using a 30-degree r.f. pulse with continuous composite pulse decoupling applied at the ^{1}H resonance frequency and using a recycle delay of 0.7 s.

Complete details for all NMR experimental conditions can be found in the Supporting Information.

3. Results

3.1. Composition of Fractions 1–4 from MPLC

From LC-MS analysis, the fractions were revealed to contain mixed components in F-1 and F-2, while F-3 and F-4 both contained largely single components. The major constituents of F-1 were putatively identified to be histamine, proline, noradrenaline, 5-aminovaleric acid, cellobiose and arginine (Figure S10). Fraction F-2 contained mainly PLA_2, as well as varying amounts of apamin, secapin and MCD peptide (Figure S11). On the other hand, melittin was the principal component of F-3 (96% purity) (Figure S12), while the organic fraction, F-4, mainly contained a new compound identified through NMR analysis as (*Z*)-9-eicosen-1-ol and trace levels of an unidentified phospholipid. The LC-MS did not detect (*Z*)-9-eicosen-1-ol due to its absolute lack of ionisation in both positive and negative ESI modes, but instead detected the trace phospholipid impurity, undetected by NMR at its concentration in the fraction (Figure S13).

3.2. Cytotoxicity of BV Fractions against U937 Cells

Cytotoxicity studies were carried out (n = 3) to obtain IC_{50} values (Figure 1). Samples F-1 and F-2 gave IC_{50} of greater than 100 µg/mL. In contrast, F-3 gave the lowest IC_{50} value at 5.4 µg/mL (or 1.9 µM). The IC_{50} value of F-4 was 68.8 µg/mL. Micrographs of the cells taken after 24 and 48 h confirmed the assay results obtained with the Alamar® Blue assay (Figure 2). These micrographs also revealed significant microscopic differences in the appearance of cells treated with F-3 and F-4 even in wells where Alamar® Blue readings were comparable. Unlike the necrosis caused by melittin, which revealed the cells to have burst to release their protoplasm, non-viable F-4-treated cells appeared to have an intact cell outline, implying that the mechanism by which the lipid exerts its cytotoxic effect on U937 cells may be different from that of melittin, which acts through cell lysis [36].

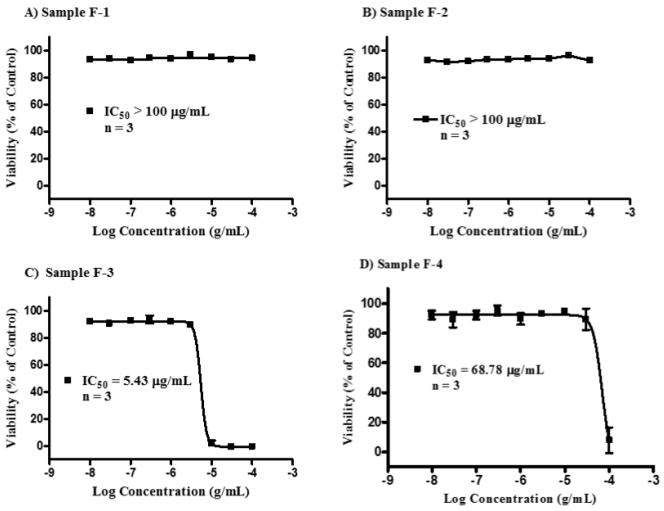

Figure 1. Cytotoxicity of the bee venom sample fractions F-1–F-4 against U937 cells. Fraction samples F-1 (**A**) and F-2 (**B**) were non-cytotoxic, each with an IC_{50} value >100 µg/mL. Fraction sample F-3 (**C**, melittin) was the most cytotoxic with an IC_{50} of 5.43 (95% CI 4.43–6.66) µg/mL, while fraction sample F-4 (**D**, lipid) had an IC_{50} value of 68.78 µg/mL.

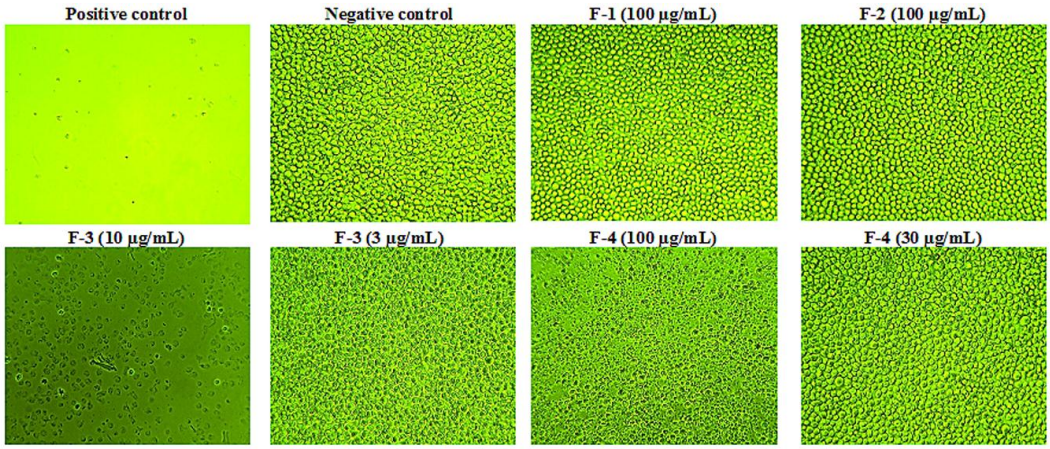

Figure 2. Cytotoxic effects of bee venom fractions on U937 cells. Fractions F-1 and F-2 were non-cytotoxic at the highest concentration of 100 µg/mL used, while F-3 was the most cytotoxic on the cells, as necrotic effects were observed even at 10 µg/mL (IC_{50} 5.4 µg/mL). On the other hand, F-4 was cytotoxic above 30 µg/mL with an IC_{50} of 68.8 µg/mL (n = 3). (Magnification = ×100).

3.3. Selection of BV and Fraction Concentrations for the Assay

ELISAs were carried out in order to determine the effect of the fractions on PMA-differentiated cells with respect to the production of three inflammatory mediators TNF-α, IL-1β and IL-6. Since the investigation of immuno-modulatory effects had to be conducted using concentrations of the fractions where the cells remained viable, concentrations were selected for each fraction that were below their respective IC_{50} values. Specifically, the highest final concentration of the fraction at which no toxicity was observed on the cells was used. Thus, F-1 and F-2 were each assayed at 100 μg/mL, F-3 and BV at 3 μg/mL, while F-4 was assayed at 30 μg/mL (Table S3 in the Supplementary Materials). The mean viability (n = 3) of the cells at the concentrations selected for each of the fractions used for the assay were F-1 (93%), F-2 (94%) and F-3 and F-4 (90% each), respectively, relative to the media control.

3.4. Effect of PMA on the U937 Cells

After the cells had been incubated in the presence of PMA, they were observed microscopically at 24 and 48 h for the presence of features that confirmed whether or not they had differentiated [37]. Micrographs were also taken of the treated cells and compared to those of U937 cells in control wells (absence of PMA) on the same plate (Figure 3), which confirmed the morphological changes expected.

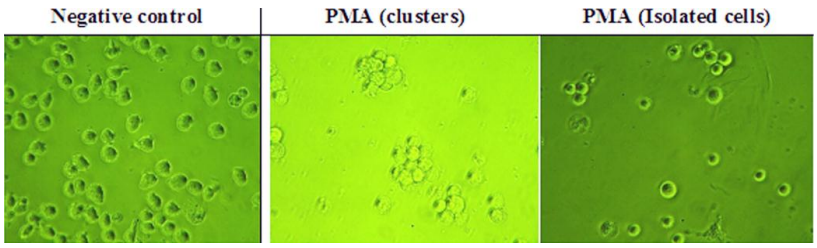

Figure 3. Effect of phorbol-12-myristate-13-acetate (PMA) on U937 cells. PMA was added to the cells at 60 ng/mL (n = 3). (Magnification = ×400).

3.5. Effect on TNF-α Production

The BV fractions on their own did not induce significant TNF-α production in PMA-differentiated U937 cells relative to the negative control (culture media). However, when used in combination with LPS, there was a noticeable enhancement (ratio >1.0) in the amount of TNF-α produced compared to LPS alone. This was statistically significant ($p < 0.05$) only with F-4, which produced a 1.6-fold increase in TNF-α release from the cells (Figure 4).

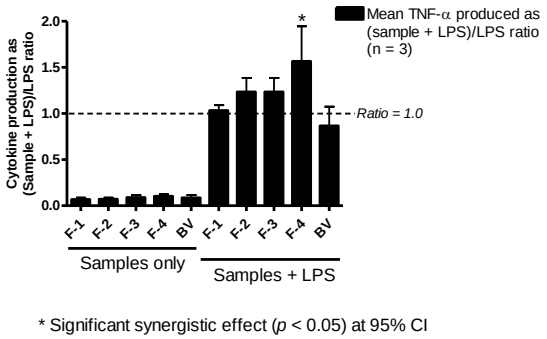

Figure 4. Effect of bee venom and its fractions of TNF-α production in PMA-differentiated U937 cells. All five samples tested produced slightly more than background levels of TNF-α, but not significantly different from those of the negative control (media). The level of TNF-α was significantly higher in fractions co-stimulated with F-4 and LPS compared to LPS, but the other fractions did not show any significant changes in the levels of the cytokine (n = 3).

3.6. Effect on IL-1β Production

The enhancement of IL-1β/IL-1F2 by BV fractions in LPS co-stimulated U937 cells was much more pronounced than that observed with TNF-α. Fractions F-2 and F-3 greatly enhanced IL-1β/IL-1F2 release in the cells by approximately nine- and six-fold, respectively. Additionally, F-1 (four-fold), F-4 (three-fold) and whole BV (two-fold) also enhanced the release of this cytokine with LPS co-stimulation, although the increase obtained with BV was not statistically significant (Figure 5). As can be seen from Figure 5, the fractions on their own did not induce any significant level of cytokine release.

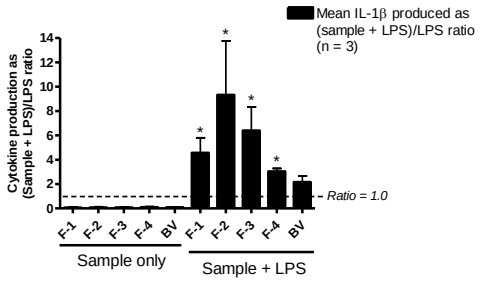

Figure 5. Effect of bee venom and its fractions of IL-1β/IL-1F2 production in PMA-differentiated U937 cells. All five been venom (BV) fractions tested produced only background levels of IL-1β/IL-1F2 when used alone. In the presence of LPS, there was significant synergy, especially with F-2 and F-3, which resulted in a nine- and six-fold increase in the production of the cytokine, respectively. Significant synergy was also observed with F-1 (four-fold) and F-4 (three-fold), but not with BV despite a two-fold increase in the latter (n = 3).

3.7. Effect on IL-6 Production

As with TNF-α and IL-1β production, the amount of IL-6 produced by the cells in the presence of BV fractions alone was undetectable (F-1–F-3) or not significantly different from levels observed in negative controls (F-4 and BV). Yet, when the same fractions were incubated together with LPS, the amount of IL-6 produced by the cells was raised, compared to that of stimulation with LPS alone, by 20%, 40%, 30% and 30% with F-1, F-2, F-3 and BV, respectively; although these were not significantly different from positive control values. Surprisingly, and contrary to observations with TNF-α and IL-1β, F-4 significantly decreased the amount of IL-6 released with LPS co-stimulation in the PMA-differentiated U937 cells by about 50% (Figure 6).

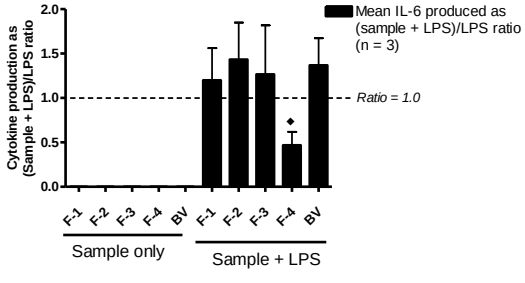

Figure 6. Effect of BV and its fractions with and without LPS on IL-6 production in PMA-differentiated U937 cells. The level of IL-6 produced by BV fractions alone was undetectable. However, in combination with LPS, Fractions F-1–F-3 and BV enhanced the level of cytokine produced by LPS though not significantly. Interestingly, F-4 significantly inhibited cytokine production by about 50% of the mean positive control (LPS) value (n = 3).

3.8. Identification of Active Compound in BV Fraction F-4

Given its unusual effect on TNF-α and IL-6 release in PMA-differentiated U937 cells, we sought to identify the component present in F-4 by NMR spectroscopy. The one-dimensional (1D) ^{1}H-NMR spectrum of F-4 (acquired at 298 K in DMSO-d_6; Figure S14) gave 10 distinguishable signals with chemical shifts and integrals as detailed in Table 1. Signal A, which corresponded to a ^{1}H chemical shift associated with a proton attached to an sp^2-hybridized carbon centre (alkene), integrated to two proton equivalents. Multiplicity-edited 2D [^{1}H, ^{13}C] HSQC-NMR data revealed that the signal was associated with a methine (CH) group, allowing the conclusion to be drawn that the molecule was likely to be a structure with close to two-fold symmetry about a double bond. The signal envelope designated H integrated to twenty two proton equivalents and suggested the presence of long chains of methylene groups typical of a lipid.

Table 1. Data arising from the 1D ^{1}H-NMR spectrum of the lipid component. Reference to the "link to ^{13}C" arises from analysis of the 2D [^{1}H, ^{13}C] HSQC-NMR spectrum that reveals $^{1}J_{HC}$ correlations where labels a–q correspond to the ^{13}C resonances shown in (Figure S12).

Label	δ (ppm)	Integral	Type	Multiplicity	Link to ^{13}C	Proposal
A	5.32	2	Alkene CH	Second order	a	Symmetric Alkene
B	4.30	1	-O<u>H</u>	t	-	-CH_2-O<u>H</u>
C	3.36	2	-CH_2-	dt	b	
D	3.32	1.7	H_2O	s	-	Water in DMSO
E	1.98	4	-CH_2-	q	m	
F	1.39	2	-CH_2-	pentet	c	
G	1.29	4	-CH_2-	q	f	
H	1.24	22	-CH_2-	-	d,e,g,h,i,j,k,l,n,o	
I	0.85	3	-C<u>H</u>$_3$	t	p	-CH_2-C<u>H</u>$_3$

To establish how many types of carbon centres existed within the molecule, ^{13}C-{^{1}H} NMR data (Figure S15) were examined. The data gave rise to 16 NMR signals corresponding to sixteen different types of ^{13}C environments. Many of these showed similar chemical shifts (signals e–l). Additionally the intensities revealed that a number of carbon centres (a, f, l, m) were twice as abundant, resulting from symmetry within the structure. It was clear in particular from these data that the carbon signal (a) was due to two alkene carbons with identical chemical shifts, confirming the expectation that the structure would be roughly symmetrical about a central double bond, the symmetry of which would remain largely unaffected by remote tail groups.

2D [^{1}H, ^{13}C] HSQC-NMR data (Figure S16) at both low and high resolution allowed the types of carbon to be distinguished for every centre, as well as editing the data to reveal protons that were not attached to carbon. As well as enabling the identification of H/C correlations within each magnetic environment, these data also made it possible to confirm the number of protons associated with the lipid chain. These data also revealed that protons giving rise to Resonances B and D were not attached to carbon. By analogy with literature examples, it was clear that Resonance D was associated with water in DMSO and could therefore be discounted from the analysis. A summary of the ^{13}C-NMR data are shown in Table 2. These data are summarized to provide a molecular formula of $C_{20}H_{40}O$, yielding a molecular weight (MW) = 296. Integration of the ^{1}H-NMR spectrum is consistent with this formula and the number of protons "counted" using the 2D [^{1}H, ^{13}C] HSQC-NMR data.

Table 2. Summary of ^{13}C-NMR data for the lipid molecule as revealed by 1D ^{13}C-{^{1}H} and 2D [^{1}H, ^{13}C] HSQC-NMR data.

Label	δ (ppm)	No. of Carbons	Type	Link to ^{1}H
a	130.09	2	CH	A
b	61.18	1	CH_2	C
c	33.03	1	CH_2	F
d	31.76	1	CH_2	H
e	29.58	1	CH_2	H
f	29.56	2	CH_2	G
g	29.50	1	CH_2	H
h	29.45	1	CH_2	H
i	29.35	1	CH_2	H
j	29.31	1	CH_2	H
k	29.17	1	CH_2	H
l	29.06	2	CH_2	H
m	27.03	2	CH_2	E
n	25.99	1	CH_2	H
o	22.57	1	CH_2	H
p	14.40	1	CH_3	I

Analysis of the remaining 2D [^{1}H, ^{1}H] COSY and TOCSY and 2D [^{1}H, ^{13}C] HSQC and HMBC-NMR data (Figures S17–S19) is summarized in Table S7 and Table S8, respectively, in the Supplementary Materials. The triplet character of ^{1}H Resonance B and its correlation with Resonance C by COSY and TOCSY indicated that the hydroxyl group was a terminal –OH attached to a methylene, whose protons gave rise to Resonance C. The triplet character of proton Signal I similarly enabled the identity of this resonance to be associated with a terminal methyl group. Correlations were traced as far as possible from both the terminal positions and the alkene proton resonances (A) until these assignment pathways merged at Resonance H. 2D [^{1}H, ^{13}C] HMBC-NMR data were used to establish longer range H/C correlations to reinforce the assignments, which remaining incomplete owing to the degeneracy at Signal H.

Following identification of coupling partners and piecing the structural evidence together, the proton and carbon assignments were allocated to a basic structure, as shown (Figure S20). It was not clear from the NMR data whether the double bond would be at the 9- or 10-position (shown in the 10-position in Figure S20). Neither was it clear from the data whether the double bond was of *E* or *Z* configuration. For this reason, simulations of the data were carried out based on both *E* and *Z* isomers of 9- and 10-eicosen-1-ol in order to throw some light on the conformation. Particular attention was paid to the appearance of proton Resonances A and E in these simulations, which would reflect directly on the conformation about the centralised double bond. The results of these simulations with their equivalent experimental counterparts are shown in Figure S21.

On balance, these data suggest a greater likelihood of the lipid existing in the (*Z*)-configuration, as shown in Figure S22. The position of the double bond is not revealed through these simulations or by experiment. Comparison with information provided directly through Beesen Co. Ltd., suppliers of the venom, suggests that the material and data are consistent with (*Z*)-eicos-9-en-1-ol.

3.9. Identification of Minor Component in F-4

Fraction F-4 was found to contain trace levels of an unidentified minor component with the $[M-H]^-$ elemental composition of $C_{43}H_{70}O_{11}P$ (0.0783 ppm mass tolerance) and MW 794.47. Collisional induced dissociation (CID) of the parental ion (*m*/*z* 793.46) at a normalised collisional energy (NCE) of 35.0 produced two daughter ions, one with *m*/*z* 493.2574 ($C_{23}H_{42}O_9P$, 2.685 ppm mass tolerance, 40%), possibly suggesting a loss of eicosapentenoic acid (MW 302), and the other with *m*/*z* 643.3608 ($C_{33}H_{56}O_{10}P$, 0.341 ppm mass tolerance, 60%) (Figure S13). This elemental composition, though inconclusive, suggested the likelihood that the unknown impurity might be a phospholipid.

4. Discussion

4.1. Cytotoxicity

The two fractions that were cytotoxic to U937 cells with IC_{50} values below 100 μg/mL contained melittin (F-3, IC_{50} 5.4 μg/mL) and (*Z*)-9-eicosen-1-ol (F-4, IC_{50} 68.8 μg/mL). The latter also contained trace levels of an unidentified phospholipid. F-1 and F-2 were relatively non-toxic to U937 cells at the concentrations tested. The former contained mainly low MW amines, such as histamine, dopamine and noradrenaline, while the latter contained mainly PLA_2, a major BV allergen [38,39]. Although one would have expected fraction F-2 to be cytotoxic due to its PLA_2 content, it may be that the enzymatic activity reduced because of its separation from melittin (*i.e.*, the venom PLA_2 and melittin act synergistically [40]) or as a result of loss of its 3D configuration during the fractionation. Fraction F-2 also contained variable amounts of the peptides apamin, MCD peptide and secapin, which were also detected in trace amounts in F-1.

Whereas the cytotoxicity of melittin is generally known in normal human and cancer cells [36,41], the biological activities of the organic fraction of BV are less well known. Melittin's cytotoxicity is thought to be due to membrane-disruption [42] and apoptotic actions mediated via mitochondrial and caspase activities [43]. During our experiments, the toxicity of F-4 (at 100 μg/mL) was also observed in adherent normal human fibroblast (HS27) cells in which growth inhibition appeared to be associated with loss of cell attachment to the cell culture well plate (data not shown). Because of this, it had been anticipated that with suspended U937 cells, the F-4 fraction would have no such cytotoxic effect below 100 μg/mL, since adherence was not a prerequisite for cell division and growth. Thus, the observed toxicity in U937 cells might suggest that F-4 acts within the cell, at least partially, rather than exclusively externally to it. Its amphiphilic structure would be consistent with an ability to penetrate and pass through cell membranes.

4.2. Effect on Cytokine Release

The enhancement of LPS-stimulated release of IL-1β in U937 cells was by far the most pronounced effect induced by all four BV fractions and crude BV, while the effects on TNF-α and IL-6 release were less marked, with variability between the fractions. The only significant effect on TNF-α release was due to F-4, while F-2 and F-3, which contained PLA_2 and melittin, respectively, were the most potent enhancers of IL-1β release by the cells following co-stimulation with LPS. Interestingly, F-4 showed anti-IL-6 effects. The IL-1 family of cytokines is closely linked to innate inflammatory and immune responses more than any other cytokine family, and IL-1β mediates auto-inflammatory diseases [44]. In the context of bees, the observed several-fold enhancement of IL-1β release by BV and all of its fractions is thus logical given the defensive function of the venom. Stimulation of IL-6 production is a key target for adjuvants due to its role in promoting B-lymphocyte differentiation into antibody-producing cells [45–47], T-cell proliferation [48] and development of cell-mediated cytotoxicity by CD8+ cells [49–51]. Thus, inhibition of IL-6 production by F-4 would suggest an immuno-suppressive action, but its concomitant stimulatory effect on TNF-α, an important cytokine involved in the development of resistance to infection and cancer with roles in necrosis and apoptosis [52], suggests a more subtle mechanism.

Among the major components of F-1, histamine was reported to increase production of IL-6, expression of histamine receptors, expression of the kinases pp38, pERK and pJNK and induction of NF-κB in nasal fibroblasts when assayed at 200 μM (~22.2 μg/mL) [14]. This concentration level was significantly higher than that present in the assay solutions of both the F-1 fraction and BV, which might explain their non-significant effects on IL-6. Bee venom PLA_2, a major allergen and main component of F-2, and apamin have been shown to possess immune-inducing effects by activating T-cells [17] and promoting T-cell proliferation [13], respectively. Thus, the effects observed with F-2 on IL-1β and IL-6 production might be related to the effects of both PLA_2 and apamin on the cells.

Additionally, melittin, the sole component of F-3, has been reported to possess adjuvant properties by enhancing the absorption of intranasal tetanus and diphtheria toxoids [23]. This would support its effect on IL-1β observed in this study. However, these findings do not suggest that melittin could reduce the effect of LPS on cells, contrary to some previous studies [26,27]. The concentration used in the current study (3 μg/mL) was sub-lethal to the U937 cells, but at 10 μg/mL, the concentration used in a previous study [27], melittin was found in the current study to be 100% cytotoxic. This was observed previously in dermal fibroblasts, mononuclear cells and fibroblast-like synoviocytes [30]. On the other hand, the study by Moon *et al.* [26] assayed both BV and melittin at 0.5–2.0 μg/mL, levels that are all markedly lower than those employed in the current study. In the same study, LPS was assayed at 0.5 μg/mL compared to 1.0 μg/mL used in this study, and the cells were initially treated with BV or melittin for 1 h before treatment with LPS, rather than being simultaneously exposed [26]. Thus, the differences observed in these *in vitro* studies in relation to melittin's role in immuno-modulation might be related to the different experimental designs and/or concentrations of melittin and LPS used. In a previous study by Stuhlmeier (2007), neither BV nor melittin was found to inhibit IL-1β-induced activation of NF-κB. Instead, there were significant increases in the levels of the mRNA of several pro-inflammatory genes and COX-2 in synoviocytes, dermal fibroblasts and mononuclear cells [30]. The results obtained in our study corroborate these findings.

The main component of F-4, identified in this study as (Z)-9-eicosen-1-ol, resembled the lipid-soluble compound reported by Pickett *et al.* (1982) in *A. mellifera* venom and structurally elucidated as (Z)-11-eicosen-1-ol [53]. The latter was described as a natural pheromone, which acted synergistically with amyl acetate, another pheromone produced by the bees [53]. Schmidt *et al.* (1997) also reported the same long chain monounsaturated alcohol to be the main component of the oily fraction of *Apis cerana* venom [54], a species related to *A. mellifera*. The compound isolated in F-4 differs from that previously described with respect to the double bond position, which might be a means of conveying subtle differences in message recognition among the bees [55].

5. Conclusions

Inflammatory responses mediated by pro-inflammatory cytokines are a key component of protective immunity against many infections. This study shows that treatment of PMA-differentiated U937 cells with BV fractions significantly enhances the IL-1β cytokine release effect of LPS in these cells. However, neither BV nor its fractions could induce any significant cytokine release on their own. The largest synergistic effect was observed for IL-1β release, which was promoted by all fractions, while only the lipid fraction, F-4, enhanced TNF-α production in the cells co-stimulated with LPS. Although fraction F-4, identified to contain (*Z*)-9-eicosen-1-ol, was stimulatory for IL-1β and TNF-α release, it produced an inhibitory effect on IL-6 production. The commercial availability of this compound in larger amounts than can be isolated from the venom will allow us in future work to explore potential synergies between it and fractions F-1–F-3. In addition, it provides a lead compound for exploring the effects of other long chain alcohols, since they are accessible via reduction of the wide range of long chain fatty acids, that is commercially available. Taken together, these results do not support some studies in the literature that suggest that BV and melittin possess potential anti-inflammatory activity by antagonising LPS-stimulation of cytokine production. Instead, BV fractions synergise with LPS in the induction of the IL-1β cytokine release in U937 cells, and the lipophilic fraction has additional orthogonal effects on TNF-α and IL-6, whereby it induces the former and inhibits the latter. Overall, these effects provide valuable preliminary information to support further evaluation of purified BV as a potential source of natural adjuvants for some vaccines.

Supplementary Materials: The following are available online at www.mdpi.com/2076-393X/4/2/11/s1.

Acknowledgments: Jonans Tusiimire and Jennifer Wallace are funded by Beesen Co. and the Korea Institute for Advancement of Technology (KIAT) partnership with Strathclyde University. Nicola Woods is sponsored through a Biotechnology and Biological Sciences Research Council (BBSRC) Case studentship.

Author Contributions: David G. Watson and Valerie A. Ferro conceived the project; Jonans Tusiimire, David G. Watson, Jennifer Wallace, John A. Parkinson and Mark J. Dufton purified and analysed the bee venom fractions; Jonans Tusiimire, Nicola Woods, Louise Young, Grainne Abbott, and Carol J. Clements performed the biology experiments and analysed their data; Jennifer Wallace, John A. Parkinson and Mark J. Dufton performed the NMR experiments and analysed their data; Jin Kyu Park and Jong Woon Jeon supplied the crude bee venom; Jonans Tusiimire, Jennifer Wallace, John A. Parkinson, Mark J. Dufton, Valerie A. Ferro and David G. Watson wrote and edited the manuscript.

Conflicts of Interest: The authors declare no conflict of interest.

References

1. Moreau, S.J. "It stings a bit but it cleans well": Venoms of Hymenoptera and their antimicrobial potential. *J. Insect Physiol.* **2013**, *59*, 186–204. [CrossRef] [PubMed]
2. Lee, J.D.; Park, H.J.; Chae, Y.; Lim, S. An overview of bee venom acupuncture in the treatment of arthritis. *Evidence-Based Complement. Alternat. Med.* **2005**, *2*, 79–84. [CrossRef] [PubMed]
3. Hider, R.C. Honeybee venom: A rich source of pharmacologically active peptides. *Endeavour* **1988**, *12*, 60–65. [CrossRef]
4. Rho, Y.H.; Woo, J.-H.; Choi, S.J.; Lee, Y.H.; Ji, J.D.; Song, G.G. A new onset of systemic lupus erythematosus developed after bee venom therapy. *Korean J. Intern. Med.* **2009**, *24*, 283–285. [CrossRef] [PubMed]
5. Zhou, J.; Zhao, J.; Zhang, S.; Shen, J.; Qi, Y.; Xue, X.; Li, Y.; Wu, L.; Zhang, J.; Chen, F.; Chen, L. Quantification of melittin and apamin in bee venom lyophilized powder from *Apis mellifera* by liquid chromatography-diode array detector-tandem mass spectrometry. *Anal. Biochem.* **2010**, *404*, 171–178. [CrossRef] [PubMed]
6. Chen, J.; Lariviere, W.R. The nociceptive and anti-nociceptive effects of bee venom injection and therapy: A double-edged sword. *Prog. Neurobiol.* **2010**, *92*, 151–183. [CrossRef] [PubMed]
7. Sciani, J.M.; Marques-Porto, R.; Lourenco Junior, A.; Orsi, R.D.O.; Ferreira Junior, R.S.; Barraviera, B.; Pimenta, D.C. Identification of a novel melittin isoform from Africanized *Apis mellifera* venom. *Peptides* **2010**, *31*, 1473–1479. [CrossRef] [PubMed]
8. Ferreira Junior, R.S.; Sciani, J.M.; Marques-Porto, R.; Lourenco Junior, A.; Orsi, R.D.O.; Barraviera, B.; Pimenta, D.C. Africanized honey bee (*Apis mellifera*) venom profiling: Seasonal variation of melittin and phospholipase A_2 levels. *Toxicon* **2010**, *56*, 355–362. [CrossRef] [PubMed]
9. Baracchi, D.; Francese, S.; Turillazzi, S. Beyond the antipredatory defence: Honey bee venom function as a component of social immunity. *Toxicon* **2011**, *58*, 550–557. [CrossRef] [PubMed]
10. Van Vaerenbergh, M.; Cardoen, D.; Formesyn, E.M.; Brunain, M.; Van Driessche, G.; Blank, S.; Spillner, E.; Verleyen, P.; Wenseleers, T.; Schoofs, L.; *et al.* Extending the honey bee venome with the antimicrobial peptide apidaecin and a protein resembling wasp antigen 5. *Insect Mol. Biol.* **2013**, *22*, 199–210. [CrossRef] [PubMed]
11. Vick, J.A.; Shipman, W.H. Effects of whole bee venom and its fractions (apamin and melittin) on plasma cortisol levels in the dog. *Toxicon* **1972**, *10*, 377–380. [CrossRef]
12. Matysiak, J.; Schmelzer, C.E.H.; Neubert, R.H.H.; Kokot, Z.J. Characterization of honeybee venom by MALDI-TOF and nanoESI-QqTOF mass spectrometry. *J. Pharm. Biomed. Anal.* **2011**, *54*, 273–278. [CrossRef] [PubMed]
13. Regnier-Vigouroux, A.; el Ayeb, M.; Defendini, M.L.; Granier, C.; Pierres, M. Processing by accessory cells for presentation to murine T cells of apamin, a disulfide-bonded 18 amino acid peptide. *J. Immunol. (Baltimore, Md.: 1950)* **1988**, *140*, 1069–1075.
14. Park, I.H.; Um, J.Y.; Cho, J.S.; Lee, S.H.; Lee, H.M. Histamine promotes the release of interleukin-6 via the H1R/p38 and NF-kappaB pathways in nasal fibroblasts. *Allergy, Asthma Immunol. Res.* **2014**, *6*, 567–572. [CrossRef] [PubMed]
15. Buku, A.; Condie, B.; Price, J.; Mezei, M. [Ala12] MCD peptide: A lead peptide to inhibitors of immunoglobulin E binding to mast cell receptors1. *J. Pept. Res.* **2005**, *66*, 132–137. [CrossRef] [PubMed]
16. Buku, A. Mast cell degranulating (MCD) peptide: A prototypic peptide in allergy and inflammation. *Peptides* **1999**, *20*, 415–420. [CrossRef]
17. Bourgeois, E.A.; Subramaniam, S.; Cheng, T.Y.; De Jong, A.; Layre, E.; Ly, D.; Salimi, M.; Legaspi, A.; Modlin, R.L.; Salio, M.; *et al.* Bee venom processes human skin lipids for presentation by CD1a. *J. Exp. Med.* **2015**, *212*, 149–163. [CrossRef] [PubMed]

18. Ichinose, M.; Miura, M.; Takahashi, T.; Yamauchi, H.; Kageyama, N.; Tomaki, M.; Endoh, N.; Sakurai, E.; Watanabe, T.; Shirato, K. Allergic airway response and potassium channels: Histamine release and airway inflammation. *Methods Find. Exp. Clin. Pharmacol.* **1995**, *17* (Suppl. C), 36–39. [PubMed]
19. Lawrence, T. The Nuclear Factor NF-κB Pathway in Inflammation. *Cold Spring Harbor Perspect. Biol.* **2009**, *1*, a001651. [CrossRef] [PubMed]
20. Buku, A.; Price, J.A.; Mendlowitz, M.; Masur, S. Mast cell degranulating peptide binds to RBL-2H3 mast cell receptors and inhibits IgE binding. *Peptides* **2001**, *22*, 1993–1998. [CrossRef]
21. Shkenderov, S.; Koburova, K. Adolapin—A newly isolated analgetic and anti-inflammatory polypeptide from bee venom. *Toxicon* **1982**, *20*, 317–321. [CrossRef]
22. Koburova, K.L.; Michailova, S.G.; Shkenderov, S.V. Further investigation on the antiinflammatory properties of adolapin—Bee venom polypeptide. *Acta Physiol. Pharmacol. Bulg.* **1985**, *11*, 50–55. [PubMed]
23. Bramwell, V.W.; Somavarapu, S.; Outschoorn, I.; Alpar, H.O. Adjuvant action of melittin following intranasal immunisation with tetanus and diphtheria toxoids. *J. Drug Target.* **2003**, *11*, 525–530. [CrossRef] [PubMed]
24. Park, H.J.; Lee, S.H.; Son, D.J.; Oh, K.W.; Kim, K.H.; Song, H.S.; Kim, G.J.; Oh, G.T.; Yoon, D.Y.; Hong, J.T. Antiarthritic effect of bee venom: Inhibition of inflammation mediator generation by suppression of NF-kappaB through interaction with the p50 subunit. *Arthritis Rheum.* **2004**, *50*, 3504–3515. [CrossRef] [PubMed]
25. Park, H.J.; Son, D.J.; Lee, C.W.; Choi, M.S.; Lee, U.S.; Song, H.S.; Lee, J.M.; Hong, J.T. Melittin inhibits inflammatory target gene expression and mediator generation via interaction with IkappaB kinase. *Biochem. Pharmacol.* **2007**, *73*, 237–247. [CrossRef] [PubMed]
26. Srivastava, R.M.; Srivastava, S.; Singh, M.; Bajpai, V.K.; Ghosh, J.K. Consequences of alteration in leucine zipper sequence of melittin in its neutralization of lipopolysaccharide-induced proinflammatory response in macrophage cells and interaction with lipopolysaccharide. *J. Biol. Chem.* **2012**, *287*, 1980–1995. [CrossRef] [PubMed]
27. Moon, D.O.; Park, S.Y.; Lee, K.J.; Heo, M.S.; Kim, K.C.; Kim, M.O.; Lee, J.D.; Choi, Y.H.; Kim, G.Y. Bee venom and melittin reduce proinflammatory mediators in lipopolysaccharide-stimulated BV2 microglia. *Int. Immunopharmacol.* **2007**, *7*, 1092–1101. [CrossRef] [PubMed]
28. Jang, H.S.; Kim, S.K.; Han, J.B.; Ahn, H.J.; Bae, H.; Min, B.I. Effects of bee venom on the pro-inflammatory responses in RAW264.7 macrophage cell line. *J. Ethnopharmacol.* **2005**, *99*, 157–160. [CrossRef] [PubMed]
29. Vick, J.A.; Mehlman, B.; Brooks, R.; Phillips, S.J.; Shipman, W. Effect of the bee venom and melittin on plasma cortisol in the unanesthetized monkey. *Toxicon* **1972**, *10*, 581–586. [CrossRef]
30. Stuhlmeier, K.M. Apis mellifera venom and melittin block neither NF-kappa B-p50-DNA interactions nor the activation of NF-kappa B, instead they activate the transcription of proinflammatory genes and the release of reactive oxygen intermediates. *J. Immunol. (Baltimore, Md.: 1950)* **2007**, *179*, 655–664. [CrossRef]
31. Sundstrom, C.; Nilsson, K. Establishment and characterization of a human histiocytic lymphoma cell line (U-937). *Int. J. Cancer* **1976**, *17*, 565–577. [CrossRef] [PubMed]
32. Minta, J.O.; Pambrun, L. *In vitro* induction of cytologic and functional differentiation of the immature human monocytelike cell line U-937 with phorbol myristate acetate. *Am. J. Pathol.* **1985**, *119*, 111–126. [PubMed]
33. Passmore, J.S.; Lukey, P.T.; Ress, S.R. The human macrophage cell line U937 as an *in vitro* model for selective evaluation of mycobacterial antigen-specific cytotoxic T-cell function. *Immunology* **2001**, *102*, 146–156. [CrossRef] [PubMed]
34. Verhoeckx, K.C.; Bijlsma, S.; de Groene, E.M.; Witkamp, R.F.; van der Greef, J.; Rodenburg, R.J. A combination of proteomics, principal component analysis and transcriptomics is a powerful tool for the identification of biomarkers for macrophage maturation in the U937 cell line. *Proteomics* **2004**, *4*, 1014–1028. [CrossRef] [PubMed]
35. Tusiimire, J.; Wallace, J.; Dufton, M.; Parkinson, J.; Clements, C.J.; Young, L.; Park, J.K.; Jeon, J.W.; Watson, D.G. An LCMS method for the assay of melittin in cosmetic formulations containing bee venom. *Anal. Bioanal. Chem.* **2015**, *407*, 3627–3635. [CrossRef] [PubMed]
36. Gajski, G.; Garaj-Vrhovac, V. Melittin: A lytic peptide with anticancer properties. *Environ. Toxicol. Pharmacol.* **2013**, *36*, 697–705. [CrossRef] [PubMed]
37. Otte, A.; Mandel, K.; Reinstrom, G.; Hass, R. Abolished adherence alters signaling pathways in phorbol ester-induced human U937 cells. *Cell Commun. Signal.* **2011**, *9*. [CrossRef] [PubMed]

38. Dhillon, M.; Roberts, C.; Nunn, T.; Kuo, M. Mapping human T cell epitopes on phospholipase A_2: The major bee-venom allergen. *J. Allergy Clin. Immunol.* **1992**, *90*, 42–51. [CrossRef]
39. Ameratunga, R.V.; Hawkins, R.; Prestidge, R.; Marbrook, J. A high efficiency method for purification and assay of bee venom phospholipase A2. *Pathology* **1995**, *27*, 157–160. [CrossRef] [PubMed]
40. Habermann, E. Bee and wasp venoms. *Science (New York, N.Y.)* **1972**, *177*, 314–322. [CrossRef]
41. Son, D.J.; Lee, J.W.; Lee, Y.H.; Song, H.S.; Lee, C.K.; Hong, J.T. Therapeutic application of anti-arthritis, pain-releasing, and anti-cancer effects of bee venom and its constituent compounds. *Pharmacol. Ther.* **2007**, *115*, 246–270. [CrossRef] [PubMed]
42. Lee, M.T.; Sun, T.L.; Hung, W.C.; Huang, H.W. Process of inducing pores in membranes by melittin. *Proc. Natl. Acad. Sci. USA* **2013**, *110*, 14243–14248. [CrossRef] [PubMed]
43. Lee, J.; Lee, D.G. Melittin triggers apoptosis in *Candida albicans* through the reactive oxygen species-mediated mitochondria/caspase-dependent pathway. *FEMS Microbiol. Lett.* **2014**, *355*, 36–42. [CrossRef] [PubMed]
44. Dinarello, C.A. Overview of the interleukin-1 family of ligands and receptors. *Semin. Immunol.* **2013**, *25*, 389–393. [CrossRef] [PubMed]
45. Bertolini, J.N.; Benson, E.M. The role of human interleukin-6 in B-cell isotype regulation and differentiation. *Cell. Immunol.* **1990**, *125*, 197–209. [CrossRef]
46. Beagley, K.W.; Eldridge, J.H.; Lee, F.; Kiyono, H.; Everson, M.P.; Koopman, W.J.; Hirano, T.; Kishimoto, T.; McGhee, J.R. Interleukins and IgA synthesis: Human and murine interleukin 6 induce high rate IgA secretion in IgA-committed B cells. *J. Exp. Med.* **1989**, *169*, 2133–2148. [CrossRef] [PubMed]
47. Hilbert, D.M.; Cancro, M.P.; Scherle, P.A.; Nordan, R.P.; Van Snick, J.; Gerhard, W.; Rudikoff, S. T cell derived IL-6 is differentially required for antigen-specific antibody secretion by primary and secondary B cells. *J. Immunol. (Baltimore, Md.: 1950)* **1989**, *143*, 4019–4024.
48. Tosato, G.; Pike, S.E. Interferon-beta 2/interleukin 6 is a co-stimulant for human T lymphocytes. *J. Immunol. (Baltimore, Md.: 1950)* **1988**, *141*, 1556–1562.
49. Van Snick, J.; Vink, A.; Uyttenhove, C.; Houssiau, F.; Coulie, P. B and T cell responses induced by interleukin-6. *Curr. Top. Microbiol. Immunol.* **1988**, *141*, 181–184. [PubMed]
50. Okada, M.; Kitahara, M.; Kishimoto, S.; Matsuda, T.; Hirano, T.; Kishimoto, T. IL-6/BSF-2 functions as a killer helper factor in the *in vitro* induction of cytotoxic T cells. *J. Immunol. (Baltimore, Md.: 1950)* **1988**, *141*, 1543–1549.
51. Houssiau, F.; Van Snick, J. IL6 and the T-cell response. *Res. Immunol.* **1992**, *143*, 740–743. [CrossRef]
52. Idriss, H.T.; Naismith, J.H. TNF alpha and the TNF receptor superfamily: Structure-function relationship(s). *Microsc. Res. Techn.* **2000**, *50*, 184–195. [CrossRef]
53. Pickett, J.A.; Williams, I.; Martin, A.P. (*Z*)-11-eicosen-1-ol, an important new pheromonal component from the sting of the honey bee, *Apis mellifera* L. (Hymenoptera, Apidae.). *J. Chem. Ecol.* **1982**, *8*, 163–175. [CrossRef] [PubMed]
54. Schmidt, J.O.; Morgan, E.D.; Oldham, N.J.; Do Nascimento, R.R.; Dani, F.R. (*Z*)-11-Eicosen-1-ol, a major component of *Apis cerana* venom. *J. Chem. Ecol.* **1997**, *23*, 1929–1939. [CrossRef]
55. Boch, R.; Morse, R.A. Discrimination of familiar and foreign queens by honey bee swarms. *Ann. Entomol. Soc. Am.* **1974**, *67*, 709–711. [CrossRef]

Supplementary Materials: Effect of Bee Venom and Its Fractions on the Release of Pro-Inflammatory Cytokines in PMA-Differentiated U937 Cells Co-Stimulated with LPS

Jonans Tusiimire, Jennifer Wallace, Nicola Woods, Mark J. Dufton, John A. Parkinson, Grainne Abbott, Carol J. Clements, Louise Young, Jin Kyu Park, Jong Woon Jeon, Valerie A. Ferro and David G. Watson

Supplementary Experimental Details: NMR Spectroscopy

NMR spectroscopy studies were carried out on 7.4 mg of a sample of fraction F4 from BV. This was dissolved in 600 μL DMSO-d_6 contained in a 5 mm Ø standard NMR tube.

NMR data were acquired on a Bruker AVANCE II$^+$ NMR spectrometer equipped with a 14.1 T Ultrashield superconducting magnet operating at a ^{1}H resonance frequency of 600.13 MHz. All data were acquired using a BBO-z-atm probehead operating at ambient temperature (298 K) regulated by means of a BCU-05 chiller unit.

1D ^{1}H-NMR spectra were acquired with 16 transients over a frequency width of 7.2 kHz (12.0 ppm) centred at a frequency offset of 5.0 ppm into 32 K data points for an acquisition time of 2.27 s using a 30 degree radio frequency (r.f.) pulse and a recycle delay of 2.0 s.

1D ^{13}C-{^{1}H} NMR spectra were acquired with 1024 transients over a frequency width of 33.33 kHz (220.8 ppm) centred at a frequency offset of 100.0 ppm into 32 K data points for an acquisition time of 491.5 ms using a 30 degree r.f. pulse with continuous composite pulse decoupling applied at the ^{1}H resonance frequency and using a recycle delay of 0.7 s.

2D [^{1}H, ^{1}H] phase-sensitive double quantum filtered COSY and TOCSY NMR data were acquired with 8 and 4 transients respectively for each of 360 TPPI t_1 increments into 2 K complex data points over ◎$_2$ and ◎$_1$ frequency widths of 3.6 kHz (6 ppm, ω_2 acquisition time = 284.7 ms) centred at a frequency offset of 3.0 ppm and using zero-quantum suppression to reduce interference from zero-quantum effects.

2D [^{1}H, ^{13}C] HSQC-NMR spectra were acquired in both traditional mode and over a reduced ω_1 frequency width using non-uniform sampling (NUS) to increase F1 resolution. Traditional low resolution NMR data were acquired using a multiplicity edited, echo-antiecho gradient selected approach with sensitivity improvement (Bruker pulse program hsqcedetgpsisp2.3). Data were acquired into 2 K complex data points over an ω_2 frequency width of 3.6 kHz (6.0 ppm) centred at a frequency offset of 3.0 ppm and an ◎$_1$ frequency width of 24.9 kHz (165.0 ppm) centred at a frequency offset of 70.0 ppm with 8 transients for each of 256 t_1 increments. High resolution data were acquired with the ω_1 frequency width set to 4.5 kHz (30.0 ppm) centred at a frequency offset of 30.0 ppm nominally using 2048 t_1 increments sampled at 25% NUS (equivalent to 256 NUS t_1 increments) using a random generator seed of 54321 for NUS purposes.

2D [^{1}H, ^{13}C] HMBC-NMR spectra were also acquired in both traditional and NUS modes into 2 K complex data points over an ω_2 frequency width of 3.6 kHz (6.0 ppm) centred at a frequency offset of 3.0 ppm and an ω_1 frequency width of 33.55 kHz (222.4 ppm) centred at a frequency offset of 100.0 ppm with 8 transients for each of 256 traditional and NUS (25% sampled) t_1 increments respectively. Data were acquired with gradient coherence selection and used a low-pass filter to reduce the appearance of artefacts from $^1J_{HC}$ coupling.

NUS data were processed using the MDD (multidimensional decomposition) algorithm developed by Orekhov *et al.* followed by Hilbert transformation to allow traditional phase correction and processing of the data.

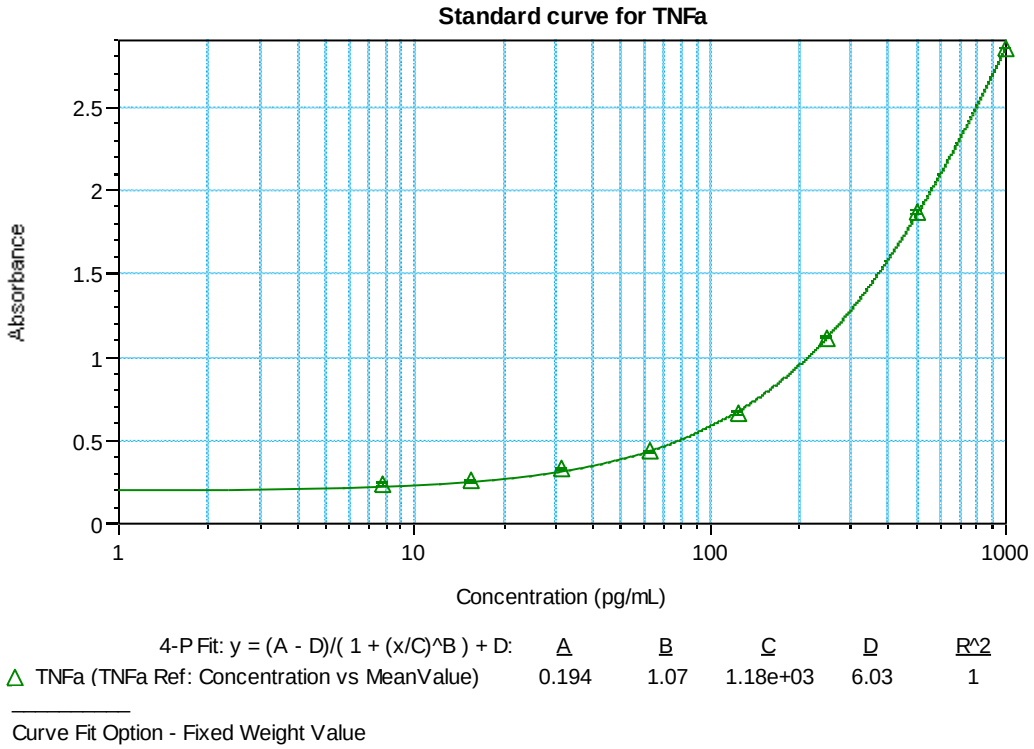

Figure S1. A representative 4-parameter logistic plot of TNF-α standard samples showing the calibration equation and the values of the constants a, b, c, and d with a perfect fit R2 values of 1.000. Error bars represent standard deviation of absorbance values for duplicate standard concentrations (n = 2).

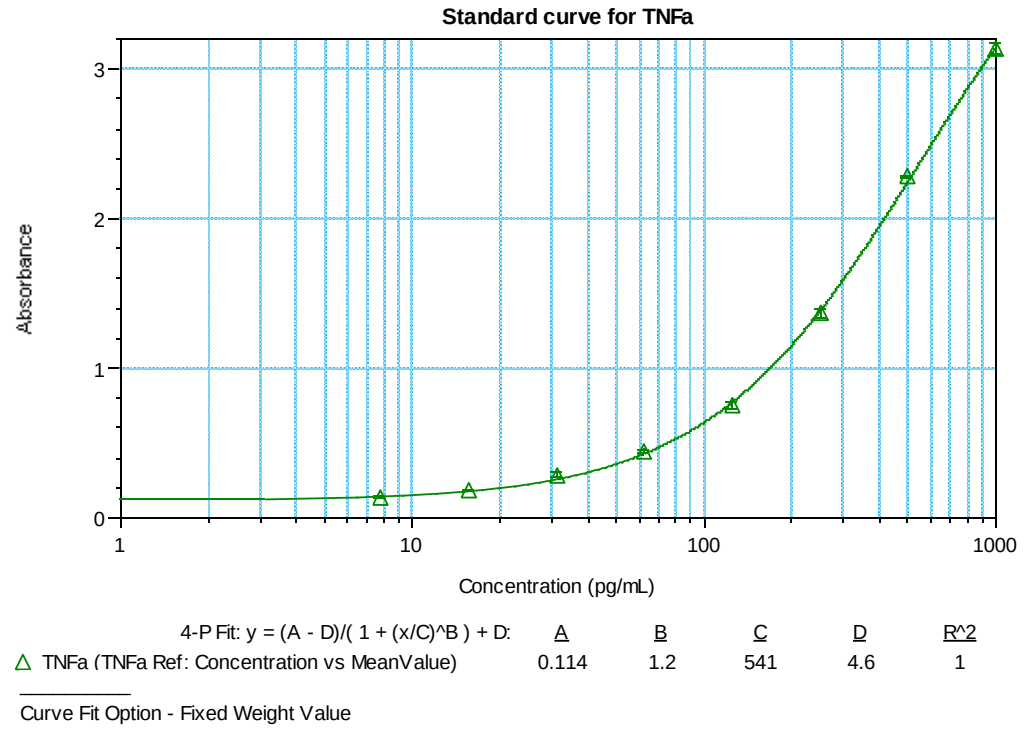

Figure S2. A representative 4-parameter logistic plot of TNF-α standard samples showing the calibration equation and the values of the constants a, b, c, and d with a perfect fit R2 values of 1.000. Error bars represent standard deviation of absorbance values for duplicate standard concentrations (n = 2).

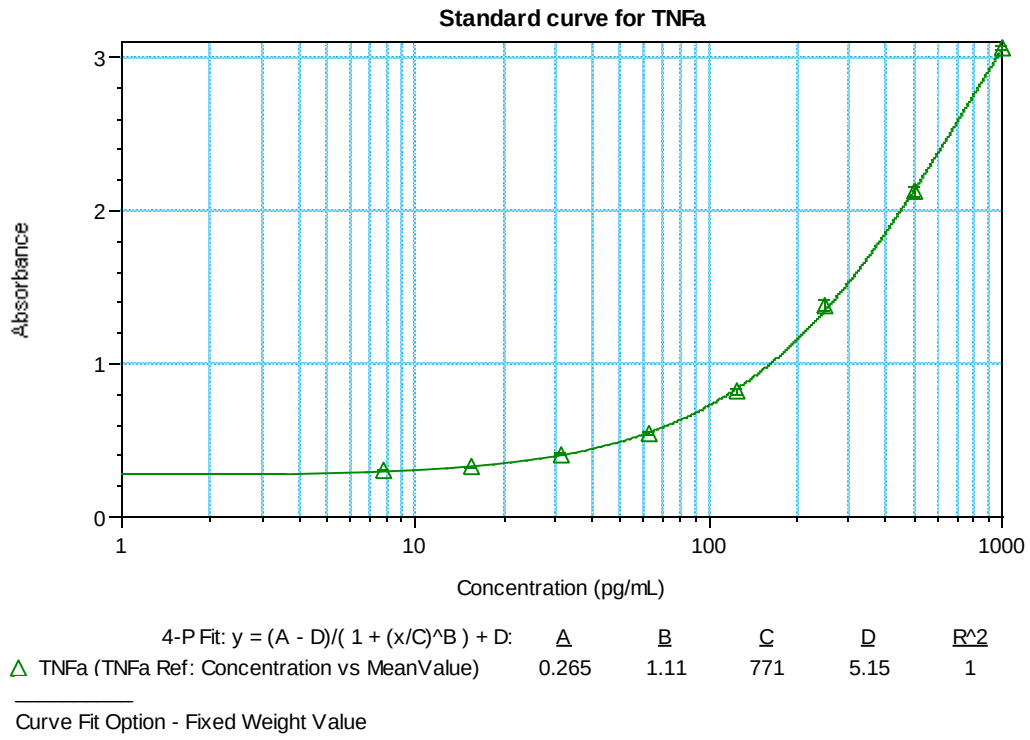

Figure S3. A representative 4-parameter logistic plot of TNF-α standard samples showing the calibration equation and the values of the constants a, b, c, and d with a perfect fit with R^2 values of 1.000. Error bars represent standard deviation of absorbance values of 1.000. Error bars represent standard deviation of absorbance values triplicate standard concentrations (n = 3).

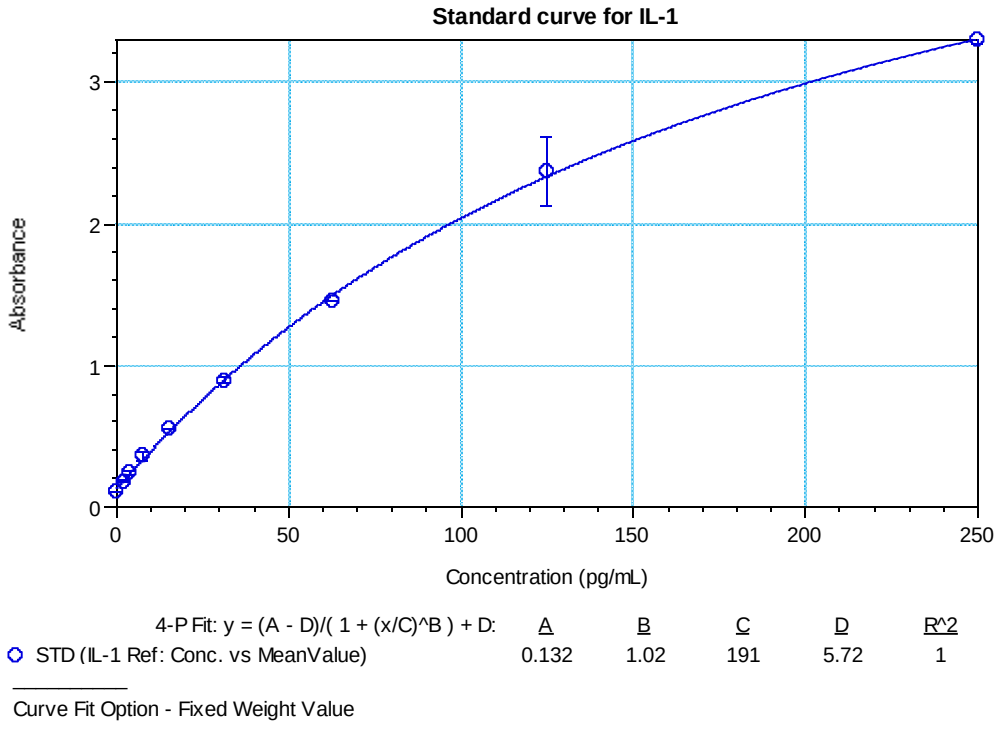

Figure S4. A sample 4-parameter logistic plot of the IL-1β/IL-1F2 standard samples showing the calibration equation and the values of the constants a, b, c, and d with a perfect fit R2 values of 1.000. Error bars represent standard deviation of absorbance values for duplicate standard concentrations (n = 2).

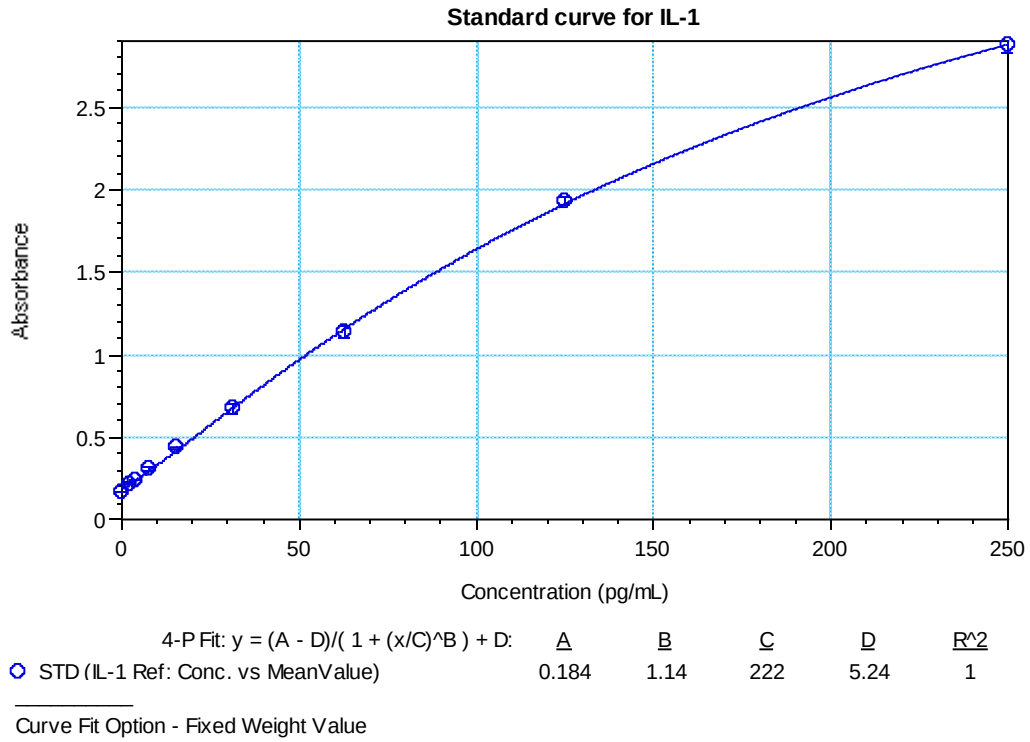

Figure S5. A sample 4-parameter logistic plot of the IL-1β/IL-1F2 standard samples showing the calibration equation and the values of the constants a, b, c, and d with a perfect fit R2 values of 1.000. Error bars represent standard deviation of absorbance values for duplicate standard concentrations (n = 2).

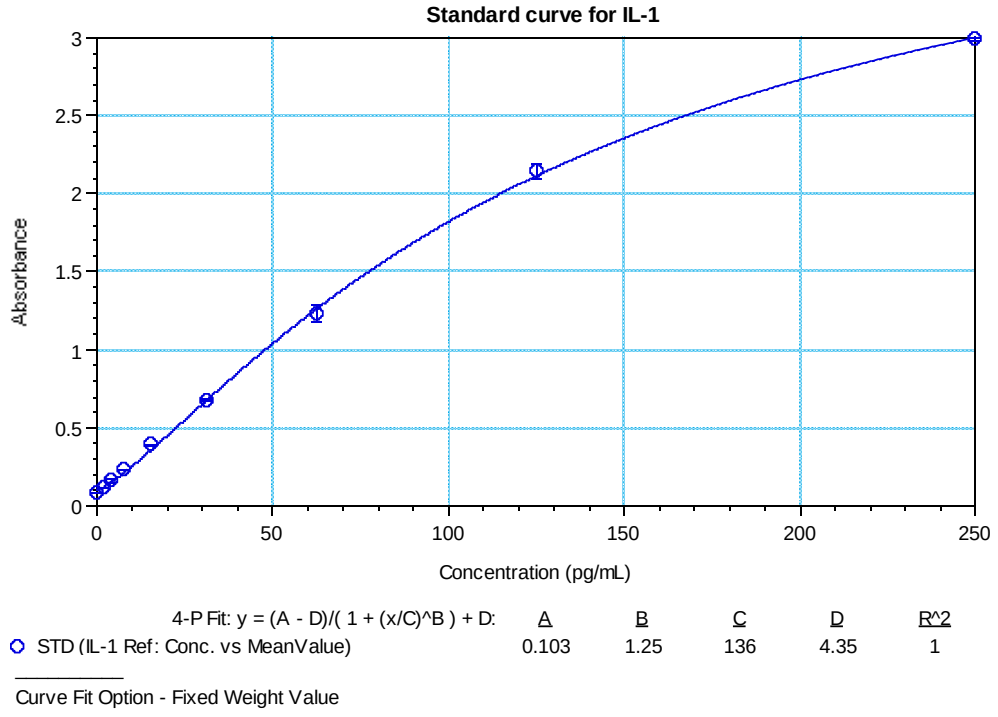

Figure S6. A sample 4-parameter logistic plot of the IL-1β/IL-1F2 standard samples showing the calibration equation and the values of the constants a, b, c, and d with a perfect fit R^2 values of 1.000. Error bars represent standard deviation of absorbance values for triplicate standard concentrations (n = 3).

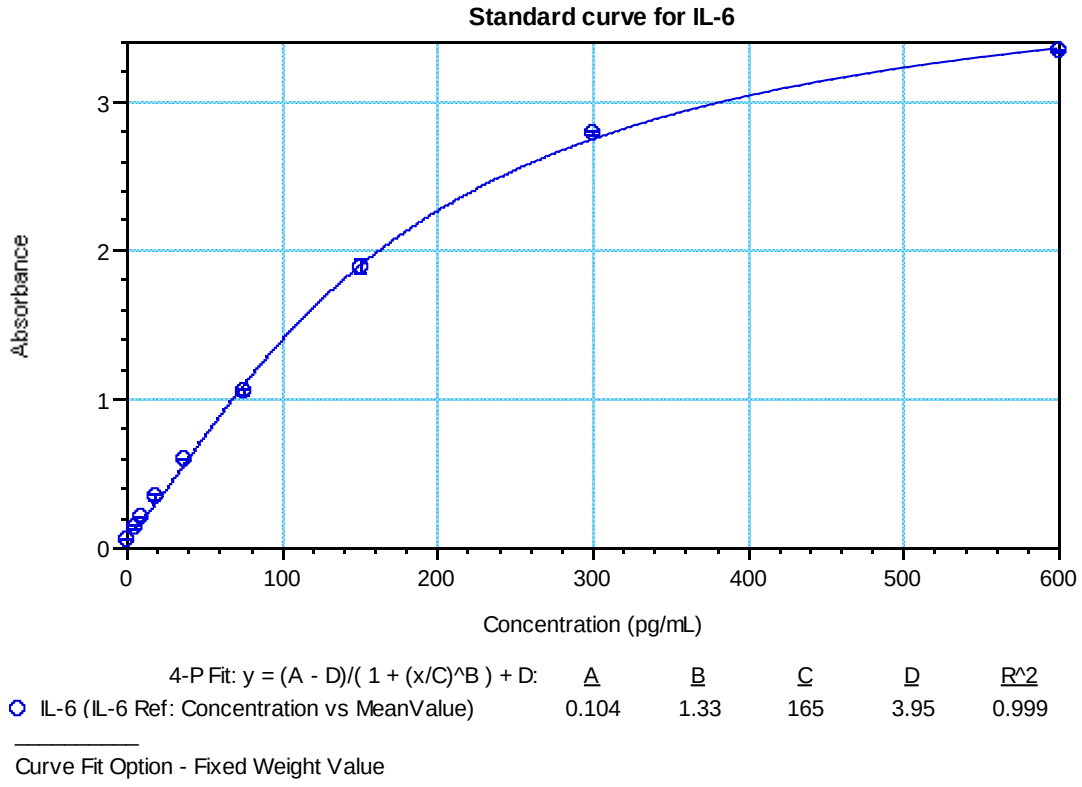

4-P Fit: y = (A - D)/(1 + (x/C)^B) + D:	A	B	C	D	R^2
IL-6 (IL-6 Ref: Concentration vs MeanValue)	0.104	1.33	165	3.95	0.999

Curve Fit Option - Fixed Weight Value

Figure S7. A sample 4-parameter logistic plot of the IL-6 standard samples showing the calibration equation and the values of the constants a, b, c, and d with a perfect fit R^2 values of 1.000. Error bars represent standard deviation of absorbance values for duplicate standard concentrations (n = 2).

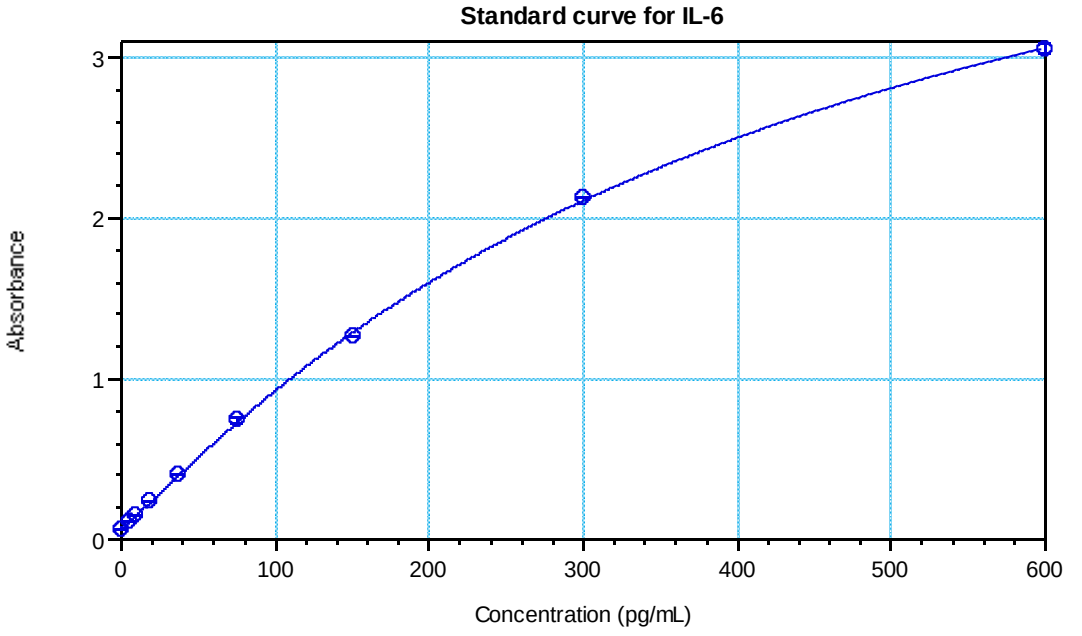

4-P Fit: y = (A - D)/(1 + (x/C)^B) + D:	A	B	C	D	R^2
IL-6 (IL-6 Ref: Concentration vs MeanValue)	0.0708	1.08	444	5.21	1

Curve Fit Option - Fixed Weight Value

Figure S8. A sample 4-parameter logistic plot of the IL-6 standard samples showing the calibration equation and the values of the constants a, b, c, and d with a perfect fit R^2 values of 1.000. Error bars represent standard deviation of absorbance values for duplicate standard concentrations (n = 2).

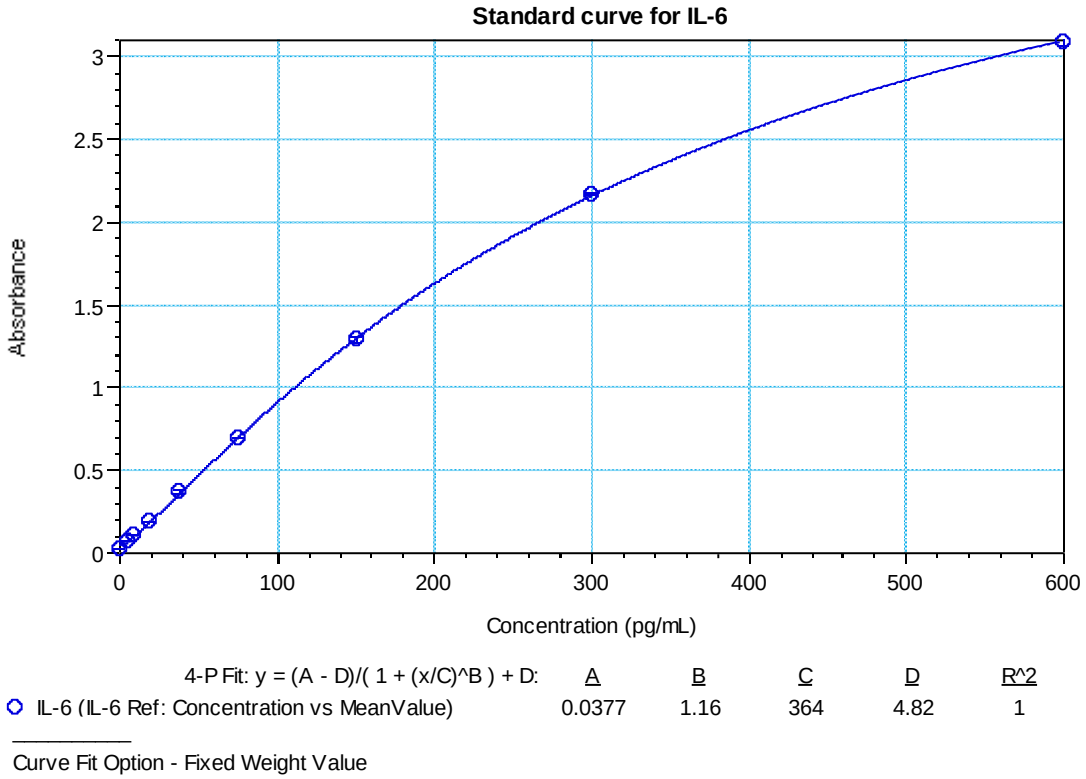

Figure S9. A sample 4-parameter logistic plot of the IL-6 standard samples showing the calibration equation and the values of the constants a, b, c, and d with a perfect fit R^2 values of 1.000. Error bars represent standard deviation of absorbance values for duplicate standard concentrations ($n = 2$).

Table S1. Volumes of LPS, fractions and media used to stimulate cytokine production in PMA-differentiated U937 cells.

Sample	Volume Added (μL)			Concentration (μg/mL)	
	Stock Solution (10 mg/mL)	*LPS (1 mg/mL)*	*Media*	*Fraction*	*LPS*
F1	80.0	8.0	1912.0	400.0	4.0
F2	80.0	8.0	1912.0	400.0	4.0
F3	2.4	8.0	1989.6	12.0	4.0
F4	24.0	8.0	1968.0	120.0	4.0
BV	2.4	8.0	1989.6	12.0	4.0
LPS	-	8.0	1992.0	-	4.0

Table S2. The constant values of the 4-PL regression curve fitted to the data of TNF-α, IL-1β and IL-6 standards respectively ($n = 3$).

Constants	TNF-α			IL-1β			IL-6		
Assay	*n = 1*	*n = 2*	*n = 3*	*n = 1*	*n = 2*	*n = 3*	*n = 1*	*n = 2*	*n = 3*
a	0.265	0.194	0.114	0.132	0.184	0.103	0.104	0.0708	0.0377
b	1.11	1.07	1.2	1.02	1.14	1.25	1.33	1.08	1.16
c	711	1180	541	191	222	136	165	444	364
d	5.15	6.03	4.6	5.72	5.24	4.35	3.95	5.21	4.82
R^2	1.000	1.000	1.000	1.00	1.000	1.000	0.999	1.000	1.000

Table S3. Concentrations of the fractions used in the assay of immuno-modulatory effects on PMA-differentiated U937 cells. For each fraction, the concentration selected was the highest non-toxic one.

SN	Fraction	IC50 (μg/mL)	Selected Concentration (μg/mL)
1	F-1	>100	100
2	F-2	>100	100
4	F-3	5.4	3.0
3	F-4	68.8	30.0

Table S4. Effect of bee venom and its fractions on TNF-α production in differentiated U937 cells in the presence or absence of LPS co-stimulation (*n* = 3).

Samples	TNF-α Concentration (pg/mL)									
Samples	Sample−LPS					Sample+LPS				
	n = 1	*n* = 2	*n* = 3	Mean	SD	*n* = 1	*n* = 2	*n* = 3	Mean	SD
F-1	6.1	6.8	3.8	5.6	1.6	68.2	126.8	70.9	88.6	33.1
F-2	5.7	7.2	4.4	5.8	1.4	74.1	162.0	90.8	109.0	46.7
F-3	7.6	8.9	5.2	7.2	1.9	69.5	161.5	84.2	105.1	49.4
F-4	8.0	9.7	8.0	8.6	1.0	88.1	160.1	143.1	130.4	37.6
BV	8.2	7.8	5.0	7.0	1.7	56.0	79.0	81.0	72.0	13.9

TNF-α Controls

Control	TNF-α Concentration (pg/mL)				
Replicate No.	*n = 1*	*n = 2*	*n = 3*	*Mean*	*SD*
Media	7.3	7.1	4.4	6.2	1.6
LPS	66.2	114.9	73.0	84.7	26.4

Table S5. Effect of bee venom and its fractions on IL-1β/IL-1F2 production in differentiated U937 cells in the presence or absence of LPS co-stimulation (*n* = 3).

Samples	IL-1β (pg/mL)									
	Sample−LPS					*Sample+LPS*				
	n = 1	*n* = 2	*n* = 3	Mean	SD	*n* = 1	*n* = 2	*n* = 3	Mean	SD
F-1	1.2	1.7	0.5	1.1	0.6	34.4	293.1	86.9	138.1	136.7
F-2	1.2	2.2	0.8	1.4	0.7	53.4	703.1	174.3	310.2	345.6
F-3	1.1	1.8	1.3	1.4	0.4	78.3	279.8	108.3	155.5	108.7
F-4	0.8	3.6	3.4	2.6	1.5	27.1	137.7	71.7	78.8	55.6
BV	<2.0	2.8	2.4	2.6	0.3	24.7	83.3	45.9	51.3	29.7

IL-1β Controls

Control	IL-1β Concentration (pg/mL)				
Replicate No.	*n = 1*	*n = 2*	*n = 3*	*Mean*	*SD*
Media	<2.0	1.2	2.5	1.8	0.9
LPS	9.1	49.1	22.0	26.8	20.4

Table S6. Effect of bee venom and its fractions on IL-6 production in differentiated U937 cells in the presence and absence of LPS co-stimulation (*n* = 3).

Samples	IL-6 Concentration (pg/mL)									
	Sample−LPS					*Sample+LPS*				
	n = 1	*n* = 2	*n* = 3	Mean	SD	*n* = 1	*n* = 2	*n* = 3	Mean	SD
F-1	<4.7	<4.7	<4.7	<4.7	n/a	93.8	199.1	126.6	139.8	53.9
F-2	<4.7	<4.7	<4.7	<4.7	n/a	113.1	235.6	160.6	169.8	61.8
F-3	<4.7	<4.7	<4.7	<4.7	n/a	112.1	159.0	152.1	141.1	25.3
F-4	<4.7	<4.7	<4.7	<4.7	n/a	32.3	63.7	71.4	55.8	20.7
BV	<4.7	<4.7	<4.7	<4.7	n/a	98.5	198.6	183.9	160.3	54.0

IL-6 Controls

Control	IL-6 Concentration (pg/mL)				
Replicate No.	*n = 1*	*n = 2*	*n = 3*	*Mean*	*SD*
Media	<4.7	<4.7	<4.7	<4.7	n/a
LPS	58.5	185.5	145.8	129.9	65.0

Additional LC-MS Data

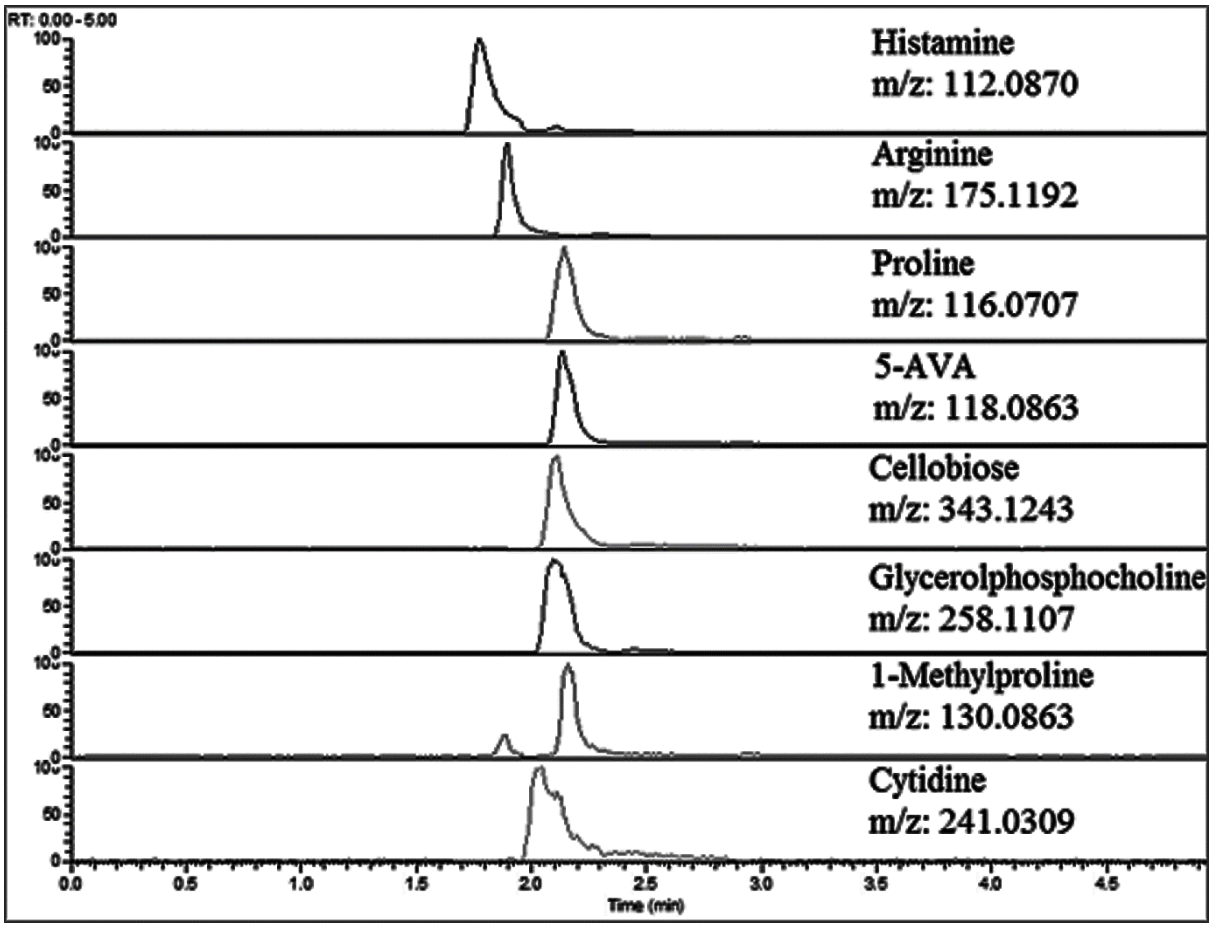

Figure S10. Extracted ion chromatograms (EICs) of the main components of F-1. The fraction was analysed by positive ion LC-ESI-MS on the Orbitrap mass spectrometer with an ACE 3 C18 column using mobile phases 0.1% formic acid in water (A) and 0.1% formic acid in acetonitrile (B) at a gradient of 20%–70% (0–10 min), 70% (10–16 min), 70%–20% (16–20 min) and 20% (20–25 min) relative to solvent B, and at a flow rate of 0.3 mL/min. The EICs were obtained within ±0.01 accuracy relative to the *m*/*z* of each ion.

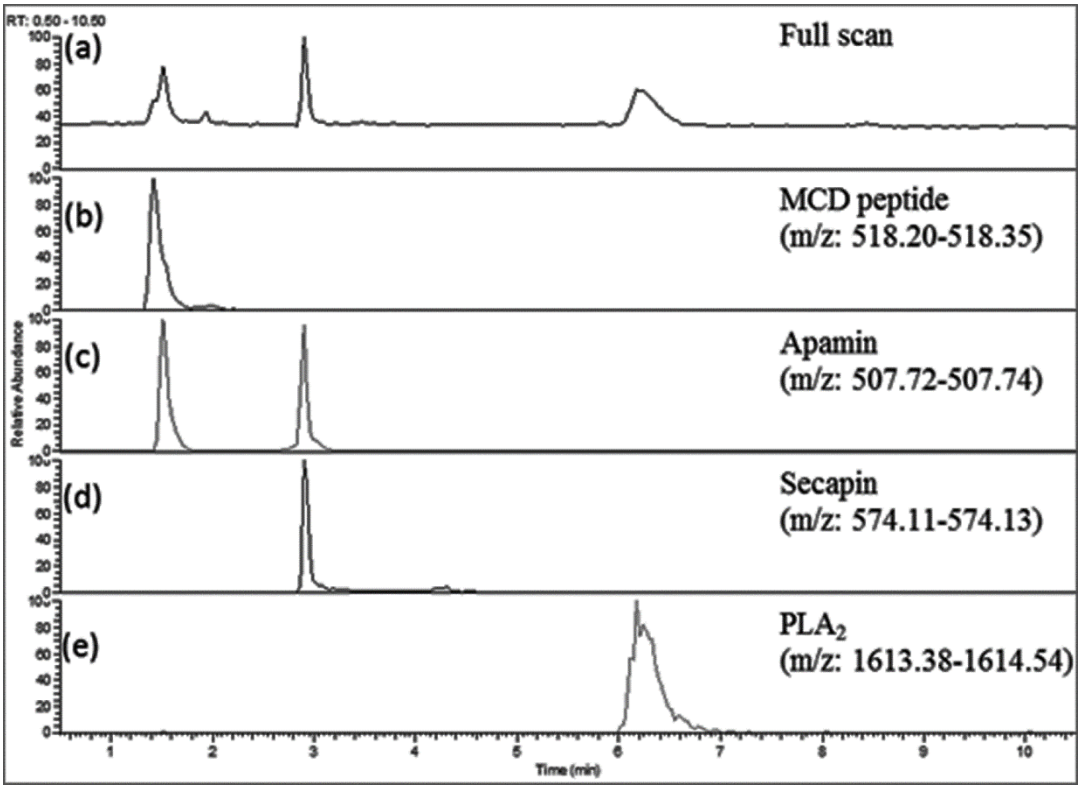

Figure S11. Full scan (**a**) and extracted ion chromatograms (**b**–**e**) of the components of F-2. The fraction was analysed by positive ion LC-ESI-MS on the Orbitrap mass spectrometer with an ACE 3 C18 column using mobile phases 0.1% formic acid in water (A) and 0.1% formic acid in acetonitrile (B) at a gradient of 20%–70% (0–10 min), 70% (10–16 min), 70%–20% (16–20 min) and 20% (20–25 min) relative to solvent B, and at a flow rate of 0.3 mL/min.

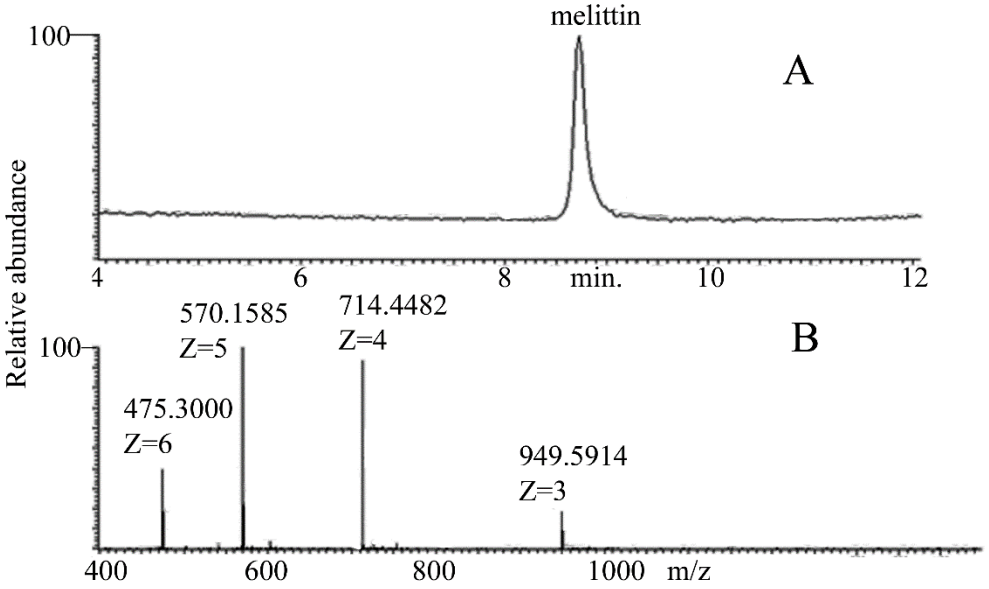

Figure S12. Chromatogram of sample from F-3 showing the melittin peak in a relatively pure form (A). The typical mass spectrum of melittin (B) shows a quintuply-charged base ion with *m*/*z* 570.1585. The fraction was analysed by positive ion LC-ESI-MS on the Orbitrap mass spectrometer with an ACE 3 C18 column using mobile phases 0.1% formic acid in water (A) and 0.1% formic acid in acetonitrile (B) at a gradient of 20%–70% (0–10 min), 70% (10–16 min), 70%–20% (16–20 min) and 20% (20–25 min) relative to solvent B, and at a flow rate of 0.3 mL/min.

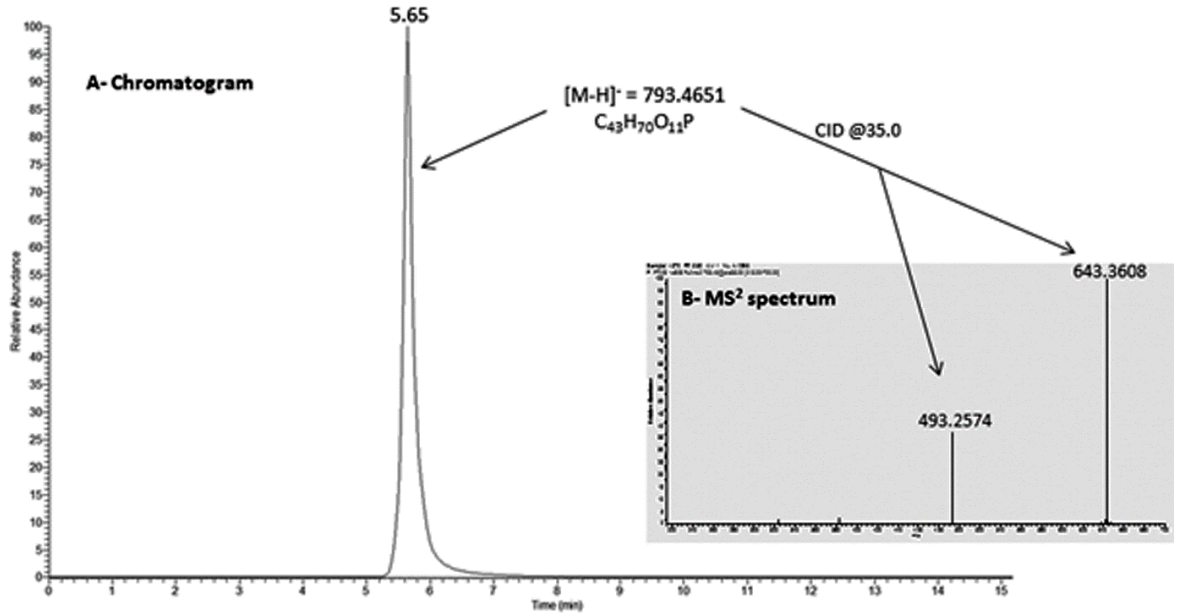

Figure S13. Chromatogram of the impurity in F-4 with [M − H] of 793.4651 and elemental composition $C_{43}H_{70}O_{11}P$. Collisional-induced dissociation (CID) of *m*/*z* 793.46 parental ion at a NCE of 35.0 gave two fragment ions of *m*/*z* 493.2574 and 643.3608 respectively. Sample analysed by LCMS using mobile phase A (0.1% formic acid in water), B (0.1% formic acid in acetonitrile), gradient [50%–95% B (0–5 min), 95% B (5–12 min), 50% B (13–16 min)], flow rate 0.4 mL/min, column ACE 3 C18 (150 × 3.0 mm), 3 μm i.d. The ions were detected on the LTQ-Orbitrap (*m*/*z* scan range 200–1200 for parental ion and 200–700 for fragment ions) in negative mode.

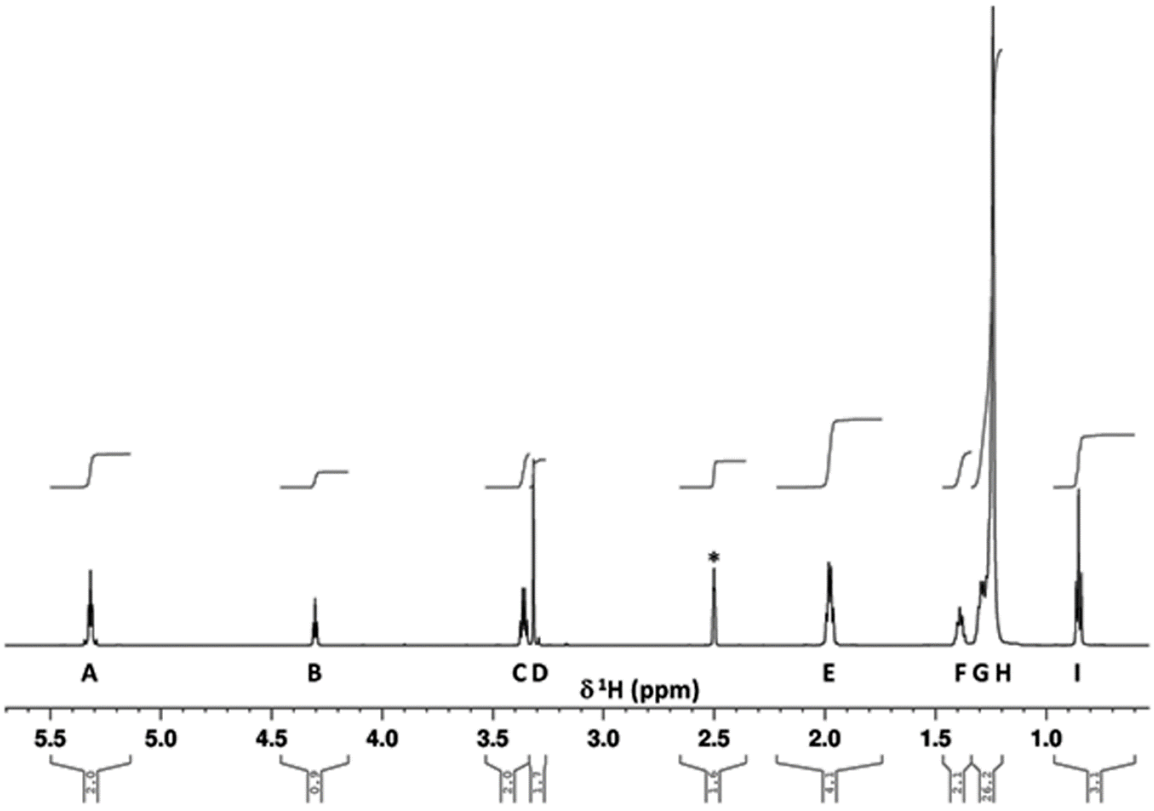

Figure S14. 600 MHz 1D ^{1}H-NMR spectrum of the lipid component from faction F-4 showing signal integrals. The signal indicated by * arises from the solvent and signal D is ascribed to water in DMSO-d_6.

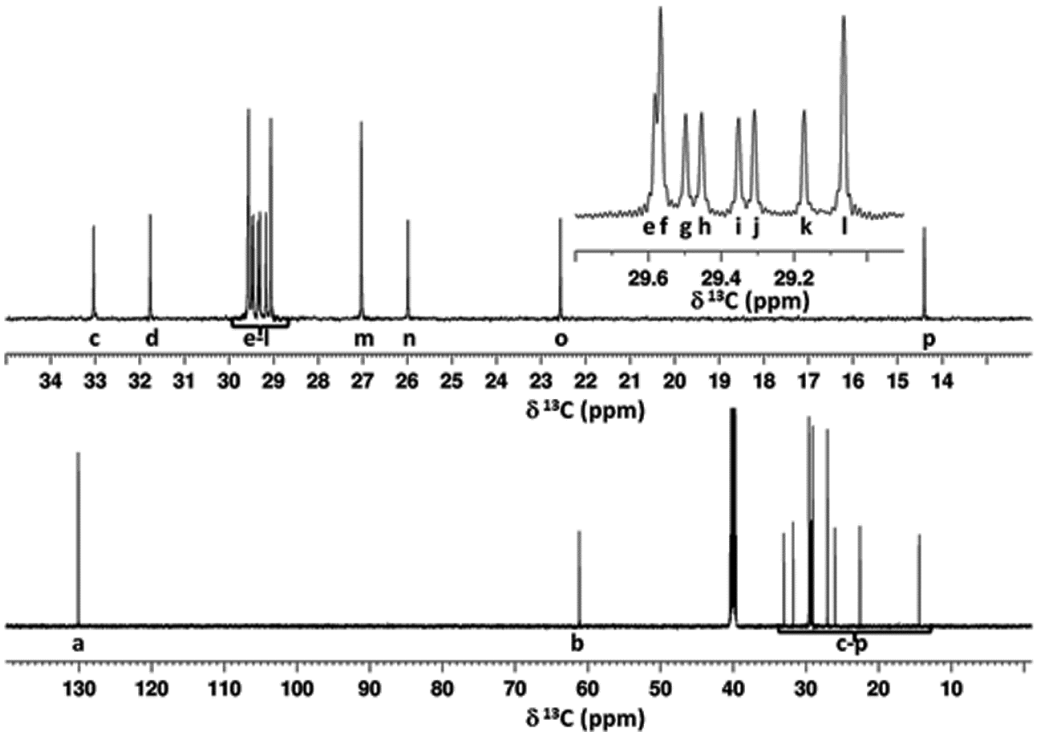

Figure S15. ^{13}C-{^{1}H} NMR spectrum of the lipid component from fraction F-4 with expansions shown to reveal details of crowded region. The expansion immediately above the full NMR spectrum shows expansion of the signal region c–p. Further expansion of the region e–l within this is shown inset as the topmost expansion.

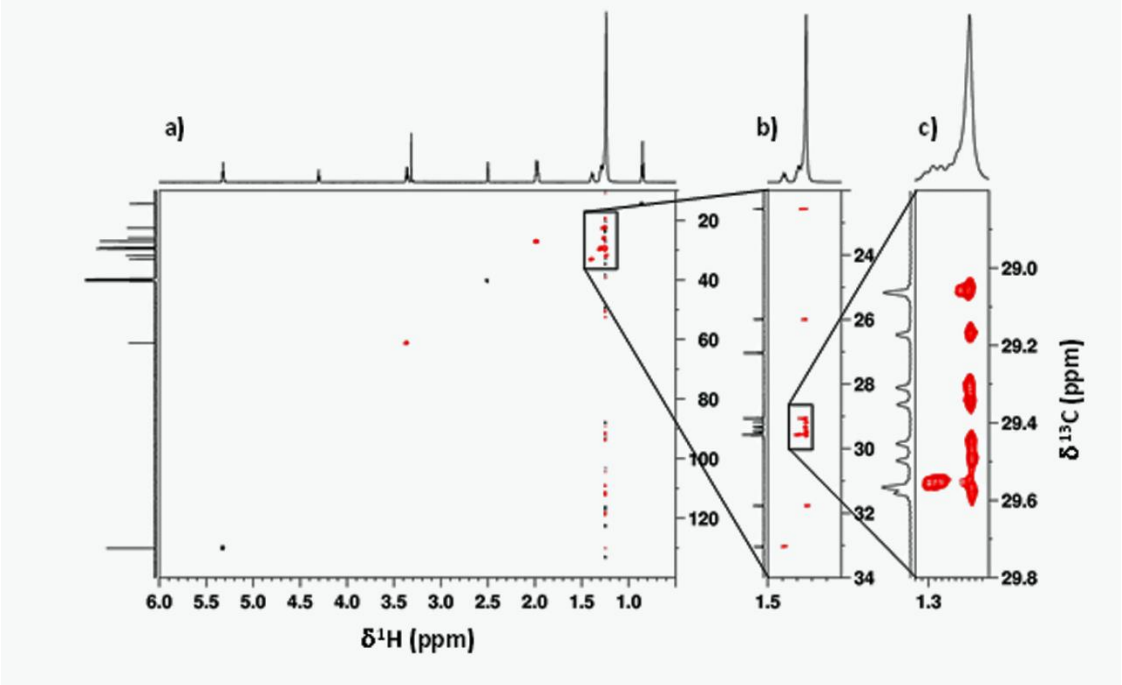

Figure S16. 600 MHz 2D [^{1}H, ^{13}C] HSQC-NMR data for the lipid component of fraction F-4. (**a**) Low resolution spectrum showing the complete data set; (**b**) Expansion of the boxed region shown in (**a**) from data acquired at high F1 resolution using non-uniform sampling; (**c**) Further expansion of the boxed region shown in (**b**) to reveal high resolution data in F1 allowing individual correlations between protons and carbons of each methylene group to be distinguished for unique carbon resonance assignment and proton counting. Black cross-peaks (positive) correspond to methine (CH) and methyl (CH_3) groups; red cross-peaks correspond to methylene (CH_2) groups.

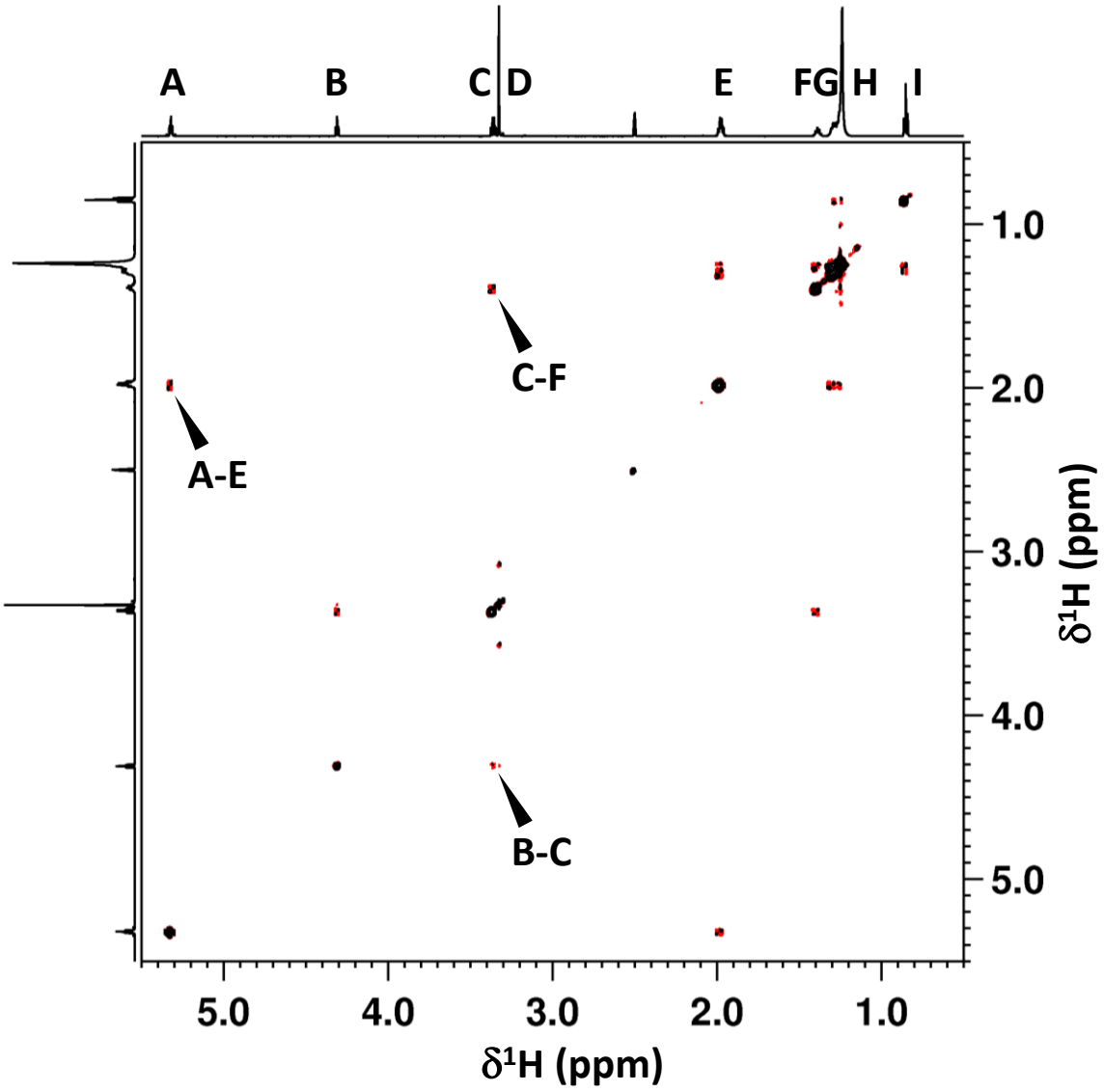

Figure S17. 600 MHz 2D [^{1}H, ^{1}H] DQFCOSY NMR spectrum of the BV F4 component molecule with 1D ^{1}H-NMR spectra shown representing horizontal and vertical projections with signal designations shown as **A**–**I**. Selected cross-peaks are highlighted. Full cross-peak assignments are summarized in Table S7.

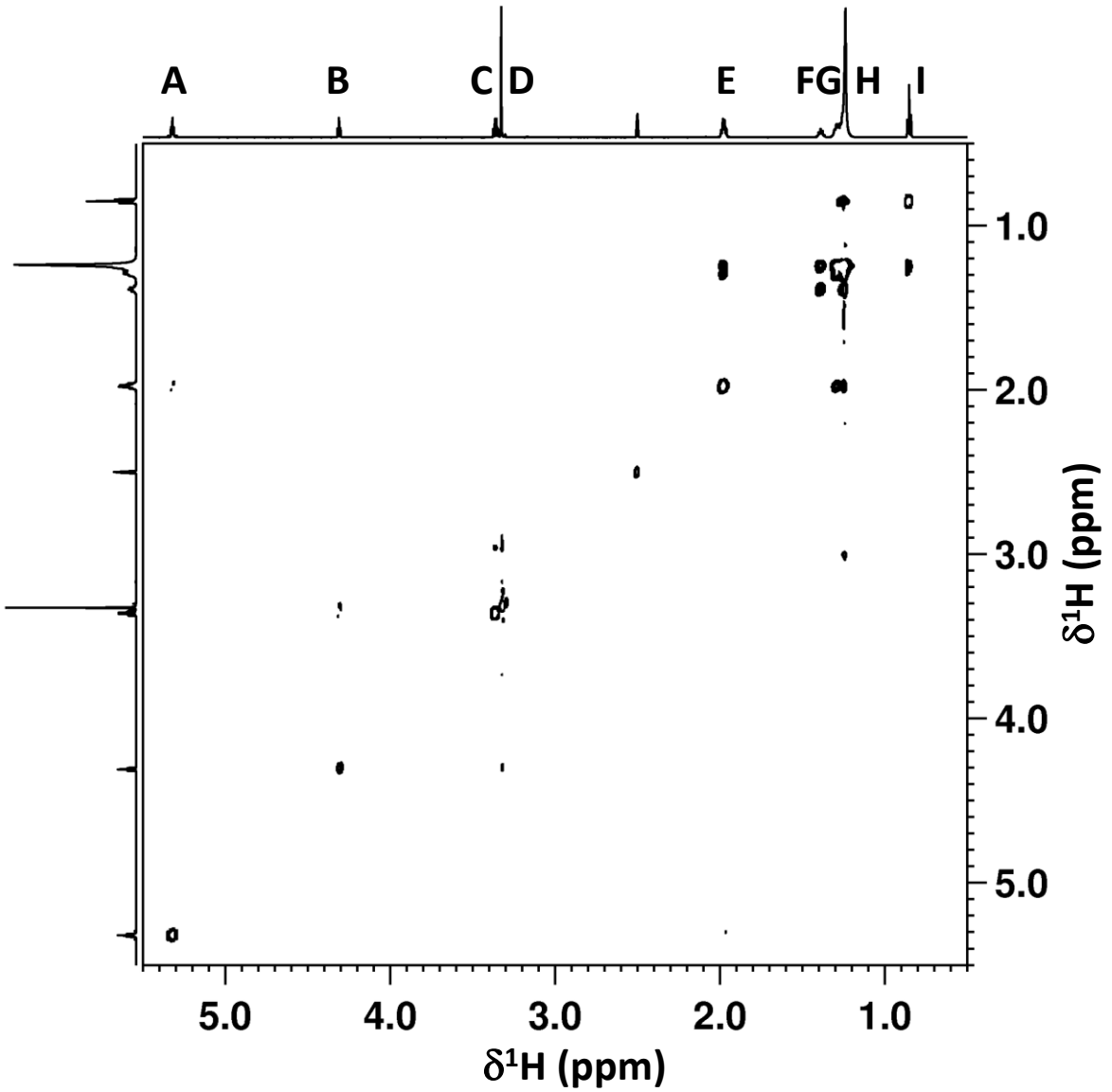

Figure S18. 600 MHz 2D [^{1}H, ^{1}H] TOCSY NMR spectrum of the BV F4 component molecule with 1D ^{1}H-NMR spectra shown representing horizontal and vertical projections with signal designations shown as **A–I**. Full cross-peak assignments are summarized in Table S7.

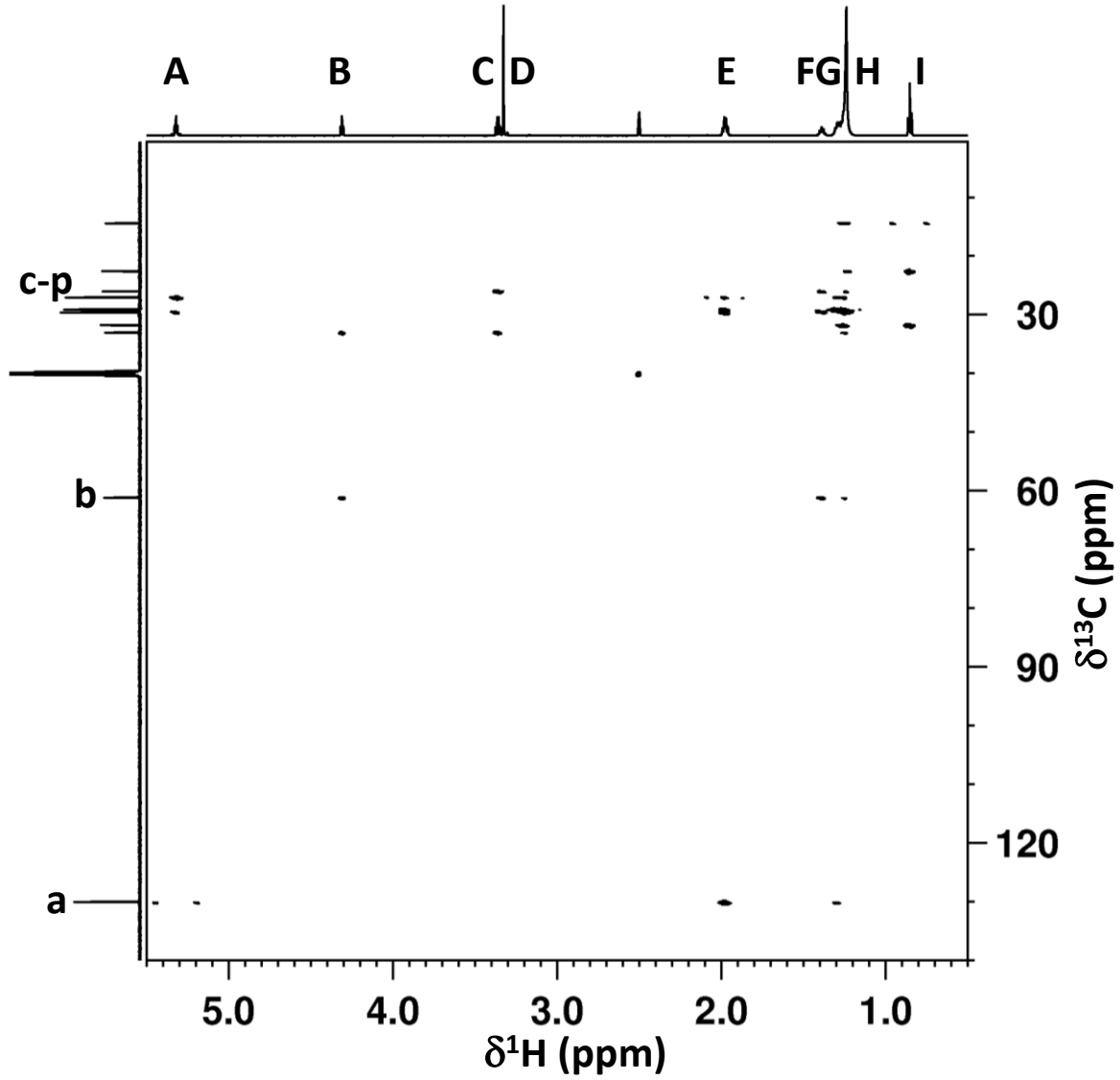

Figure S19. 600 MHz 2D [^{1}H, ^{13}C] HMBC-NMR spectrum of the BV F4 component molecule with 1D ^{1}H-NMR spectrum shown representing the horizontal projection and 1D ^{13}C-{^{1}H} NMR spectrum shown representing the vertical projection with signal designations shown as **A–I** and **a–p** respectively. Full cross-peak assignments are summarized in Table S8.

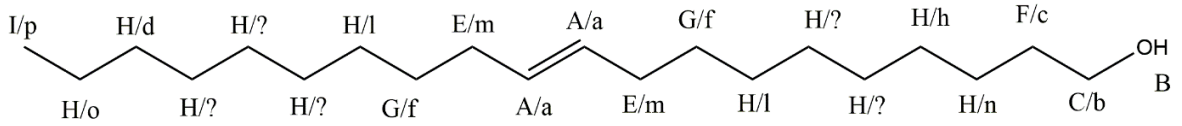

Figure S20. Basic lipid structure from an analysis of the NMR data showing the signal assignments associated with protons (upper case labels) and carbons (lower case labels) at each position. The *E*-layout about the double bond is purely for convenience and has no bearing on the final structure.

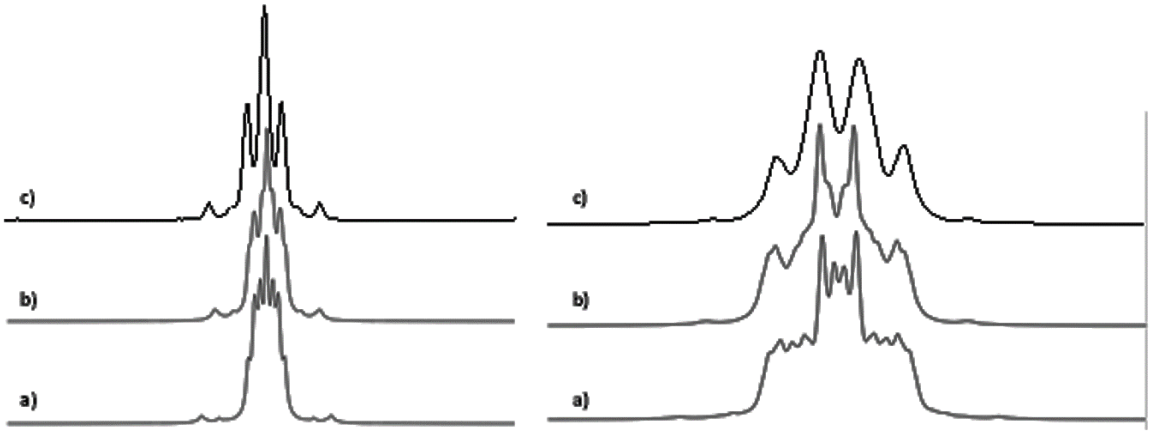

Figure S21. Simulations and experimental data for two possible configurations of the lipid molecule for ^{1}H resonances A (**left**) and E (**right**). (**a**) Simulated signals for the *E*-configuration; (**b**) simulated signals for the *Z*-configuration; (**c**) experimental data.

Table S7. Coupling partners revealed through 2D [^{1}H, ^{1}H] COSY (C) and TOCSY (T) NMR data

Label	A	B	C	D	E	F	G	H	I
A					C, T				
B			C, T						
C		C, T				C, T			
D									
E	C, T						C, T	C, T	
F			C, T					C, T	
G					C, T			C, T	
H					C, T	C, T	C, T		C, T
I								C, T	

Table S8. Coupling partners revealed by analysis of 2D [^{1}H, ^{13}C] HSQC (HS) and HMBC (HM) NMR data for the lipid component.

Labels	A	B	C	D	E	F	G	H	I
a	HS				HM		HM		
b		HM	HS			HM		HM	
c		HM	HM			HS		HM	
d								HSHM	HM
e								HS	
f	HM				HM		HS		
g								HS	
h						HM		HS	
i								HS	
j								HS	
k								HS	
l					HM		HM	HS	
m	HM				HS		HM	HM	
n			HM			HM		HS	
o								HS	HM
p								HM	HS

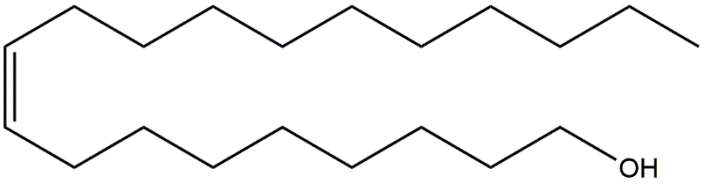

Figure S22. (*Z*)-eicos-9-en-1-ol.

References

1. Thrippleton, M.J.; Keeler, J. Elimination of Zero-Quantum Interference in Two-Dimensional NMR Spectra. *Angew. Chem. Int. Ed.* **2003**, *42*, 3938–3941
2. Jaravine, V.; Zhuravleva, A.; Permi, P.; Ibraghimov, I.; Orekhov, V.Y. Hyperdimensional NMR spectroscopy with nonlinear sampling. *J. Am. Chem. Soc.* **2008**, *130*, 3927–3936.

metabolites

MDPI

Article

Metabolomic Profiling of the Effects of Melittin on Cisplatin Resistant and Cisplatin Sensitive Ovarian Cancer Cells Using Mass Spectrometry and Biolog Microarray Technology

Sanad Alonezi [1], Jonans Tusiimire [1], Jennifer Wallace [2], Mark J. Dufton [2], John A. Parkinson [2], Louise C. Young [1], Carol J. Clements [1], Jin Kyu Park [3], Jong Woon Jeon [3], Valerie A. Ferro [1] and David G. Watson [1,*]

1 Strathclyde Institute of Pharmacy and Biomedical Sciences, University of Strathclyde, Glasgow G4 0RE, UK; alonezi-sanad-mohammed-z@strath.ac.uk (S.A.); jonans.tusiimire@strath.ac.uk (J.T.); louise.c.young@strath.ac.uk (L.C.Y.); c.j.clements@strath.ac.uk (C.J.C.); v.a.ferro@strath.ac.uk (V.A.F.)

2 WestCHEM, Department of Pure and Applied Chemistry, University of Strathclyde, 295 Cathedral Street, Glasgow G1 1XL, UK; jennifer.wallace.101@strath.ac.uk (J.W.); mark.dufton@strath.ac.uk (M.J.D.); john.parkinson@strath.ac.uk (J.A.P.)

3 Beesen Co. Ltd., Bio Venture Town, Yuseong Daero 1662, Dae Jeon 34054, Korea; jkypark@live.co.kr (J.K.P.); confessor@hanmail.net (J.W.J.)

* Correspondence: d.g.watson@strath.ac.uk; Tel.: +44-141-548-2651

Academic Editor: Peter Meikle

Received: 7 September 2016; Accepted: 11 October 2016; Published: 13 October 2016

Abstract: In the present study, liquid chromatography-mass spectrometry (LC-MS) was employed to characterise the metabolic profiles of two human ovarian cancer cell lines A2780 (cisplatin-sensitive) and A2780CR (cisplatin-resistant) in response to their exposure to melittin, a cytotoxic peptide from bee venom. In addition, the metabolomics data were supported by application of Biolog microarray technology to examine the utilisation of carbon sources by the two cell lines. Data extraction with MZmine 2.14 and database searching were applied to provide metabolite lists. Principal component analysis (PCA) gave clear separation between the cisplatin-sensitive and resistant strains and their respective controls. The cisplatin-resistant cells were slightly more sensitive to melittin than the sensitive cells with IC_{50} values of 4.5 and 6.8 μg/mL respectively, although the latter cell line exhibited the greatest metabolic perturbation upon treatment. The changes induced by melittin in the cisplatin-sensitive cells led mostly to reduced levels of amino acids in the proline/glutamine/arginine pathway, as well as to decreased levels of carnitines, polyamines, adenosine triphosphate (ATP) and nicotinamide adenine dinucleotide (NAD+). The effects on energy metabolism were supported by the data from the Biolog assays. The lipid compositions of the two cell lines were quite different with the A2780 cells having higher levels of several ether lipids than the A2780CR cells. Melittin also had some effect on the lipid composition of the cells. Overall, this study suggests that melittin might have some potential as an adjuvant therapy in cancer treatment.

Keywords: metabolomics; Melittin; LC-MS; ovarian cancer; A2780 cells; cisplatin resistance

1. Introduction

Growth of cancers is associated with various metabolic changes at the cellular level, which can be used as biomarkers for diagnosis, prognosis and evaluation of anticancer therapies [1]. For instance, unlike normal cells, cancer cells are more dependent on aerobic glycolysis, fatty acid synthesis, and glutaminolysis for proliferation [2]. Thus, evaluation of the concentrations of specific metabolites in a cell can provide insights into its metabolic state relative to the physiological norm. The metabolic

profile of cancer cells can also provide an understanding of the process of carcinogenesis and the mechanism of chemoresistance leading to development of better diagnostic and therapeutic tools [3].

Worldwide, more than 230,000 women are diagnosed with ovarian cancer each year, and this disease is responsible for an estimated 140,000 deaths per year [4]. Platinum (e.g., cisplatin) and taxane (e.g., paclitaxel)-based chemotherapies are currently the first line treatments for ovarian cancer, but relapse occurs in 70% of patients [3]. Although most ovarian cancers remain sensitive to these therapies, there is growing resistance against them which reduces the time to disease progression following the initial treatment, and minimises their efficacy upon further treatment during relapse [5]. The anticancer activity of platinum arises from its ability to form irreparable intra-strand DNA crosslinks/adducts, which leads to cell apoptosis [6], as well as induction of oxidative and endoplasmic reticulum stress [7–9]. On the other hand, platinum resistance in cancer results from various adaptive mechanisms including reduced cellular uptake, increased DNA repair and tolerance [10], and inactivation by glutathione [10,11]. It has been previously reported that platinum-sensitive (A2780) and resistant (C200) ovarian cancer cell lines have distinct metabolic profiles in various interdependent pathways [3].

Melittin, is the main component of honey bee venom and has demonstrated a variety of biological and pharmacological applications [12,13]. It has natural anti-bacterial, anti-viral, and anti-inflammatory properties [12,13]. It has also been shown to have diverse anticancer effects in several different cancer cell lines including those of gastric [14,15], breast [12,16], ovarian [16,17], liver [18,19], prostate [16], cervical [16], and lung [20] origins. The mechanisms by which melittin, an amphipathic haemolytic peptide, exerts its potential anticancer effects include inhibition of cell proliferation [12,17], induction of apoptosis [12,14,15,21], and direct necrosis [14,15]. The mechanism of apoptosis appears to be related to the activation of the caspase-dependent pathway [15,16,21]. On the other hand, necrosis arises from damage to the cell membranes through necrotic cytotoxicity, as has been observed in rat thymocytes, murine skeletal muscle cells, gastrointestinal (GI) tumour cells, erythrocytes, lymphocytes, lymphoblastoid cells, rat primary alveolar cells, and intestinal Caco-2 cells [15,21]. Melittin can also cause cell cycle arrest leading to inhibition of cell proliferation and growth. It can contribute to inhibition of angiogenesis through its ability to suppress epidermal growth factor (EGF)-induced vascular endothelial growth factor (VEGF) secretion and inhibit the creation of new blood vessels by influencing hypoxia-inducible factor (HIF)-1a [22]. Previous studies on ovarian cancer cells have shown that melittin inhibits their growth through induction of apoptosis mediated via inhibition of signal transducer and activator of transcription 3 (STAT3) and activation of Janus kinase 2 (JAK2), both of which are critical during angiogenesis [16]. Melittin can also prevent EGF-induced cell invasion through its inhibition of the PI3K/Akt/mTOR signaling pathway, but this is primarily related to breast cancer cells [12]. In hepatocellular carcinoma, melittin appears to inhibit cell proliferation through its influence on methyl-CpG binding protein 2 ($MeCP_2$), which is a critical element in tumour growth and development [19]. As a consequence, melittin induces a delay in G_0/G_1 cell cycle progression, which it is able to accomplish without causing apoptosis [19]. Based on these observations, it is apparent that melittin affects cancer cells in a variety of ways that are different from those induced by platinum-based agents. This difference in molecular action could be reflected at cellular level in terms of differences in the metabolite profiles, and would suggest an opportunity for synergy between the two agents and a possible lack of cross-resistance. By determining the metabolite differences between platinum-sensitive and resistant cancer cells after treatment with melittin, it could be possible to understand the latter's metabolic effects on these cells in relation to their platinum chemosensitivity.

Metabolomics is a growing and powerful technology capable of detecting hundreds to thousands of metabolites in tissues and biofluids [23–26]. With recent advances in both instrumental and computational metabolomics technologies, it is now possible to gain deeper understanding of the metabolic processes occurring within cancer cells, including how they exploit the process of glycolysis. Cancer cells are known to rely on higher rates of glycolysis, an observation that is known as the "Warburg effect". With metabolomic profiling, it is possible to relate the "Warburg effect"

to the production of amino acids, nucleotides, and lipids necessary for tumour proliferation and vascularisation [27]. Some researchers have suggested that metabolic profiling can be an invaluable tool in the evaluation of drug targets and analysis of malignant phenotypes, including the diagnosis of cancer [28]. For instance, by comparing the metabolite profile of cancer cell lines such as ovarian cancer cells pre- and post-treatment, it is possible to identify relevant metabolic changes that relate to specific treatments, which not only helps in determining the efficacy of the treatment, but is also essential in elucidating its pharmacodynamics and identifying the essential biomarkers involved. Thus, metabolomic analysis of lysates from cell cultures has many potential applications and advantages over conventional methods of analytical biochemistry and cell line testing. It is anticipated that as more robust platforms for metabolomics of cell cultures become available, this will facilitate greater understanding of drug actions both in vitro and in vivo, as well as aiding the rapid incorporation of drug leads into novel therapeutic agents [29].

Phenotype Microarrays (PMs) use a patented redox chemistry, employing cell respiration as a universal reporter. These assays potentially provide a natural fit to support data obtained from metabolomics screens. The redox assay provides for both amplification and precise quantitation of phenotypes. Redox dye mixes contain a water-soluble nontoxic tetrazolium reagent that can be used with virtually any type of animal cell line or primary cell [30]. The dyes used in Biolog (Hayward, CA, USA) assays measure output of nicotinamide adenine dinucleotide reduced form (NADH) production from various catabolic pathways present in the cells being tested. If cell growth is supported by the medium in an assay well, the actively metabolizing cells reduce the tetrazolium dye. Reduction of the dye results in colour formation in the well, and the phenotype is considered "positive." If metabolism is hampered or growth is poor, then the phenotype is "weakly positive" or "negative," and little or no colour is formed in the well. This colorimetric redox assay allows examination of the effect of treatment on the metabolic rate produced by different substrates and thus is an excellent technique to combine with examination of metabolic output via metabolomics screens.

The current study sought to examine the metabolic effects of melittin on cisplatin-resistant (A2780CR) and cisplatin-sensitive (A2780) human ovarian cancer cell lines via mass spectrometry-based metabolic profiling in combination with Biolog microarray assays. Each of the cell lines was separately treated with sub-lethal doses of melittin for 24 h before extraction and global metabolite analysis of cell lysates by LC-MS using a high performance liquid chromatography (HPLC) system coupled to an Orbitrap Exactive mass spectrometer using a ZIC-pHILIC column. The resulting data were extracted by MZMine and subsequently analysed by univariate and multivariate approaches with SIMCA-P.

2. Results

2.1. Melittin Sensitivity of the Ovarian Cancer Cells

Figure S1 shows the cell viability plots for A2780 and A2780CR cells treated with cisplatin. Melittin exhibited toxicity against both A2780CR and A2780 cells, with IC_{50} values of 4.5 and 6.8 μg/mL, respectively (Figure 1). Thus, the cisplatin-resistant A2780CR cells were more sensitive to melittin than the cisplatin-sensitive A2780 cells and exhibited a response curve suggestive of a dose-response relationship.

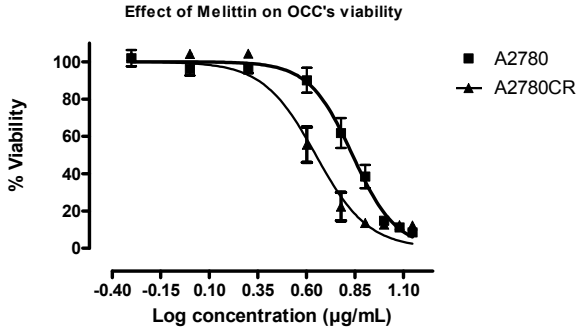

Figure 1. Effect of melittin on the viability of the ovarian cancer cells A2780 and A2780CR. Cell viability was determined following treatment with varying doses of melittin for 24 h (IC_{50} = 6.8 µg/mL A2780; IC_{50} = 4.5 µg/mL A2780CR).

2.2. Phenotypic MicroArray (PM) Assay of Untreated and Melittin Treated A2780 and A2780CR Cells

The cells were tested by using standard protocols for metabolic phenotype microarray-mammalian (PM-M) cell assays (Biolog, Hayward, CA, USA). In order to select the proper dye mix, an optimisation experiment was performed in order to determine which of the two Biolog redox dyes (MA or MB) was most appropriate for phenotypic microarray (PM) assay of both A2780 and A2780CR cells. Figure S2 shows the layout of the carbon sources in the PM-M1 microplate. Figure S3 shows the colours which developed in the plates after inoculation with A2780 and A2780CR cells in the presence and absence of melittin. Figure 2 indicates the extent of utilisation of the different carbon sources by the resistant and sensitive cells. A number of the carbon sources were used by both cell lines. However, many of the substrates in the microarray plate do not appear to be useful as carbon sources. There were clear phenotypic differences and the A2780CR cells would appear to have a slightly more active glycolytic pathway as judged by the rate of utilization of glucose and fructose phosphates, although the rates of glucose and pyruvate utilisation were higher in the A2780 cell line. Inosine also appears to be a very favourable carbon source and is used by the A2780CR cells to a greater extent than by the A2780 cells. Neither Krebs cycle intermediates nor short chain fatty acids appear to be useful as carbon sources underlining the dependence of both cell lines on glycolysis, which is generally the case in cancer cell lines [2].

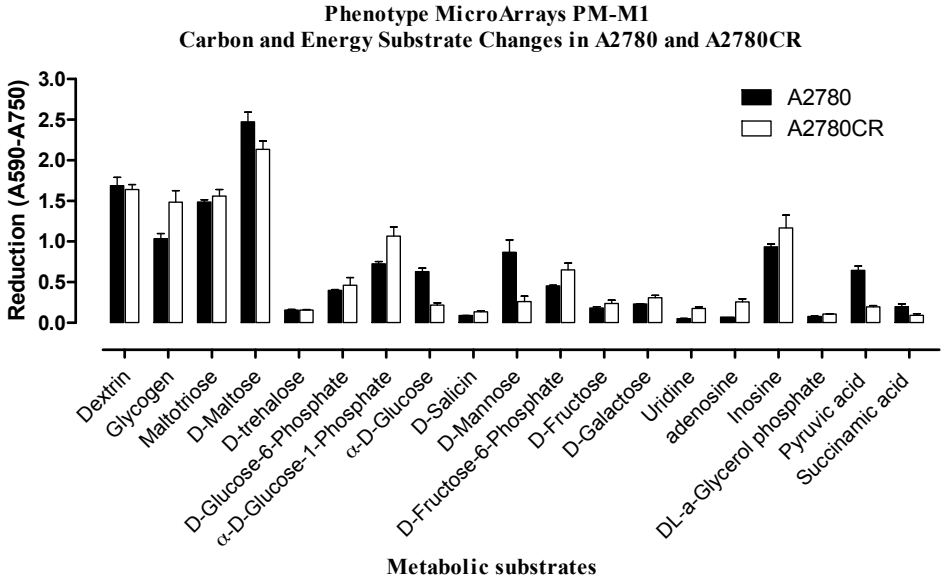

Figure 2. Comparison of substrate metabolism in A2780 and A2780CR. Dye reduction rates calculated following 24 h incubation of cells.

Treatment of the cells with melittin produced a very different effect on the sensitive cells in comparison with the resistant cells. In the resistant cells carbon metabolism was not that strongly affected and the cells continued to produce NADH, but in the sensitive cells there was a huge reduction in carbon metabolism (Figures 3 and 4). This suggests that there may be differences in the mechanisms by which the two cell lines respond to melittin, which could lead to different mechanisms of cell death induced by the treatment.

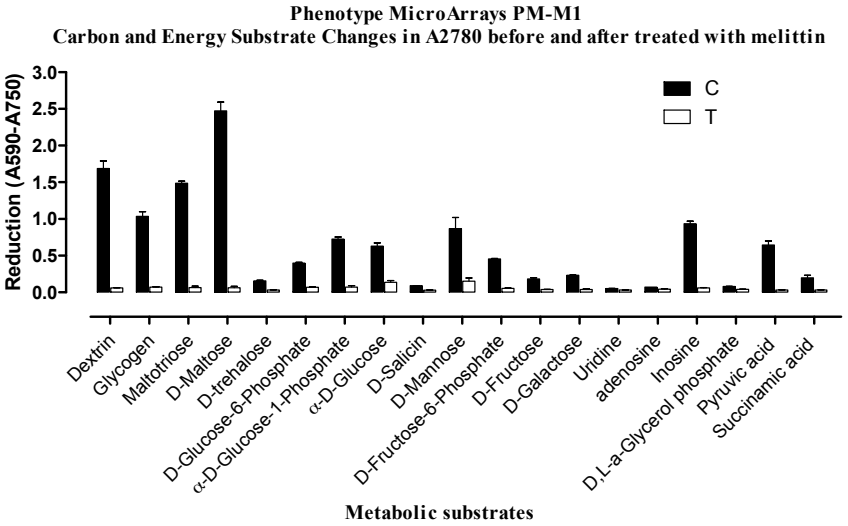

Figure 3. Comparison of substrate metabolism in A2780 cells following melittin exposure. Dye reduction rates calculated following 24 h incubation of cells with melittin at IC_{50} (6.8 μg/mL) concentration. C = untreated controls; T = melittin treated.

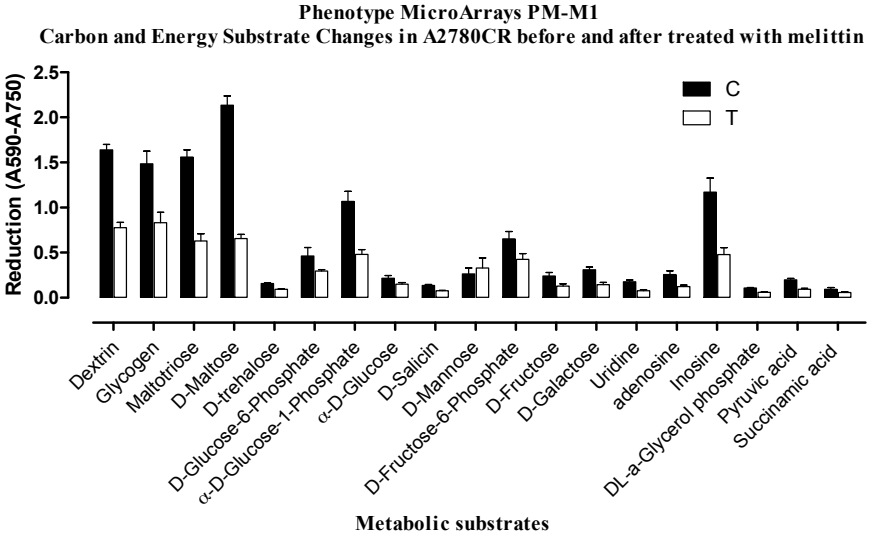

Figure 4. Comparison of substrate metabolism in A2780CR cells following melittin exposure. Dye reduction rates calculated following 24 h incubation of cells with melittin at IC_{50} (4.5 μg/mL) concentration. C = untreated controls; T = melittin treated.

2.3. Effect of Melittin on the Metabolomes of Both Cell Lines

In order to gain a better understanding of the mechanism of melittin toxicity in the two cell lines, differences in the levels of metabolites induced by treatment with melittin at concentrations corresponding to IC_{50} with respect to each cell line were assessed. PCA and HCA analyses were used to classify the metabolic phenotypes and identify the differentiating metabolites. A clear separation

of melittin-treated A2780 and A2780CR cells, and their respective untreated controls, was achieved indicating unique metabolite profiles for the treated and control cells on a PCA scores plot (Figure 5). The model parameters and validation of the plot suggested a good model (2 components, R^2X = 0.814; Q^2 = 0.526). The HCA groupings of the metabolomics data showed distinct separation between the cell lines themselves as well as between the control and treated samples of each cell line.

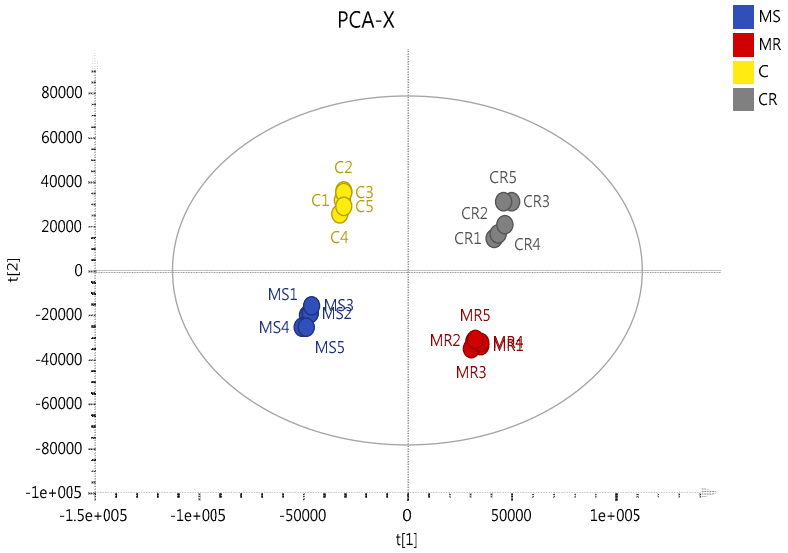

Figure 5. Multivariate data analysis of the ovarian cancer cells A2780 and A2780CR treated with melittin. PCA scores plot generated from PCA using LC-MS normalised data of treated cells and controls. MS circles: A2780-treated cells; C circles: untreated A2780 cells; MR circles: A2780CR -treated cells; CR circles: untreated A2780CR.

Table 1 shows the metabolic differences between the sensitive and resistant cell lines. The low levels of ATP in the A2780 cells reflected the Biolog data suggesting that these cells have reduced rates of glycolysis in comparison with the resistant cells. Several metabolites in the TCA cycle differed between the sensitive and resistant cells including citrate, 2-oxoglutarate, and malate. None of the TCA intermediates supplied in the Biolog array were utilised by the cell lines as carbon sources. However, pyruvate was used as a carbon source and presumably enters the Krebs cycle. Treatment with melittin further reduced the levels of ATP in the A2780 cells whereas melittin had little effect on the ATP levels in the A2780CR cells. There were marked differences in levels of some carnitines between the sensitive and resistant cells with the sensitive cells having much higher levels of butyryl carnitine. However, there was no evidence from the Biolog data that short chain fatty acids were utilised as carbon sources.

The most marked differences between the sensitive and resistant cells were in the polyamine pathway where 14 metabolites in the pathway were altered in the sensitive cells in comparison with the resistant cells. The polyamines spermidine, putrescine and *N*-acetylputrescine were markedly higher in the sensitive cells and, correspondingly, many of their precursors, especially arginine, were down regulated. Melittin treatment decreased the levels of polyamines in the sensitive cells and the levels of arginine present in the cells were reduced almost to zero.

There were important differences in lipid composition between the two cell lines before and after treatment with melittin. Figure 6 shows a heat map of the top 50 lipids by intensity extracted from the A2780 cells in comparison with A2780CR cells. The top 10 most abundant lipids are similar between the two cell lines and make up a large proportion of the lipids extracted. However, it is clear that the A2780 cell line generally contains more lipids than the A2780CR cell line. The really marked differences between the two cell lines are in several sphingolipids such as dehydrosphinganine and lactosylceramide, and in some ether lipids such as PC38:4 and PC38:6, all of which are lower in the resistant cells. The differences in lipid composition of the two cell lines suggest that either remodelling

of the cell membrane might have occurred in order for the A2780CR cells to become resistant, or there is decreased biosynthesis and/or increased utilisation of lipids in cisplatin resistant cells as has been suggested by others [3]. Melittin appears to have some effect on lipid composition in the A2780 cells with the levels of the abundant lipid PC34:1 decreasing, but the effect on this lipid in the A2780CR cells is less marked. Overall there are many changes in lipid abundance in response to melittin but they are generally quite small and restricted to the less abundant lipids (Table S1). The decrease in the lipids induced by treatment with melittin is less in the case of the A2780CR cells suggesting less membrane damage in the case of these cells.

m/z	Rt(min)	Met Name	Mean S	Mean R	Mean MS	Mean MR
760.5846	13.9	PC34:1				
786.6	13.9	PC36:2				
732.5539	14.0	PC32:1				
746.6055	14.1	PC34:0				
788.6156	13.9	PC36:1				
734.5691	14.0	PC32:0				
758.5694	13.9	PC34:2				
703.5745	14.5	SPPC16:0				
720.5899	14.2	PC32:2 ether lipid				
718.5746	14.1	PC32:0 ether lipid				
706.5382	14.1	PC30:0				
784.5847	13.8	PC36:3				
782.5672	13.7	PC36:4				
768.5529	9.7	PC38:4				
808.5836	13.7	PC38:5				
810.5995	13.7	PC38:4				
768.5885	13.8	PC36:3 ether lipid				
744.5905	13.9	PC34:1 ether lipid				
794.6051	13.8	PC38:5 ether lipid				
796.6206	13.8	PC38:4 ether lipid				
752.5584	9.6	PE38:5				
813.6838	14.4	SM42:2				
804.5759	14.0	PS37:0				
812.6155	13.8	PC38:3				
814.6312	13.9	PC38:2				
744.5534	10.1	PE36:2 ether lipid				
772.621	14.0	PC 36:1 ether lipid				
300.2893	10.4	Dehydrosphinganine				
774.6007	13.9	PC35:1				
752.5583	9.6	PE38:5 ether lipid				
766.5367	9.6	PE38:5				
750.5427	9.6	PE38:4 ether lipid				
724.5273	9.7	PE36:5 ether lipid				
772.5851	13.9	PC35:2				
774.6365	14.1	PC36:0 ether lipid				
770.6052	13.9	PC36:2 ether lipid				
731.6057	14.5	SM36:2				
718.538	10.3	PE34:1				
692.5589	14.2	PC30:2 ether lipid				
730.5382	13.9	PC32:2				
862.6244	3.1	C18:0 Lactosylceramide				
746.569	10.2	PE34:1 ether lipid				
792.5897	13.7	PC38:6 ether lipid				
282.2788	10.4	Octadecenamide				
834.5994	13.7	PC40:6				
836.6151	13.7	PC40:5				
863.5661	3.7	PI36:1				
790.5586	11.4	PS36:1				
756.5523	13.9	PC34:3				
887.5643	3.6	PI38:3				

Figure 6. Heat Map showing the relative abundance of lipids in A2780 (S), A2780CR (R) and melittin treated (MS & MR) cells. Red = 5×10^7, Yellow = 8% of highest value, Blue = 0%.

Table 1. Statistically differentiating metabolites in melittin treated and untreated A2780 and A2780CR cells.

m/z	RT	Metabolite Name	S/R		MS/MR		MR/R		MS/S	
			p-Value	Ratio	*p*-Value	Ratio	*p*-Value	Ratio	*p*-Value	Ratio
Proline/glutamate/arginine/polyamine metabolism										
116.071	12.8	* Proline	<0.01	0.837	<0.001	0.409	ns	1.056	<0.001	0.516
128.035	10.3	1-Pyrroline-3-hydroxy-5-carboxylate	<0.05	0.839	<0.001	0.364	ns	1.114	<0.001	0.453
130.051	14.4	Glutamate-5-semialdehyde	ns	0.944	<0.001	0.607	ns	1.065	<0.001	0.658
131.083	11.4	* Ornithine	<0.001	4.774	<0.001	3.573	ns	1.001	<0.001	0.749
132.030	15.2	* Aspartate	ns	1.091	<0.001	1.229	ns	1.055	<0.01	1.159
146.046	10.8	Glutamate	<0.001	0.608	<0.001	0.113	ns	0.999	<0.001	0.187
147.076	14.9	* Glutamine	<0.001	0.299	<0.001	0.503	<0.001	1.204	<0.001	1.906
173.104	24.6	* Arginine	<0.001	0.155	<0.001	0.004	ns	1.023	<0.05	0.026
188.057	14.4	* *N*-Acetyl-L-glutamate	<0.001	0.637	<0.001	0.146	<0.001	1.348	<0.001	0.313
89.107	15.4	** Putrescine	<0.001	2.339	<0.001	1.490	ns	1.051	<0.001	0.670
131.118	8.24	*N*-Acetylputrescine	<0.001	5.175	<0.001	1.603	ns	1.021	<0.001	0.316
146.165	26.2	** Spermidine	<0.001	2.354	ns	1.150	ns	1.127	<0.001	0.550
150.058	11.4	* Methionine	<0.001	0.422	<0.001	0.669	<0.01	1.127	<0.001	1.594
298.096	6.42	* 5′-Methylthioadenosine	0.003	1.92	ns	0.830	ns	0.839	<0.001	0.361
TCA cycle/glycolysis										
133.014	16.4	* Malate	<0.001	0.647	<0.001	0.238	<0.001	1.129	<0.001	0.418
145.014	15.9	* 2-Oxoglutarate	ns	0.972	<0.001	0.173	<0.001	1.217	<0.001	0.221
191.020	18.4	* Citrate	<0.001	2.207	<0.001	0.534	ns	1.098	<0.001	0.265
508.003	16.6	* ATP	<0.001	0.267	<0.001	0.118	ns	0.963	<0.001	0.415
Carnitine metabolism/fatty acid metabolism										
162.112	13.3	* Carnitine	<0.001	0.253	<0.001	0.164	ns	1.065	<0.001	0.676
204.123	11.0	* Acetylcarnitine	<0.001	0.273	<0.001	0.050	ns	1.016	<0.001	0.190
232.154	8.7	Butanoylcarnitine	<0.001	14.083	ns	1.992	ns	0.903	<0.001	0.131
664.117	14.3	* NAD+	<0.001	0.487	<0.001	0.135	<0.001	1.228	<0.001	0.336
Miscellaneous										
104.106	19.6	* Choline	<0.001	0.019	<0.001	0.231	<0.001	1.423	<0.001	7.270
166.086	10.0	* Phenylalanine	<0.001	0.381	<0.05	0.873	<0.01	1.157	<0.001	2.358
118.086	12.4	* Valine	<0.001	1.148	<0.01	2.257	<0.01	1.148	<0.001	2.257
120.065	14.3	* Threonine	<0.001	0.610	ns	0.948	<0.05	1.140	<0.001	1.704
88.040	14.7	* Alanine	ns	0.965	<0.001	0.385	ns	1.098	<0.001	0.442
179.056	17.1	* Hexose	<0.001	0.564	<0.001	0.364	<0.01	0.931	<0.001	0.605
195.051	13.7	* Gluconic acid	<0.001	0.559	<0.001	0.103	<0.001	0.837	<0.001	0.154
258.110	14.4	* Glycerophosphocholine	<0.001	0.020	<0.001	0.031	<0.001	1.529	<0.001	2.342

RT: retention time (in min); MR: melittin treated A2780CR cells; R: untreated A2780CR cells; MS: melittin treated A2780 cells; S: untreated A2780 cells; ns: non-significant.
* Retention time matches standard on ZIC-pHILIC column; ** Retention time matches standard on ZIC-HILIC column.

2.4. Assessment of Necrotic and Apoptotic Cell Death in A2780 and A2780CR Cells

LDH (lactate dehydrogenase) release in the medium is an enzymatic indicator that illustrates the breakdown of membrane integrity, apoptosis, or necrosis of a cell. A2780 and A2780CR cancer cells were incubated with increasing concentrations of melittin for 24 h and intracellular LDH release increased as a result of the breakdown of the cell or plasma membrane. The results suggest that compared to control cells (untreated cells), melittin produced an increase in LDH leakage when incubated with ovarian cancer cells at levels $\geq$6 μg/mL (Figure S4); the amount of LDH released appeared to be concentration-dependent in A2780, but not in A2780CR, cells. However, in comparison to staurosoporine, melittin did not induce high levels of caspase activity particularly at 6 h (Figure S5). This suggests that the mechanism of cell death promoted by melittin was via necrosis rather than apoptosis.

3. Discussion

In this study, untargeted metabolomics was performed in order to determine the effects of melittin on the metabolic output of A2780 and A2780CR ovarian cancer cell lines. The altered metabolites in both cells encompassed several pathways including those of lipid, amino acid, energy, and carbohydrate metabolism. In a previous study it was found that docetaxel, the chemotherapeutic agent used for treatment of ovarian cancer, caused significant metabolic changes in amino acid and carbohydrate metabolism in ovarian cancer cells (OVCAR-3) [31]. In addition, recent metabolomics based studies in ovarian cancer cells have demonstrated that gossypol decreases cellular levels of glutathione (GSH), aspartic acid, and flavin adenine dinucleotide (FAD) [32]. Thus, the results obtained with melittin in this study add to the growing body of evidence regarding the utility of metabolomics as a tool for evaluating metabolic alterations in cancer cells induced by various agents. However, while there have been some previous metabolomics studies on the comparison between platinum-sensitive and resistant ovarian cancer cell lines [3], and between effects of nicotinamide phosphoribosyltransferase on ovarian and colorectal cancers [33], this is the first metabolomics-based study to evaluate the effects of melittin on human ovarian cancer cell lines as a potential anticancer therapeutic agent.

The overall impression is that the cisplatin-sensitive cells exhibit a much stronger metabolic response to melittin treatment than the resistant cells, possibly indicating a greater capacity of the former cell line to neutralise the effects of melittin given its higher IC_{50} value against this cell line. In particular, the levels of several amino acids including proline, pyrroline-3-hydroxy-5-carboxylate, glutamate, glutamate-5-semialdehyde, *N*-acetyl-L-glutamate, and arginine were all markedly decreased in A2780 cells following melittin exposure. In a previous study by Poisson et al. (2015) to compare the metabolic profiles of untreated cisplatin-resistant and sensitive cell lines [3], arginine was found to be significantly higher in the latter. In contrast, our study shows that arginine was higher in the resistant compared to sensitive cell lines both pre- and post-treatment with melittin. However, it should be noted that the Poisson et al. study [3] compared the sensitive A2780 cells with C200, a different cisplatin resistant cell line from the one used in the current study. Thus, our findings suggest that the A2780CR cell line contains more arginine than both the cisplatin sensitive A2780 and cisplatin-resistant C200 cell lines and, unlike in A2780 cells where it is lowered, the arginine level in A2780CR cells is unperturbed by treatment with melittin. In correspondence to lower levels of intermediates in the arginine pathway, ornithine, putrescine, *N*-acetylputrescine and spermidine were all upregulated suggesting that the levels of arginine and its precursors are lower in the A2780 cells since they are being directed towards polyamine biosynthesis. The lower level of methionine in these cells correlates with an increased requirement for it in the biosynthesis of spermidine. High levels of polyamines have been linked to high rates of cell proliferation. Treatment of the sensitive cells with melittin results in an almost complete depletion of arginine within the cells and further lowering of arginine precursors. The lack of arginine as a precursor appears to result in a fall in the level of ornithine and polyamines within the cells although the levels still remain higher than those in

the resistant cells and methionine is higher after treatment suggesting that the requirement for it in spermidine biosynthesis is reduced because of the depletion of spermidine. Polyamine metabolism in the resistant cells remains unaffected by melittin. Polyamines are known to act to stabilise membranes through interaction with phospholipid head groups [34]. It has been speculated that polyamines stabilise membrane flow, which involves fusion between the plasma membrane and Golgi derived vesicles [35,36]. The resistant cells contain higher levels of arginine and lower levels of polyamines suggesting a slower rate of biosynthesis of polyamines from arginine in these cells. Treatment of the resistant cells with melittin does not affect the levels of either the polyamines or arginine to any great extent. If the hypothesis regarding the role of polyamines in stabilising membrane flow is true, then it is possible that the lower levels of polyamines might result in reduced capability in these cells to repair membrane damage caused by melittin. In addition there is a link between polyamine depletion and the inhibition of apoptotic cell death [37]. This further underlines possible differences in the mechanism of cell death between these two cell lines.

The A2780 cells have lower levels of ATP both before and after melittin treatment in comparison with the A2780CR cells. The Biolog data also indicates lower levels of glycolysis in the A2780 cells in comparison with the A2780CR cells. Since ATP generation in cancer cells is primarily from glycolysis as opposed to oxidative phosphorylation, even under normoxic conditions [38], the observed effect implies that glycolysis may be a potential target for melittin as an anticancer agent. The strong dependence of cancer cells on glycolysis could be the basis for melittin's selective toxicity against them [13–19]. On the other hand, levels of ATP in A2780CR cells were higher than in A2780 at the outset and were not greatly affected by melittin treatment. The Biolog data also suggested a smaller effect of melittin on ATP production in A2780CR cells since the production of NADH by the cells was much less affected by melittin treatment than in the case of the A2780 cells. ATP levels have been linked to the capability of cells to undergo apoptotic as opposed to necrotic cell death and this suggests that the A2780CR cells may be undergoing apoptotic cell death in response to melittin whereas the A2780 cells may be undergoing necrotic cell death. However, the effect of melittin on caspase levels does not support this. In our study, we found that melittin inhibited glycolysis in A2780 cells by reducing the level of NAD+, but this biomarker was increased in A2780CR cells. Cancer cells require increased NAD+ biosynthesis to support anabolic metabolism, to sustain signalling processes including sirtuin activity and ADP-ribosylation, and to maintain a redox balance. Accordingly, inhibitors of nicotinamide phosphoribosyltransferase (NamPT), the enzyme that catalyses the rate-limiting step in NAD+ biosynthesis, have been shown to possess moderate anti-tumour activity in monotherapy both in vitro and in vivo [39]. The peptide toxin ricin was found to promote apoptosis by decreasing both ATP and NAD levels in U937 cells [40] although it was proposed that necrotic mechanisms might also be operating.

Levels of choline, methionine, phenylalanine, valine and threonine observed were raised in both cell lines when treated with melittin and they were significantly higher in A2780 cells. These findings resemble those from a previous study in which the levels of phenylalanine and methionine were elevated in A2780 and HCT-116 (colorectal cancer) cell lines following treatment with FK866, a small molecule inhibitor of NamPT [41]. However, the levels of metabolic intermediates of the TCA cycle, such as citrate, 2-oxoglutarate, and malate were decreased in A2780 cells by melittin, but they were increased in A2780CR. Some recent studies have demonstrated higher levels of TCA cycle intermediates (including succinate, fumarate, and malate) observed in tissue samples from ovarian carcinoma without treatment [42–44] and our study shows as well that there are significant differences in citrate and malate levels in the untreated cells (negative controls) in which malate is decreased and citrate is increased in A2780 relative to A2780CR cells respectively. However, the previously mentioned study by Poisson et al. did not find significant differences in TCA cycle metabolites between untreated platinum-sensitive (A2780) and resistant (C200) cells [3], suggesting that the A2780CR cell line has relatively specific distinctions in its metabolome. Some acyl carnitines were also found to respond to melittin treatment in A2780, but not in A2780CR cells. The dose-dependent decreases in *L*-carnitine,

acetylcarnitine and butanoylcarnitine levels in A2780 cells after melittin exposure might be explained based on cell-specific alteration of metabolic pathways. Carnitine serves an important role in the regulation of energy production from fatty acids and glucose at the cellular level. It is involved in the transport of long-chain fatty acids across the inner mitochondrial membrane, as well as facilitating chain-shorted acyl group transportation from the peroxisomes, where they are produced, to the mitochondria for further energy metabolism [45].

There are some significant differences in the lipid composition between A2780 cells and A2780CR cells. Several sphingomyelin (SM) lipids are higher in the A2780 cells in comparison to the A2780CR cells. This differs from previous reports of increased ceramide lipids, particularly glucosylceramides and galactosylceramides, in multidrug resistant ovarian cancer cells [46] and breast cancer cells [47]. However, in these previous studies ceramides or glycosylceramides were measured rather than sphingomyelin lipids. In common with Veldman et al. [46], we have observed lower levels of lactosylceramide in the resistant cells. It has also been previously reported that ether lipids are elevated in vinblastine-resistant human leukaemic lymphoblasts compared with sensitive cells [48], although in the current case many ether lipids are elevated in the cisplatin-sensitive cells and lowered in the resistant ones. Ether lipids increase membrane impermeability due to their ability to form hydrogen bonds with cholesterol and their resistance to hydrolysis by phospholipases [48].

The presence of lower levels of many lipids in the resistant cells, particularly those lipids whose function involves promoting membrane stability, suggests that cisplatin resistance in this cell line is unconventional. Cisplatin, a polar drug, does not cross cell membranes by passive diffusion but via action of organic cation transporters of which several have been identified [49]. Thus, it is possible that cisplatin resistance could be mediated through mechanisms other than augmentation of membrane lipids. This possibility is supported by two of our findings which suggest that melittin, an agent known to destabilise cell membranes, was more active on the cisplatin resistant compared to cisplatin sensitive cells, and that polyamines were higher in the sensitive cells. Both observations further illustrate the fact that the A2780 cell line had a more stable cell membrane. Why membrane stability of the A2780 cells would make them more vulnerable to cisplatin still remains unclear.

Following treatment with melittin, lipids were significantly altered in both A2780 and A2780CR cells although the fold changes are quite small. The observed effect was much more marked in the cisplatin-sensitive cells, where there was a larger number of lipids significantly decreased, suggesting that the latter undergo much more extensive membrane re-modelling in response to melittin in comparison with the resistant cells.

4. Materials and Methods

4.1. Cell Lines and Cultures

The cisplatin-sensitive (A2780) and resistant (A2780CR) human ovarian carcinoma cells were obtained from ECACC (Porton Down, Salisbury, UK) and maintained at 75×10^4 cells/mL in RPMI 1640 medium (Lonza, Verviers, Belgium) supplemented with 1% (*v*/*v*) *L*-glutamine (Invitrogen, Paisley, UK), 100 IU/mL/100 µg/mL penicillin/streptomycin (Invitrogen, Paisley, UK), and 10% (*v*/*v*) foetal bovine serum (FBS) (Life Technologies, Carlsbad, CA, USA). In addition, the cultures for the A2780CR cells contained 1 µM cisplatinum (Tocris Bioscience, Bristol, UK) in the first three passages. Sub-confluent cultures were split by trypsinisation every 4–5 days and maintained at 37 °C in a humidified atmosphere saturated with 5% CO_2.

4.2. Cell Viability Assay against Melittin

Melittin was purified from bee venom (supplied by Beesen Co. Ltd., Dae Jeon, Korea) by reversed phase liquid chromatography [50] and reconstituted in sterile water to form a stock solution of 1 mg/mL before storage at −20 °C until required for analysis. Cell viability was assessed by an Alamar® Blue (AB) cell viability reagent (Thermo Fisher Scientific, Loughborough, UK). Both A2780

and A2780CR cells were seeded at 1×10^4 cells/well in 96-well plates (Corning®, Sigma-Aldrich, Dorset, UK) and incubated at 37 °C and 5% CO_2 in a humidified atmosphere for 24 h. After this incubation period, the cells were treated with various concentrations of melittin ranging from 0.5 to 14 µg/mL in 100 µL of medium, and re-incubated at 37 °C and 5% CO_2 for a further 24 h. Triton X at 1% (*v*/*v*) and cell culture media were used as positive and negative controls, respectively. After this, AB was added at a final concentration of 10% (*v*/*v*) and the resultant mixture was incubated for a further 4 h at 37 °C and 5% CO_2. Then, the plates were read at an excitation wavelength of 560 nm and the emission at 590 nm was recorded on a SpectraMax M3 microplate reader (Molecular Devices, Sunnyvale, CA, USA). Background-corrected fluorescence readings were converted to cell viability data for each test well by expressing them as percentages relative to the mean negative control value.

4.3. Determination of IC_{50}

GraphPad Prism for Windows (version 5.00, GraphPad Software, San Diego, CA, USA) was employed to produce dose-response curves by performing nonlinear regression analysis of the cell viability data. The mean inhibitory concentration (IC_{50}) values were calculated from at least three measurements of independent experiments ($n = 3$).

4.4. Determination of Effect of Melittin on Cell Metabolomes

The A2780 and A2780CR cell lines were separately treated with melittin at concentrations of 6.8 and 4.5 µg/mL respectively for 24 h ($n = 5$). The cells were seeded at 75×10^4 cells/mL in T-25 cell culture flasks and incubated for 1 doubling time (48 h) before treatment with the melittin and incubation for an additional 24 h. After the treatment, the medium was removed and the cells were washed twice with 3 mL of phosphate-buffered saline (PBS) at 37 °C before lysis. Cell lysates were prepared by extraction with ice cold methanol:acetonitrile:water (50:30:20) (1 mL per 2×10^6 cells). Lipids were extracted with isopropanol (4 °C) (Sigma-Aldrich, Dorset, UK). The cells were scraped and cell lysates mixed on a Thermo mixer at 1440 rotations per minute (r.p.m.) for 12 min at 4 °C, before being centrifuged at 13,500 r.p.m. for 15 min at 0 °C. The supernatants were collected and transferred into HPLC vials for LC-MS analysis. During the analysis, the temperature of the autosampler was maintained at 4 °C. Mixtures of authentic standard metabolites (Sigma-Aldrich, Dorset, UK), prepared as previously described [51], and the pooled quality control (QC) sample, were injected in each analysis run in order to facilitate identification and to evaluate the stability and reproducibility of the analytical method, respectively. The pooled QC sample was obtained by taking equal aliquots from all the samples and placing them into the same HPLC vial.

4.5. Optimisation of Phenotype Microarray Experiment Parameters

(1) A2780 and A2780CR cells were cultured in a 75 cm^2 culture flask containing 10 ml RPMI-1640 medium lacking phenol red but containing 5% (*v*/*v*) FBS, *L*-glutamine and Pen/Strep (Gibco™ by Life Technologies, Paisley, UK).

(2) The medium was removed from the culture flask and saved in a 15 mL sterile conical tube. The remaining medium was aspirated and discarded from the culture flask. The adherent cells were washed twice with 10 mL of Dulbecco's Phosphate-Buffered Saline (D-PBS) (Gibco, Paisley, UK) and any remaining D-PBS was aspirated and discarded.

(3) The cells were then detached by adding 2 mL of 0.25 % (*v*/*v*) Trypsin-EDTA (Gibco, Paisley, UK) and incubated at 37 °C for 3 min.

(4) Then, 3 mL of culture medium was taken from the 15 mL conical tube was added to quench the detachment reaction and the cell suspension mixed by gently pipetting up and down several times to disperse the cells.

(5) The cells were harvested by transferring the cell suspension to the 15 mL conical tube containing the culture medium and centrifuged at 350× *g* for 5 min. After centrifugation, the medium was

aspirated and 10 mL of D-PBS was added. After that, the cell pellet was suspended in the D-PBS by pipetting up and down several times, then centrifuged again at 350× *g* for 5 min.

(6) After the second centrifugation, the medium was aspirated and 10 mL of pre-warmed MC-0 was added. The cell pellet in the MC-0 Assay Medium was suspended by pipetting up and down several times. The MC-0 medium was composed of IF-M1 (Technopath Distribution, Tipperary, Ireland) medium supplemented with 5.3% (*v*/*v*) dialysed foetal bovine serum (dFBS) (Gibco™ by Life Technologies, Paisley, UK), 1.1% of 100× Pen/Strep solution (Gibco™ by Life Technologies, Paisley, UK), and 0.16% (*v*/*v*) of 200 mM glutamine (final concentration 0.3 mM).

(7) The cell number was determined and cell viability was assessed by trypan blue dye exclusion (Sigma-Aldrich, Dorset, UK).

(8) The cells were suspended in enough MC-0 Assay Medium to fill the selected number of PM panels and to achieve a density of 4×10^5 cells/mL.

(9) After that, 50 µL/well of the cell suspension was added on two sets of PM-M1 plates (Technopath Distribution, Tipperary, Ireland) so that each well had 20,000 cells. The first one was used as the control set, where untreated A2780 and A2780CR were cultured. A2780 and A2780CR seeded in the second set of plates were exposed to melittin. Both sets of PMs containing A2780 and A2780CR were first incubated for 24 h to allow cells to catabolise all nutrients in medium MC-0. The treated cells set was subsequently inoculated with 25 µL of Melittin/well of three PM-M1 plates at IC_{50} concentration, while 25 µL of MC-0 medium was added to each well in the control set of three PM-M1 plates.

(10) Then, the PM plates were incubated at 37 °C in a humidified atmosphere with 95% Air-5% CO_2 for 18 h, after which the Biolog Redox Dye Mix MA was added to all wells (15 µL/well to the plate). The plate was sealed with tape to prevent off-gassing of CO_2.

(11) The plates were incubated for an additional 6 h with Biolog Redox Dye Mix MA (Technopath Distribution, Tipperary, Ireland).

(12) Tetrazolium reduction was determined with a microplate reader (SpectraMax M3, Molecular Devices, Sunnyvale, CA, USA). The endpoint read was performed at 590 nm with subtraction of a 750 nm reference reading (A590-750) which corrects for any background light scattering.

4.6. LC-MS Conditions

Liquid chromatographic separation was carried out on an Accela HPLC system interfaced to an Exactive Orbitrap mass spectrometer (Thermo Fisher Scientific, Bremen, Germany) using a hydrophilic interaction liquid chromatography (HILIC) column (ZICp-HILIC, 150 × 4.6 mm, 5 µm particle size) supplied by Hichrom Ltd. (Reading, UK). Since chromatographic separation of polyamines is poor on a ZIC-pHILIC column [51], a ZIC-HILIC column (150 × 4.6 mm, 5 µm particle size), supplied by Hichrom Ltd. (Reading, UK) was employed for the determination of putrescine and spermidine in the samples. The mobile phase for ZIC-pHILIC consisted of 20 mM ammonium carbonate (Sigma-Aldrich, Dorset, UK) in water purified by Direct-Q 3 Ultrapure water purification system (Millipore, Watford, UK) at pH 9.2 (solvent A) and acetonitrile (Sigma-Aldrich, Dorset, UK) (solvent B) at a flow rate of 0.3 mL/min. The elution gradient was an A:B ratio of 20:80 at 0 min, 80:20 at 30 min, 92:8 at 35 min and finally 20:80 at 45 min as described previously [52]. In the case of the ZIC-HILIC column, the mobile phase was 0.1% (*v*/*v*) formic acid in water (A) and 0.1% (*v*/*v*) formic acid in acetonitrile (B) with a gradient of A:B 50:50 at 0 min, 95:5 from 20–30 min, and 50:50 from 31–36 min. The nitrogen sheath and auxiliary gas flow rates were maintained at 50 and 17 mL/min. The electrospray ionisation (ESI) interface was operated in a positive/negative dual polarity mode. The spray voltage was 4.5 kV for positive mode and 4.0 kV for negative mode, while the ion transfer capillary temperature was 275 °C. Full scan data were obtained in the mass-to-charge ratio (*m*/*z*) range of 75 to 1200 for both ionisation modes with settings of AGC target and resolution as Balanced (1E6) and High (50,000) respectively. Mass calibration was performed for both positive and negative ESI polarities before the analysis using the standard Thermo Calmix solution (Thermo Fisher Scientific, Bremen, Germany) with additional

coverage of the lower mass range with signals at m/z 83.0604 (2 × ACN + H) for the positive and m/z 91.0037 (2 × $HCOO^-$) for the negative modes respectively. The resulting data were recorded using the XCalibur 2.1.0 software package (Thermo Fisher Scientific, Bremen, Germany). Analysis of lipids was carried out on an ACE silica gel column (150 × 4.6 mm, 3 µm, Hichrom, Reading, UK) as described previously [52].

4.7. Data Extraction and Analysis

Data extraction for each of the samples was carried out by MZmine-2.10 software [53,54]. The extracted ions, with their corresponding m/z values and retention times, were pasted into an Excel macro of the most common metabolites prepared in–house to facilitate identification, and a library search was also carried out against accurate mass data of the metabolites in the Human Metabolome, KEGG, and Metlin databases. The lists of the metabolites obtained from these searches were then carefully evaluated manually by considering the quality of their peaks and their retention time match with the standard metabolite mixtures run in the same sequence. All metabolites were within 3 ppm of their exact masses. Statistical analyses were performed using both univariate and multivariate approaches. The p-values from univariate analyses were adjusted using the Bonferroni correction and differences in the levels (or peak areas) of the metabolites between treated and control cells were considered significant at $p < 0.05$. SIMCA-P software version 14.0 (Umetrics, Crewe, UK) was used for unsupervised multivariate analysis of the metabolite data with Pareto scaling prior to principal component (PCA) and hierarchical clustering (HCA) analyses.

4.8. LDH Assay

The cytotoxicity of the melittin was determined by the lactate dehydrogenase (LDH) release assay on A2780 and A2780CR cells. LDH release into the medium is due to the loss of membrane integrity either due to apoptosis or necrosis. Briefly, A2780 and A2780CR cells were seeded at 1×10^4 cells/well in 96-well plates and incubated at 37 °C and 5% CO_2 in a humidified atmosphere for 24 h. The cells were treated with different concentrations of the melittin for 24 h. Then, the supernatant (50 µL) of the treated cells was transferred into 96-well flat-bottomed plates, and 50 µL of the LDH reaction mix (Lactate Dehydrogenase Activity Assay Kit, MAK066, Sigma-Aldrich, Dorset, UK) was added for 30 min. Finally, the intensity of orange colour in the samples indicating the LDH activity was measured at 490 nm. LDH release increased in a dose-dependent manner in melittin treated A2780 and A2780CR cells compared with untreated cells. The values are represented as the means ± SD of three separated experiments.

4.9. Caspase Activity Assay

Fluorometric assays of caspase activity were carried out by using the substrate Ac-DEVD-AMC (BD Pharmingen, San Diego, CA, USA) for caspase-3. Both A2780 and A2780CR cells were seeded at 1×10^4 cells/well in costar 96-well black plates and incubated at 37 °C and 5% CO_2 in a humidified atmosphere for 24 h. Then, the cells were treated for 6 and 24 h with different concentrations of melittin to measure caspase-3 activity. Staurosporine (Sigma-Aldrich, Dorset, UK) was used to induce apoptosis at a concentration of 10 µM. The control cells were treated with media alone. The caspase-3 assay buffer was prepared as described previously [55]. The caspase-3 assay buffer (3×) was added to each well and incubated at 37 °C in 5% CO_2 for 1 h. Fluorescence was measured at 360 nm (excitation) and 460 nm (emission) using a Spectramax M3 microplate reader. The average fluorescence values of the background were subtracted from the fluorescence values of experimental wells. Statistical analysis was done using one-way ANOVA followed by Bonferroni's Multiple Comparison test.

5. Conclusions

In conclusion, this study shows that the cisplatin sensitive A2780 cells contain relatively higher levels of ether lipids and polyamines, which might result in increased membrane stability and

repair and thus resistance to the lytic action of melittin in comparison with the cisplatin resistant A2780CR cells. After exposure to melittin, the levels of most of the significantly altered metabolites, particularly amino acids and TCA cycle intermediates, were lower in A2780 compared to A2780CR cells, suggesting different metabolic responses in the two cell lines. The large increases in choline and glycerophosphocholine in A2780 cells may be related to increased de novo lipid synthesis and re-direction of cellular metabolism. Thus, analysis of the full lipidome could offer a more valuable insight. Given that melittin interacts with cell membranes, the observed effects might suggest that the membranes are less adaptable in the cisplatin resistant cells compared to the sensitive ones. Over all, this study shows that a LC-MS based metabolomics approach for the assessment of drug effects in vitro provides a powerful tool for obtaining insights into the mechanism of action of potential therapeutic agents, while offering the possibility to identify key metabolite markers for in vivo monitoring of tumour responsiveness to standard chemotherapy. Melittin might serve as a valuable adjuvant in cancer chemotherapy for overcoming chemoresistance.

Supplementary Materials: The following are available online at http://www.mdpi.com/2218-1989/6/4/35/s1, Table S1: Differences in the top 50 lipids between A2780 cells and A2780CR cells before and after melittin treatment, Figure S1: Cell viability determined following treatment with cisplatin for 24 h (A) IC_{50} = 10.8 μg/mL A2780CR; (B) IC_{50} = 4.9 μg/mL A2780. Figure S2: Layout of carbon sources in the wells on the PM-M1 microplate, Figure S3: Changes in the metabolism of ovarian cancer A2780 and A2780CR cells, Figure S4: Lactate dehydrogenase (LDH) assay, Figure S5: Effect of Melittin on caspase-3 activity in A2780 and A2780CR cells.

Acknowledgments: Sanad Alonezi is funded by the government of Saudi Arabia (Armed Forces Medical Services Ministry of Defence). Jonans Tusiimire and Jennifer Wallace are both funded by Beesen Co. Ltd. (Dae Jeon, Korea) through a partnership between Strathclyde University and Korea Institute for Advancement of Technology (KIAT).

Author Contributions: David G. Watson conceived the project; Jonans Tusiimire, David G. Watson, Jennifer Wallace, John A. Parkinson and Mark J. Dufton purified and characterized the melittin; Sanad Alonezi, Carol J. Clements and Louise C. Young performed the biological assays and analyzed the data; Sanad Alonezi, Jonans Tusiimire and David G. Watson performed LC-MS experiments and analyzed the data; Jin Kyu Park and Jong Woon Jeon supplied the crude bee venom and provided preliminary scientific input; Sanad Alonezi, Jonans Tusiimire, John A. Parkinson, Valerie A. Ferro and David G. Watson wrote and edited the manuscript. All authors have read and approved the final manuscript.

Conflicts of Interest: The authors declare no conflict of interest.

References

1. Vermeersch, K.A.; Styczynski, M.P. Applications of metabolomics in cancer research. *J. Carcinog.* **2013**, *12*, 9. [PubMed]
2. Vander Heiden, M.G.; Cantley, L.C.; Thompson, C.B. Understanding the Warburg effect: The metabolic requirements of cell proliferation. *Science* **2009**, *324*, 1029–1033. [CrossRef] [PubMed]
3. Poisson, L.M.; Munkarah, A.; Madi, H.; Datta, I.; Hensley-Alford, S.; Tebbe, C.; Buekers, T.; Giri, S.; Rattan, R. A metabolomic approach to identifying platinum resistance in ovarian cancer. *J. Ovarian Res.* **2015**, *8*. [CrossRef] [PubMed]
4. Wang, D.; Lippard, S.J. Cellular processing of platinum anticancer drugs. *Nat. Rev. Drug Discov.* **2005**, *4*, 307–320. [CrossRef] [PubMed]
5. Matsuo, K.; Eno, M.L.; Im, D.D.; Rosenshein, N.B.; Sood, A.K. Clinical relevance of extent of extreme drug resistance in epithelial ovarian carcinoma. *Gynecol. Oncol.* **2010**, *116*, 61–65. [CrossRef] [PubMed]
6. Zwelling, L.A.; Kohn, K.W. Mechanism of action of cis-dichlorodiammineplatinum (II). *Cancer Treat. Rep.* **1978**, *63*, 1439–1444.
7. Siddik, Z.H. Cisplatin: Mode of cytotoxic action and molecular basis of resistance. *Oncogene* **2003**, *22*, 7265–7279. [CrossRef] [PubMed]
8. Galluzzi, L.; Senovilla, L.; Vitale, I.; Michels, J.; Martins, I.; Kepp, O.; Castedo, M.; Kroemer, G. Molecular mechanisms of cisplatin resistance. *Oncogene* **2012**, *31*, 1869–1883. [CrossRef] [PubMed]
9. Mandic, A.; Hansson, J.; Linder, S.; Shoshan, M.C. Cisplatin induces endoplasmic reticulum stress and nucleus-independent apoptotic signaling. *J. Biol. Chem.* **2003**, *278*, 9100–9106. [CrossRef] [PubMed]
10. Rabik, C.A.; Dolan, M.E. Molecular mechanisms of resistance and toxicity associated with platinating agents. *Cancer Treat. Rev.* **2007**, *33*, 9–23. [CrossRef] [PubMed]

11. Byun, S.S.; Kim, S.W.; Choi, H.; Lee, C.; Lee, E. Augmentation of cisplatin sensitivity in cisplatin-resistant human bladder cancer cells by modulating glutathione concentrations and glutathione-related enzyme activities. *BJU Int.* **2005**, *95*, 1086–1090. [CrossRef] [PubMed]
12. Jeong, Y.-J.; Choi, Y.; Shin, J.-M.; Cho, H.-J.; Kang, J.-H.; Park, K.-K.; Choe, J.-Y.; Bae, Y.-S.; Han, S.-M.; Kim, C.-H. Melittin suppresses EGF-induced cell motility and invasion by inhibiting PI3K/Akt/mTOR signaling pathway in breast cancer cells. *Food Chem. Toxicol.* **2014**, *68*, 218–225. [CrossRef] [PubMed]
13. Kohno, M.; Horibe, T.; Ohara, K.; Ito, S.; Kawakami, K. The Membrane-Lytic Peptides K8L9 and Melittin Enter Cancer Cells via Receptor Endocytosis following Subcytotoxic Exposure. *Chem. Biol.* **2014**, *21*, 1522–1532. [CrossRef] [PubMed]
14. Mahmoodzadeh, A.; Morady, A.; Zarrinnahad, H.; Ghasemi-Dehkordi, P.; Mahdavi, M.; Shahbazzadeh, D.; Shahmorady, H. Isolation of melittin from bee venom and evaluation of its effect on proliferation of gastric cancer cells. *Tehran Univ. Med. Sci.* **2013**, *70*, 760–767.
15. Mahmoodzadeh, A.; Zarrinnahad, H.; Bagheri, K.P.; Moradia, A.; Shahbazzadeh, D. First report on the isolation of melittin from Iranian honey bee venom and evaluation of its toxicity on gastric cancer AGS cells. *J. Chin. Med. Assoc.* **2015**, *78*, 574–583. [CrossRef] [PubMed]
16. Jo, M.; Park, M.H.; Kollipara, P.S.; An, B.J.; Song, H.S.; Han, S.B.; Kim, J.H.; Song, M.J.; Hong, J.T. Anti-cancer effect of bee venom toxin and melittin in ovarian cancer cells through induction of death receptors and inhibition of JAK2/STAT3 pathway. *Toxicol. Appl. Pharmacol.* **2012**, *258*, 72–81. [CrossRef] [PubMed]
17. Liu, M.; Zong, J.; Liu, Z.; Li, L.; Zheng, X.; Wang, B.; Sun, G. A novel melittin-MhIL-2 fusion protein inhibits the growth of human ovarian cancer SKOV3 cells in vitro and in vivo tumor growth. *Cancer Immunol. Immunother.* **2013**, *62*, 889–895. [CrossRef] [PubMed]
18. Qian, C.-Y.; Wang, K.-L.; Fang, F.-F.; Gu, W.; Huang, F.; Wang, F.-Z.; Li, B.; Wang, L.-N. Triple-controlled oncolytic adenovirus expressing melittin to exert inhibitory efficacy on hepatocellular carcinoma. *Int. J. Clin. Exp. Pathol.* **2015**, *8*, 10403. [PubMed]
19. Wu, X.; Zhao, B.; Cheng, Y.; Yang, Y.; Huang, C.; Meng, X.; Wu, B.; Zhang, L.; Lv, X.; Li, J. Melittin induces PTCH1 expression by down-regulating MeCP2 in human hepatocellular carcinoma SMMC-7721 cells. *Toxicol. Appl. Pharmacol.* **2015**, *288*, 74–83. [CrossRef] [PubMed]
20. Oh, S.-B.; Hwang, C.J.; Song, S.-Y.; Jung, Y.Y.; Yun, H.-M.; Sok, C.H.; Sung, H.C.; Yi, J.-M.; Park, D.H.; Ham, Y.W. Anti-cancer effect of tectochrysin in NSCLC cells through overexpression of death receptor and inactivation of STAT3. *Cancer Lett.* **2014**, *353*, 95–103. [CrossRef] [PubMed]
21. Gajski, G.; Garaj-Vrhovac, V. Melittin: A lytic peptide with anticancer properties. *Environ. Toxicol. Pharmacol.* **2013**, *36*, 697–705. [CrossRef] [PubMed]
22. Shin, J.-M.; Jeong, Y.-J.; Cho, H.-J.; Park, K.-K.; Chung, I.-K.; Lee, I.-K.; Kwak, J.-Y.; Chang, H.-W.; Kim, C.-H.; Moon, S.-K. Melittin suppresses HIF-1α/VEGF expression through inhibition of ERK and mTOR/p70S6K pathway in human cervical carcinoma cells. *PLoS ONE* **2013**, *8*, e69380. [CrossRef] [PubMed]
23. Zhang, T.; Watson, D.G.; Wang, L.; Abbas, M.; Murdoch, L.; Bashford, L.; Ahmad, I.; Lam, N.Y.; Ng, A.C.; Leung, H.Y. Application of Holistic Liquid Chromatography-High Resolution Mass Spectrometry Based Urinary Metabolomics for Prostate Cancer Detection and Biomarker Discovery. *PLoS ONE* **2013**, *8*, e65880. [CrossRef] [PubMed]
24. Zhang, T.; Watson, D.G. A short review of applications of liquid chromatography mass spectrometry based metabolomics techniques to the analysis of human urine. *Analyst* **2015**, *140*, 2907–2915. [CrossRef] [PubMed]
25. Zhang, R.; Zhang, T.; Ali, A.M.; Al Washih, M.; Pickard, B.; Watson, D.G. Metabolomic Profiling of Post-Mortem Brain Reveals Changes in Amino Acid and Glucose Metabolism in Mental Illness Compared with Controls. *Comput. Struct. Biotechnol. J.* **2016**, *14*, 106–116. [CrossRef] [PubMed]
26. Frezza, C.; Zheng, L.; Tennant, D.A.; Papkovsky, D.B.; Hedley, B.A.; Kalna, G.; Watson, D.G.; Gottlieb, E. Metabolic profiling of hypoxic cells revealed a catabolic signature required for cell survival. *PLoS ONE* **2011**, *6*, e24411. [CrossRef] [PubMed]
27. Beger, R.D. A review of applications of metabolomics in cancer. *Metabolites* **2013**, *3*, 552–574. [CrossRef] [PubMed]
28. Griffin, J.L.; Shockcor, J.P. Metabolic profiles of cancer cells. *Nat. Rev. Cancer* **2004**, *4*, 551–561. [CrossRef] [PubMed]
29. Čuperlović-Culf, M.; Barnett, D.A.; Culf, A.S.; Chute, I. Cell culture metabolomics: Applications and future directions. *Drug Discov. Today* **2010**, *15*, 610–621. [CrossRef] [PubMed]

30. Bochner, B.R.; Siri, M.; Huang, R.H.; Noble, S.; Lei, X.H.; Clemons, P.A.; Wagner, B.K. Assay of the multiple energy-producing pathways of mammalian cells. *PLoS ONE* **2011**, *6*, e18147. [CrossRef] [PubMed]
31. Vermeersch, K.A.; Wang, L.; McDonald, J.F.; Styczynski, M.P. Distinct metabolic responses of an ovarian cancer stem cell line. *BMC Syst. Biol.* **2014**, *8*. [CrossRef] [PubMed]
32. Wang, J.; Jin, L.; Li, X.; Deng, H.; Chen, Y.; Lian, Q.; Ge, R.; Deng, H. Gossypol induces apoptosis in ovarian cancer cells through oxidative stress. *Mol. BioSyst.* **2013**, *9*, 1489–1497. [CrossRef] [PubMed]
33. Sasada, S.; Miyata, Y.; Tsutani, Y.; Tsuyama, N.; Masujima, T.; Hihara, J.; Okada, M. Metabolomic analysis of dynamic response and drug resistance of gastric cancer cells to 5-fluorouracil. *Oncol. Rep.* **2013**, *29*, 925–931. [PubMed]
34. Schuber, F. Influence of polyamines on membrane functions. *Biochem. J.* **1989**, *260*, 1–10. [CrossRef] [PubMed]
35. Moinard, C.; Cynober, L.; de Bandt, J.-P. Polyamines: Metabolism and implications in human diseases. *Clin.Nutr.* **2005**, *24*, 184–197. [CrossRef] [PubMed]
36. Morré, D.J.; Kartenbeck, J.; Franke, W.W. Membrane flow and interconversions among endomembranes. *Biochim. Biophys. Acta Rev. Biomembr.* **1979**, *559*, 71–152. [CrossRef]
37. Seiler, N.; Raul, F. Polyamines and apoptosis. *J. Cell. Mol. Med.* **2005**, *9*, 623–642. [CrossRef] [PubMed]
38. Uetaki, M.; Tabata, S.; Nakasuka, F.; Soga, T.; Tomita, M. Metabolomic alterations in human cancer cells by vitamin C-induced oxidative stress. *Sci. Rep.* **2015**, *5*, 13896. [CrossRef] [PubMed]
39. Moore, Z.; Boothman, D.A. Tumor-specific targeting of the NAD metabolome with β-lapachone and NamPT inhibition. *Cancer Res.* **2014**, *74* (Suppl. S19). [CrossRef]
40. Komatsu, N.; Nakagawa, M.; Oda, T.; Muramatsu, T. Depletion of Intracellular NAD+ and ATP Levels during Ricin-Induced Apoptosis through the Specific Ribosomal Inactivation Results in the Cytolysis of U937 Cells. *J. Biochem.* **2000**, *128*, 463–470. [CrossRef] [PubMed]
41. Tolstikov, V.; Nikolayev, A.; Dong, S.; Zhao, G.; Kuo, M.-S. Metabolomics Analysis of Metabolic Effects of Nicotinamide Phosphoribosyltransferase (NAMPT) Inhibition on Human Cancer Cells. *PLoS ONE* **2014**, *9*, e114019. [CrossRef] [PubMed]
42. Ben Sellem, D.; Elbayed, K.; Neuville, A.; Moussallieh, F.M.; Lang-Averous, G.; Piotto, M.; Bellocq, J.P.; Namer, I.J. Metabolomic Characterization of Ovarian Epithelial Carcinomas by HRMAS-NMR Spectroscopy. *J. Oncol.* **2011**, *2011*, 174019. [CrossRef] [PubMed]
43. Denkert, C.; Budczies, J.; Kind, T.; Weichert, W.; Tablack, P.; Sehouli, J.; Niesporek, S.; Könsgen, D.; Dietel, M.; Fiehn, O. Mass spectrometry–based metabolic profiling reveals different metabolite patterns in invasive ovarian carcinomas and ovarian borderline tumors. *Cancer Res.* **2006**, *66*, 10795–10804. [CrossRef] [PubMed]
44. Halama, A.; Guerrouahen, B.S.; Pasquier, J.; Diboun, I.; Karoly, E.D.; Suhre, K.; Rafii, A. Metabolic signatures differentiate ovarian from colon cancer cell lines. *J. Transl. Med.* **2015**, *13*, 223. [CrossRef] [PubMed]
45. Zammit, V.A.; Ramsay, R.R.; Bonomini, M.; Arduini, A. Carnitine, mitochondrial function and therapy. *Adv. Drug Deliv. Rev.* **2009**, *61*, 1353–1362. [CrossRef] [PubMed]
46. Veldman, R.J.; Klappe, K.; Hinrichs, J.; Hummel, I.; van der Schaaf, G.; Sietsma, H.; Kok, J.W. Altered sphingolipid metabolism in multidrug-resistant ovarian cancer cells is due to uncoupling of glycolipid biosynthesis in the Golgi apparatus. *FASEB J.* **2002**, *16*, 1111–1113. [CrossRef] [PubMed]
47. Lavie, Y.; Cao, H.-T.; Bursten, S.L.; Giuliano, A.E.; Cabot, M.C. Accumulation of Glucosylceramides in Multidrug-resistant Cancer Cells. *J. Biol. Chem.* **1996**, *271*, 19530–19536. [CrossRef] [PubMed]
48. May, G.L.; Wright, L.C.; Dyne, M.; Mackinnon, W.B.; Fox, R.M.; Mountford, C.E. Plasma membrane lipid composition of vinblastine sensitive and resistant human leukaemic lymphoblasts. *Int. J. Cancer* **1988**, *42*, 728–733. [CrossRef] [PubMed]
49. Yonezawa, A.; Inui, K.-I. Organic cation transporter OCT/SLC22A and H+/organic cation antiporter MATE/SLC47A are key molecules for nephrotoxicity of platinum agents. *Biochem. Pharmacol.* **2011**, *81*, 563–568. [CrossRef] [PubMed]
50. Tusiimire, J.; Wallace, J.; Dufton, M.; Parkinson, J.; Clements, C.J.; Young, L.; Park, J.K.; Jeon, J.W.; Watson, D.G. An LCMS method for the assay of melittin in cosmetic formulations containing bee venom. *Anal. Bioanal. Chem.* **2015**, *407*, 3627–3635. [CrossRef] [PubMed]
51. Zhang, R.; Watson, D.G.; Wang, L.; Westrop, G.D.; Coombs, G.H.; Zhang, T. Evaluation of mobile phase characteristics on three zwitterionic columns in hydrophilic interaction liquid chromatography mode for liquid chromatography-high resolution mass spectrometry based untargeted metabolite profiling of Leishmania parasites. *J. Chromatogr. A* **2014**, *1362*, 168–179. [CrossRef] [PubMed]

52. Zheng, L.; T'Kind, R.; Decuypere, S.; von Freyend, S.J.; Coombs, G.H.; Watson, D.G. Profiling of lipids in Leishmania donovani using hydrophilic interaction chromatography in combination with Fourier transform mass spectrometry. *Rapid Commun. Mass Spectrom.* **2010**, *24*, 2074–2082. [CrossRef] [PubMed]
53. Pluskal, T.; Castillo, S.; Villar-Briones, A.; Oresic, M. MZmine 2: Modular framework for processing, visualizing, and analyzing mass spectrometry-based molecular profile data. *BMC Bioinform.* **2010**, *11*, 395. [CrossRef] [PubMed]
54. Katajamaa, M.; Orešič, M. Processing methods for differential analysis of LC/MS profile data. *BMC Bioinform.* **2005**, *6*, 179. [CrossRef] [PubMed]
55. Carrasco, R.A.; Stamm, N.B.; Patel, B.K. One-step cellular caspase-3/7 assay. *Biotechniques* **2003**, *34*, 1064–1067. [PubMed]

Supplementary Materials: Metabolomic Profiling of the Effects of Melittin on Cisplatin Resistant and Cisplatin Sensitive Ovarian Cancer Cells Using Mass Spectrometry and Biolog Microarray Technology

Sanad Alonezi, Jonans Tusiimire, Jennifer Wallace, Mark J. Dufton, John A. Parkinson, Louise C. Young, Carol J. Clements, Jin Kyu Park, Jong Woon Jeon, Valerie A. Ferro and David G. Watson

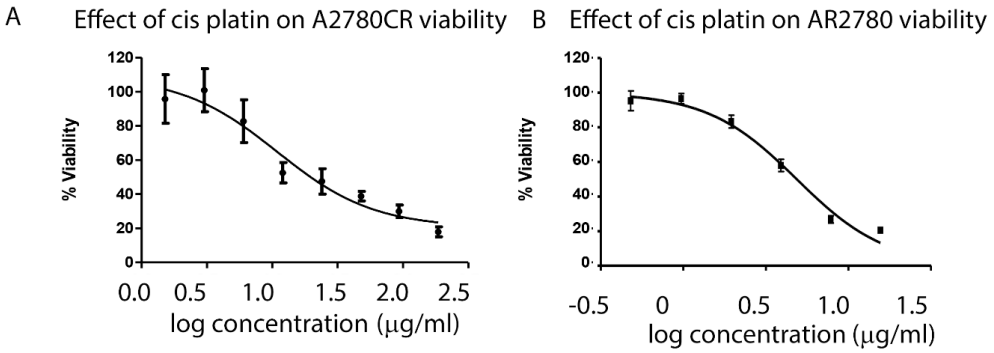

Figure S1. Cell viability was determined following treatment with cisplatin for 24 h (**A**) IC_{50} = 10.8 µg/mL A2780CR; (**B**) IC_{50} = 4.9 µg/mL A2780.

PM-M1 MicroPlate™ - Carbon and Energy Sources

A1 Negative Control	A2 Negative Control	A3 Negative Control	A4 α-Cyclodextrin	A5 Dextrin	A6 Glycogen	A7 Maltitol	A8 Maltotriose	A9 D-Maltose	A10 D-Trehalose	A11 D-Cellobiose	A12 β-Gentiobiose
B1 D-Glucose-6-Phosphate	B2 α-D-Glucose-1-Phosphate	B3 L-Glucose	B4 α-D-Glucose	B5 α-D-Glucose	B6 α-D-Glucose	B7 3-O-Methyl-D-Glucose	B8 α-Methyl-D-Glucoside	B9 β-Methyl-D-Glucoside	B10 D-Salicin	B11 D-Sorbitol	B12 N-Acetyl-D-Glucosamine
C1 D-Glucosaminic Acid	C2 D-Glucuronic Acid	C3 Chondroitin-6-Sulfate	C4 Mannan	C5 D-Mannose	C6 α-Methyl-D-Mannoside	C7 D-Mannitol	C8 N-Acetyl-β-D-Mannosamine	C9 D-Melezitose	C10 Sucrose	C11 Palatinose	C12 D-Turanose
D1 D-Tagatose	D2 L-Sorbose	D3 L-Rhamnose	D4 L-Fucose	D5 D-Fucose	D6 D-Fructose-6-Phosphate	D7 D-Fructose	D8 Stachyose	D9 D-Raffinose	D10 D-Lactitol	D11 Lactulose	D12 α-D-Lactose
E1 Melibionic Acid	E2 D-Melibiose	E3 D-Galactose	E4 α-Methyl-D-Galactoside	E5 β-Methyl-D-Galactoside	E6 N-Acetyl-Neuraminic Acid	E7 Pectin	E8 Sedoheptulosan	E9 Thymidine	E10 Uridine	E11 Adenosine	E12 Inosine
F1 Adonitol	F2 L- Arabinose	F3 D-Arabinose	F4 β-Methyl-D-Xylopyranoside	F5 Xylitol	F6 Myo-Inositol	F7 Meso-Erythritol	F8 Propylene glycol	F9 Ethanolamine	F10 D,L- α-Glycerol-Phosphate	F11 Glycerol	F12 Citric Acid
G1 Tricarballylic Acid	G2 D,L-Lactic Acid	G3 Methyl D-lactate	G4 Methyl pyruvate	G5 Pyruvic Acid	G6 α-Keto-Glutaric Acid	G7 Succinamic Acid	G8 Succinic Acid	G9 Mono-Methyl Succinate	G10 L-Malic Acid	G11 D-Malic Acid	G12 Meso-Tartaric Acid
H1 Acetoacetic Acid (a)	H2 γ-Amino-N-Butyric Acid	H3 α-Keto-Butyric Acid	H4 α-Hydroxy-Butyric Acid	H5 D,L-β-Hydroxy-Butyric Acid	H6 γ-Hydroxy-Butyric Acid	H7 Butyric Acid	H8 2,3-Butanediol	H9 3-Hydroxy-2-Butanone	H10 Propionic Acid	H11 Acetic Acid	H12 Hexanoic Acid

Figure S2. Layout of carbon sources in the wells on the PM-M1 microplate.

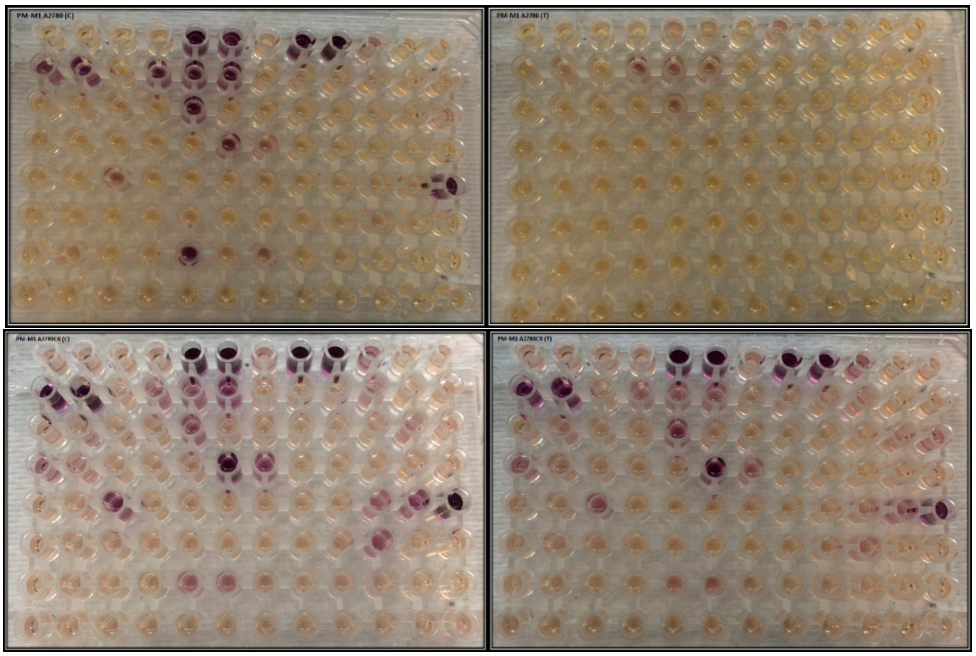

Figure S3. Changes in the metabolism of ovarian cancer A2780 and A2780CR cells. Top left was A2780 without treated. Top right was A2780 after exposure to melittin. Bottom left was A2780CR without treated. Bottom right was A2780 after exposure to melittin.

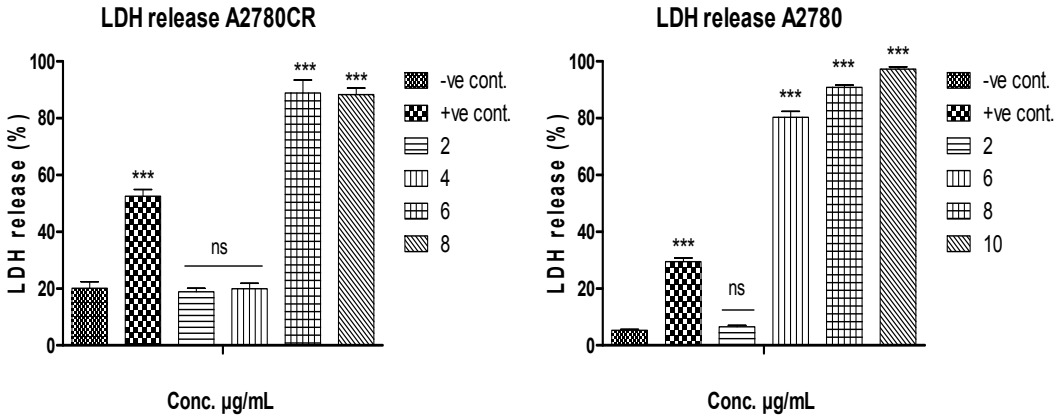

Figure S4. Lactate dehydrogenase (LDH) assay. Effect of melittin on leakage of lactate dehydrogenase (LDH) from A2780 and A2780CR cell lines. The cells were incubated with melittin at different concentrations for 24 h. LDH activity was measured at 490 nm using an LDH cytotoxicity kit. Data were expressed as the mean ± SD of three independent experiments. Significant difference in LDH activity of melittin compared to untreated cells was tested by one-way ANOVA followed by Bonferroni's Multiple Comparison test to determine the differences between the experimental groups. Differences were considered significant at $p < 0.001$ (***) and ns: no significance.

$$\% \text{ Cytotoxicity} = \frac{\text{Experimental} - \text{Culture Medium Background}}{\text{Maximum LDH Release} - \text{Culture Medium Background}} \times 100$$

Effect of Melittin on Caspase-3 Activity

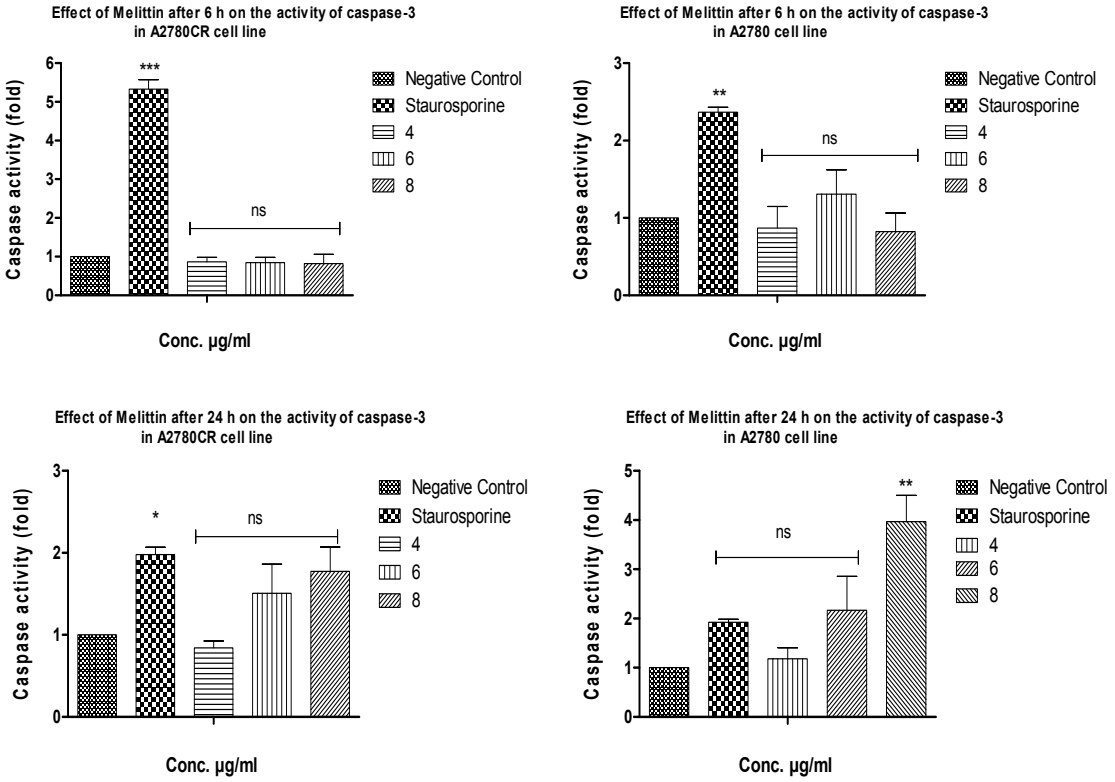

Figure S5. Effect of Melittin on caspase-3 activity in A2780 and A2780CR cells. Both cell lines were incubated with different concentrations of melittin to measure caspase-3 activity. Staurosporine (10 µM) was used as a positive control. Following 6 and 24 h, cell were incubated with the caspase detection buffer and the fluorescence signal was measured following 1 h at 360 nm (excitation) and at 460 nm (emission). Data are presented as the fold change compare to untreated cells (negative control). Data were expressed as the mean ± SD of three independent experiments. Significant difference in caspase-3 activity of melittin compared to untreated cells was tested by one-way ANOVA followed by Bonferroni's Multiple Comparison test to determine the differences between the experimental groups. Differences were considered significant at the level of $p < 0.05$ and ns: no significance.

Table S1. Differences in the top 50 lipids between A2780 cells and A2780CR cells before and after melittin treatment.

m/*z*	Rt(min)	Met Name	*p* Value S/R	Ratio S/R	MS/S *p* Value	Ratio MS/S	MR/R *p* Value	MR/R Ratio	MS/MR *p* Value	Ratio MS/MR
760.5846	13.9	PC34:1	0.03	1.36	0.01	0.64	0.09	0.82	0.58	1.05
786.6	13.9	PC36:2	0.29	1.10	0.03	0.75	0.12	0.85	0.77	0.97
732.5539	14.0	PC32:1	0.01	1.87	0.01	0.56	0.00	0.59	< 0.001	1.76
746.6055	14.1	PC34:0	< 0.001	3.28	0.03	0.74	0.07	0.82	< 0.001	2.95
788.6156	13.9	PC36:1	0.94	0.99	0.02	0.65	0.33	1.11	0.02	0.58
734.5691	14.0	PC32:0	0.01	1.44	0.01	0.61	0.04	0.79	0.31	1.10
758.5694	13.9	PC34:2	0.01	1.58	0.02	0.73	0.01	0.69	< 0.001	1.68
703.5745	14.5	SM14:1	< 0.001	1.87	0.63	0.96	0.69	1.05	< 0.001	1.72
720.5899	14.2	PC32:2 ether lipid	< 0.001	4.62	0.12	0.82	0.01	0.69	< 0.001	5.50
718.5746	14.1	PC32:0 ether lipid	0.00	3.31	0.11	0.83	0.17	1.17	< 0.001	2.35
706.5382	14.1	PC30:0	0.03	1.31	0.00	0.49	0.00	0.61	0.47	1.06
784.5847	13.8	PC36:3	0.02	1.58	0.05	0.76	0.45	0.93	0.03	1.30
782.5672	13.7	PC36:4	0.01	1.76	0.57	0.95	0.18	1.20	0.03	1.39
768.5529	9.7	PC38:4	0.01	1.87	0.23	1.12	0.00	1.41	< 0.001	1.48
808.5836	13.7	PC38:5	0.03	1.64	0.32	1.12	0.11	1.30	0.03	1.41
810.5995	13.7	PC38:4	0.02	1.88	0.44	0.90	0.02	1.84	0.54	0.93
768.5885	13.8	PC36:3 ether lipid	< 0.001	4.56	0.78	0.98	0.01	1.62	0.00	2.75
744.5905	13.9	PC34:1 ether lipid	< 0.001	1.88	0.45	0.94	0.17	1.19	0.01	1.49
794.6051	13.8	PC38:5 ether lipid	< 0.001	3.58	0.11	1.19	0.01	2.11	< 0.001	2.01
796.6206	13.8	PC38:4 ether lipid	< 0.001	5.72	0.39	0.92	0.01	1.73	< 0.001	3.03
752.5584	9.6	PE38:5	< 0.001	3.20	0.51	0.94	0.01	1.31	< 0.001	2.29
813.6838	14.4	SM42:2	< 0.001	1.84	0.88	0.99	0.62	1.07	< 0.001	1.71
804.5759	14.0	PS37:0	0.69	0.96	< 0.001	1.32	0.13	1.14	0.05	1.11
812.6155	13.8	PC38:3	0.01	1.84	0.01	0.60	0.30	1.14	0.80	0.97
814.6312	13.9	PC38:2	0.01	0.67	0.02	0.60	0.08	0.81	0.01	0.49
744.5534	10.1	PE36:2 ether lipid	0.26	0.89	0.02	0.69	0.01	0.75	0.06	0.82
772.621	14.0	PC 36:1 ether lipid	0.00	2.08	0.06	0.80	0.81	0.97	0.00	1.70
300.2893	10.4	Dehydrosphinganine	0.00	6.21	0.00	0.66	0.00	0.62	0.00	6.63
774.6007	13.9	PC35:1	0.08	1.24	0.13	0.84	0.13	1.21	0.21	0.87
752.5583	9.6	PE38:5 ether lipid	0.01	3.33	0.21	0.80	0.03	1.27	0.00	2.12
766.5367	9.6	PE38:5	0.03	1.99	0.35	0.85	0.44	0.95	0.00	1.80
750.5427	9.6	PE38:4 ether lipid	0.01	1.78	0.39	0.92	0.50	1.04	0.00	1.57
724.5273	9.7	PE36:5 ether lipid	0.02	1.51	0.74	1.03	0.01	1.41	0.14	1.11

772.5851	13.9	PC35:2	0.03	1.41	0.42	0.93	0.33	0.90	0.01	1.45
774.6365	14.1	PC36:0 ether lipid	0.00	3.40	0.02	0.69	0.03	0.76	0.00	3.11
770.6052	13.9	PC36:2 ether lipid	0.00	2.70	0.01	0.63	0.55	1.07	0.01	1.58
731.6057	14.5	SM36:2	0.00	2.97	0.24	1.10	0.63	1.07	0.00	3.07
718.538	10.3	PE34:1	0.16	1.14	0.00	0.58	0.00	0.61	0.42	1.08
692.5589	14.2	PC30:2 ether lipid	0.00	3.45	0.02	0.62	0.02	0.77	0.00	2.80
730.5382	13.9	PC32:2	0.00	3.79	0.01	0.70	0.00	0.58	0.00	4.61
862.6244	3.1	C18:0 Lactosylceramide	< 0.001	5.11	0.20	0.86	0.03	1.16	0.00	3.79
746.569	10.2	PE34:1 ether lipid	0.01	0.69	0.01	0.66	0.03	0.78	0.01	0.59
792.5897	13.7	PC38:6 ether lipid	0.01	2.36	0.81	1.03	0.02	1.91	0.08	1.27
282.2788	10.4	Octadecenamide	0.00	5.26	0.00	0.67	0.00	0.62	0.00	5.68
834.5994	13.7	PC40:6	0.68	1.05	0.08	0.74	0.07	1.42	0.02	0.55
836.6151	13.7	PC40:5	0.33	1.16	0.17	0.79	0.10	1.34	0.06	0.68
863.5661	3.7	PI36:1	0.07	0.87	0.09	1.15	0.08	1.22	0.07	0.82
790.5586	11.4	PS 36:1	0.28	1.10	0.03	0.74	0.12	0.87	0.37	0.93
756.5523	13.9	PC34:3	0.00	2.16	0.04	0.81	0.02	0.76	0.00	2.33
887.5643	3.6	PI38:3	0.00	2.32	0.00	1.52	0.58	0.96	0.00	3.66

metabolites

MDPI

Article

Metabolomic Profiling of the Synergistic Effects of Melittin in Combination with Cisplatin on Ovarian Cancer Cells

Sanad Alonezi [1], Jonans Tusiimire [1,2], Jennifer Wallace [3], Mark J. Dufton [3], John A. Parkinson [3], Louise C. Young [1], Carol J. Clements [1], Jin-Kyu Park [4], Jong-Woon Jeon [4], Valerie A. Ferro [1] and David G. Watson [1,*]

1 Strathclyde Institute of Pharmacy and Biomedical Sciences, University of Strathclyde, G4 0RE Glasgow, UK; alonezi-sanad-mohammed-z@strath.ac.uk (S.A.); jonanstusiimire@must.ac.ug (J.T.); Louise.c.young@strath.ac.uk (L.Y.); c.j.clements@strath.ac.uk (C.J.C.); v.a.ferro@strath.ac.uk (V.A.F.)

2 Department of Pharmacy, Faculty of Medicine, Mbarara University of Science and Technology, P.O. Box 1410 Mbarara, Uganda

3 WestCHEM Department of Pure and Applied Chemistry, University of Strathclyde, G1 1XL Glasgow, UK; jennifer.wallace.101@strath.ac.uk (J.W.); mark.dufton@strath.ac.uk (M.J.D.); john.parkinson@strath.ac.uk (J.A.P.)

4 #204, Beesen Co. Ltd., Bio Venture Town, Yuseong Daero 1662, 34054 Dae Jeon, Korea; jkypark@live.co.kr (J.-K.P.); confessor@hanmail.net (J.-W.J.)

* Correspondence: d.g.watson@strath.ac.uk; Tel.: +44-141-548-2651

Academic Editor: Peter Meikle
Received: 17 March 2017; Accepted: 12 April 2017; Published: 14 April 2017

Abstract: Melittin, the main peptide present in bee venom, has been proposed as having potential for anticancer therapy; the addition of melittin to cisplatin, a first line treatment for ovarian cancer, may increase the therapeutic response in cancer treatment via synergy, resulting in improved tolerability, reduced relapse, and decreased drug resistance. Thus, this study was designed to compare the metabolomic effects of melittin in combination with cisplatin in cisplatin-sensitive (A2780) and resistant (A2780CR) ovarian cancer cells. Liquid chromatography (LC) coupled with mass spectrometry (MS) was applied to identify metabolic changes in A2780 (combination treatment 5 μg/mL melittin + 2 μg/mL cisplatin) and A2780CR (combination treatment 2 μg/mL melittin + 10 μg/mL cisplatin) cells. Principal components analysis (PCA) and orthogonal partial least squares discriminant analysis (OPLS-DA) multivariate data analysis models were produced using SIMCA-P software. All models displayed good separation between experimental groups and high-quality goodness of fit (R^2) and goodness of prediction (Q^2), respectively. The combination treatment induced significant changes in both cell lines involving reduction in the levels of metabolites in the tricarboxylic acid (TCA) cycle, oxidative phosphorylation, purine and pyrimidine metabolism, and the arginine/proline pathway. The combination of melittin with cisplatin that targets these pathways had a synergistic effect. The melittin-cisplatin combination had a stronger effect on the A2780 cell line in comparison with the A2780CR cell line. The metabolic effects of melittin and cisplatin in combination were very different from those of each agent alone.

Keywords: melittin; cisplatin; synergy; sensitive and resistant ovarian cancer cells; metabolomics

1. Introduction

Combination therapy has long been studied in the treatment of cancer, including ovarian cancer [1]. It is a logical approach, focusing on increasing the response and tolerability to treatment, while also decreasing resistance [2]. Unfortunately, it can be difficult to assess whether a particular

combination will behave in a synergistic, additive, or antagonist fashion when used on a particular cancer patient. The only known way of determining their effectiveness is to identify specific measures, such as response rate, survival, or time to progression, and assess if or whether the new combination is able to achieve a significant improvement [2]. Combination therapy is essentially cooperative: each agent involved should have non-overlapping toxicities, different mechanisms of action with minimal cross-resistance, and individually proven in treatment by itself [2].

Several cancers, including ovarian cancer, have demonstrated resistance or reduced sensitivity to cisplatin treatment, leading to decreased time to disease progression, increased likelihood of relapse, and reduced efficacy upon re-treatment during relapse [3,4]; cisplatin itself causes significant health problems, such as nephrotoxicity [5]. Ideally, cisplatin in combination with a drug that diminishes its negative effects while enhancing the therapeutic effects would decrease resistance or relapse while mitigating its negative effects. For example, cisplatin (or another platinum agent) in combination with taxanes (e.g., paclitaxel) is now regarded as standard chemotherapy in ovarian cancer, where the taxane enhances the tumour's radiosensitivity. Cisplatin and the adenovirus OBP-301 have also been shown to work synergistically [1].

Cisplatin shares cytotoxic synergy with bee venom [1]. Bee venom makes sense as a complement to cisplatin: it has protective effects in many areas of the body such as the blood and nerves [6]; it is able to inhibit cell growth in tumours [7]; and has even been examined and used in complementary treatments that are necessitated by the effects of chemotherapy, such as allodynia [8] and neuropathy [9]. Cisplatin in combination with bee venom has been successfully used against human cervical and laryngeal carcinoma cells, including their drug-resistant sublines [10], and human glioblastoma [11]. Several studies have found that phospholipase A_2, another component of bee venom, not only mitigates the negative impact of cisplatin on kidneys [12], but also boosts regulatory T cell (Treg) numbers in the spleen and enhances Treg traffic to the kidneys following cisplatin exposure. This is important, as Tregs play a significant role in many mechanisms, including inflammation and autoimmunity suppression [4,12,13]. A significant bonus in this dynamic is that bee venom has no negative impact on the anti-cancer properties of the cisplatin [4], meaning it in no way diminishes the effect of the cisplatin treatment. This is critical; a combinatory agent which diminishes any positive effects of the primary treatment undermines its effectiveness overall. The effects that cisplatin and bee venom have together on ovarian cancer cells emerge from the synergistic relationship between the two agents [14]. Alizadehnohi et al. report that separately and together, the two agents induce apoptosis in human ovarian cancer cells; bee venom appears to enhance the cytotoxic impact of cisplatin [14]. It also appears that melittin provokes responses in cisplatin-sensitive cells which lead to decreasing levels of amino acids, which in turn affect the energy metabolism of the tumour [15].

In order to understand these effects and the metabolic changes that the cisplatin-melittin combination has on ovarian cancer cells, metabolomic investigations can be undertaken. Metabolomics in the context of oncology usefully focuses on diagnosis and prognosis, as well as on evaluating the effectiveness of therapy [16,17]. For instance, one study employed nuclear magnetic resonance (^{1}H-NMR) spectroscopy and was able to accurately separate serum metabolite profiles of three groups of patients: namely women with ovarian cancer, normal premenopausal women, and women with a benign ovarian disease [18]. In addition, LC-MS in combination with Biolog Microarray assays revealed that treatment of cisplatin-resistant and sensitive ovarian cancer cells with melittin distinctively altered their lipid profiles and their ability to metabolise certain carbon energy sources, [15]. NMR spectroscopy has also been used to produce and examine metabolic profiles in other cancers such as hepatocellular carcinoma [19].

In essence, the effects of the cytotoxic mechanisms of both cisplatin and melittin, together and separately, cause changes in cells which can be identified and measured through metabolomic analysis. The current study aimed to examine the metabolic effects of melittin in combination with cisplatin on A2780 and A2780CR human ovarian cancer cell lines using a LC-MS based metabolomics approach employing a ZIC-pHILIC column. Multivariate data analysis was performed based on PCA and OPLS-DA models constructed using the SIMCA-P software.

2. Results

2.1. The Cytotoxicity of Melittin in Combination with Cisplatin

The viabilities of the cisplatin-sensitive and cisplatin-resistant ovarian cancer cells (OCCs) (A2780 and A2780CR, respectively) treated with melittin or cisplatin were compared. Both single treatments exerted a concentration-dependent cytotoxic effect on A2780 and A2780CR cells (Figure 1). The cisplatin mediated growth inhibition of the sensitive cell line (A2780) was significantly greater than that of the melittin over the concentration range of 1 to 8 μg/mL (Figure 1A; $p < 0.05$). However, the A2780CR cells, as expected, were more resistant to cisplatin than the A2780 cells (Figure 1B). The 24 h half maximal inhibitory concentrations (IC_{50}) of cisplatin in A2780CR and A2780 cells were 10.8 and 4.9 μg/mL, respectively. Melittin exhibited toxicity against both A2780CR and A2780 cells, with IC_{50} values of 4.5 and 6.8 μg/mL, respectively [15] (Figures S1 and S2). The cytotoxicity of melittin in combination with cisplatin against A2780 and A2780CR cells was studied by using an Alamar® Blue assay [15]. The A2780 and A2780CR cells were treated for 24 h at various concentrations of melittin in combination with cisplatin. The percentage of surviving cells decreased in a dose-dependent manner in both cell lines. The cytotoxic effects of melittin in combination with cisplatin on A2780 and A2780CR cell lines are shown in Figures 2A and 3A, respectively.

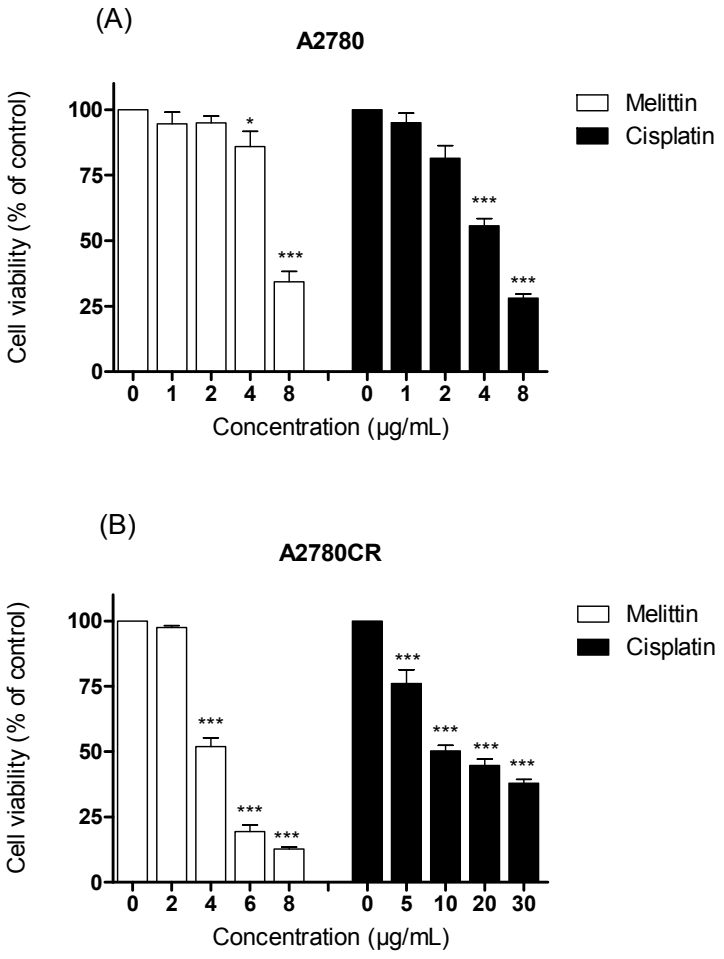

Figure 1. Examination of cell viability after treatment with either cisplatin or melittin alone with various concentrations on (**A**) A2780 and (**B**) A2780CR cell lines. * Significantly different from zero. concentration at <0.05; *** Significant at <0.001.

2.2. The Combination Index (CI)

In order to qualitatively evaluate whether the combination of melittin with cisplatin might cause synergistic cytotoxic effects, the value of CI, a commonly used evaluation index, was calculated. It has been proposed that CI values be interpreted as follows: <0.1 very strong synergism, 0.1–0.3 strong synergism, 0.3–0.7 synergism, 0.7–0.9 moderate to slight synergism, 0.9–1.1 nearly additive, 1.1–1.45 slight to moderate antagonism, 1.45–3.3 antagonism, and >3.3 strong to very strong antagonism [22].

The CI analyses showed that synergistic cytotoxic activity on A2780 cells occurred with the melittin + cisplatin combinations at concentrations of 5 + 2 (CI = 0.647) and 6 + 2 (CI = 0.512) μg/mL, and with the cisplatin+melittin combinations at concentrations of 4 + 3 (CI = 0.789) and 5 + 3 (CI = 0.711) μg/mL, respectively. However, the calculated CI was found to be >1 in A2780 cells treated with the melittin + cisplatin combinations at concentrations of 3 + 2 (CI = 2.812) and 4 + 2 (CI = 1.259) μg/mL, and thus could represent an antagonistic effect (Figure 2B). The melittin + cisplatin combinations had CI between 0.7–0.9, indicating a moderate to slight synergism relationship in A2780CR at 2 + 10 (CI = 0.888) and 5 + 10 (CI = 0.741) μg/mL, as shown in Figure 3B. The CI value of melittin + cisplatin was 0.985 at concentrations of 3 + 10 μg/mL and 0.921 at concentrations of 4 + 10 μg/mL used to treat A2780CR, indicating a nearly additive effect. However, the calculated CI was found >1 in A2780CR with the cisplatin+melittin combination at concentrations of 20 + 2 and 30 + 2 μg/mL and thus could represent an antagonism effect. The combination of melittin and cisplatin thus shows potential in the treatment of the resistant cells since there is no evidence of cross resistance against melittin which might be expected as a feature of multidrug resistance.

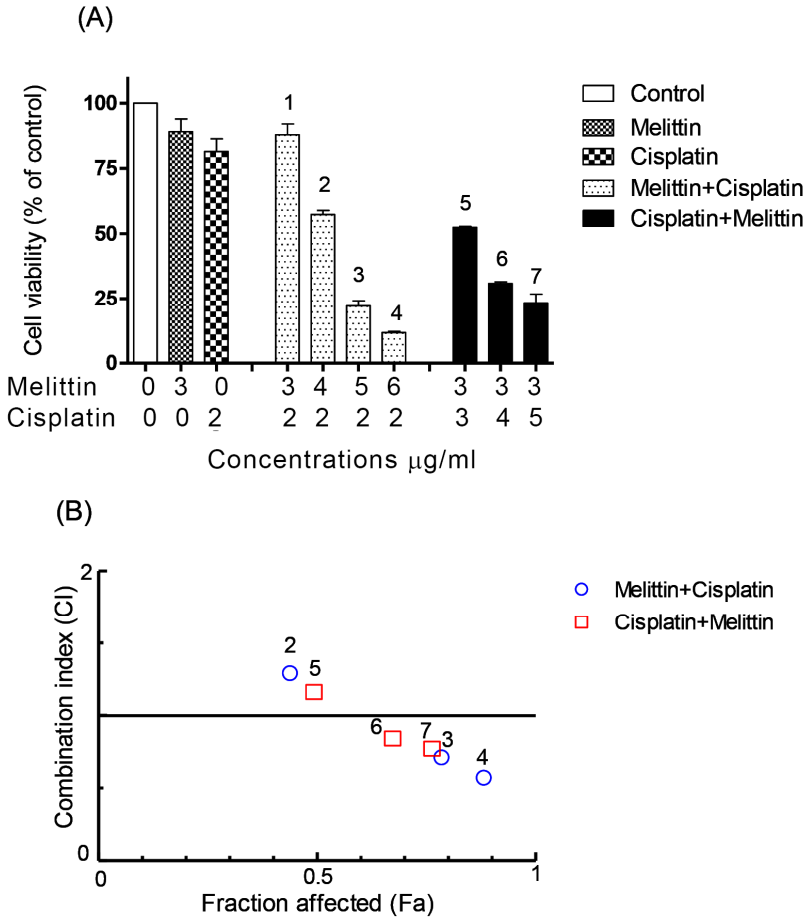

Figure 2. Effects of melittin in combination with cisplatin on (**A**) cell viability of A2780 cell lines and (**B**) combination index. (**A**) The A2780 cells were treated with various concentrations of the melittin + cisplatin combination for 24 h. Bar graphs represent mean ± SD values. (**B**) Combination index (CI) analysis was generated using the method of Chou and Talalay [20,21] to determine the extent of synergy, if any, for the melittin + cisplatin combination on A2780 cell lines.

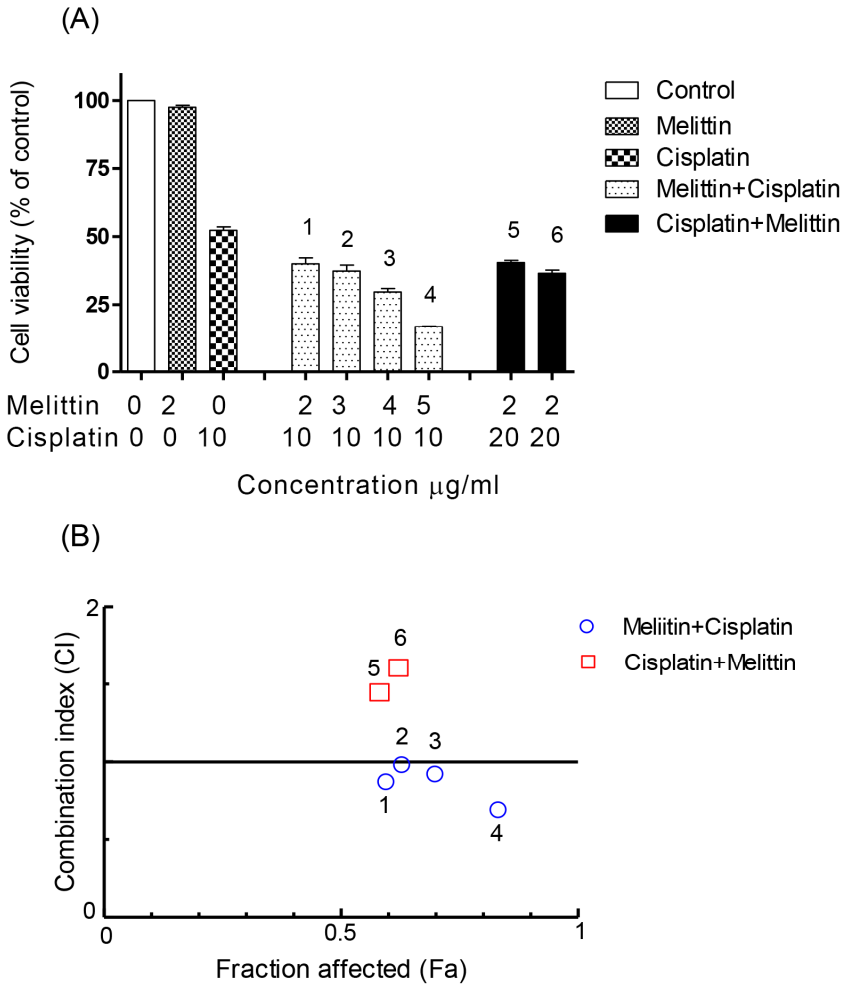

Figure 3. Effect of melittin in combination with cisplatin on (**A**) cell viability of A2780CR cell lines and (**B**) combination index. (**A**) The A2780CR cells were treated with various concentrations of the melittin + cisplatin combination for 24 h. Bar graphs represent mean ± SD values. (**B**) Combination index (CI) analysis was generated using the method of Chou and Talalay [20,21] to determine the extent of synergy, if any, for the melittin + cisplatin combination on A2780CR cell lines.

2.3. Metabolome Analysis

The metabolic effects of melittin in combination with cisplatin on ovarian cancer cells were assessed using an LC-MS based metabolomic approach. Univariate and multivariate statistical analyses were used to examine the effect of combination 1 (5 μg/mL of melittin + 2 μg/mL cisplatin) and combination 2 (2 μg/mL of melittin + 10 μg/mL cisplatin) on A2780 and A2780CR cells, respectively.

A clear separation of A2780 and A2780CR cells was achieved indicating unique metabolite profiles for the treated and control cells on the PCA and OPLS-DA scores plots at both treatment combinations (Figure 4A,B, respectively). The pooled quality control (QC) samples injected at intervals in the analysis run to assess the precision of the measurements and confirm stability of the analytical method produced a single tight cluster in the center of the dataset (Figure 4A), thus validating the analysis. The PCA model parameters and validation of the plot suggested a good model (four components, R2X (cum) = 0.918; Q2 (cum) = 0.856). There was also very clear separations between the treated and control A2780 and A2780CR cells in the OPLS-DA, a supervised model for classifying samples. The OPLS-DA model parameters and validation of the plot suggested a strong model (four components, R2X (cum) = 0.916, R2Y (cum) = 1, Q2 (cum) = 0.975), and the CV-ANOVA for this model was 1.28×10^{-24}. Hierarchical clustering analysis (HCA) of the metabolomics data showed distinct separation between the control and treated samples (Figure S3).

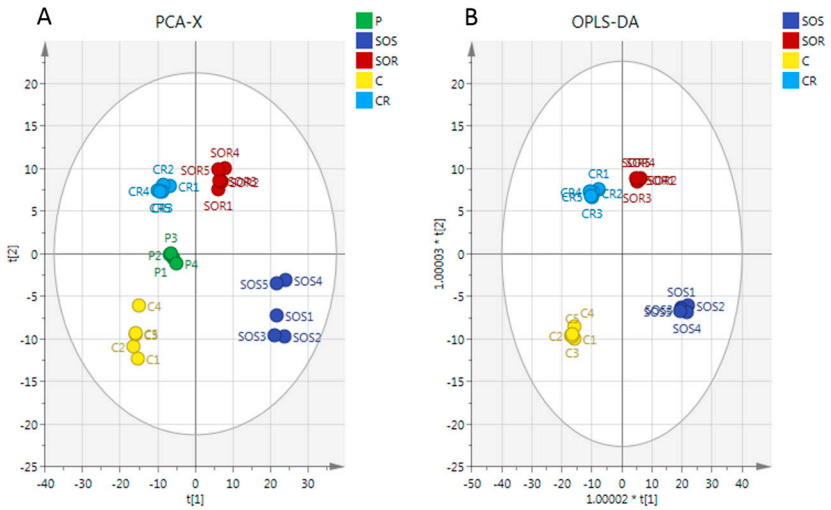

Figure 4. (**A**) Principal components analysis (PCA) vs. (**B**) Orthogonal Partial Least Squares Discriminant Analysis (OPLS-DA). PCA and OPLS-DA scores plot generated from PCA and OPLS-DA using LC-MS normalised data of cells after exposure to the combination (melittin + cisplatin) and controls of A2780 and A2780CR cell lines. A2780-treated cells at 5 μg/mL melittin + 2 μg/mL cisplatin (SOS); untreated A2780 cells (C) ; A2780CR-treated cells at 2 μg/mL melittin + 10 μg/mL cisplatin (SOR) ; untreated A2780CR (CR) ; pooled quality control (QC) samples (P).

There was a very clear separation of the treated versus untreated A2780 cells obtained by using the OPLS-DA model based on the significant metabolites (Figure 5A). The model parameters and validation of the plot suggested a strong model (two components, R2X (cum) = 0.965, R2Y (cum) = 1, Q2 (cum) = 0.996, CV-ANOVA= 2.62×10^{-6}). To test the validity, a receiver operator characteristic (ROC) curve and permutation test were also applied (Figure S3). The area under the curve (AUC) for the ROC curve is regarded as excellent when AUC > 0.9. The OPLS-DA model classified the treated and untreated A2780 cells into two groups, and the AUC of the ROC for the groups were in the excellent to perfect classification.

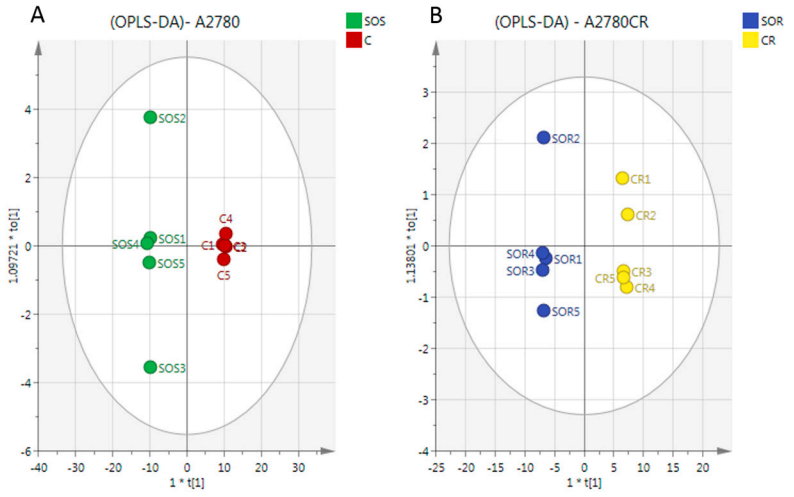

Figure 5. OPLS-DA score plot of (**A**) A2780 cells and (**B**) A2780CR before and after treatment with melittin + cisplatin respectively. Separation of the treated and untreated cells in both cell lines in the model suggests that there are significant metabolite differences induced by treatment in both cell lines. The metabolites responsible for the observed separation are shown in Table 1.

In the case of the A2780CR cells, OPLS-DA models were also generated by comparing control and treated samples based on the significant metabolites (Figure 5B). As in A2780 cells, a clear separation was also found between the treated and untreated A2780CR samples and the CV-ANOVA

for this model was 8.42×10^{-6} (two components, R2X (cum) = 0.966, R2Y (cum) = 1, Q2 (cum) = 0.994). Furthermore, the validity of the ROC and permutation test showed that the constructed OPLS-DA model was valid (Figures S4 and S5).

For univariate statistical analysis of candidate specific biomarkers in ovarian cancer cells after exposure to the treatment combinations, the false discovery rate statistical test (FDR) was used to reduce the probability of false positive results [23]. Significant changes in the levels of various classes of metabolites, especially those in the mitochondrial TCA cycle, energy metabolism, and nucleotide and amino acids metabolism were observed as summarised in Table 1. The major impression is that the combination of melittin and cisplatin produces distinct metabolic profiles in both cell lines that are unlike those produced when either of the agents are used alone as previously reported [15,24].

It can be observed that there is a strong reduction in the levels of metabolites involved in Krebs cycle and energy metabolism. Several metabolites in the TCA cycle, including citrate, 2-oxoglutarate, malate, and phosphoenolpyruvate were significantly decreased in both sensitive and resistant cells after treatment with the melittin + cisplatin combination. The treatment also reduced the levels of adenosine triphosphate (ATP) in both cell lines. It should be noted that the combination treatment had a stronger effect on ATP levels in the A2780 cells than in the A2780CR cells, although the treatments were not the same as they were based on cell sensitivities towards the two agents. There were also marked decreases in the levels of pentose phosphate pathway metabolites in both cell lines after the combination treatment. Moreover, there were important differences in the levels of purine and pyrimidine metabolites between the two cell lines after treatment with the combinations. With the exception of hypoxanthine and guanine (both purines) which were increased, the rest of these metabolites were significantly decreased by the combination treatment in both cell lines.

The most affected metabolites due to the combination treatment in both cell lines compared to the other pathways were involved in amino acid metabolism. In A2780 cells, the valine metabolite, 3-methyl-2-oxobutanoic acid, increased, while there were decreases in many amino acids related to arginine and proline metabolism. In A2780CR cells, significant increases were observed in the levels of S-adenosyl-L-methionine, 5′-methylthioadenosine, L-lysine, and L-serine.

Table 1. Metabolites significantly altered by treatment with melittin in combination with cisplatin at 5 μg/mL melittin + 2 μg/mL cisplatin on A2780 and at 2 μg/mL melittin + 10 μg/mL cisplatin on A2780CR.

m/z	RT (min)	Metabolites	SR/CR		SS/C	
			p-Value	Ratio	*p*-Value	Ratio
Citrate cycle (TCA cycle)/glycolysis						
338.989	18.1	* D-Fructose 1,6-bisphosphate	<0.001	0.278	<0.001	0.246
115.004	16.0	* Fumarate	<0.001	0.227	<0.01	0.402
133.014	16.1	* (S)-Malate	<0.001	0.218	<0.001	0.062
145.014	15.7	* 2-Oxoglutarate	<0.001	0.324	<0.001	0.048
191.02	18.1	* Citrate	<0.001	0.588	<0.001	0.172
173.009	17.9	* cis-Aconitate	<0.001	0.490	<0.001	0.072
166.975	17.5	* Phosphoenolpyruvate	<0.001	0.344	<0.05	0.082
Oxidative phosphorylation						
664.116	14.2	* NAD+	<0.001	0.294	<0.001	0.067
508.003	16.2	* ATP	<0.001	0.362	<0.001	0.073
Glycine/Serine/Cysteine and Glutathione						
241.031	16.3	* L-Cystine	ns	1.739	ns	1.832
427.095	17.1	S-Glutathionyl-L-cysteine	ns	0.750	<0.001	0.218
152.002	14.6	3-Sulfino-L-alanine	ns	0.706	<0.001	0.139
308.091	14.5	* Glutathione (GSH)	<0.001	0.562	<0.001	0.092
179.048	14.4	L- Cysteinylglycine (Cys-Gly)	<0.001	0.521	<0.001	0.067
223.074	17.1	* L-Cystathionine	<0.001	0.438	<0.001	0.004
76.0394	15.7	* Glycine	ns	1.050	<0.001	0.142
116.035	10.8	L-2-Amino-3-oxobutanoic acid	<0.001	0.319	<0.001	0.317
106.050	15.8	* L-Serine	<0.001	7.112	<0.001	0.420

RT: min; SR: combination 2 treated A2780CR; CR: control A2780CR; SS: combination 1 treated A2780; C: control A2780; ns: non-significant. * Retention time matches standard.

Table 1. *Cont.*

m/z	RT (min)	Metabolites	SR/CR		SS/C	
			p-Value	Ratio	*p*-Value	Ratio
Pentose phosphate pathway						
195.051	13.7	* D-Gluconic acid	<0.001	0.147	<0.001	0.093
308.978	16.5	D-Ribose 1,5-bisphosphate	<0.001	0.259	<0.001	0.124
149.046	11.9	* D-Ribose	<0.001	0.222	<0.001	0.285
229.012	15.8	* D-Ribose 5-phosphate	<0.001	0.545	<0.001	0.131
Lysine biosynthesis						
170.046	14.3	2,3,4,5-Tetrahydrodipicolinate	<0.001	0.245	<0.001	0.112
147.113	24.3	* L-Lysine	<0.001	1.966	ns	0.724
162.112	13.3	* L-Carnitine	<0.001	0.508	<0.001	0.135
243.074	17.2	5-Phosphonooxy-L-lysine	<0.001	0.303	<0.001	0.006
128.071	15.5	2,3,4,5-Tetrahydropyridine-2-carboxylate	<0.001	0.433	<0.001	0.271
Purine metabolism						
137.046	10.2	* Hypoxanthine	<0.001	16.99	<0.01	7.87
152.056	12.4	* Guanine	<0.001	13.19	<0.01	102.21
348.07	13.8	* AMP	<0.001	0.372	<0.001	0.190
428.036	15.0	* ADP	<0.001	0.376	<0.001	0.163
442.018	17.8	GDP	<0.001	0.509	ns	0.104
521.984	18.9	* GTP	<0.001	0.442	<0.001	0.079
426.013	16.9	Adenylyl sulfate	<0.001	0.271	<0.01	0.014
Pyrimidine metabolism						
155.01	10.3	* Orotate	<0.001	0.218	<0.001	0.050
129.066	14.8	5,6-Dihydrothymine	<0.001	0.326	<0.001	0.120
480.982	15.8	dTTP	<0.001	0.337	<0.001	0.347
175.036	16.8	N-Carbamoyl-L-aspartate	<0.001	0.036	<0.001	0.017
115.05	14.7	5,6-Dihydrouracil	<0.001	0.383	<0.001	0.079
402.995	16.4	* UDP	<0.001	0.485	<0.001	0.035
484.975	17.6	* UTP	<0.001	0.465	<0.001	0.059
323.029	15.2	* UMP	ns	1.195	<0.001	0.282
Arginine/ Proline/ Glutamate/Methionine						
188.057	14.3	N-Acetyl-L-glutamate	<0.001	0.241	<0.001	0.029
176.103	15.8	* L-Citrulline	<0.001	0.521	<0.001	0.189
173.104	25.8	* L-Arginine	ns	1.161	<0.001	0.379
130.051	14.5	L-Glutamate-5-semialdehyde	<0.001	0.538	<0.001	0.235
116.071	12.8	* L-Proline	<0.001	0.568	<0.001	0.228
399.144	16.3	* S-Adenosyl-L-methionine	<0.001	2.005	<0.001	0.115
298.096	6.4	* 5′-Methylthioadenosine	<0.05	2.016	<0.001	0.158
146.093	15.1	* 4-Guanidinobutanoate	<0.001	0.325	<0.001	0.055
291.129	16.8	N-(L-Arginino) succinate	<0.001	0.260	<0.001	0.010
247.14	14.2	N_2-(D-1-Carboxyethyl)-L-arginine	<0.001	0.170	<0.001	0.010
174.087	15.3	5-Guanidino-2 oxopentanoate	<0.001	0.680	<0.001	0.058
132.077	14.7	* Creatine	<0.001	0.403	<0.001	0.075
210.029	15.2	* Phosphocreatine	<0.001	0.422	<0.001	0.051
Miscellaneous						
110.027	14.9	Hypotaurine	<0.001	0.139	<0.001	0.009
115.04	8.2	3-Methyl-2-oxobutanoic acid	<0.001	0.191	<0.05	5.604
166.053	13.4	L-Methionine S-oxide	<0.01	0.470	<0.001	0.250
218.067	13.9	O-Succinyl-L-homoserine	<0.001	0.082	<0.001	0.011
181.051	9.0	3-(4-Hydroxyphenyl)lactate	<0.001	0.656	<0.001	0.087
204.123	11.1	* O-Acetylcarnitine	<0.001	0.137	<0.001	0.021
176.056	10.3	4-Hydroxy-4-methylglutamate	ns	1.911	<0.001	0.022
159.076	15.8	4-Methylene-L-glutamine	<0.001	0.607	ns	0.258
175.025	14.4	* Ascorbate	<0.001	0.067	<0.001	0.024
165.041	13.0	L-Arabinonate	<0.001	0.372	<0.001	0.166
179.056	17.1	Hexose	<0.05	0.670	<0.05	0.334

RT: min; SR: combination 2 treated A2780CR; CR: control A2780CR; SS: combination 1 treated A2780; C: control A2780; ns: non-significant. * Retention time matches standard.

3. Discussion

Cisplatin is one of the most effective anticancer drugs currently used for treating many types of cancer, however, it comes with serious side effects. Combination therapy has been used in cancer treatment in order to increase therapeutic response and tolerability, and to decrease resistance [2].

The present study aimed to determine whether or not melittin, a cytotoxic peptide from bee venom, possesses a synergistic inhibitory effect in combination with cisplatin on A2780 and A2780CR cells. In addition, the study was intended to determine the metabolomics effects of the melittin + cisplatin combination treatment on the two cell lines which would corroborate any observed synergistic cytotoxic effects.

Cell viability assays using the Alamar® Blue method confirmed the synergistic cytotoxic effects of melittin in combination with cisplatin at certain concentrations, although at other concentrations, antagonistic effects were observed. CI analysis of the cytotoxicity data showed that, on A2780 cells, the combinations had synergistic effects at 2 μg/mL of melittin plus either 5 or 6 μg/mL of cisplatin, respectively. In contrast, at melittin + cisplatin concentrations of 3 + 2 and 4 + 2 μg/mL, respectively, antagonistic effects were observed. Synergistic effects were observed in A2780CR cells when the melittin was combined with cisplatin at 2 + 10 and 5 + 10 μg/mL, while with a fixed concentration of melittin (2 μg/mL) and variable concentrations of cisplatin (20 and 30 μg/mL) in the combination, antagonist effects were observed. The CI analysis used the median effect equation of Chou and the combination index equation of Chou and Talalay to quantify synergism or antagonism at different concentrations, and to select the best pair of drugs to combine for potentially maximal antitumor efficacy [21,25]. This method of analysis has been useful in identifying effective combinations of anticancer drugs [26,27].

Recent studies have reported that components of bee venom may exert an anti-tumour effect on human ovarian cancer and that the venom has the potential for enhancing the cytotoxic effect of the antitumor agent cisplatin [14]. Different melittin + cisplatin mechanisms could interact to either reduce or increase anticancer efficacy, thus producing three possible effects: (1) Additive, when the combined effect is equal to the sum of individual effects; (2) Antagonistic, when the effect of one or both compounds is less than when they are applied together than when individually applied; (3) synergism, when the effect of combined substances is greater than the sum of the individual effects [24]. Our findings show that these effects can occur depending on the concentrations of melittin and cisplatin in the combination.

With respect to OCCs, several previous studies have analysed the metabolic responses of OCCs to various compounds [28–30]. Additionally, there have been some previous metabolomic studies on the comparison between the effects of cisplatin on squamous cancer cell lines sensitive and resistant to cisplatin [31], and the effects of docetaxel on ovarian cancer stem cells [30]. Our previous study employed a metabolomics approach to assess the effects of melittin monotherapy on OCCs that revealed significant changes in amino acid and carbohydrate metabolism [15]. In addition, clear differences were previously observed in the metabolomes of the untreated cells [15]. Although our study demonstrated profound metabolic changes in the cells after melittin monotherapy, there has been no metabolomics study to date that has comparatively profiled the metabolite composition of OCCs treated with a combination of melittin and cisplatin. A previous study suggested that combination therapy is more effective than monotherapy on cancer cells such as hepatocellular carcinoma [19]. In the current untargeted metabolomics study, metabolic profiles of A2780 and A2780CR cells treated with melittin + cisplatin combinations were assessed using a LC-MS based metabolomics approach, with OPLS-DA models displaying good separation between the experimental groups, high-quality goodness of fit (R^2), and high-quality goodness of prediction (Q^2).

The metabolomics analysis demonstrated distinct metabolic profiles for the treated A2780 and A2780CR cells, although the treatments were adjusted in accordance with cell sensitivities. Specifically, the concentrations of melittin and cisplatin used were chosen based on cytotoxicity assays and CI values for synergy to allow detection of a combination effect rather than to achieve a maximal anticancer effect. The most altered metabolites in A2780 and A2780CR cells could be categorised under amino acid, energy, carbohydrate, and nucleotide metabolism. Most of the altered

metabolites participate in more than one pathway in significant ways, and the change in that one metabolite could have a resonating effect for other pathways.

There was a very clear effect of the combination treatment on the purine and pyrimidine pathways. This was very different from the metabolic shifts observed for melittin and cisplatin alone [15,24], suggesting the combination has quite a different effect on cell metabolism. There was a very large increase in the levels of the adenine metabolite, hypoxanthine, and guanine in both cell lines. This possibly indicates that the combination of melittin with cisplatin is promoting greater adduct formation between cisplatin and DNA in comparison with the treatment with cisplatin alone, where there was no strong evidence for effects on the levels of DNA bases [24]. Adducts formed with cisplatin are mainly intra-strand crosslinks joining two guanine residues and to a lesser extent intra-strand links between guanine and adenine [32]. DNA is repaired by excision of damaged bases and this would correlate with largely increased levels of guanine and hypoxanthine, although this presumes that the cisplatin adduct somehow breaks down during the excision. The levels of the purine metabolites adenosine monophosphate (AMP), adenosine diphosphate (ADP), and guanosine triphosphate (GTP) were decreased in both cell lines by the combination treatment. In a previous study, it was found that FK866, a small molecule inhibitor of nicotinamide phosphoribosyltransferase (NAMPT), caused significant metabolic changes in purine metabolism in ovarian cancer and colorectal cancer cells [30]. Moreover, Zhou et al. described a study in hepatocellular carcinoma (HepG2 cells) that showed that high-dose treatment with sorafenib, an oral multikinase inhibitor, affects purine metabolism with significant decreases in GTP levels [33]. Despite the profound dose-dependent metabolic changes in HepG2 cells induced by sorafenib monotherapy, Zhou et al. showed that everolimus, another anticancer agent, in combination with first-line sorafenib therapy results in more pronounced metabolic changes to pyruvate, amino acid, methane, glyoxylate, and dicarboxylate, and glycolysis or gluconeogenesis in hepatocellular carcinoma cells [33]. Other than purine metabolite changes, consistent variations were observed for pyrimidine metabolism. The levels of pyrimidine metabolites such as orotate, dihydrothymine, dihydrouracil, and uridine triphosphate (UTP) were reduced in both cell lines after exposure to the melittin + cisplatin combinations. The reason for the decrease in pyrimidine metabolites is not clear. Normally DNA damage might be associated with increased levels of dihydrothymine which is produced by excision of damaged thymine residues from DNA.

There were many altered metabolites belonging to several pathways for amino acid metabolism. Most of the metabolites grouped under the arginine and proline pathways were reduced in sensitive cells after the combination treatments; while the arginine metabolite was non-significantly altered in resistant cells. Similarly, our previous study examined the effect of melittin on A2780 and A2780CR cells which showed that the level of arginine was downregulated in cisplatin sensitive cells compared with resistant cells [15]. A number of studies have reported that arginine deficiency enhances apoptosis in different cell lines including human lymphoblastic cell lines [34], mesothelioma cells [35], and melanoma cell lines [36]. Some human cancers, such as melanoma and hepatocellular carcinoma [37], do not express arginosuccinase synthase and therefore are unable to synthesise arginine from citrulline [38]. A recent study observed that ovarian carcinoma SKOV3 cells under arginine deprivation showed increased sensitivity to treatment with paclitaxel, a chemotherapy drug used to treat cancers, at low doses. In this context, it is to be noted that paclitaxel is a disruptor of the cytoskeleton and negatively impacts on the autophagosome-lysosome fusion step [39]. A previous study suggested that combinational treatment based on arginine deprivation and an autophagy inhibitor (for example chloroquine, a known nontoxic antimalarial drug) can potentially be applied as a second line treatment for a subset of ovarian carcinomas deficient in argininosuccinate synthetase [39]. It was also observed that the development of chemoresistance to platinum compounds in ovarian carcinomas leads to collateral appearance of arginine auxotrophy due to the downregulation of argininosuccinate synthetase [40]. The exact mechanism whereby deficiency arginine biosynthesis confers resistance remains unclear.

There was a strong effect of the combination treatment on cellular cysteine and glutathione metabolism; S-glutathionyl-L-cysteine, 3-sulfino-L-alanine, glutathione, L-cysteinylglycine, and L-

cystathionine were all lower in cisplatin sensitive cells compared with resistant cells after being treated with the combinations. In a previous study, it was found that the level of glutathione was higher in resistant cells (A2780-CP20) than in sensitive cells (A2780) [41]. This finding resembles the current results in which the level of glutathione was higher in resistant cells than sensitive cells following combination treatment. Two of the main reasons for platinum resistance in OCCs are the p53 mutation and drug-induced increases in intracellular glutathione concentration. A study by Mohell et al. showed that methylene quinuclidinone (MQ), in addition to binding to cysteine residues in p53, also binds to glutathione, decreasing intracellular glutathione levels in OCCs [42]. Therefore, it is possible that the combination promotes greater binding of cisplatin to glutathione thus depleting its levels which occurs to a greater extent in the sensitive cells. Mohell et al. also observed that combination effects of APR-246 (which is a prodrug that is converted to the active compound MQ) with doxorubicin were the cause of a DNA damage response, including activation of the p53 pathway leading to apoptosis [42]. Moreover, recent metabolomics based studies in OCCs have demonstrated that gossypol decreases cellular levels of GSH and induces apoptosis through oxidative stress [30]. In our previous study it was observed that the levels of GSH were no different between resistant and sensitive cells. However, in the current study GSH is depleted by the combination treatment to a much greater extent in the sensitive cells. The depletion appears to be related to the ability of the cells to synthesise GSH. Although there is no difference between the cysteine levels in the two cell lines, there are marked differences in key intermediates which can be used to synthesise both cysteine and GSH including glycine, serine, cystathionine, and glutathione cysteine. There are also lower levels of S-adenosylmethionine in the treated sensitive cells which is a source of homocysteine which is also a precursor of cysteine.

Increased serine biosynthesis is one of many metabolic changes that have been reported in cancer cells [43,44], and serine is a central node for the biosynthesis of many molecules such as glycine and cysteine [45]. High levels of serine in cancer cells have been linked to increased rates of cell proliferation [46]. The level of serine was increased in resistant cells following the combination treatment. In contrast, treatment of the sensitive cells with the combination resulted in a decrease of serine within the cells and a further lowering of the nonessential amino acid glycine. Glycine is incorporated directly into purine nucleotide bases and into GSH. The conversion of serine to glycine, catalysed by serine hydroxymethyltransferase (SHMT), donates a one-carbon unit to tetrahydrofolate to produce 5, 10-methylenetetrahydrofolate (CH_2-THF). CH_2-THF is used in thymidine synthesis and is a precursor of other folate species that contribute to purine synthesis [46]. The difference in OCCs could be reflected at the cellular level in terms of differences in the metabolite profiles. Serine is required for a number of biosynthetic and signalling pathways, including the production of phospholipids such as sphingolipids and phosphatidylserine [46]. Previous studies have shown that serine biosynthesis appears to be part of an adaptive response to oxidative stress [47]. The tumour suppressor p53 is emerging as an important regulator of cellular metabolism. P53 is a key player in the cellular response to stress in the form of numerous challenges, including DNA damage, hypoxia, and oncogene activation [48]. Cells lacking p53 fail to respond to serine starvation due to oxidative stress, which leads to reduced viability and severely impaired proliferation [49].

The level of ATP was found to be reduced in both cell lines after the combination treatment. ATP was found to be more reduced in both cell lines when treated with the combinations compared with the results observed previously with melittin monotherapy [15]. It is known that glycolysis provides ATP and energy in most cell types, but cancer cells extensively use glycolysis to sustain anabolism, which is necessary for tumour growth [50]. We found that the combinations inhibited glycolysis in both cell lines as indicated by lower levels of fructose bisphosphate and phosphopyruvate. In addition, several TCA cycle intermediates were lowered. Cell death can be executed by different mechanisms, including apoptosis, autophagy, necrosis, or combinations of these processes. Although different cell death mechanisms are unique in their molecular signalling cascades, one molecule is involved in the processes that mediates all types of cell death; ATP. During late-stage apoptosis, ATP levels sharply drop, mostly because of the loss of mitochondrial function and consumption by ATP-dependent proteases. In autophagy, a rescue process of self-degradation to compensate for energy

paucity occurs, that also features ATP insufficiency prior to cell death [50,51]. During necrosis, depletion of ATP precedes mitochondrial permeability changes [52]. The fact that ATP deprivation occurs in all types of cell death suggests that energy metabolism may play a critical role in the survival of cancer cells under stress. Thus, it could be possible that the A2780 cells may be undergoing late-stage apoptosis cell death in response to the combination treatment whereas the A2780CR may be undergoing early-stage apoptosis cell death. In our study, we found that combination treatment probably inhibited glycolysis in A2780 cells by depletion of NAD^+. Moreover, the level of NAD^+ was found to be decreased in A2780CR cells after combination treatment. It appears that the combinations had more impact on the oxidative phosphorylation pathway in both cell lines in comparison with melittin as a single treatment [15]. The inhibition of NAMPT leads to suppression of tumour cell growth and induction of apoptosis due to NAD^+ depletion [53]. NAMPT represents a promising therapeutic target for the development of potential novel cancer drugs [54,55]. In most cancer cells, poly (ADP-ribose) polymerase is activated due to DNA damage and cell death induced by oxidative stress [56,57]. Therefore, NAMPT inhibition leads to attenuation of glycolysis, resulting in further alteration of the carbohydrate metabolism in the cells [53].

4. Materials and Methods

4.1. Cell Lines and Cultures

The cisplatin-sensitive (A2780) and resistant (A2780CR) human ovarian carcinoma cells were obtained from ECACC (Porton Down, Salisbury, UK) and maintained at 75×10^4 cells/mL in RPMI 1640 medium (Lonza, Verviers, Belgium) supplemented with 1% (v/v) L-glutamine (Invitrogen, Paisley, UK), 100 IU/mL/100 μg/mL penicillin/streptomycin (Invitrogen, Paisley, UK), and 10% (v/v) foetal bovine serum (FBS) (Life Technologies, Carlsbad, CA, USA). In addition, the cultures for the A2780CR cells contained 3 μg/mL of cisplatinum (Tocris Bioscience, Bristol, UK) in the first three passages. Sub-confluent cultures were split by trypsinisation every 4–5 days and maintained at 37 °C in a humidified atmosphere saturated with 5% CO_2.

4.2. Cell Viability Assay

Cisplatin was purchased from Tocris Bioscience (Bristol, UK) and was dissolved in sterile water with gentle warming according to the manufacturer's instructions. Melittin was purified from bee venom (supplied by Beesen Co. Ltd, Dae Jeon, Korea) by reversed phase liquid chromatography [58] and reconstituted in sterile water to form a stock solution of 1 mg/mL before storage at −20 °C until required. Cell viability was assessed by an Alamar® Blue cell assay (Thermo Fisher Scientific, Loughborough, UK), as previously described [15].

To test the synergistic cytotoxic effect, experiments were performed with A2780 and A2780CR cell lines using various combinations of melittin with cisplatin in medium, to assess possible synergistic/additive effects. Both A2780 and A2780CR cells were seeded at 1×10^4 cells/well in 96-well plates (Corning®, Sigma-Aldrich) and incubated at 37 °C and 5% CO_2 in a humidified atmosphere for 24 h. For the A2780 cell line, 3, 4, 5, and 6 μg/mL of melittin was combined with 2 μg/mL of cisplatin and 3, 4, and 5 μg/mL of cisplatin was combined with 3 μg/mL of melittin. For the A2780CR cell line, 2, 3, 4 and 5 μg/mL of melittin was combined with 10 μg/mL of cisplatin and 20 and 30 μg/mL of cisplatin was combined with 2 μg/mL of melittin. Twenty hours after drug treatment, AB was added at a final concentration of 10% (v/v) and the resultant mixture was incubated for a further 4 h at 37 °C and 5% CO_2. Then, the plates were read at an excitation wavelength of 560 nm and the emission at 590 nm was recorded on a SpectraMax M3 microplate reader (Molecular Devices, Sunnyvale, CA, USA). All experiments were performed in triplicate.

4.3. Calculation of CI

The specific interaction between melittin and cisplatin on A2780 and A2780CR cancer cell lines was evaluated by the CI analysis. Drug combination synergy was performed using CompuSyn software [59]. CI values and CI-Fa plot (plot representing CI versus Fa, the fraction affected by a

particular dose) were calculated by CompuSyn program (Compusyn Inc, Paramus, NJ, USA). All experiments were repeated at least three times.

4.4. Statistical Analysis

GraphPad Prism for Windows (version 5.00, GraphPad Software, San Diego, California, USA) was employed to produce dose-response curves by performing nonlinear regression analysis of the cell viability data. The mean IC_{50} values were calculated from at least three measurements of independent experiments ($n = 3$).

4.5. Determination of the Effect of Melittin in Combination with Cisplatin on Cell Metabolomes

The A2780 cell line was treated with the combination of melittin and cisplatin at concentrations of 5 and 2 μg/mL, respectively, for 24 h ($n = 5$). The A2780CR cells were treated with the combination of melittin and cisplatin at concentrations of 2 and 10 μg/mL, respectively, for 24 h ($n = 5$). The cells were seeded at 75×10^4 cells/mL in T-25 cell culture flasks and incubated for 1 doubling time (48 h) before treatment with the combinations and incubation for an additional 24 h. After the treatment, the medium was removed and the cells were washed twice with 3 mL of phosphate-buffered saline (PBS) at 37 °C before lysis. Cell lysates were prepared by extraction with ice cold methanol:acetonitrile:water (50:30:20) (1 mL per 2×10^6 cells). The cells were scraped and cell lysates mixed on a Thermo mixer at 1440 rotations per minute (r.p.m.) for 12 min at 4 °C, before being centrifuged at 13500 r.p.m. for 15 min at 0 °C. The supernatants were collected and transferred into HPLC vials for LC-MS analysis. During the analysis, the temperature of the autosampler was maintained at 4 °C. Mixtures of standard metabolites (Sigma-Aldrich, Poole, UK) and the pooled quality control (QC) sample were injected in each analysis run in order to facilitate identification and to evaluate the stability and reproducibility of the analytical method. The pooled QC sample was obtained by taking equal aliquots from all the samples and placing them into the same HPLC vial.

4.6. LC-MS Conditions

Liquid chromatographic separation was carried out on an Accela HPLC system interfaced to an Exactive Orbitrap mass spectrometer (Thermo Fisher Scientific, Bremen, Germany) using a hydrophilic interaction liquid chromatography (HILIC) column (ZIC-pHILIC, 150 × 4.6 mm, 5 μm particle size) supplied by Hichrom Ltd. (Reading, UK). The method was reported previously [60]. Briefly, the mobile phase for ZIC-pHILIC consisted of 20 mM ammonium carbonate (Sigma-Aldrich, Poole, UK) in water purified by Direct-Q3 Ultrapure water purification system (Millipore, UK) at pH 9.2 (solvent A) and acetonitrile (Sigma-Aldrich, Poole, UK) (solvent B) at a flow rate of 0.3 mL/min. The elution gradient was an A:B ratio of 20:80 at 0 min, 80:20 at 30 min, 92:8 at 35 min, and finally 20:80 at 45 min.

4.7. Data Extraction and Analysis

Data extraction for each of the samples was carried out by MZmine-2.10 software (mzmine.github.io/) using identical parameters for peak detection, deconvolution, deisotoping, alignment, filtering, and gap filling in order to make multiple data files comparable [23]. The extracted ions, with their corresponding m/z values and retention times, were pasted into an Excel macro of the most common metabolites prepared in–house to facilitate identification, and a library search was also carried out against accurate mass data of the metabolites in the Human Metabolome, Kyoto Encyclopedia of Genes and Genomes, and Metlin databases. The lists of the metabolites obtained from these searches were then carefully evaluated manually by considering the quality of their peaks and their retention time match to the standard metabolite mixtures run in the same sequence. The MS data were $\log_2$-transformed and mean-centred with unit variance scaling for statistical analysis. Statistical analyses were performed using both univariate and multivariate approaches. The *p*-values from univariate analysis were adjusted using the FDR control and differences in the levels (or peak areas) of the metabolites between treated and control cells were considered significant at $p < 0.05$.

MetaboAnalyst®, a web-based metabolomic data processing tool [60], was used for supporting fold-change analysis, and t-tests. SIMCA-P software version 14.0 (Umetrics, Crewe, UK) was also used for multivariate analysis of the metabolite data with Pareto scaling prior to modelling with PCA and OPLS-DA. OPLS-DA models were validated based on multiple correlation coefficient (R^2) and cross-validated R^2 (Q^2) in cross-validation and permutation tests.

5. Conclusions

Based on the results presented, a metabolic signature for the cisplatin and melittin combination treatment for A2780 and A2780CR OCCs is proposed. Melittin and cisplatin together have different metabolic effects on these cells compared to melittin alone, which preferentially affects fatty acids, amino acids, and TCA cycle intermediates. The most significantly affected metabolites due to the melittin + cisplatin combination treatment in both cell lines were in the TCA cycle, oxidative phosphorylation, purine and pyrimidine metabolism, and arginine/proline pathways. This distinct mechanism of action of the melittin + cisplatin combination may provide a new paradigm for overcoming chemoresistance in ovarian cancer therapy. Our results provide rationale for the ongoing study of melittin in combination with cisplatin that could produce improved therapy for platinum resistance in ovarian cancer.

Supplementary Materials: The following are available online at www.mdpi.com/2218-1989/7/2/14/s1, Figure S1: Cell viability was determined following treatment with cisplatin for 24 h (A) IC_{50}= 10.8 μg/mL A2780CR; (B) IC_{50}= 4.9 μg/mL A2780, Figure S2: Cell viability was determined following treatment with melittin for 24 h (IC_{50}= 6.8μg/mL A2780; IC_{50}= 4.5μg/mL A2780CR), Figure S3: Hierarchical clustering analysis (HCA) of 20 ovarian cancer cell samples. It shows two main groups and four subgroups. The groups: CR, control of cisplatin resistance cell lines; SOR: A2780CR after treatment with melittin + cisplatin; C, control of cisplatin sensitive cell lines; SOS, A2780 after treatment with melittin + cisplatin, Figure S4: (A) Permutation analysis of OPLS-DA model derived from A2780 cells treated with melittin/cisplatin and controls cells. Statistical validation of the OPLS-DA model by permutation analysis using 100 different model permutations. The goodness of fit (R2) and predictive capability (Q2) of the original model are indicated on the far right and remain higher than those of the 100 permuted models to the left. OPLS-DA, orthogonal partial least squares discriminant analysis. (B) Receiver Operating Characteristics (ROC) curve shows sensitivity (true positive rate (TPR)) on the y-axis versus (false positive rate (FPR = 1 - Specificity)) on the x-axis. The area under ROC curve (AUROCC) =1 for SOS and C groups, Figure S5: (A) Permutation analysis of OPLS-DA model derived from A2780CR cells treated with melittin/cisplatin and controls cells. Statistical validation of the OPLS-DA model by permutation analysis using 100 different model permutations. The goodness of fit (R2) and predictive capability (Q2) of the original model are indicated on the far right and remain higher than those of the 100 permuted models to the left. OPLS-DA, orthogonal partial least squares discriminant analysis. (B) Receiver Operating Characteristics (ROC) curve shows sensitivity (true positive rate (TPR)) on the y-axis versus (false positive rate (FPR = 1 - Specificity)) on the x-axis. The area under ROC curve (AUROCC) =1 for SOR and CR groups.

Acknowledgments: Sanad Alonezi is funded by the government of Saudi Arabia (Armed Forces Medical Services Ministry of Defence). Jonans Tusiimire and Jennifer Wallace are both funded by Beesen Co. Ltd. (Dae Jeon, Korea) through a partnership between Strathclyde University and the Korea Institute for Advancement of Technology (KIAT).

Author Contributions: David G. Watson conceived the project; Jonans Tusiimire, David G. Watson, Jennifer Wallace, John A. Parkinson, and Mark J. Dufton purified and characterised the melittin; Sanad Alonezi, Carol J. Clements, and Louise Young performed the biological assays and analysed the data; Sanad Alonezi, Jonans Tusiimire, and David G. Watson performed the LC-MS experiments and analysed the data; Jin Kyu Park and Jong Woon Jeon supplied the crude bee venom and provided preliminary scientific input; Sanad Alonezi, Jonans Tusiimire, John A. Parkinson, Valerie A. Ferro, and David G. Watson wrote and edited the manuscript. All authors have read and approved the final manuscript.

Conflicts of Interest: The authors declare no conflict of interest.

References

1. Takakura, M.; Nakamura, M.; Kyo, S.; Hashimoto, M.; Mori, N.; Ikoma, T.; Mizumoto, Y.; Fujiwara, T.; Urata, Y.; Inoue, M. Intraperitoneal administration of telomerase-specific oncolytic adenovirus sensitizes ovarian cancer cells to cisplatin and affects survival in a xenograft model with peritoneal dissemination. *Cancer Gene Ther.* **2010**, *17*, 11–19.
2. Pinto, A.C.; Moreira, J.N.; Simões, S. *Combination Chemotherapy in Cancer: Principles, Evaluation and Drug Delivery Strategies*; INTECH Open Access Publisher: Rijeka, Croatia, 2011.
3. Fontaine, F.; Overman, J.; François, M. Pharmacological manipulation of transcription factor protein-protein interactions: Opportunities and obstacles. *Cell Regen.* **2015**, *4*, 2.
4. Kim, H.; Lee, G.; Park, S.; Chung, H.-S.; Lee, H.; Kim, J.-Y.; Nam, S.; Kim, S.K.; Bae, H. Bee venom mitigates cisplatin-induced nephrotoxicity by regulating CD4. *Evid.-Based Complement. Altern. Med.* **2013**, *2013*, doi:10.1155/2013/879845.
5. Kim, H.; Lee, H.; Lee, G.; Jang, H.; Kim, S.-S.; Yoon, H.; Kang, G.-H.; Hwang, D.-S.; Kim, S.K.; Chung, H.-S. Phospholipase A_2 inhibits cisplatin-induced acute kidney injury by modulating regulatory T cells by the CD206 mannose receptor. *Kidney Int.* **2015**, *88*, 550–559.
6. Chvetzoff, G.; Bonnotte, B.; Chauffert, B. Anticancer chemotherapy. Prevention of toxicity. *Presse Med.* **1998**, *27*, 2106–2112.
7. Choi, K.E.; Hwang, C.J.; Gu, S.M.; Park, M.H.; Kim, J.H.; Park, J.H.; Ahn, Y.J.; Kim, J.Y.; Song, M.J.; Song, H.S. Cancer cell growth inhibitory effect of bee venom via increase of death receptor 3 expression and inactivation of NF-kappa B in NSCLC cells. *Toxins* **2014**, *6*, 2210–2228.
8. Lim, B.-S.; Moon, H.J.; Li, D.X.; Gil, M.; Min, J.K.; Lee, G.; Bae, H.; Kim, S.K.; Min, B.-I. Effect of bee venom acupuncture on oxaliplatin-induced cold allodynia in rats. *Evid.-Based Complement. Altern. Med.* **2013**, *2013*, doi:10.1155/2013/369324.
9. Yoon, J.; Jeon, J.-H.; Lee, Y.-W.; Cho, C.-K.; Kwon, K.-R.; Shin, J.-E.; Sagar, S.; Wong, R.; Yoo, H.-S. Sweet bee venom pharmacopuncture for chemotherapy-induced peripheral neuropathy. *J. Acupunct. Meridian Stud.* **2012**, *5*, 156–165.
10. Gajski, G.; Čimbora-Zovko, T.; Rak, S.; Osmak, M.; Garaj-Vrhovac, V. Antitumour action on human glioblastoma A1235 cells through cooperation of bee venom and cisplatin. *Cytotechnology* **2016**, *68*, 1197–1205.
11. Gajski, G.; Čimbora-Zovko, T.; Rak, S.; Rožman, M.; Osmak, M.; Garaj-Vrhovac, V. Combined antitumor effects of bee venom and cisplatin on human cervical and laryngeal carcinoma cells and their drug resistant sublines. *J. Appl. Toxicol.* **2014**, *34*, 1332–1341.
12. Lee, G.; Bae, H. Bee venom phospholipase A_2: Yesterday's enemy becomes today's friend. *Toxins* **2016**, *8*, 48.
13. Kinsey, G.R.; Okusa, M.D. Expanding role of T cells in acute kidney injury. *Curr. Opin. Nephrol. Hypertens.* **2014**, *23*, 9.
14. Alizadehnohi, M.; Nabiuni, M.; Nazari, Z.; Safaeinejad, Z.; Irian, S. The synergistic cytotoxic effect of cisplatin and honey bee venom on human ovarian cancer cell line A2780cp. *J. Venom Res.* **2012**, *3*, 22.
15. Alonezi, S.; Tusiimire, J.; Wallace, J.; Dufton, M.J.; Parkinson, J.A.; Young, L.C.; Clements, C.J.; Park, J.K.; Jeon, J.W.; Ferro, V.A. Metabolomic profiling of the effects of melittin on cisplatin resistant and cisplatin sensitive ovarian cancer cells using mass spectrometry and Biolog microarray technology. *Metabolites* **2016**, *6*, 35.
16. Palmnas, M.S.; Vogel, H.J. The future of NMR metabolomics in cancer therapy: Towards personalizing treatment and developing targeted drugs? *Metabolites* **2013**, *3*, 373–396.
17. Spratlin, J.L.; Serkova, N.J.; Eckhardt, S.G. Clinical applications of metabolomics in oncology: A review. *Clin. Cancer Res.* **2009**, *15*, 431–440.
18. Odunsi, K.; Wollman, R.M.; Ambrosone, C.B.; Hutson, A.; McCann, S.E.; Tammela, J.; Geisler, J.P.; Miller, G.; Sellers, T.; Cliby, W. Detection of epithelial ovarian cancer using ^{1}H-NMR-based metabonomics. *Int. J. Cancer* **2005**, *113*, 782–788.
19. Zheng, J.-F.; Lu, J.; Wang, X.-Z.; Guo, W.-H.; Zhang, J.-X. Comparative metabolomic profiling of hepatocellular carcinoma cells treated with sorafenib monotherapy vs. sorafenib-everolimus combination therapy. *Med. Sci. Monit. Int. Med. J. Exp. Clin. Res.* **2015**, *21*, 1781.
20. Chou, T.-C.; Talalay, P. Analysis of combined drug effects: A new look at a very old problem. *Trends Pharmacol. Sci.* **1983**, *4*, 450–454.

21. Chou, T.-C.; Talalay, P. Quantitative analysis of dose-effect relationships: The combined effects of multiple drugs or enzyme inhibitors. *Adv. Enzyme Regul.* **1984**, *22*, 27–55.
22. Patrick Reynolds, C.; Maurer, B.J. Evaluating response to antineoplastic drug combinations in tissue culture models. *Chemosensitivity* **2005**, *110*, 173–183.
23. Xia, J. and Wishart, D.S. Using MetaboAnalyst 3.0 for Comprehensive Metabolomics Data Analysis. *Curr. Protoc. Bioinform.* **2016**, doi:10.1002/cpbi.11.
24. Alonezi, S.; Al Washih M.; Clements, C.J.; Young, L.; Ferro, V.A.; Watson, D.G. Current liquid chromatography mass spectrometry (LCMS) and phenotype microarray profiling of ovarian cancer cells after exposure to cisplatin. *Curr. Metabol.* **2017**, *5*, doi:10.2174/2213235X05666170203120840.
25. Chou, T.-C.; Motzer, R.J.; Tong, Y.; Bosl, G.J. Computerized quantitation of synergism and antagonism of taxol, topotecan, and cisplatin against human teratocarcinoma cell growth: A rational approach to clinical protocol design. *J. Natl. Cancer Inst.* **1994**, *86*, 1517–1524.
26. Chang, T.; Gulati, S.; Chou, T.; Vega, R.; Gandola, L.; Ibrahim, S.E.; Yopp, J.; Colvin, M.; Clarkson, B. Synergistic effect of 4-hydroperoxycyclophosphamide and etoposide on a human promyelocytic leukemia cell line (HL-60) demonstrated by computer analysis. *Cancer Res.* **1985**, *45*, 2434–2439.
27. Bible, K.C.; Kaufmann, S.H. Cytotoxic synergy between flavopiridol (NSC 649890, L86-8275) and various antineoplastic agents: The importance of sequence of administration. *Cancer Res.* **1997**, *57*, 3375–3380.
28. Wang, J.; Jin, L.; Li, X.; Deng, H.; Chen, Y.; Lian, Q.; Ge, R.; Deng, H. Gossypol induces apoptosis in ovarian cancer cells through oxidative stress. *Mol. BioSyst.* **2013**, *9*, 1489–1497.
29. Vermeersch, K.A.; Wang, L.; McDonald, J.F.; Styczynski, M.P. Distinct metabolic responses of an ovarian cancer stem cell line. *BMC Syst. Biol.* **2014**, *8*, 134.
30. Tolstikov, V.; Nikolayev, A.; Dong, S.; Zhao, G.; Kuo, M.-S. Metabolomics analysis of metabolic effects of nicotinamide phosphoribosyltransferase (NAMPT) inhibition on human cancer cells. *PLoS ONE* **2014**, *9*, e114019.
31. Huang, Y.; Bell, L.N.; Okamura, J.; Kim, M.S.; Mohney, R.P.; Guerrero-Preston, R.; Ratovitski, E.A. Phospho-ΔNp63α/SREBF1 protein interactions: Bridging cell metabolism and cisplatin chemoresistance. *Cell Cycle* **2012**, *11*, 3810–3827.
32. Chaney, S.G.; Campbell, S.L.; Bassett, E.; Wu, Y. Recognition and processing of cisplatin- and oxaliplatin-DNA adducts. *Crit. Rev. Oncol./Hematol.* **2005**, *53*, 3–11.
33. Zhou, S.; Luo, R. Metabolomic response to sorafenib treatment in human hepatocellular carcinoma cells. *FASEB J.* **2013**, *27*, 663–667.
34. Gong, H.; Zölzer, F.; Von Recklinghausen, G.; Havers, W.; Schweigerer, L. Arginine deiminase inhibits proliferation of human leukemia cells more potently than asparaginase by inducing cell cycle arrest and apoptosis. *Leukemia* **2000**, *14*, 826.
35. Szlosarek, P.W.; Klabatsa, A.; Pallaska, A.; Sheaff, M.; Smith, P.; Crook, T.; Grimshaw, M.J.; Steele, J.P.; Rudd, R.M.; Balkwill, F.R. In vivo loss of expression of argininosuccinate synthetase in malignant pleural mesothelioma is a biomarker for susceptibility to arginine depletion. *Clin. Cancer Res.* **2006**, *12*, 7126–7131.
36. Feun, L.; You, M.; Wu, C.; Kuo, M.; Wangpaichitr, M.; Spector, S.; Savaraj, N. Arginine deprivation as a targeted therapy for cancer. *Curr. Pharm. Des.* **2008**, *14*, 1049–1057.
37. Ensor, C.M.; Holtsberg, F.W.; Bomalaski, J.S.; Clark, M.A. Pegylated arginine deiminase (ADI-SS $PEG_{20,000\ mw}$) inhibits human melanomas and hepatocellular carcinomas in vitro and in vivo. *Cancer Res.* **2002**, *62*, 5443–5450.
38. Lind, D.S. Arginine and cancer. *J. Nutr.* **2004**, *134* (Suppl. S10), 2837S–2841S.
39. Shuvayeva, G.; Bobak, Y.; Igumentseva, N.; Titone, R.; Morani, F.; Stasyk, O.; Isidoro, C. Single amino acid arginine deprivation triggers prosurvival autophagic response in ovarian carcinoma SKOV3. *BioMed Res. Int.* **2014**, *2014*, doi:10.1155/2014/505041.
40. Nicholson, L.J.; Smith, P.R.; Hiller, L.; Szlosarek, P.W.; Kimberley, C.; Sehouli, J.; Koensgen, D.; Mustea, A.; Schmid, P.; Crook, T. Epigenetic silencing of argininosuccinate synthetase confers resistance to platinum-induced cell death but collateral sensitivity to arginine auxotrophy in ovarian cancer. *Int. J. Cancer* **2009**, *125*, 1454–1463.
41. Poisson, L.M.; Munkarah, A.; Madi, H.; Datta, I.; Hensley-Alford, S.; Tebbe, C.; Buekers, T.; Giri, S.; Rattan, R. A metabolomic approach to identifying platinum resistance in ovarian cancer. *J. Ovarian Res.* **2015**, *8*, 13.

42. Mohell, N.; Alfredsson, J.; Fransson, Å.; Uustalu, M.; Byström, S.; Gullbo, J.; Hallberg, A.; Bykov, V.; Björklund, U.; Wiman, K. Apr-246 overcomes resistance to cisplatin and doxorubicin in ovarian cancer cells. *Cell Death Dis.* **2015**, *6*, e1794.
43. Davis, J.L.; Fallon, H.J.; Morris, H.P. Two enzymes of serine metabolism in rat liver and hepatomas. *Cancer Res.* **1970**, *30*, 2917–2920.
44. Snell, K. Enzymes of serine metabolism in normal, developing and neoplastic rat tissues. *Adv. Enzyme Regul.* **1984**, *22*, 325–400.
45. Locasale, J.W. Serine, glycine and one-carbon units: Cancer metabolism in full circle. *Nat. Rev. Cancer* **2013**, *13*, 572–583.
46. Mattaini, K.R.; Sullivan, M.R.; Vander Heiden, M.G. The importance of serine metabolism in cancer. *J. Cell Biol.* **2016**, *214*, 249–257.
47. Maddocks, O.D.; Berkers, C.R.; Mason, S.M.; Zheng, L.; Blyth, K.; Gottlieb, E.; Vousden, K.H. Serine starvation induces stress and p53-dependent metabolic remodelling in cancer cells. *Nature* **2013**, *493*, 542–546.
48. Vousden, K.H.; Prives, C. Blinded by the light: The growing complexity of p53. *Cell* **2009**, *137*, 413–431.
49. Amelio, I.; Cutruzzolá, F.; Antonov, A.; Agostini, M.; Melino, G. Serine and glycine metabolism in cancer. *Trends Biochem. Sci.* **2014**, *39*, 191–198.
50. Lemasters, J.J.; Qian, T.; He, L.; Kim, J.-S.; Elmore, S.P.; Cascio, W.E.; Brenner, D.A. Role of mitochondrial inner membrane permeabilization in necrotic cell death, apoptosis, and autophagy. *Antioxid. Redox Signal.* **2002**, *4*, 769–781.
51. Skulachev, V. Bioenergetic aspects of apoptosis, necrosis and mitoptosis. *Apoptosis* **2006**, *11*, 473–485.
52. Vanlangenakker, N.; Berghe, T.V.; Krysko, D.V.; Festjens, N.; Vandenabeele, P. Molecular mechanisms and pathophysiology of necrotic cell death. *Curr. Mol. Med.* **2008**, *8*, 207–220.
53. Tan, B.; Dong, S.; Shepard, R.L.; Kays, L.; Roth, K.D.; Geeganage, S.; Kuo, M.-S.; Zhao, G. Inhibition of nicotinamide phosphoribosyltransferase (NAMPT), an enzyme essential for NAD^+ biosynthesis, leads to altered carbohydrate metabolism in cancer cells. *J. Biol. Chem.* **2015**, *290*, 15812–15824.
54. Giannetti, A.M.; Zheng, X.; Skelton, N.J.; Wang, W.; Bravo, B.J.; Bair, K.W.; Baumeister, T.; Cheng, E.; Crocker, L.; Feng, Y. Fragment-based identification of amides derived from trans-2-(pyridin-3-yl) cyclopropanecarboxylic acid as potent inhibitors of human nicotinamide phosphoribosyltransferase (NAMPT). *J. Biol. Chem.* **2014**, *57*, 770–792.
55. Zheng, X.; Bauer, P.; Baumeister, T.; Buckmelter, A.J.; Caligiuri, M.; Clodfelter, K.H.; Han, B.; Ho, Y.-C.; Kley, N.; Lin, J. Structure-based discovery of novel amide-containing nicotinamide phosphoribosyltransferase (NAMPT) inhibitors. *J. Biol. Chem.* **2013**, *56*, 6413–6433.
56. Yu, S.-W.; Wang, H.; Poitras, M.F.; Coombs, C.; Bowers, W.J.; Federoff, H.J.; Poirier, G.G.; Dawson, T.M.; Dawson, V.L. Mediation of poly (ADP-ribose) polymerase-1-dependent cell death by apoptosis-inducing factor. *Science* **2002**, *297*, 259–263.
57. Du, L.; Zhang, X.; Han, Y.Y.; Burke, N.A.; Kochanek, P.M.; Watkins, S.C.; Graham, S.H.; Carcillo, J.A.; Szabó, C.; Clark, R.S. Intra-mitochondrial poly (ADP-ribosylation) contributes to NAD^+ depletion and cell death induced by oxidative stress. *J. Biol. Chem.* **2003**, *278*, 18426–18433.
58. Tusiimire, J.; Wallace, J.; Dufton, M.; Parkinson, J.; Clements, C.J.; Young, L.; Park, J.K.; Jeon, J.W.; Watson, D.G. An LCMS method for the assay of melittin in cosmetic formulations containing bee venom. *Anal. Bioanal. Chem.* **2015**, *407*, 3627–3635.
59. Chou, T.; Martin, N. *Compusyn for Drug Combinations: Pc Software and User's Guide: A Computer Program for Quantitation of Synergism and Antagonism in Drug Combinations, and the Determination of IC_{50} and ED_{50} and LD_{50} Values*; ComboSyn Inc.: Paramus, NJ, USA, 2005.
60. Zhang, R.; Watson, D.G.; Wang, L.; Westrop, G.D.; Coombs, G.H.; Zhang, T. Evaluation of mobile phase characteristics on three zwitterionic columns in hydrophilic interaction liquid chromatography mode for liquid chromatography-high resolution mass spectrometry based untargeted metabolite profiling of leishmania parasites. *J. Chromatogr. A* **2014**, *1362*, 168–179.

Supplementary Materials: Metabolomic Profiling of the Synergistic Effects of Melittin in Combination with Cisplatin on Ovarian Cancer Cells

Sanad Alonezi, Jonans Tusiimire, Jennifer Wallace, Mark J. Dufton, John A. Parkinson, Louise C. Young, Carol J. Clements, Jin-Kyu Park, Jong-Woon Jeon, Valerie A. Ferro and David G. Watson

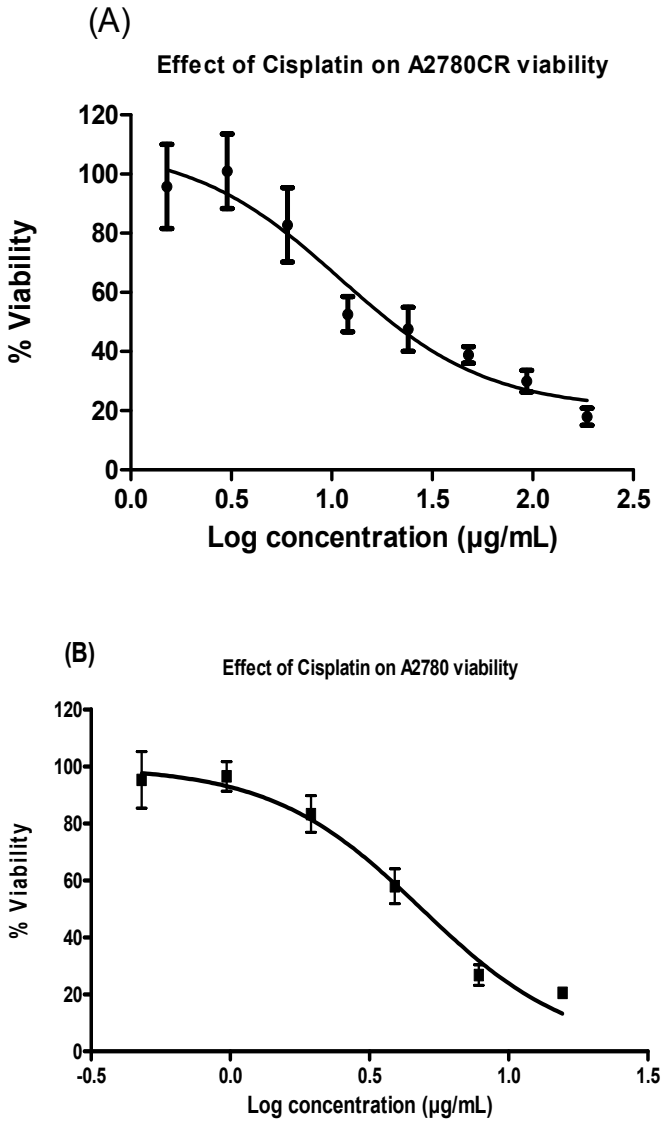

Figure S1. Cell viability was determined following treatment with cisplatin for 24 h (A) IC_{50} = 10.8 µg/mL A2780CR; (B) IC_{50} = 4.9 µg/mL A2780.

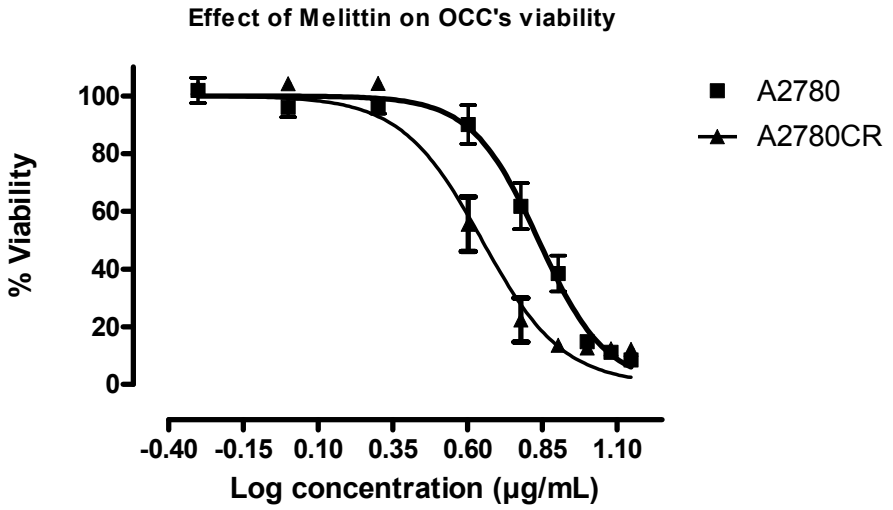

Figure S2. Cell viability was determined following treatment with melittin for 24 h (IC_{50} = 6.8µg/mL A2780; IC_{50} = 4.5µg/mL A2780CR).

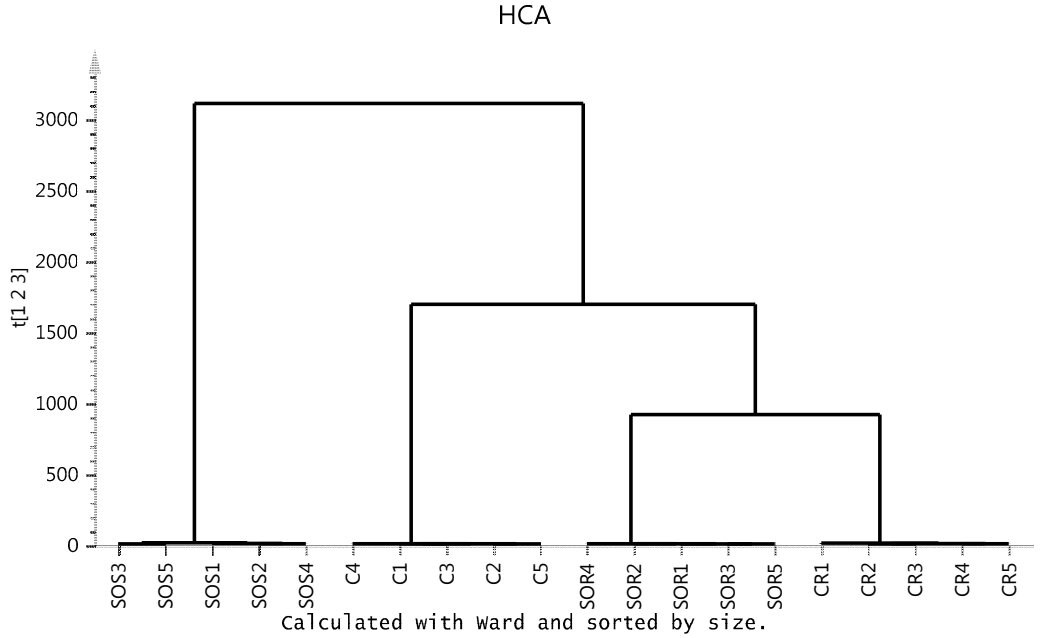

Figure S3. Hierarchical clustering analysis (HCA) of 20 ovarian cancer cell samples. It shows two main groups and four subgroups. The groups: CR, control of cisplatin resistance cell lines; SOR: A2780CR after treatment with melittin + cisplatin; C, control of cisplatin sensitive cell lines; SOS, A2780 after treatment with melittin + cisplatin.

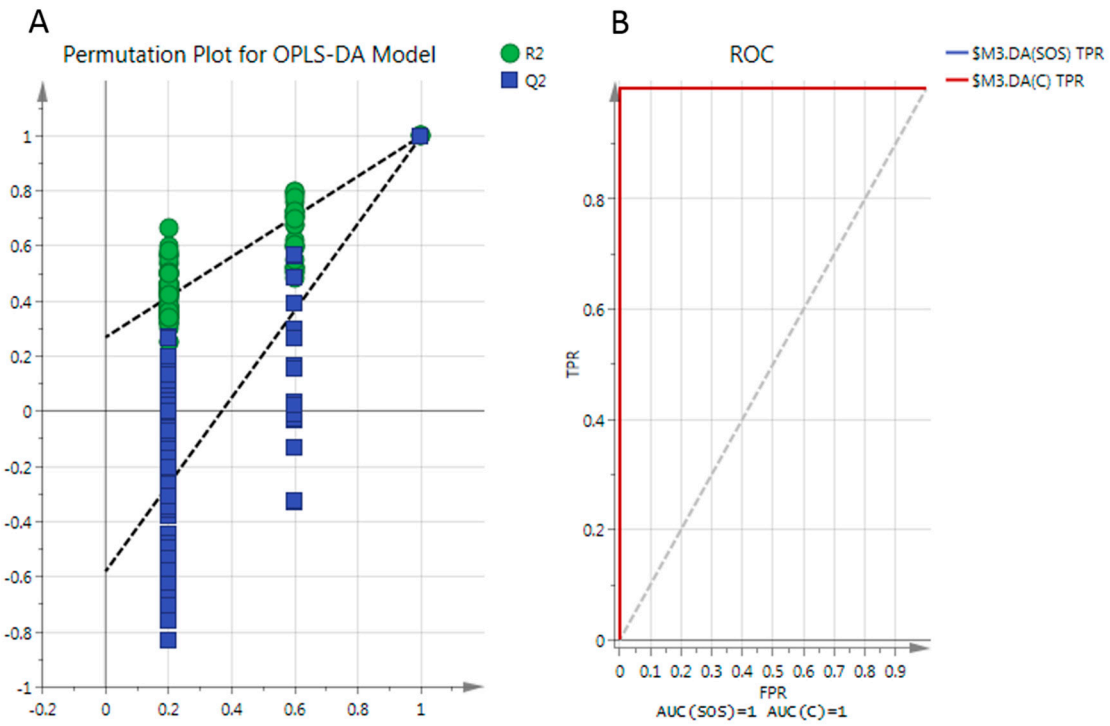

Figure S4 (A) Permutation analysis of OPLS-DA model derived from A2780 cells treated with melittin/cisplatin and controls cells. Statistical validation of the OPLS-DA model by permutation analysis using 100 different model permutations. The goodness of fit (R2) and predictive capability (Q2) of the original model are indicated on the far right and remain higher than those of the 100 permuted models to the left. OPLS-DA, orthogonal partial least squares discriminant analysis. **(B)** Receiver Operating Characteristics (ROC) curve shows sensitivity (true positive rate (TPR)) on the y-axis versus (false positive rate (FPR = 1 − Specificity)) on the x-axis. The area under ROC curve (AUROCC) = 1 for SOS and C groups.

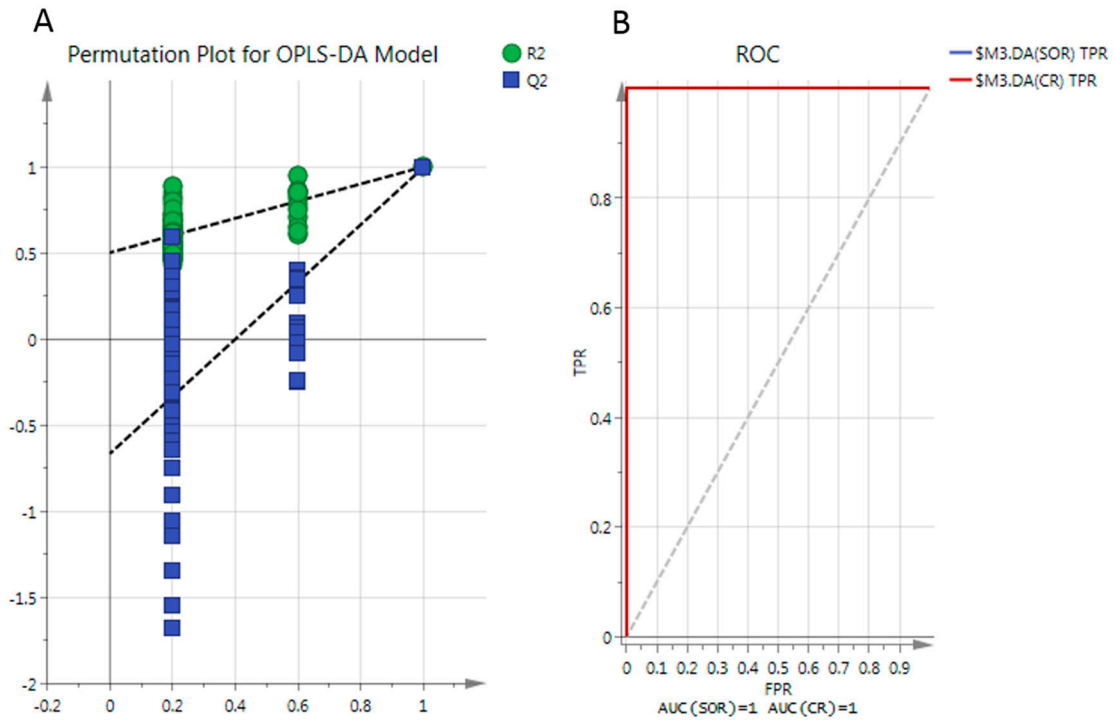

Figure S5 (A) Permutation analysis of OPLS-DA model derived from A2780CR cells treated with melittin/cisplatin and controls cells. Statistical validation of the OPLS-DA model by permutation analysis using 100 different model permutations. The goodness of fit (R2) and predictive capability (Q2) of the original model are indicated on the far right and remain higher than those of the 100 permuted models to the left. OPLS-DA, orthogonal partial least squares discriminant analysis. **(B)** Receiver Operating Characteristics (ROC) curve shows sensitivity (true positive rate (TPR)) on the y-axis versus (false positive rate (FPR = 1 − Specificity)) on the x-axis. The area under ROC curve (AUROCC) = 1 for SOR and CR groups.